Dissertations, Theses, and Masters Projects

Theses, Dissertations, & Master Projects

1995

Fabrication of thermoplastic polymer composite ribbon

Donald Allan Sandusky
College of William and Mary - Virginia Institute of Marine Science

Follow this and additional works at: https://scholarworks.wm.edu/etd

Part of the Materials Science and Engineering Commons, Mechanical Engineering Commons, and the Polymer Science Commons

Recommended Citation

INFORMATION TO USERS

This manuscript has been reproduced from the microfilm master. UMI films the text directly from the original or copy submitted. Thus, some thesis and dissertation copies are in typewriter face, while others may be from any type of computer printer.

The quality of this reproduction is dependent upon the quality of the copy submitted. Broken or indistinct print, colored or poor quality illustrations and photographs, print bleedthrough, substandard margins, and improper alignment can adversely affect reproduction.

In the unlikely event that the author did not send UMI a complete manuscript and there are missing pages, these will be noted. Also, if unauthorized copyright material had to be removed, a note will indicate the deletion.

Oversize materials (e.g., maps, drawings, charts) are reproduced by sectioning the original, beginning at the upper left-hand corner and continuing from left to right in equal sections with small overlaps. Each original is also photographed in one exposure and is included in reduced form at the back of the book.

Photographs included in the original manuscript have been reproduced xerographically in this copy. Higher quality 6" x 9" black and white photographic prints are available for any photographs or illustrations appearing in this copy for an additional charge. Contact UMI directly to order.

UMI

FABRICATION OF THERMOPLASTIC POLYMER
COMPOSITE RIBBON

A Dissertation

Presented to the Program in

Applied Science (Polymer Track)

The College of William & Mary in Virginia

In Partial Fulfillment

Of the Requirements for the Degree of

Doctor of Philosophy

---

by

Donald A. Sandusky

1995

UMI Number: 9537551

UMI

300 North Zeeb Road
Ann Arbor, MI 48103
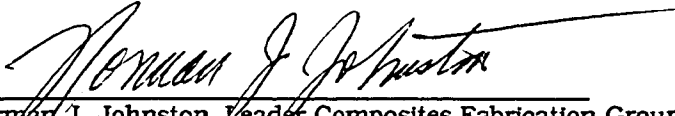
Approval Sheet

This dissertation is submitted in partial fulfillment of

the requirements for the degree of

Doctor of Philosophy
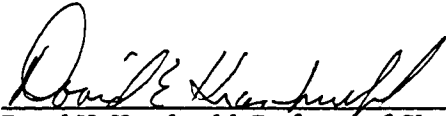
<u>Donald A. Sandusky</u>

Author
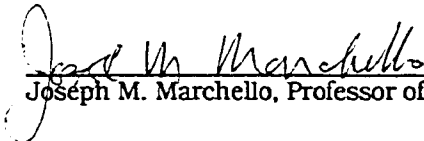
Approved, February 1995

Norman J. Johnston, Leader Composites Fabrication Group (NASA Langley Research Center, Composites and Polymers Branch) and Adjunct Professor of Applied Science

David H. Kranbuehl, Professor of Chemistry

Joseph M. Marchello, Professor of Civil Engineering (Old Dominion University)

Robert A. Orwoll, Professor of Chemistry

John N. Shoosmith, Chief Scientist, (NASA Langley Research Center, Analysis and Computation Division) and Adjunct Professor of Applied Science

ii

Acknowledgments

Thank you to the U.S. tax-payers who funded my research via the NASA Graduate Student Researcher Fellowship program and the NASA High Speed Research program. I have done my level-best to make your investment worth-while. Thanks to each and every member of the NASA Langley Research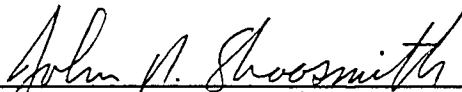 Center Composites and Polymers Branch. I have never known a finer group of people, especially Norman J. Johnston, Joseph M. Marchello and Terry L. St.Clair. I have learned volumes from each of you. Thanks to the faculty of the College of William & Mary Program in Applied Science for the opportunity to attend such a fine academic institution. Thanks to my committee members for their constructive criticism and support. Thanks to my student peers, especially Michael Glasgow, for their friendship and care. Thanks to my colleagues Steven Wilkinson and Maylene Hugh for helping me maintain perspective and drive when things were tough. Thank you to my parents, Susanne and Terry, and my sister Jennie, for teaching me how to follow our Fathers will, and providing me unconditional refuge. Thank you to Captain Charles L. Wyman who instilled the fundamental seeds of wanderlust and confidence in my life, and taught me how to thrive. Thank you to Mark T. Wyman whose recommendation opened the first door to the rest of my engineering career. And finally, the greatest honor of my life is to call Jennifer my wife. Thank you Jennifer, for your kindness, patience, and strength.

Table of Contents

v

vi

List of Tables

vii

List of Figures

viii

ix

x

Abstract

The goal of this research was to develop a controllable process to convert a thermoplastic powder-coated carbon-fiber towpreg into uniform and consolidated ribbon. The approach comprised four primary activities. 1) The patent and processing literature was studied to evaluate the state of the art. 2) A functional ribbon fabrication technique was developed by scaling-up, in a novel configuration, hardware components found in the literature. 3) The *ex parte* ribbonizing process was characterized by calibrating equipment, determining steady state and studying cause and effect between process parameters and ribbon quality. 4) Process design and control methods were derived from heat transfer and pulling force analyses.

The *ex parte* ribbonizer process comprises a material handling system, a preheat region, a heated stationary bar assembly, and a cooled nip roller assembly. Appropriate timing of important contacts is key to fabricating quality ribbon. Process characterization and analyses revealed key flow mechanisms. Ribbon microstructure changes most at the bars. Ribbon macrostructure changes most at the nip. An isothermal bar contact is a practical processing constraint for ensuring uniform squeeze flow bar spreading. All bar drag force is attributed to shear stress in the interfacial viscous boundary layer between the towpreg and the stationary bar surface. Continually sensing pulling force is a good indication of process control.

The research goal was achieved because the *ex parte* ribbonizer can be used to convert polymer powder towpreg into uniform and fully-consolidated ribbon in a controllable manner.

xi

FABRICATION OF THERMOPLASTIC POLYMER

COMPOSITE RIBBON

Chapter 1   Introduction

To encourage continued growth in the general technology base, U.S. and foreign government agencies have strategically generated tax-funded development programs which inherently require continued high-risk research (large capital expenditure for long term or no pay-off), over a broad scope of topics. Many such programs are classified under the guise of national security or competitiveness while others, like the U.S. space program, are widely disseminated to achieve complex socioeconomic and political goals. These technology growth programs, have provided the silicon chip, Velcro™ and countless other devices which have since been developed into consumer products.

Over the last few decades, NASA and components of the U.S. Department of Defense have generated various research programs contributing to the development of fiber-reinforced polymer composites. Carbon fiber-reinforced polymer composites have demonstrated desirable mechanical properties and are considered useful in a broad range of applications. Access to strong, yet light, building materials provides intuitively obvious benefit to consumers who live in a mobile society. Although these high-performance composite materials have existed for decades, their use has

not been generally prolific due to the complexity of polymer matrix composite fabrication and high cost. Materials research and fabrication technology development efforts are required to bring costs down, thereby promoting broad use of polymer composites.

Background

Fiber-reinforced polymer composite materials enable novel structure design and applications. The anisotropic properties of these materials command a unique and intrinsic paradigm shift in fabrication methodology. Unlike conventional metal machining technology, removing material from a carbon fiber composite billet is difficult and, more importantly, limits the extent to which anisotropic composite properties may be utilized. Consequently, an entirely different fabrication process is often used for building polymer composite structures. One of the more commonly encountered fabrication methods is to apply tacky thermoset prepreg lamina, layer by layer, to a build-up a laminate part. After vacuum bagging and autoclave cure, these parts exhibit highly engineered anisotropic mechanical properties. Although this hand "lay-up" composite fabrication method is enabling, it is also laborious and inherently costly.

A government program funded the automation of thermoset prepreg lay-up in an effort to develop the enabling technology needed to build large and complex polymer composite structures. The so-called "filament winding" process was developed to perform automated lay-up of carbon fiber-reinforced thermoset

polymer matrix prepreg to fabricate composite structures of closed-section and convex shapes. "Fiber placement" technology was developed later as an improvement over filament winding. The more complex fiber placement technology is capable of fabricating open-section and concave structures in addition to those made by filament winding. After filament winding or fiber placement, lay up the thermoset laminate is usually vacuum bagged and autoclave cured, both of which are inherently costly.

As material requirements evolved with new government application programs, thermoplastic matrix composites became desirable over thermoset matrix composites for their toughness properties. Furthermore, thermoplastic matrix composites promised the potential for in situ fabrication to net shape, which is like the inverse of metal machining. After in-situ lay-up, the vacuum bag and autoclave processes are theoretically unnecessary because there is no required cure for thermoplastics. The filament winding process was enhanced to accommodate thermoplastic prepreg giving rise to the so called "hot-head filament winding" technology. Closed-section and convex shape limitations of the filament winding process led to the development of the so-called in situ "advanced tow placement" (ATP) technology which, while still in its infancy, purports to fabricate open- and closed-section structures of simple laminate design using boardy thermoplastic ribbonized carbon fiber-reinforced prepreg. Machine constraints and capability limitations of the in situ ATP process have led to modifications enabling in situ placement of wide bands comprising several adjacent thermoplastic ribbons. Research is continuing in order to advance the state of-the-art ATP process so it

can be used to fabricate complex open-section structures of high-performance carbon fiber-reinforced thermoplastic ribbon material.

This Research Program

.

A recent government program is aimed at developing non-autoclave methods to fabricate high-performance carbon fiber-reinforced composites. A sub-task of this government program required in situ ATP fabrication of structures from carbon fiber-reinforced polyimide matrix ribbon. The in situ ATP sub-task was delayed because ribbon of the specified composition was not available in research quantities from either commercial, government or university laboratories. For good reason, the ribbon was not available because, the ribbon fabrication technology had not yet been successfully developed. Consequently, developing a ribbonizing technique, especially one that could be applied to thermoplastic polyimides, was a critical issue for the program and therefore became the purpose of this research.

Background For This Research

The fabrication of thermoplastic ribbon requires two key steps. In the first step, polymer is impregnated into the carbon fiber roving (tow) producing a preimpregnated tow (towpreg). In the second step, the towpreg is consolidated into a uniform ribbon. High molecular weight thermoplastic polyimides, for example, are not particularly amenable to conventional solution impregnation or hot-melt

impregnation. They tend to exhibit particularly high melt viscosity and many are insoluble in conventional processing solvents. The high melt viscosity, combined with the fine diameter of the carbon filaments, cause particular resistance to state of-the-art impregnation and ribbon forming.

Conventional solution, and hot-melt impregnation technology was defined by several prepregging patents [1-6]. Alternative prepregging methods such as organic, and aqueous slurry prepregging technology [7,8] were developed as alternatives for materials such as polyimides. Even simpler, dry powder impregnation by electrostatic fluidized bed [9], turbulent fluidized bed [10] and powder curtain [11] impregnation processes were also developed and patented. Each novel prepregging process exhibited the ability to impregnate tow with thermoplastic polymer powder resulting in a flexible powder-coated towpreg. These towpregs were not fully consolidated and were not ideally suited for in situ ATP. They needed to be ribbonized.

The body of ribbonizing literature is very limited. Some commercial interests were understood to have the capability to fabricate thermoplastic towpreg ribbon but unfortunately, were not engaged in the government project and their work was not found in the literature. Three publications presented research efforts consistent with thermoplastic powder towpreg ribbonizing. A 1993 University of Delaware Ph.D. dissertation by P. Hepola [12] provided useful information and modeling regarding the pultrusion of unidirectional towpreg ribbon. The pultrusion process was combined with on-line dry powder impregnation. A 1993 Georgia Institute of

Technology M.S. thesis by M. Rammoorthy [13] evaluated the pultrusion of powder-coated towpreg in which the latter was made by electrostatic powder fusion impregnation. This study also evaluated a heated roller consolidation of the towpreg rather than pultrusion. A 1992 Tampere University of Technology (Finland) study by P. Peltonen et al. [14] described a cross-head extruder/impregnation device used in conjunction with a stationary pin spreading device to fabricate polyethylene/fiberglass towpreg ribbon.

1.1   Research Goal

In contrast to the previously mentioned literature on ribbon fabrication literature, the research presented here was based on a slightly different premise. It was assumed that good quality powder-coated towpreg could be fabricated by any of the known powder impregnation methods. Rather than focusing on the impregnation method, the towpreg consolidation (ribbonizing) method was considered to be the critical issue.

The goal of this effort was to develop a controllable process which could convert high temperature, thermoplastic powder-coated, carbon fiber towpreg into uniform, consolidated ribbon with the condition that the ribbon exhibit quality attributes satisfactory for in situ ATP fabrication of composite structures. In short, the goal was to fabricate thermoplastic polymer carbon fiber-reinforced composite ribbon with special emphasis on polyimide matrix composition.

1.2   General Approach

The approach comprised four primary activities. 1) The patent and processing literature was studied to evaluate the state of-the-art. 2) A functional ribbon fabrication technique was developed by scaling-up, in a novel configuration, hardware components found in the literature. 3) The *ex parte* ribbonizing process was characterized by calibrating equipment, determining steady state and studying cause and effect between process parameters and ribbon quality. 4) Process design and control methods were derived from heat transfer and pulling force analyses.

The first and second actives comprise Chapter 2 wherein the development of the *ex parte* ribbonizing process is discussed. The third activity comprises Chapter 3. The fourth activity comprises Chapters 4 and 5. A summary of observations, conclusions and future work comprises Chapter 6.

1.3   End Notes

1   Chabrier, G.; Moine, G.; Maurion, R.; Szabo, R. U.S. Patent 4 626 306, 1986.

2   Cogswell, F.N.; Hezzell, D.J. U.S. Patent 4 549 920, 1985.

3   Courtney, A.L. U.S. Patent 3 249 484, 1966.

4   Wickwire, A.M., Jr. U.S. Patent 2 407 335, 1946.

5   XXX. U.S.S.R. Patent 422 469, 1974.

6   Hashizume, S. Japanese Patent 405 050 432, 1993.

7   Johnston, N. J.; Towell, T. W. U. S. Patent 5 252 168, 1993.

8   Towell, T. W.; Hirt, D. E.; Johnston, N. J. *IntL SAMPE Tech. Conf. Series*, **1990**, *22*, 1156-69 .

9   Muzzy, J.D.; Colton, J.S. U.S. Patent 5 295 064, 1994.

10   Baucom, R. M.; Snoha, J.; Marchello, J. M. U. S. Patent 5 057 338, 1991.

11   Baucom, R. M.; Marchello, J. M. *SAMPE Series*, **1993**, *38*, 1902-15.

12   Hepola, P.J. Ph.D. Dissertation, The University of Delaware, Newark, DE., 1993.

13   Rammoorthy, M. M.S. Thesis, Georgia Institute of Technology, Atlanta, GA., 1993.

14   Peltonen, P.; Lahteenkorva, K.; Paakkonen, E.J.; Jarvela, P.K.; Tormala, P. *J. ThermopL Comp. Mat.*, **1992**, *5*, 318-43.

2   Ribbonizing Process Development

The goal of this research was to design and build an apparatus that could be used to fabricate towpreg ribbon comprising high-temperature performance polyimide polymer and carbon fiber. The general approach was to study the state of-the-art, evaluate prototype devices, and scale-up the optimal design configuration.

2.1   Related Processing Literature Survey

Thermoplastic towpreg ribbonizing can be classified as a component part of the more general prepregging process. A review of prepregging patents and pertinent processing research publications delineated the important issues and potential deficiencies in the state of-the-art. Thermoset and thermoplastic prepregging methods constituted most of the related patent literature. Key thermoplastic processing research studies, relevant to the present objective, were also studied to gain knowledge of other ribbon fabrication efforts.

Relevant Thermoset Prepregging Patents

The state of-the-art in thermoset prepregging is defined by the patent literature. In

1966, Courtney [1] patented an impregnation apparatus for making flat tapes of thermoset precursor coated filaments. No consolidation mechanism was mentioned because filament band spreading was achieved prior to impregnation and the resin solution exhibited low viscosity. The importance of filament tow spreading was however stressed by Courtney. In 1973, Avis *et al.* [2] patented thermoset prepregging technology which made use of solution dip pan impregnation, roller consolidation and film coating of several adjacent fiber tows to produce wide tacky prepreg tapes. In 1976, Hardwick [3] taught an impregnation method using significant spreading, a novel resin coating mechanism and sinuous rollers for flattening the tacky prepreg into a wide tape. A 1974 U.S.S.R. Patent [4] utilized impregnation mechanisms with sinuous stationary spreader bars rather than rollers. In 1990, Dyksterhouse *et al.* [5] taught a impregnation process similar to that of Avis *et al.* for primarily water soluble, thermosetting matrix polymer precursors which were compatible with polymeric binding agents. From these references, the key concept of thermoset prepregging was determined to be wet-out, which could be achieved best with substantial tow spreading prior to impregnation and some sort of smoothing, nipping or spreading technique after impregnation.

Relevant Thermoplastic Prepregging Patents

An object of thermoplastic prepregging is to evenly distribute the polymer about the filaments. A common way to accomplish wet-out is to liquefy thermoplastic polymer prior to impregnation. Two primary methods are available to soften the polymers for prepregging, solvation and melting. Some thermoplastics are soluble in conventional processing solvents (e.g., PEEK™/diphenylsulphone) at elevated temperature, while

others (e.g., most polyimides) are not particularly soluble. Thermoplastics with reasonably flexible backbone structure (e.g., aliphatic) and low molecular weight exhibit substantially lower melt viscosity than rigid backbone (e.g., imide), high molecular weight polymers indicating the compromise between processing properties and mechanical properties of the composites made from them.

In 1987, O'Conner [6] patented a prepregging process wherein fibers were impregnated with thermoplastic poly (arylene sulfide) which consolidated to form a laminate. O'Conner described a powder slurry impregnation component with a pultrusion consolidation component. The 15 (cm min^{-1}) production rates were limited by the consolidation rather than by the impregnation component. O'Conner also referred to fiber jamming at the die entrance which required frequent stoppages. In 1992, all of O'Conners claims were canceled due to prior art.

In 1989, O'Conner et al. [7] taught a complicated pultrusion process wherein a preferred embodiment described the prepregging and pultrusion of 1/4 inch diameter carbon fiber rods from a carbon fiber tow, slurry impregnated with poly (phenylene sulfide) powder. Processing rates for laminates were noted at 15 (in min^{-1}) which are considered slow for thin lamina fabrication.

A method for impregnation and consolidation, all in one resin extrusion/pultrusion (crosshead) die, was taught in 1976 by Moyer [8]. Heated stationary spreader bars were situated downstream of the crosshead die impregnation chamber. In a preferred embodiment, the partially consolidated lamina could exit the die and then be formed and solidified by cooled nip rollers. In one example, Moyer illustrated the

ribbonization of a 10K carbon fiber tow with Nylon™ 6.6 at 36 (ft min⁻¹) which was considered reasonably fast. This technique was also taught in 1993 by Hashizume [9] where rolling spreader bars rather than fixed bars were utilized just downstream from the crosshead impregnation component.

In 1986, Chabrier *et al.* [10] taught slurry powder impregnation followed by heating and cooled roller forming. A fiber tow was pulled through a slurry impregnation chamber forming a towpreg, then through a heating oven to melt the polymer and after exiting the malleable towpreg was formed into a uniform ribbon by contact with a cool nip roller. The preferred embodiments of this patent seem in conflict with those of the 1992 patent by Muzzy *et al.* [11] wherein the preferred embodiments included many variations of dry powder impregnation and many variations of partial consolidation. Another very similar patent application was awarded to Muzzy *et al.* [12] in 1994, again teaching a method for impregnating and partially consolidating high melt viscosity matrix composite lamina. Melt wetting and pultrusion or nip forming resulted in a partially consolidated flexible towpreg known as Towflex™.

Precedence exists for claiming the novelty and utility of only the impregnation component of a prepregging process. In 1991, Soules [13] taught an apparatus and method for impregnation of thermoplastic polymer by drawing a fiber tow through a slurry bath to form a towpreg. Although the figures of the patent illustrate a heated pultrusion die for consolidation of the lamina, no claims for consolidation were allowed.

In 1946, Wickwire Jr. [14] taught smoothing of thermoplastic hot-melt coatings by using several stationary blades, over which a hot-melt impregnated fiber web (comprising several adjacent tows) passed. This combination impregnation and consolidation device was understood to work very well for polymer systems exhibiting low melt viscosity. In 1989 Angell Jr. et al. [15] taught a hot-melt prepregging process with a hot-melt impregnation section and a "kneading section" comprising several sinuously spaced spreading rollers. In a preferred embodiment, these rollers were situated in such a manner to impose substantial wrapping of the lamina around the forming rollers. This configuration of the kneading section was confusing since it appeared that the nip was situated in an awkward configuration such that if the nip was cooled, the tape would be curled and, if the nip was heated, the polymer would stick and cause filament wrapping and tearing.

In 1985, Cogswell et al. [16] taught a prepregging process which took advantage of the reduced melt viscosity of high-solids-content solutions compared to the high melt viscosity of the neat polymer. In a preferred embodiment, impregnation took place within a heated dip pan, a modification of those commonly used for thermoset prepregging, with some number of stationary bar spreaders. Upon exiting the impregnation pan, the web was forced between two metering rods forming a fixed nip which controlled the quantity of solution pick-up. In a subsequent step, the high boiling solvent was vaporized. Residual solvent was defined to be plasticizer, a beneficial toughening modifier. This impregnation technique was especially useful for polymer systems with particularly high melt viscosity, but required the polymer to be partially soluble in a conventional processing solvent. Typical processing rates were suggested to be near 20 (cm min^{-1}). This impregnation technique was material

specific (especially for PEEK™/diphenylsulphone) in application, although many types of thermoplastics were included in the patent claims.

In 1985, Cogswell *et al* [17] taught a thermoplastic prepregging process which was not material specific. In a preferred embodiment, a filament web was drawn into a heated region where the filaments were spread between a stationary nip. At the location just upstream of the nip, polymer powder was dropped onto the spread fiber web. The polymer melted on contact and was forced into the fibers by the fixed nip and subsequent bars or rollers within the heated region. This process made no mention of further forming or consolidation after the impregnation and spreading.

Relevant Thermoplastic Consolidation Patents

Dating back to 1955, Hartland [18] taught a pultrusion apparatus with two separate dies where the first was heated to cause the polymer to melt and flow and the second was cooled to solidify the composite to form a solid profile. In 1989, Beever *et al* [19] taught the further development of this concept to include an improved oversized heated pultrusion die to aid in the melt flow and compaction process. Precedence for claiming a "consolidation only" apparatus and method was set here by Beever *et al*. The method included individual components where the first heated component was intended to partially consolidate "rough forming" and a second cooling component to fully consolidate, "final forming". Addition of an impregnation method was included as an alternate embodiment but was not claimed specifically in the patent. This apparatus and method were intended for use in the pultrusion of composite laminates. The process required occasional stoppage to open the cooling die to remove fiber ball slag which was considered a substantial nuisance.

Related Process Development Research

Three publications were identified which presented research efforts consistent with thermoplastic powder towpreg ribbonizing. A 1993 University of Delaware Ph.D. dissertation by P. Hepola [20] provided useful information and modeling regarding the fabrication of unidirectional composites with on-line dry powder impregnation followed by pultrusion. A 1993 Georgia Institute of Technology M.S. thesis by M. Rammoorthy [21] evaluated the Muzzy *et al.* [11] process with electrostatic powder fusion impregnation and also evaluated a heated roller consolidation mechanism. A 1992 study by P. Peltonen *et al.* [22] evaluated the utility of a cross-head extruder/impregnation device in conjunction with a stationary pin spreading device (similar to that taught by Moyer [8]) for the production of thermoplastic polyethylene/fiberglass ribbon. The stationary pin spreading device provided substantial improvements over pultrusion in terms of void content and processing speed, but was not sufficient to provide a uniformly profiled cross-section. Each of these process studies investigated methods which were intended to impregnate and consolidate on-line, which is at variance with the present goal of the present effort to develop a controllable method to ribbonize an already impregnated powder towpreg.

2.2   Prototype Equipment Evaluation

Several prototype apparatus were built and evaluated to determine their potential for towpreg ribbonizing. Some were similar to those described by the literature, some were novel and others comprised various components of several different methods. Based on the evaluation of over 20 different hardware components, the optimal

configuration was determined to be a combination of a material handling system combined with a heated tool and a cooled machine located in functional proximity to a premelting chamber.

Prototype Evaluation Summary

Heated and cooled prototype hardware were evaluated independently. A description of each prototype and its corresponding analysis was published in a 1994 SAMPE preprint [23] found in **Appendix A**. A material handling system was used to pull powder towpreg through various process prototypes to evaluate the attributes of each prototype. The heated apparatus evaluated by this study comprised both stationary tools (fixtures) and assemblies (machines). The cooled apparatus also comprised both fixtures and machines. The heated or cooled fixtures imposed sliding contact with the towpreg whereas heated or cooled machines imposed rolling contact.

Heated stationary fixtures were superior to heated machines due to undesirable adhesion between polymer coated fibers and rolling surfaces. Contact between the towpreg and the heated rollers caused fiber wrapping, requiring frequent and prohibitive cleaning stops. Adhesion also occurred for stationary fixtures causing stray fiber stripping however, the accumulated fiber balls and "slag" were observed to break free periodically. This was considered a manageable nuisance.

Evaluation of cooled hardware required preheating to soften the polymer. Preheating was accomplished by pulling powder-coated towpreg through a tube furnace at a functional speed so that on entering the cooled fixture or machine the towpreg was softened. Cooled machines were superior to cooled fixtures due to the advantageous

product release resulting from the polymer's rapid solidification on contact. In contrast to the heated apparatus which facilitated melt flow, bubble expulsion and wet-out, the cooled apparatus facilitated cross-section shaping by solidifying the polymer under constrained conditions. In general, the heated apparatus improved the towpreg's microstructure whereas the cooled apparatus provided uniform ribbon macrostructure.

The Optimal Configuration, the "Ex parte Ribbonizer"

The evaluations from this study lead to the development of a unique thermoplastic towpreg processing method called the *ex parte* ribbonizer comprising a preheat region, a heated stationary bar fixture (heated tool) and a cooled nip roller assembly (cooled machine). *Ex parte* (*Latin*) is usually used in legal context describing an argument "from one side or perspective only". Here *ex parte* serves metaphorically, as an adjective describing, in particular, the bar fixture region where the towpreg band is contacted on only one side at a time.

The most influential references for this process were the patents of Moyer [8], Hashizume [9], Cogswell *et al.* [17] and Chabrier *et al.* [10], who together, defined state of-the-art thermoplastic prepregging technology. The *ex parte* process apparatus and method were considered unique due to their utility and improvement over the state of-the-art for ribbonizing previously powder-coated towpreg. All of the claims in a U.S. patent application for the *ex parte* ribbonizer were allowed in 1994 and the patent will issue in 1995.

Summary

A study of the state of-the-art in polymer composite prepregging revealed several approaches for converting thermoplastic powder-coated towpreg into consolidated and uniform cross section ribbon. Towpreg band spreading was accomplished best by heated stationary bar fixture spreading and ribbon forming was best accomplished by cooled nip rolling. A novel process called the *ex parte* ribbonizer was developed comprising a material handling system, a premelting chamber, a stationary bar assembly and a cooled nip roller assembly.

The next chapter offers a detailed characterization of the *ex parte* ribbonizing process in terms of design, utility and calibration. Photographs and apparatus descriptions are followed by discussion of the purpose of each item to develop understanding of the process parameters and the requirements for process control.

2.3   End Notes

1   Courtney, A.L. U.S. Patent 3 249 484, 1966.

2   Avis, V.A.; Matthews, A.J. U.S. Patent 3 737 352, 1973.

3   Hardwick, J.G. G.B. Patent 1 434 926, 1976.

4   XXX. U.S.S.R. Patent 422 469, 1974.

5   Dyksterhouse R.; Dyksterhouse, J.A.; Handermann, A.C.; Western, E.D. U.S. Patent 4 919 739, 1990.

6   O'Conner, J.E. U.S. Patent 4 680 224, 1987.

7   O'Conner, J.E.; Beever, W.H.; Dancer, J.W.; Beaulieu, W.B.; Selby, L.M.;

       Rhodes Jr., V.H. U.S. Patent 4 883 552, 1989.

8   Moyer, R.L. U.S. Patent 3 993 726, 1976.

9   Hashizume, S. Japanese Patent 405 050 432, 1993.

10   Chabrier,G.; Moine, G.; Maurion, R.; Szabo, R, U.S. Patent 4 626 306, 1986.

11   Muzzy, J.D.; Varughese, B. U.S.Patent 5 094 883,1992.

12   Muzzy, J.D.; Colton, J.S. U.S. Patent 5 296 064, 1994.

13   Soules, D.A. U.S. Patent 5 019 427, 1991.

14   Wickwire, A.M., Jr. U.S. Patent 2 407 335, 1946.

15   Angell, Jr., R.G.; Michno, Jr., M.J.; Konrad, J.M.; Hobbs, K.E. U.S. Patent

       4 804 509, 1989.

16   Cogswell, F. N.; Staniland, P.A. U.S. Patent 4 541 884, 1985.

17   Cogswell, F.N.; Hezzell, D.J. U.S. Patent 4 549 920, 1985.

18   Hartland, U.S. Patent 2 702 408, 1955.

19   Beever, W.H.; Selby, L.M. U.S. Patent 4 820 366, 1989.

20   Hepola, P.J., Ph.D. Dissertation, The University of Delaware, Newark, DE.,

       1993.

21   Rammoorthy, M. M.S. Thesis, Georgia Institute of Technology, Atlanta, GA.,

       1993.

22   Peltonen, P.; Lahteenkorva, K.; Paakkonen, E.J.; Jarvela, P.K.; Tormala, P. *J.

       Thermopl. Comp. Mat.*, **1992**, *5*, 318-43.

23   Sandusky, D.A.; Marchello, J.M.; Johnston, N.J. *SAMPE Series,* **1994** *39*,

       2612-25.

Chapter 3 *Ex parte* **Ribbonizing Process Characterization**

The purpose of this chapter is to characterize the *ex parte* ribbon fabrication process in broad terms. Three primary efforts are discussed; a hardware description, a study of the control parameters' cause and effect with ribbon quality, and a study of the mechanism of microstructure melt-flow to identify potential rate determining steps.

The objective of the *ex parte* ribbonizing process and a schematic description of the

overall process is described to define some of the vernacular used throughout the dissertation. The *ex parte* ribbonizer comprises four primary hardware components: a material handling system, a tube furnace, a stationary bar assembly and a nip roller assembly. Each of these components is characterized in terms of design, utility and calibration. The role of process control variables on ribbon quality is established. Ribbon quality attributes consistent with the state of-the-art ATP requirements are defined. A cause and effect study of the changes in ribbon quality as a function of process control variables is discussed. A photographic and digital image analysis experiment is conducted to investigate the cross section microstructure changes experienced by the towpreg.

3.1   Hardware Description and Calibration

The primary objective of the *ex parte* ribbonizing process was to convert a thermoplastic coated towpreg into a consolidated ribbon. **Figure 3.1** is a side view and a top view of the *ex parte* ribbonizer apparatus. The supply means **101** delivers the incoming towpreg band **102** under substantial and uniformly distributed tension. The towpreg band comprises a plurality of contiguous towpregs. This band is unconsolidated with some volume percentage occupied by air or other fluid medium. The towpreg band **102** is drawn through the pre-melting chamber **103** the stationary bar assembly **107** and the nip roller assembly **104** by the take-up **105**. As a consequence of contacting the apparatus, the towpreg **102** is partially consolidated first into a malleable band **106** and then is formed into a consolidated ribbon **108**.

Figure 3.2 is a side view and a top view of the premelting chamber and stationary bar

assembly. The pre-melting chamber **201** and stationary bar assembly **202** are

integrally related within a tube furnace **203** having a steel tube liner **204**. The pre-

melting chamber is located within and is first encountered by the towpreg band at the

entrance plane of the tube furnace **205**. Within the pre-melting chamber, the polymer

component of the towpreg band **206** melts from the solid to a viscous liquid state

causing wetting of the filaments. This wetting phenomenon is observed to reduce the

overall bulk of the band and form a neck-down region **207**. Near the exit **208** of the

tube furnace is the stationary bar assembly **202**.

Figure 3.4 is a top view and a side view of the stationary bar assembly. The bar

fixture **401** comprises a plurality of bar templates **402**, and at least two stationary

bars **403**, **404** fixed perpendicular to the towpreg band. The bars each have at least

one side with a curved surface. The bars are constructed of materials which maintain

structural integrity at temperatures above the processing temperature of the polymer

component of the prepreg band. The entire stationary bar assembly is passively

heated by the tube liner throughout process operation. An alternate embodiment

would accommodate directly heated bars in place of passively heated bars.

The towpreg band is pulled over a first stationary bar **404** and then under a second

stationary bar **403**. The application of these contacts facilitates the expulsion of

bubbles and the redistribution of the polymer and filaments causing the prepreg band

106 to become partially consolidated.

After exiting the stationary bar assembly, the band exits the tube furnace and cools

under ambient conditions. On cooling the polymer matrix transitions between a

viscous liquid to a solid state, described here as "malleable viscoelastic solid". The partially consolidated malleable towpreg band 106 next enters the nip roller assembly 104 which is placed in an operable relationship to the exit plane of the tube furnace near the stationary bar fixture 107. This positioning allows sufficient distance between the exit of the tube furnace and nip point such that the partially consolidated malleable prepreg band cools yet remains warm and soft enough to be shaped on contact.

Figure 3.3 is a front view of the nip roller assembly. The nip assembly is a spring loaded, cooled nip-roller apparatus and comprises two hollow, matched grooved nip-rollers 301, 302 which are actively cooled under forced convection via load bearing shafts 303, 304. One of the rollers 301 is loaded 305 against a fixed roller 302. The resilient loading allows for passing of anomalies, such as filament balls, in the partially consolidated malleable towpreg band. Under both the applied load from the nip-rollers 301, 302 and the thermal gradient imposed by the cool roller surfaces, the malleable plastic solid transitions to solid elastic and the partially consolidated band is simultaneously shaped to match the gap 306 between the two nip-rollers. An advantage to having the nip-rollers cooled rather than heated is product release.

3.1.1 Material Handling System

A spool creel, a tensioning device (capstan), a single take-up and some alignment rollers comprise the material handling system. Each component is described in this section in terms of utility and calibration as appropriate.

Take-up

The ribbon take-up shown in **Figure 3.5** consists of a puller motor mounted on a traverse platform driven by a traverse motor. Both motors are 1/8 hp. Bodine™ DC gear motors with 40:1, right angle, single reduction, worm gear box. The two motors are controlled separately. This take-up does not have the capability of level winding because the traverse moves at a constant velocity, changing directions when the traverse platform contacts one of the two proximity relays mounted at either end of the traverse range. The motor controllers allows only for shaft speed control. **Figure 3.6** is a calibration plot showing the linear relationship between analog take-up setting and take-up speed.

Creel Rack

The spooled prepreg is mounted on a unique multi-station creel rack, **Figure 3.7**, with permanent magnet braking mechanisms on each spool shaft . The range of tension for the spool brakes is between 5g and 20g which is sufficient to keep the spools form over spinning. At the downstream end of the creel rack resides a ceramic eyelet array through-which the towpreg rovings are arranged in a uniform pattern. These abrasive contact points cause only minor quantities of powder to be stripped away from the towpreg and therefore are considered a nuisance rather than a prohibitive impediment.

Tensioning Capstans

In order to apply substantial back tension to the towpreg, a Century Design, Inc. model number CD 8820 braking capstan is employed. In the case where multiple towpregs are necessary to form a ribbon of predetermined cross section dimensions, each towpreg is required to experience identical back tension to reduce the potential for only one towpreg to carry most the capstan load (non-uniform catenary effects). To reduce the potential for this non-uniform catenary effect, each towpreg roving is afforded its own tensioning capstan. **Figure 3.8** is a photograph of one of these capstans. The electromagnetic braking range begins at 5 (N) and increased by analog scale to at least 20 (N).

Alignment Rollers

Since all of the apparatus are not ideally situated, alignment rollers are employed. To reduce friction, 1 3/8" x 3" AirStar™ (model XB-24973) air bearings are utilized. Two air bearing assemblies are plumbed with Tygon™ tubing and are mounted in custom fixtures of aluminum construction. A 40 psig source of dry shop air is attached to a custom manifold which provides multiple attachment points. **Figure 3.9** is a photograph of one of the alignment rollers assemblies and the manifold.

3.1.2 Premelting Chamber

In the *ex parte* process the purpose of the "oven" consists of three primary functions. The oven is necessary 1) to provide a premelting chamber so that the polymer is fully melted prior to contact with the processing bars, 2) to passively heat the stationary bar assembly and 3) to provide a rigid housing into which the stationary bar fixture is

attached.

Furnace Apparatus Description

The 6KW Lindberg™ tube furnace (model #58434-P) was designed by the manufacturer with a "split" clam shell configuration which can be opened from the front as shown in **Figure 3.10**, to reveal the functional components. The resistive heating elements are divided into 3 zones consisting of insulated heater coil arrays arranged in a matched semicircular shell configuration. When the oven is closed, each zone forms a cylindrical chamber. The three zones are axially situated to form an extended cylindrical region about 4 inches in diameter and 45 inches long. The temperature of each heating element zone is monitored by a single control thermocouple. These 3 control thermocouples extend through the insulation material at the top center of each upper semi-cylindrical shell. The control thermocouples are unshielded beads and therefore monitored the radiant temperature located about 1 inch below the top center of each zone. The controller device is used to set and maintain the temperature of each thermocouple bead. The controller comprises three separate modules which monitor and maintain the temperature within each of the three corresponding zones. The power input to each heater array is continually adjusted by the controller to maintain a steady radiant temperature at each of the three control thermocouples.

A stainless steel tube liner is situated within the furnace cavity in a concentric configuration. The tube is 48 inches long with an inside diameter of 3 inches and an outside diameter of 3.25 inches. The steel liner protrudes about 2 inches from the inlet side of the tube furnace and 1 inch from the exit side. As an option, an

essentially inert atmosphere within the heated region can be provided when the nitrogen bleed assembly shown in **Figure 3.11** is utilized.

3.1.2.1   Steady State Temperature Profile

The thin-walled cylindrical stainless steel tube liner is approximately 0.125 inch thick. Prior to experimentation the temperature of the inner and outer surfaces were expected to be similar, however the temperature along the axial direction was expected to vary. Furthermore, the temperature of the tube was expected to be reasonably uniform in the theta direction for a given axial location, due to the symmetry of the heating coil arrays and good insulation of the heating cavity.

The first approach for characterizing the axial tube liner temperature profile was to weld thermocouple beads directly to the tube liners external surface. Heavy gage glass wrap-glass braid thermocouple wire (Omega™ HH-K-20) was cut into 10 pieces each being approximately 10 feet long. A Unitech™, spot welder was used to simultaneously form a bead and weld the wire ends to the tube liner. The 10 beads were distributed evenly along the tubes length.

The thermocouple wire leads were attached to a Hydra™ Data Acquisition Unit (Model 2620A) manufactured by John Fluke Mfg. Co., Inc. All wiring connections were attached in the detachable Input Module which was subsequently placed into the Acquisition Module. The temperature induced bead voltages were calibrated and converted to degrees by the Acquisition Module and were displayed digitally. All of the temperature values were transmitted to a Hewlett Packard ThinkJet™ Printer via

were input into a Microsoft™ Excel spreadsheet. The steady state sample means and standard deviations were calculated.

The typical oven profile experiment began with all equipment at ambient temperature. On the heat-up, the radiative elements were on full power. This intense heat attacked the thermocouple lead fiberglass insulation. The polymer sizing on the fiberglass was burned off. Nonetheless, temperature measurements were recorded. After cool down, the leads were inspected and were determined unreliable for subsequent measurements as the fiberglass insulation was brittle and easy to rub off. Since many profiles needed to be evaluated, an alternative yet reliable test method was considered.

A thermocouple probe assembly shown in **Figure 3.12** was constructed so that it could be placed inside the tube liner, thereby, shielding the thermocouple wire insulation from direct exposure to the furnaces radiating elements. Several thermocouple leads of the same Omega™ HH-K-20 wire were attached with strapping wire to a 1.4 meter long by 1 cm diameter steel rod. Each bead was extended upward approximately 3 cm. The thermocouple probe was placed inside the tube from the inlet end and turned over so that each thermocouple bead contacted the inner surface of the tube. After temperature data were taken and the furnace was cooled down, the thermocouple lead insulation appeared to be only slightly degraded near the center region of the tube. This probe was considered to be reusable.

The temperature data gained from both the previously mentioned methods under identical conditions are presented in **Figure 3.13.** Continuous tube temperature

profiles were interpolated between measured data. It is important to note that comparison of the profiles measured by the two different methods indicates radiation shielding. The horizontal axis corresponds to the axial location along the tube liner from the entrance plane to the exit plane. The outermost shaded regions of the figure correspond to the overhang of the tube liner which extend beyond the end of the tube furnace on either side. The lighter shaded regions correspond to the insulated region of the furnace where there are no heating elements but rather there is intimate contact between the tube furnace insulation material and the tube liner. The innermost regions, zone 1,2 and 3 correspond to the heated sections which offer heating coils surrounding the tube liner.

Each zone is controlled separately and so furnace set points are identified by three temperatures separated by a slash (e.g., 500/475/500°C) for zones 1,2 and 3. Note that zone 3 corresponds to the entrance side of the tube. This tube furnace hardware configuration provides a temperature profile which is roughly parabolic when all three zone temperatures are set to the same value. The manufacturer recognized this issue and in an attempt of level the shape of the profile, set the controllers for zone 1 and 3 to 0°C at room temperature while zone 2 was set to 23°C at room temperature. Note that if a furnace is set to 500/475/500°C, the furnace is actually maintaining 523/475/523°C, explaining why some of the measured profile temperatures near the inlet side of zone 3 and the exit side of zone 1 were found to be greater than the set temperatures.

Steady State Tube Liner Temperature Profile

The furnace steady-state is defined by the passively heated stationary bar temperature rather than the heater zone control thermocouples. The processing steady-state is monitored externally to the oven temperature control device. The surface temperature of the passively heated processing bars is used to define the end of the heat-up period. Bar surface temperature is continually monitored by a thermocouple bead which is fit through a cylindrical hole through one of the bar templates and pressed to the surface of a processing bar.

At steady state the temperature profile along the length of the tube was observed to be reasonably constant. **Figure 3.14** presents the experimental results for the start up corresponding to a tube furnace setting of 465/445/465°C. Each data curve represents the inner tube temperature at the noted axial distance from the entrance. Of primary importance was the bar surface temperature as it tended to lag the tube surface temperature. This was reasonable because the stationary bar assembly was heated passively by the tube liner. Steady-state was attained after the measured bar temperature reached a value not varying more than 2°C per 5 second interval. Warm-up time was about 1 hour. This experiment was repeated for several zone temperature set-points. Warm-up time was not found to vary significantly between trials at similar zone settings.

3.1.2.2   Temperature Profile Sensitivity Analysis

The thermocouple probe was placed within the tube to evaluate the steady state tube

liner temperature profile for a variety of zone set points and equipment configurations. **Figure 3.15** illustrates four different steady state profiles which correspond to different zone set temperatures. Mean values are plotted with ±3 standard deviation error bars. **Figure 3.16** displays the effect of increasing the temperature in zone 1 relative to the others. The zone set temperatures can be altered to reflect a desired shape of the steady state profile. Reassurance was obtained by recognizing the stability of the profile over time. These profiles were generated from mean values calculated from data taken at one minute intervals over 30 minutes. During that half hour, outside doors were opened and closed and occasional changes in local air flow were experienced.

The effect of partially blocking the ends of the tube were characterized by conducting two steady state profiles at the same set point. **Figure 3.17** illustrates the sensitivity to heat loss out the ends of the tube. Substantial change in the profiles was observed near the ends of the tube, but near the middle, little change was observed.

3.1.3 Stationary Bar Assembly

The stationary bar assembly provides a tool against which the towpreg is generally flattened and debulked. The assembly is required to be of simple construction and to be reusable in the high-temperature and abrasive environment for its intended use. The materials selection for each of the three primary components was considered carefully. A sturdy fixture with reusable bars is required.

3.1.3.1   Materials Evaluation

The stationary bar fixture was constructed of a low alloy stainless steel sheet metal having good malleability, oxidative stability at elevated temperature, strength and stiffness. The thermal conductivity of the steel made the external end of the fixture a heat sink. The intent of the assembles design was to passively and advantageously heat the bars by radiation from the tube liner. To insulate the bars from the steel fixture, the bar templates were constructed of a stiff ablative ceramic material which exhibited desirable machinability, stiffness and low thermal conductivity. The template material allowed for several configurations of bar geometry since fabrication of new templates was simple and inexpensive.

The appropriate material attributes of the stationary bars was initially unknown, so several materials were evaluated. **Figure 3.18** is a photograph of the silica glass, carbon graphite, Armalox™ machinable ceramic and aluminum oxide ceramic bars.

Experimental Evaluation Method

The *ex parte* ribbonizer was set-up without the nip roller assembly. A single polyimide powder-coated towpreg was pulled through the experimental apparatus at nominal processing conditions. After several minutes of operation the stationary bar assembly was removed from the tube furnace and allowed to cool. The towpreg was peeled away and the bars were inspected for wear and slag build-up so that the general utility of the material could be established. This was repeated for several different bar types.

Glass stir rod (10 (mm) diameter) was recovered from a chemistry laboratory glass disposal. Two 70 (mm) long rods were polished with a butane torch to provide a smooth surface. The cylindrical glass bars were press fit into bar templates forming a subassembly which was then placed into the stationary bar fixture forming the stationary bar assembly. During a 10 minute experimental ribbonizing interval only minimal slag build-up was accumulated on the bars, however the bar surfaces showed wear. The 400°C processing temperature softened the glass enough so that some fibers cut into the glass surface. Furthermore, the load applied by the towpreg deformed both bars. Residual polymer and fibers, remaining adhered to the glass bars was difficult to remove. By prying slag off the bar surface, glass fragments broke-off. In general, the glass bars provided a smooth ribbon but were not rigid, abrasion resistant nor reusable.

Bulk carbon graphite was machined into two 10 (mm) diameter, 35 (mm) long rods. These rods were press fit into the same templates as the glass rod. After experimental ribbon fabrication, only minimal slag build-up was observed. The carbon bar surfaces were easily rid of residual slag by rubbing with a woven heavy gauge copper fabric. Close inspection of the bar surfaces revealed grooves which had been cut by fibers. This indicated the possibility of graphite deposits on the ribbon surfaces which was considered undesirable. The graphite bars proved sufficiently stiff at high-temperature, smooth and reusable but were not abrasion resistant.

Armalox™ machinable ceramic was milled from a billet, into a modified triangular shape with a 10 (mm) diameter curvature on the top. After machining, the "green" ceramic precursor was fired at 3000°C for 8 hours. This firing process eliminated the

residual liquid in the "green" material and consequently resulted in a porous ceramic bar. Templates were prepared which matched the shape of the bars so that a press fit was not necessary. Two powder-coated towpregs were pulled through the *ex parte* process. During the 2 hour experimental evaluation, clumps of slag broke free about every 5 to 10 minutes, and exited the tube with the towpreg. The "hair balls" caused jamming difficulties at nip roller and occasionally the take-up was stopped to remove the anomaly so that the process could continue. After the experiment was completed the bar assembly was removed and allowed to cool to room temperature. The towpreg was well adhered to the ceramic bar surface and was difficult to remove from the bar. A razor was placed between the towpreg and the bar surface so that the towpreg was pried away. Once the towpreg sample was broken free, the bar surface was observed to have regions where the ceramic chipped away from the surface similar to that observed for the silica glass bars. This was attributed to the mechanical bonding of the polymer to the porous ceramic surface which was inherently weak in tension. The Armalox™ bars were then placed into a 1000°F turbulent convection oven for 3 to 5 hours. The high-temperature cleaned all the polymer and fiber slag away from the ceramic bar surface. The pitted bar surface was sanded with silicone carbide emery cloth. These bars were reusable several times because they could be cleaned. The Armalox™ bars were not ideal because there was considerable surface roughness resulting in "hair balls" and provided a porous surface for bonding with the polymer. The fabrication of these bars was costly and complicated but not necessarily prohibitive.

Greenleaf Inc. makes high density ceramic tool bits for metal milling machines on a regular basis. An improved bar design was sent to Greenleaf where several aluminum

oxide ceramic bars were fabricated at a reasonable cost. Ribbonizing experiments were conducted for several hours. The average time between "hair balls" was on the order of 30 minutes. The "Greenleaf" bars were found to be much denser than the Armalox™ bars and correspondingly were also observed to be more abrasion resistant, less porous and much stronger in tension. At room temperature, the towpreg material was mildly adhered to the bars surfaces and could usually be picked off with fingers. No pitting or abrasion of the bar surfaces was observed. The minor amount of polymer and fiber slag remaining on the tool surface was easily removed in a high-temperature oven. The aluminum oxide bars were superior to the others because they were wear resistant, smooth, reusable and inexpensive.

3.1.3.2   Bar Surface Temperature

The bar surface temperature was of particular interest for process control and modeling. The bars are passively heated by the tube liner and are insulated from the bar fixture by the ceramic templates. Steady state bar surface temperature at several locations were measured with a six inch long Omega™ temperature probe (JMQSS-020G-6) placed onto the bar surface from the exit side of the tube liner. The bars were found to be hottest near the tube liner and coolest near the centerline of the tube. **Figure 3.19** is an illustration indicating the bar surface temperatures measured at several locations for zone settings 475/490/465°C. Note that the measured temperature at location 1 is similar to the temperature at the center of the hottest bar at location 5. The measured temperature at location 1 was therefore assumed to provide a reasonable approximation for the maximum bar surface temperature encountered by the towpreg.

3.1.4 Cool Nip Roller Assembly

The nip roller assembly shown in **Figure 3.20** rotates passively. By nature of the spring-loaded nip, the rollers rotate at a tangential velocity equal to the take up speed of the towpreg. The nip rollers are air cooled to ensure sufficient cooling to solidify the towpreg matrix on contact. The shape of the nip region is designed to facilitate the formation of profiled ribbons. The magnitude of the transverse nip load affected ribbon quality.

The complex heat transfer phenomenon was left for future work, and therefore was not characterized by this analysis. For a given set of processing conditions, if the nip was too close to the tube liner exit plane, insufficient cooling at the nip would occur and the ribbon would exhibit non-uniform cross section. If the nip was too far away (downstream) from the tube liner exit plane, the towpreg was not hot enough to be able to be formed and again the ribbon would exhibit non-uniform cross section. The range of operable distance from the tube liner exit plane was usually between 2 (cm) and 15 (cm).

3.1.4.1   Transverse Nip Load Calibration

The transverse nip load was considered a process variable. A first approximation for the nip load was characterized in terms of the compression of the nip spring. The load was applied to the nip region by compressing the spring which forced the top roller onto the bottom fixed roller. This spring was compressed by turning the load bolt clockwise. The spring was assumed to strain elasticity, and so there existed a

basic relationship between the torque on the load bolt and the transverse nip load. This relationship was linear for a dry friction interface at the load bolt threads.

Special care was taken to ensure the friction between the load bolt threads and the nut fixture threads was uniform. The load cell nut fixture was fitted with a Helicoil™ insert to provide a stiff and smooth thread. The 2 1/2" x 1/2"-21 load bolt was hardened steel with a 3/8" hex-head and 1" shank. The combination of fine bolt threads and hard nut fixture threads provided a good smooth matching surface, increasing the likelihood of a consistent dry friction interface. The head of the bolt was fitted with a polymer washer to reduce the likelihood of substantial friction away from the threads.

The bottom fixed roller and its shaft were removed altogether in order to make room for a compression load cell made by Transducer, Load Cell Inc. (RTL-FF63-CS-50#-8688) The load cell provided approximately 3 (mV V^{-1}) output signal for loads up to 50 lbf. The load cell calibration was conducted with known weights and indicated a sensitivity constant of 0.337 ± 0.001 (lbf mV^{-1}).

The spring was compressed by turning the load bolt, which forced the top roller against a load cell positioned directly below. Break-away torque was measured with an analog Snap-On™ TorqMeter™ (Model TQ 3) with a 3/8" hex-head adapter, at several spring compression settings. The nip loads shown in **Figure 3.21** indicate the linear trend as expected, but also indicated a shift to the right of zero at the origin. This shift was attributed to the friction at the polymer washer. The break-away torque measurements corresponded to the amount of static torque required to start

loosening the nip load, not the dynamic torque indicated on tightening. This measurement technique was biased toward high torque values since the break-away torque also included contributions from static friction between the bolt and washer as well as the static thread friction. Note that both of these contributions were higher than their respective dynamic torque values and therefore this break-away method was more precise than the dynamic method. As long as this technique was used consistently and none of the concerned surfaces abraded significantly, this calibration technique provided a good first approximation for the nip load.

3.1.4.2   Product Release

An advantage to having cooled nip rollers as opposed to heated rollers was that the contact between the hot sticky polymer and the metal rollers did not require release paper. Release papers are generally restricted in maximum use temperatures, precluding their use in high-temperature performance thermoplastic processing.

The release phenomenon of the cooled nip rollers was attributed to the difference in coefficient of thermal expansions of the polymer and the smooth aluminum rollers. The thermoplastic polymer was well above its glass transition temperature when contacted by the nip rollers so adhesion likely occurred. The polymer was constrained by the adhesive bond so that it could not shrink freely on cooling and so, the polymer bond interface retained residual thermal stresses. On cooling and changing phase through Tg, these thermal stresses were substantial enough to sacrifice the adhesive bond, and separation occurred.

3.2   Role of Process Parameters

The primary processing parameters for the *ex parte* ribbonizer are set temperatures, capstan tension, bar contact angle, take-up speed axial nip load. Appropriate settings for these parameters are expected to cause redistribution of the towpregs constituent components to form a uniform consolidated ribbon. The extent to which this redistribution is necessary depends on the initial quality of the towpreg material.

Ribbon quality was defined and analysis were performed, to understand the cause and effect between processing parameters and resulting ribbon quality. Ribbon quality was defined by this analysis in terms the requirements for in situ ATP. General ribbon quality comprised both desirable microstructure and macrostructure attributes. A study by Peltonen *et al.* [1] discussing the role of process parameters on ribbon microstructure was reviewed. Photomicrographic and digital image analysis experiments were performed and discussed, revealing key mechanisms contributing to ribbon wet-out and formation.

3.2.1   Definition of Ribbon Quality

Microstructure is usually characterized by cross section analysis to reveal wet-out, distribution of voids, filaments and matrix. As an initial screening test, microstructure can be indicated by "bending and snapping" a ribbon. A "clean" fracture surface indicates good wet-out, whereas dry, unbroken fibers indicate poorly wet-out ribbon. Macrostructure is often determined by dimensional tolerance, void and fiber volume fraction and composite density. Good macrostructure and good

microstructure are independent and therefore, ribbon quality characterization often considers both.

Ribbon macrostructure can be characterized by measuring cross sectional dimensions and their deviations along the axial direction. A procedure was established to characterize ribbon macrostructure. At or near the end of each ribbon spool, a representative 18 foot long sample is obtained. This sample is evaluated to provide mean width, thickness, and component volume percentages. Each ribbon sample's mass is measured on a balance. Since the ribbon is known to consist of a specific length of carbon fiber, the mass of a similar 18 foot length sample of dry carbon fiber is obtained. This "dry versus wet" method provides the ratio of fiber mass m_f (g) to the total composite ribbon mass m_c (g) and yields the weight fraction, w_f of fiber.

$$w_f = \frac{m_f}{m_c}$$
[3.1]

The theoretical density ρ_{ct} (g cm^{-3}) of the composite material is obtained in terms of the fiber density ρ_f (g cm^{-3}) and polymer matrix density ρ_m (g cm^{-3}) and their weight fractions.

$$\frac{1}{\rho_{ct}} = \frac{w_f}{\rho_f} + \frac{w_m}{\rho_m}$$
[3.2]

The experimental density ρ_{ce} (g cm^{-3}) includes the bubble (void) contributions. The relative density of the 18 foot long sample of ribbon is measured by ASTM D792. Isopropyl alcohol is used as the displacement medium instead of water to take

advantage of its superior wetting. Relative density values (commonly called specific gravity) for void free composites in isopropyl alcohol are corrected to absolute densities. The respective volume fractions of each volume contributing component, V_f, V_m, and V_v for each ribbon sample are therefore known by the following equations.

$$V_f = w_f \frac{\rho_{ce}}{\rho_f} \qquad [3.3]$$

$$V_m = w_m \frac{\rho_{ce}}{\rho_m} \qquad [3.4]$$

$$V_v = \frac{\rho_{ct} - \rho_{ce}}{\rho_{ct}} \qquad [3.5]$$

Width and thickness were measured at 1 foot intervals along each 18 foot long sample. Mean values and standard deviations were calculated. The remnants of each sample were acid digested via ASTM D3171 procedure as a check on the previously explained "dry versus wet" method. Analysis of ribbon macrostructure can be utilized to characterize quality and therefore indicate process control.

3.2.2 Process Parameter Cause and Effect

The process parameters (left column of **Table 3.1**) categorized in association with their hardware systems (bold) were evaluated in terms of some of the more important effects (top row of **Table 3.1**) which contribute to the fabrication of good quality ribbon. A cause and effect relationship between variations of these parameters and

ribbon quality is indicated by a check mark. Most of these parameters were observed to be interdependent. The qualitative cause and effect relationships were observed and noted in this table because they provided a general basis for subsequent heat transfer and pulling force modeling.

Table 3.1 *Ex parte* **Process Parameters Affecting Towpreg Ribbon Quality**

	Towpreg Spread Width	Towpreg Wet-out (impregnation)	Towpreg Surface Abrasion	Ribbon Shaping
Material Handling System	√	√	√	√
Towpreg Alignment	√	√	√	√
Capstan Tension	√	√	√	√
Take-up Speed				√
Premelting Chamber	√	√	√	√
Zone Set Temperatures	√	√	√	√
Bar Surface Temperature	√	√	√	√
Stationary Bar Assembly	√	√	√	√
Bar Diameter	√	√	√	√
Centerline Angle	√	√	√	√
Centerline Distance	√	√	√	√
Contact Angle	√	√	√	√
Number of Bars		√	√	√
Cool Nip Roller Assembly				√
Transverse Nip Load				√
Cooling Air Flow Rate				√
Distance From Tube Exit				√

† Passively Controlled by Zone #3 Set Temperature and Other Processing Conditions.

Ribbon microstructure is most often characterized in qualitative terms. Good microstructure implies full wet-out and even distribution of the filaments and matrix. Poor microstructure implies incomplete wet-out, uneven distribution and excessive void content. Cross section analysis of the ribbon reveals the microstructure. A detailed study of the influence of melt impregnation processing parameters on the degree of impregnation of a poly (propylene)/glass fiber prepreg [1] was conducted by

Peltonen *et al.* Their quantitative observations were similar to observations of the stationary bar assembly of the *ex parte* ribbonizing process and therefore, this section discusses their results in detail.

A cross-head extrusion/pultrusion impregnation chamber with one of two adjacent modular pin consolidation assemblies was used to impregnate glass fiber roving with high molecular weight polypropylene. The bench scale apparatus was similar to that described by Moyer [2] and to a lesser extent by Courtney [3] and Hashizume [4]. The key feature of the process studied by Peltonen *et al.* was the pin consolidation assembly which was similar to the stationary bar assembly of the *ex parte* process. In the normal configuration, glass fiber tow was pulled through a cross-head extruder so that an annular film of molten polymer was applied around the bundle. To wet-out the fiber roving, the prepreg was drawn through several sets of parallel pins. On exiting the chamber, the towpreg was drawn through a "shaping nozzle".

Analysis of the Peltonen *et al.* Study

The microscopic analysis provided useful data to Peltonen *et al.* regarding the role of the process control parameters on the degree of impregnation (D_{imp}) of the resulting ribbon, measured by a cross section photographic analysis technique. As an approximation, D_{imp} was defined as the number of wet-out fiber ends divided by the total number of fibers in the cross section. The cross section area void percent or void content was $(1-D_{imp})$. Processing parameters were varied from low settings to high settings so that the roles of temperature, tension, speed, contact length and hydrostatic polymer melt pressure, could be characterized quantitatively.

Table 3.2 is a list of the process parameter values and corresponding experimental D_{imp} values. For temperature, contact length and back tension, the D_{imp} increased asymptotically from 70% to a maximum value approaching 95%. For increasing pulling speed and hydrostatic extrusion pressure the D_{imp} reduced asymptotically over a similar range. Several key observations were discussed regarding each experiment.

Table 3.2   Partial List of Peltonen et al. Experimental Results

Parameter	Low Setting	D_{imp}	High Setting	D_{imp}
Length of Contact Surface (mm)	3	62%	17	94%
Resin Temperature (°C)	180	71%	230	90%
Pay-out Back Tension (N)	0	75%	60	91%
Pulling Speed (cm/s)	0.7	92%	8.6	75%
Polymer Gage Pressure (bars)	0	92%	11	71%

Every pin was 4mm in diameter and the distance between pin pairs was 5mm. The pin pairs were rotated so that the contact angle was increased and correspondingly the contact length was increased from a minimum (3mm) to a maximum (18mm) causing an increase in D_{imp} from 61% to 94%. This identified several important points. After impregnation in the cross-head die and prior to contact with any consolidation pins, the towpreg exhibited area void content of at least 38% , and was probably resin rich around the fiber bundles periphery. Also, increasing the contact length provided a substantial (over 30%) improvement in wet-out. This same contact length of 18mm could have been achieved by increasing the diameter of the pins

rather than by rotating the pin pair assemblies. Note that it is unlikely that the same increase in D_{imp} would have been achieved by increasing the pin diameters.

Two approaches to increase melt temperature were utilized. By the first method, an antioxidant was added to the polypropylene at 0.2 weight percent so that the extruder temperature could be increased. As expected, D_{imp} increased with increasing temperature due to the corresponding decrease in melt viscosity. In the second method, the pins inside the consolidation chamber were actively heated from 210°C up to 300°C, yielding only modest improvements in D_{imp} which were within statistical deviation of the measurements.

The pulling force was measured by monitoring the calibrated input current for the "haul off" motor. The pay-out (back) tension was provided by a resistance friction braking mechanism on the fiber spool. As expected, when the back tension was increased, the wet out increased. There was no mention of spreading or damage to the towpreg as a result of increased tension. An important observation was that under a back tension of zero, the authors noted a drag force of 37 (N) which was attributed to the frictional drag between the prepreg and the stationary pins. No further analysis of the pulling force was indicated.

With this processing analysis, the difficulty of melt flow wet-out was clearly illustrated. The cross-head impregnation did not wet-out the bundle. The best consolidation was achieved by processing at slow speed, the highest allowable temperature, low extruder pressure, high contact length (or contact angle) and high pretension braking force. These observations (with the exception of the impregnation

pressure) were consistent with those observed for the *ex parte* ribbonizer process.

3.3   *Ex parte* Ribbonization Flow Mechanism Study

The goal of this study is to understand the redistribution and polymer flow mechanisms and their significance to forming good ribbon. The *ex parte* ribbonizing process consists of two critical and sequential steps involving first, the heated stationary bar assembly and second, the cool nip roller assembly. The first facilitates melt flow while the latter results in ribbon forming. Towpreg microstructure changes resulting from the ribbonizing process were studied to understand the intraply consolidation flow mechanisms.

Consolidation of the towpreg is expected to involve six sequential mechanisms. The first three result from contact with the stationary bars. Composite squeeze-flow spreads the towpreg into a wide, flat band causing 1) gas bubble (void) redistribution, 2) transverse, permeative melt flow (general wet-out) and 3) filament alignment. On contact with the cool nip roller assembly, the towpreg undergoes 4) residual void compression, 5) elastic compaction of the filament network and 6) net axial cross section shaping. The relative importance of each of these mechanisms depends on material properties, process conditions and towpreg quality.

The approach was to prepare towpreg samples exhibiting various degrees of intraply consolidation and observe redistribution patterns in the axial cross sections which would agree with an expected interply consolidation mechanisms. The samples were cross-sectioned at locations along the fiber direction corresponding to the contacts

with the hot stationary bars and the cooled nip. The microstructural changes observed between sample layers were assumed to mimic those encountered in real-time ribbon fabrication. The expected consolidation mechanisms were reasonably validated by this study.

3.3.1 Experimental Sample Preparation

The *ex parte* ribbonizing process was set-up and operated at steady state for several minutes. Once the process exhibited nominal steady state production, the take-up motor and tube furnace were turned off. The towpreg, still under tension, cooled below the polymer's Tg, usually over a 20 to 35 minute interval. Next, the solidified towpreg sample, still adhered to the stationary bar surfaces, was peeled away and preserved. This sample was assumed to represent the steady state at a moment frozen in time. The sample was then potted in a transparent epoxy compound. The solidified potted sample was then cut and polished so that axial cross sections could be inspected. Several layers were evaluated to characterize the changes in microstructure resultant from contact with the stationary bars and nip rollers. **Figure 3.22** illustrates a towpreg sample at the bar assembly and indicates the nominal cross section layer locations A through I. This diagram is used as a locator key for the following analyses.

3.3.2 Qualitative Photomicrographic Characterization

A Reichert™MeF3 metallograph was used to obtain black and white Polaroid™ photos of each cross section. Several adjacent photographs were digitized to gray scale with

an Epson™ color scanner and a Macintosh™ Quadra 800. The adjacent images were combined to form a collage with an Adobe Photoshop® application.

Sample #062194A and #062194B Photomicrographs

[12K IM-7™ / LaRC™-IAX (4% offset stoichiometry) polyimide powder]

Powder towpreg was fabricated by the powder curtain process [5] at NASA Langley Research Center. The towpreg exhibited excellent distribution of powder within the filament array. A sample consisting of two towpregs was prepared, and was later cut in half to form samples #062194A and B. **Figure 3.23** organizes several sequential cross section photomicrograph collages which indicate the transformation of the towpreg from a circular cross section to a wide and flat cross section. Photograph I was located about 2 (cm) prior to the first bar contact and photograph V corresponded to the location just prior to contact with the first bar surface. Photographs II, III and IV were equally spaced between I and V. **Figure 3.24** is another series of photographs indicating the spreading which occurred as a result of contact with the bar surfaces. This high quality towpreg resulted in a high quality ribbon.

Sample #101893 Photomicrographs

[12K IM-7™ / Aurum™-400A polyimide powder]

A slurry impregnation process was utilized to fabricate a powder towpreg exhibiting poor powder distribution; consequently, on melting in the heated section of the *ex*

parte ribbonizer, complete wet-out was not achieved. Again, two towpregs were utilized to prepare a sample, with back tension set reasonably low. At 10 (N) back tension for each of the two 12K towpregs, minimal spreading occurred. A sample was prepared and several cross sections were photographed. The dark regions in the middle of layers F and G of **Figure 3.25** are not voids but rather are ends of fiberglass filaments which serve as a flag. Note the decreasing void content from layer B to C as air bubbles appear to be expelled. Layers D and E correspond to the locations between the bars where an apparent enlargement of gas bubbles is observed. Note that the perspective angle is different for each photograph and therefore the images do not reflect the true axial cross sections. The contact with the second bar at F and G appears to substantially reduce the bubble size. After exiting the last bar, the malleable towpreg assumes an unrestrained microstructure depicted in layer I. To the left of center in layer I, an area exists that was incompletely wet-out. To the right of center, several gas bubbles appear substantially larger than those observed in layers F and G. Furthermore, most of the bubbles in Layer I appear to reside near the center of the cross section.

Sample # 072594 Photomicrographs

[12K IM-7™ / PIXA™ polyimide powder]

Poor quality towpreg was fabricated by a slurry impregnation process. Here, a sample was prepared with a single towpreg, under low back tension 5 (N). **Figure 3.26** depicts the changing microstructure for a towpreg of exceptionally poor powder distribution as evidenced by layer A where most of the polymer is on the top surface of

the fiber bundle. As this towpreg contacts the first bar surface (layers B, C and D), very little wet-out or spreading is apparent. In contrast, substantial spreading occurs during contact with the second bar surface (layers F, G and H). Just downstream from the bar surface, the towpreg has substantial void content, most of which is attributed to the poor quality of the poorly wet-out towpreg.

Nipped Ribbon Sample Photomicrographs

[Various Material Systems]

Figure 3.27 illustrates three characteristic ribbon cross section shapes formed by the present embodiment of the *ex parte* ribbonizing process. The shape of the resulting ribbon depends primarily on towpreg spread width at the bar contact. The cross section labeled A is a photomicrograph of a ribbon made from material similar to sample #072594 (**Figure 3.26**) which was spread too wide at the bar contacts in an attempt to facilitate wet-out of the poor quality towpreg. The groove width in the nip rollers was narrower than the towpreg spread width. The cross sections labeled B resulted from process conditions similar to those described in the preparation of sample #101893 (**Figure 3.25**), where just the right amount of bar spreading occurred. Note that the apparent void content of layer I in **Figure 3.25** is greater than that of ribbon B in **Figure 3.27**, indicating bubble compression. Also, note the substantial change in the cross section geometry which resulted from nip contact, implying some elastic compression of the filament network. The anomaly at either end of the ribbon cross section is attributed to squeeze-by between the sides of the tongue and groove of the nip rollers. Cross sections labeled C resulted from towpreg

similar to that shown in sample #062194A and B (**Figures 3.23 and 3.24**) with insufficient spreading.

3.3.3 Quantitative Digital Image Characterization

The potted and polished sample was transferred to an OLYMPUS™ CUE 2 Image Analyzer which utilized an OLYMPUS™ BH-2-UMA optical microscope and a personal computer operated with OLYMPUS™ Planomorphometry Software 3.0. A quantitative description of the distribution of the samples' constituent components was obtained. Each image was digitized into pixels of various shade. Filaments, matrix polymer, voids and the potting epoxy were each clearly distinguishable because each reflected incident light differently. Sub-areas of the cross section could be selected and analyzed based on threshold segregation of the digitized image.

Perspective Angle Measurement by Digital Image Analysis

Filament ends were assumed circular in axial cross section. **Figure 3.28** illustrates the perspective angle where the non-axial measured areas could be corrected by the geometry. A portion of the cross section layer with several isolated filament ends was magnified 2000X and then digitized. The maximum diameter (D_{max}) and minimum diameter (D_{min}) of each selected, oval-shaped image was measured by the analysis program. The average of the maximums and average of the minimums were utilized to calculate the perspective angle.

$$\text{Perspective Angle} = \tan^{-1}\left(\frac{D_{min}}{\sqrt{D_{max}^2 - D_{min}^2}}\right) \qquad [3.6]$$

It is important to note that these maximum and minimum diameters were not necessarily vertical or horizontal relative to the sample but rather the oval shapes were observed to be slightly skewed to one side. This skew suggested some misalignment, out of the plane of interest, and therefore the perspective angle did not reflect the true perspective relative to the axial direction. Although the perspective angle approximation was not ideal, the application was consistently utilized for all layers and so the relative trend was valid.

Total Composite Area Measurement by Digital Image Analysis

Magnification by 50X was required to obtain sufficient detail of the cross section perimeter. The sub area of the digitized image which contained the total cross section was selected by tracing the border and measuring the enclosed area. These total area measurements included some of the potting epoxy for poorly wet-out regions. This was considered reasonable since the total area was intended to represent the bulky towpreg including "voids". Care was taken to exclude from the analysis bubbles on the sample surface which clearly resulted from the potting process.

Void Area Measurement Technique by Digital Image Analysis

Magnification by 100X was necessary to distinguish void regions. The voids were darker than the potting epoxy, the matrix polymer and the filaments which were

respectively brighter. The perimeter of the towpreg section was outlined and isolated as a subsection. By adjusting the thresholding function, only the voids were highlighted and the software counted the calibrated pixels and provided the void area.

Sample #101893 Digital Image Analysis

[12K IM-7™ / Aurum™-400A polyimide powder]

The perspective angle axial total composite area, and axial void area were determined for several cross section layers. The nominal location of each layer was determined by visual comparison with sample length measurements made prior to potting. **Figure 3.29** is a plot of the area data obtained for sample #101893 after being corrected for the axial perspective. **Figure 3.30** is the corresponding plot of area void percent for the same sample. Note that there appeared to be a substantial void content reduction and recovery for both bar contacts.

Sample #072594 Digital Image Analysis

[12K IM-7™ / PIXA™ polyimide powder]

Sample #072594 was prepared with one half the back tension of the previous sample #101893. The perspective angle, axial total composite area and axial void area were again determined for several cross section layers. **Figure 3.31** is a plot of the measurements obtained for sample #072594 and corrected to the axial perspective. **Figure 3.32** is the corresponding plot of area void percent. Note the appearance of a

substantial void content reduction at both bar contacts but only a void recovery at for the second bar contact.

3.3.4 Preheating Region Discussion

The preheating region provides a means to heat the towpreg prior to contact with the bar surfaces. Some wetting and void reduction occurs simply by liquefying the polymer and was primarily dependent on the quality of the towpreg. Good quality towpreg exhibits even distribution of powder throughout the entire cross section of the towpreg. Poor towpreg is usually polymer deficient near the center and polymer rich near the surface and on melting, the towpreg exhibits high void content. Here, "void content" comprises two types of undesirable attributes, (1) incomplete filament wet-out and (2) entrapped gas bubbles.

During preheating, the towpreg assumes a nominally cylindrical cross section shape. This effect is attributed to two mechanisms, wetting and a filament catenary effect. Wetting by the viscous liquid onto the filaments tends to promote a symmetrical shape which minimizes the liquid surface area, and therefore, a circular cross section is favored. The towpreg catenary effect arises because only some of the fibers carry the tensile load. Most filaments are simply constrained by the load carrying filaments and the distribution of these non-load bearing filaments is uniform about the filaments in tension.

Preheating alone of good quality towpreg results in nearly void-free intra-tow microstructure. Preheating of poor to moderate quality towpreg usually results in

only partial wet-out of the intra-tow region. Substantial cross section area void contents of 55% to 40% are common for poor to moderate quality towpreg, respectively.

3.3.5 Stationary Bar Contact Region Discussion

On contact with the stationary bars, filament wetting, towpreg spreading, bubble expulsion and bubble compression are observed. The cross section wet-out appears to improve as a result of contact with the stationary bars. Since permeative flow is time dependent and the viscosity of high molecular weight polyimide thermoplastics is very high, wet-out by transverse permeative flow is unlikely. The time interval over which the bar contact occurs is on the order of 0.01 to 0.05 seconds, corresponding to sample preparation time intervals greater than 20 minutes. Consequently, only moderate improvements in wet-out are expected at normal processing speeds. To achieve full wet-out of poor quality towpreg, prohibitively slow processing speeds are required.

Gas bubbles appear uniformly sized throughout each cross section layer but are smaller for layers near the center of the bar contacts and larger for layers near the tangent points. Gas bubbles appear to be both expelled near the surfaces and compressed near the middle of the cross section. After exiting the bar surfaces, the residual gas bubbles are generally distributed near the center of the towpreg and larger in diameter. This bubble reduction, compression and recovery phenomenon is observed to be repetitive and diminishing on successive bar contacts.

The mechanism for void expulsion is expected to be driven by the thinning cross section rather than bubble flow. On spreading, the viscous composite is effectively moved away from the bubbles. The time dependence for this squeeze flow is dependent on the viscosity of the composite mixture and the forces applied. Towpreg spreading at the bar contact is routinely observed for nominal processing speeds. Consequently, substantial bubble reduction near the towpreg surfaces is expected, even at time intervals associated with nominal processing speeds.

The rate determining step for ribbonizing poor quality towpreg is the transverse permeative flow mechanism. The rate determining step for ribbonizing good quality towpreg is the squeeze flow spreading mechanism allowing release of entrapped gas bubbles. The time duration required for the latter is usually very short and therefore, it is desirable to ribbonize good quality towpreg.

3.3.6 Nip Region Discussion

The towpreg does not become a fully consolidated ribbon until after it passes through the nip region. The role of the nip roller assembly is to consolidate and shape the malleable towpreg into a uniform cross section ribbon. The primary functions are to compress residual air bubbles and shape the macrostructure thus presenting an apparently uniform composite ribbon.

Since the nip rollers are cooled, the malleable towpreg undergoes substantial cooling on contact with the nip. Due to the short contact time interval and the processing conditions, the surface of the towpreg, which becomes the surface of the ribbon,

usually cools below Tg while interior sections remain warmer. An objective during ribbon fabrication is to cool the entire cross section below Tg on contact with the nip region. This constraint allows little time for squeeze flow and so only moderate surface shaping and interior bubble compression can possibly be achieved before the composite solidifies.

Depending on the processing conditions, the size and shape of the malleable towpreg cross section can vary. For poorly wet-out towpreg, the tendency is to spread as much as possible to attempt to improve wet-out. In contrast, for well wet-out towpreg the tendency is to spread the towpreg to exactly the same width as the size of the groove in the nip region. When the towpreg is spread wider than the size of the nip groove, the resulting ribbon is usually thicker on one side of the cross section than the other. This non-uniformity is considered undesirable. When the towpreg is not sufficiently spread, the cross section is usually thicker than desired.

3.4   Characterization Summary and Conclusions

The *ex parte* ribbonizing process was characterized in terms of hardware descriptions and calibration. The material handling system is of simple construction and provides a means by which to pull the towpreg through the premelting chamber, stationary bar assembly and nip assembly, while maintaining uniform and substantial back tension. The premelting chamber is characterized in terms of heat-up time and steady state temperature profile analysis. The stationary bar assembly is built of abrasion resistant and reusable materials and contains the necessary attributes to be heated passively by the premelting chamber and to serve as a fixed tool, against which melt

consolidation of the towpreg occurred. The cool nip roller assembly is of rigorous construction and provides calibrated transverse nip load and appropriate product release to facilitate ribbon formation. The role of process parameters was discussed in terms of macro- and microstructural ribbon quality attributes. A flow mechanism study was performed to understand the redistribution of the towpregs constituent components occurring at the stationary bar assembly and the nip assembly.

Hardware Description and Calibration

The material handling system control parameters: capstan tension (5 to 20 (N)) and pulling speed (0 to 50 (cm s^{-1})), are variable by analog setting. The premelting chamber control variables comprise three zone set temperatures. The tube liner heat-up time to the steady state tube liner surface temperature profile is less than 1 hour. The stationary bar assembly control parameter constitutes the bar subassembly geometry . The bars are passively heated by the steel tube liner of the premelting chamber. The cool nip roller control parameter is transverse nip load.

Role of Process Parameters

All of the process control parameters affect ribbon quality to some extent. Ribbon quality is defined to include low void content and uniform cross sectional shape. Modeling is necessary to understand the specific contribution of each parameter.

Ex parte Ribbonization Flow Mechanism Study

The microstructure analysis of the samples cross sections revealed key phenomena encountered by the towpreg which were consistent with the six expected mechanisms: gas bubble (void) redistribution, transverse, permeative melt flow (general wet-out) and filament alignment, residual void compression, elastic compaction of the filament network and net axial cross section shaping. The cylindrical symmetry during preheating is attributed to "towpreg catenary effect". Spreading at the bar contacts is attributed to composite squeeze flow.

As a consequence of contact with the stationary bars, gas bubbles near the towpreg outer surface are expelled. Bubbles not close to the surface do not escape but appear to compress and re-expand. After exiting the last bar contact, the towpreg cross section is generally wide and flat but usually contains some gas bubbles near the center plane. Since permeative melt flow wet-out of viscous polymer melts requires substantial residence time and the bar contacts occurr over such short time intervals, only limited transverse flow wet-out is expected to occur at normal processing speeds. Filament alignment is implicitly observed by the towpreg band spreading and the uniformity of the perspective angles measured for each cross section layer. On contact with the nip rollers, voidy towpreg is formed into lower void content ribbon by sequentially compressing the voids and solidifying the polymer. Elastic compaction of the filament network is implicit by observing the formation of a profiled cross section.

The towpreg "void content" comprises two components, incompletely wet-out regions and gas bubbles. Fabrication of void free towpreg ribbon is observed to be dependent

and gas bubbles. Fabrication of void free towpreg ribbon is observed to be dependent on the initial quality of the powder towpreg. In general, the even distribution of the powder, throughout the towpreg cross section results in ribbon with even wet-out. The key to forming good ribbon microstructure is to maximize wet-out and minimize entrapped gas bubbles. To reduce the volume of compressed gasses, it is recommended that the towpreg band be spread as wide and thin as possible. The limitation to the spreading occurred downstream of the bars, at the nip region where excessive spreading causes undesirable overlapped macrostructure. The key to good macrostructure is to optimize bar spread width to be nearly identical to the desired ribbon width.

3.5   End Notes

1   Peltonen, P.; Lahteenkorva, K.; Paakkonen, E.J.; Jarvela, P.K.; Tormala, P. *J. Thermopl. Comp. Mat.*, 1992, 5, 318-43.

2   Moyer, R.L. U.S. Patent 3 993 726, 1976.

3   Courtney, A.L. U.S. Patent 3 249 484, 1966.

4   Hashizume, S. Japanese Patent 405 050 432, 1993.

5   Baucom, R.M.; Marchello, J.M. *SAMPE Series*, **1993** *38*, 1902-.

3.6   Chapter 3 Figures
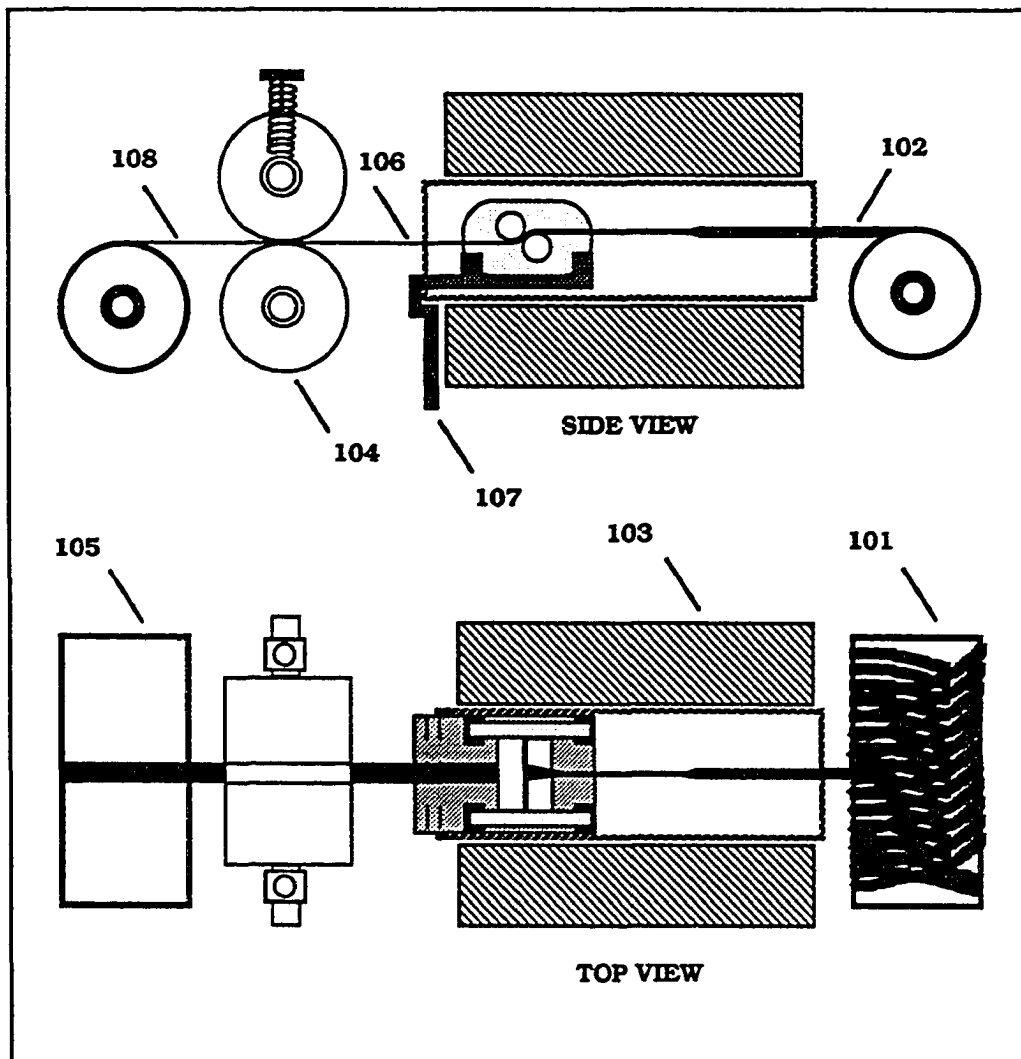
Figure 3.1 Illustration of the *Ex parte* Ribbonizer Apparatus
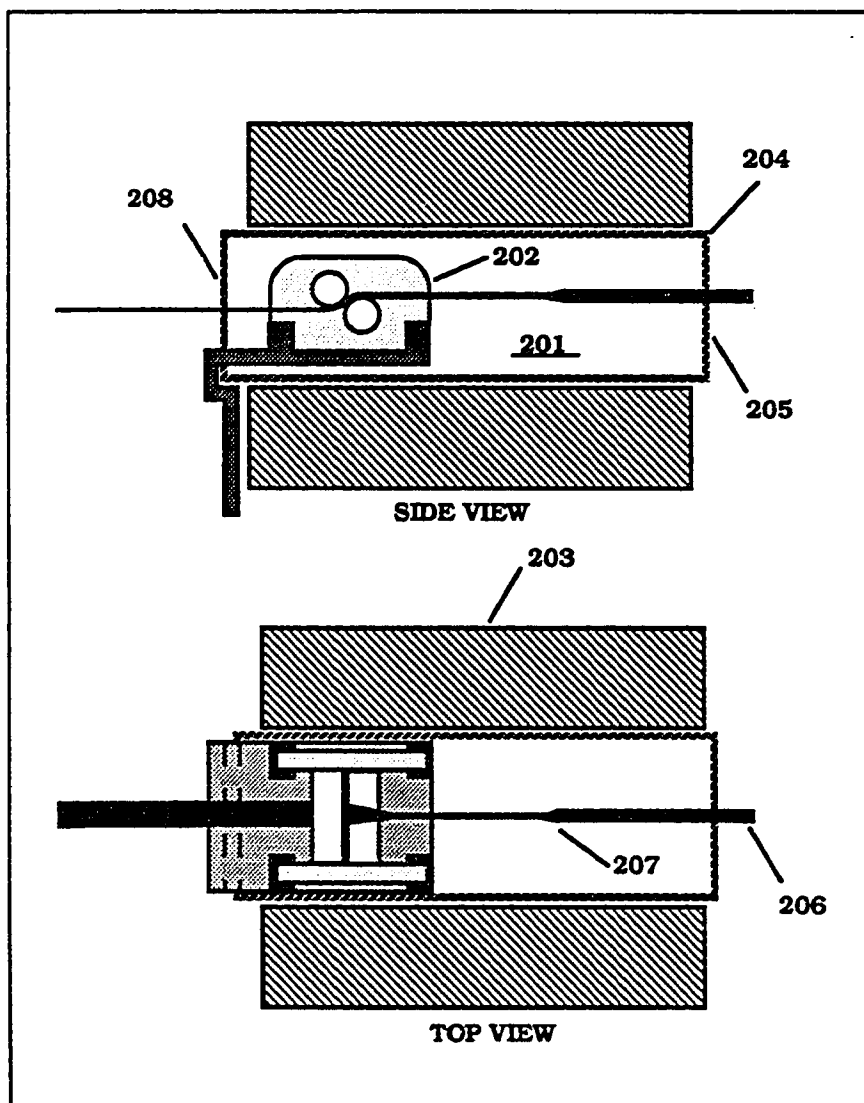
Figure 3.2 Illustration of the Premelting Chamber and Stationary Bar Assembly
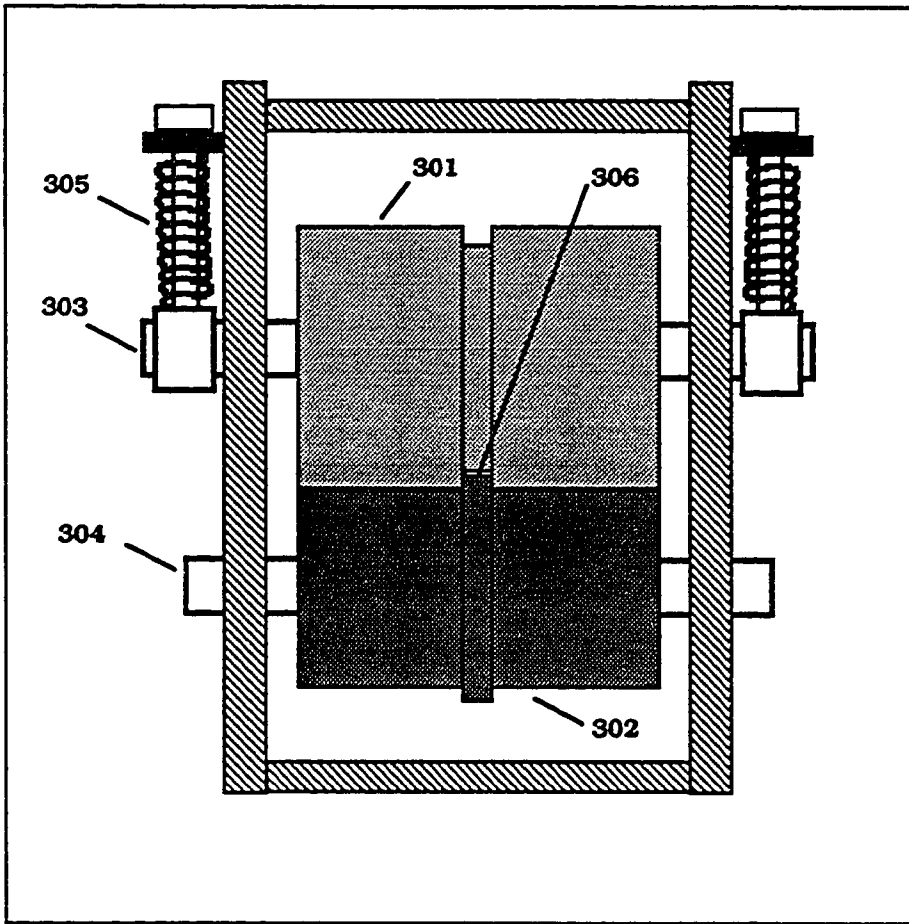
Figure 3.3 Front View Illustration of the Nip Roller Assembly
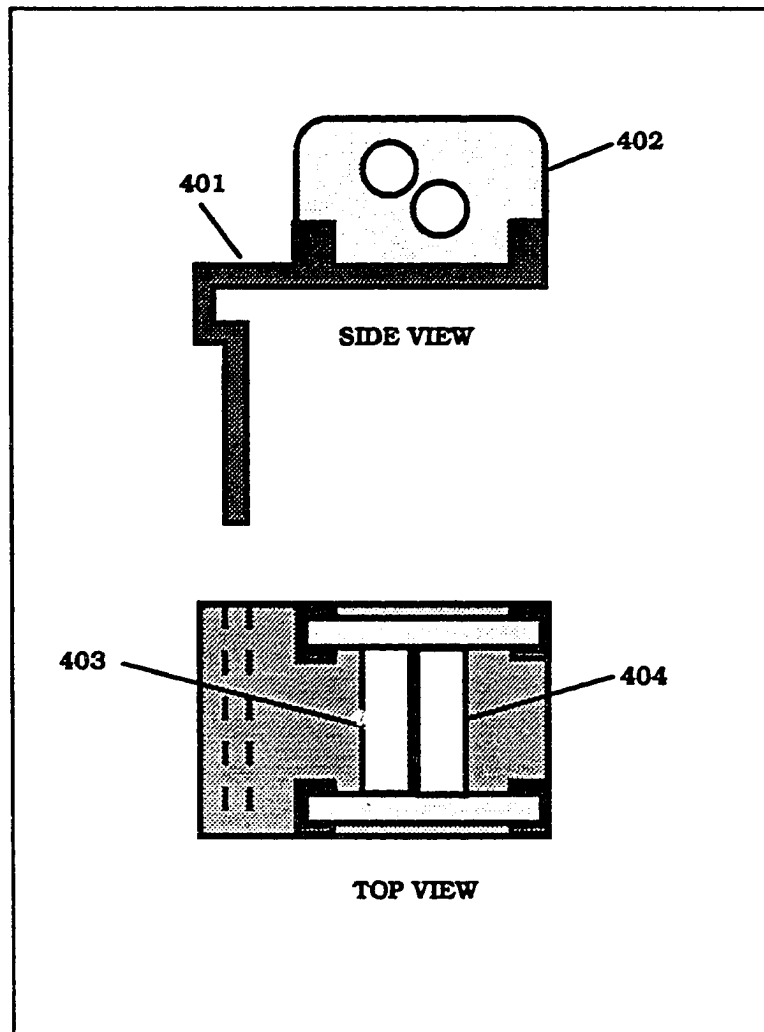
Figure 3.4. Illustration of the Stationary Bar Assembly
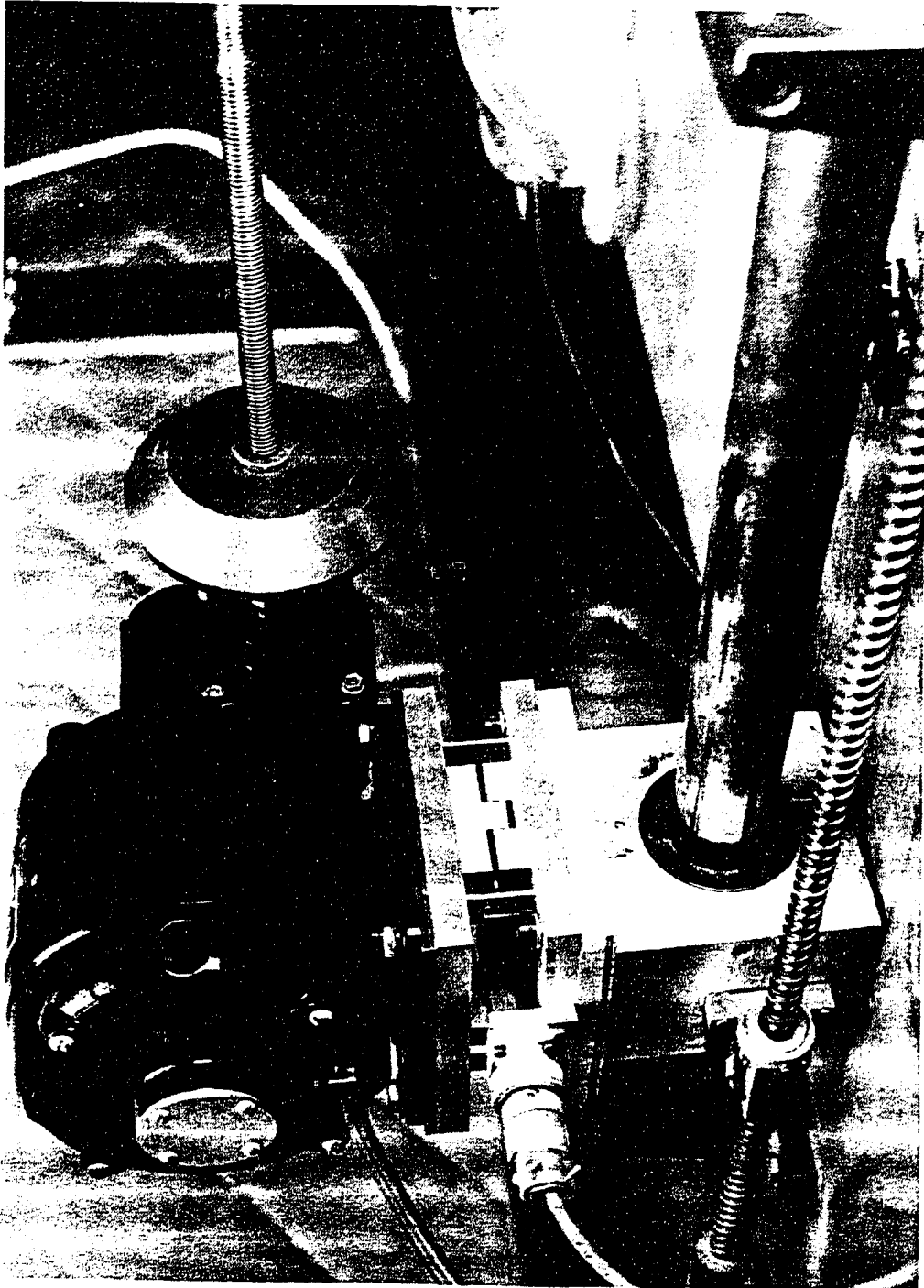
Figure 3.5   Ribbon Take-up Photograph
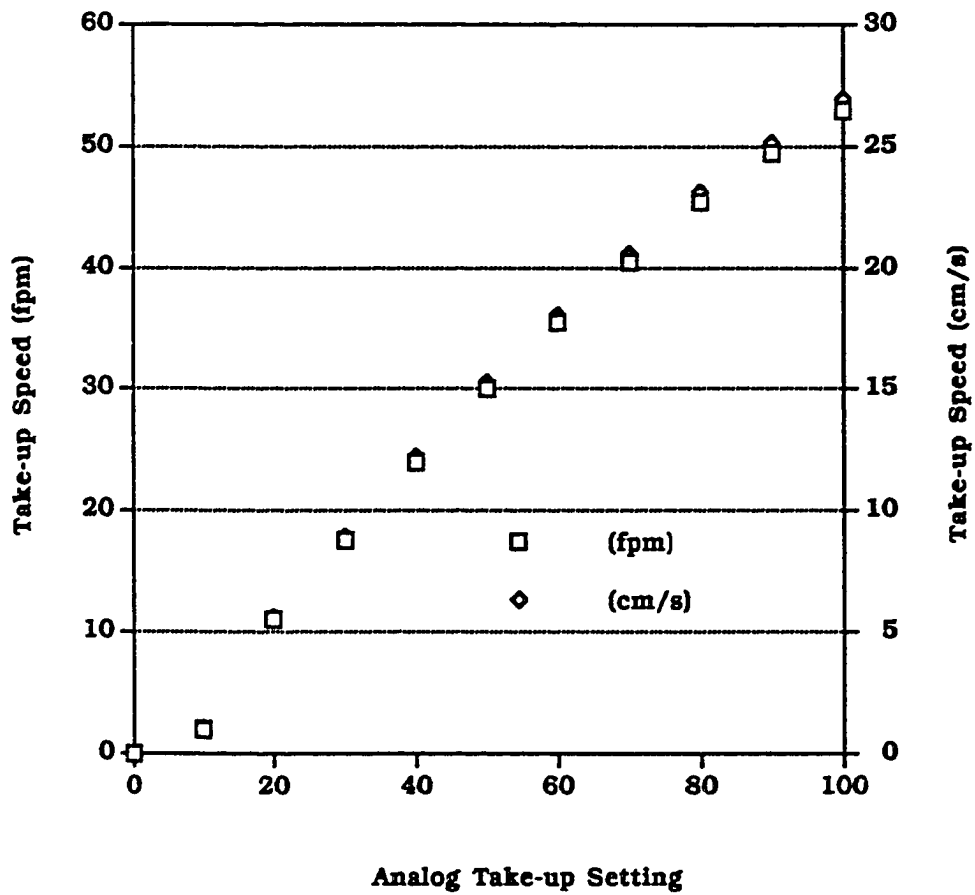
Figure 3.6 Take-up Speed Calibration Plot

Figure 3.7 Creel Rack Photograph
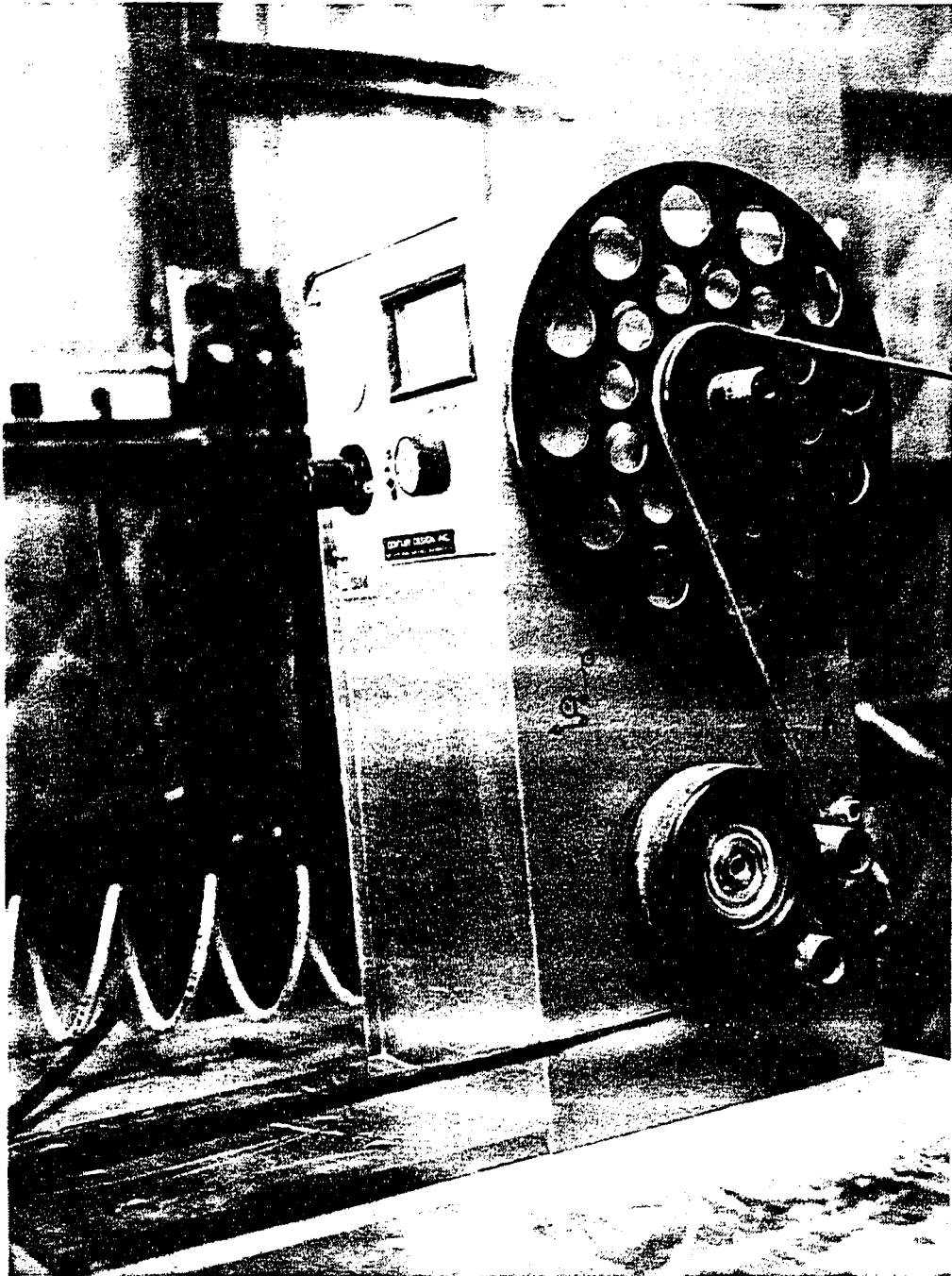
Figure 3.8   Tensioning Capstan Photograph
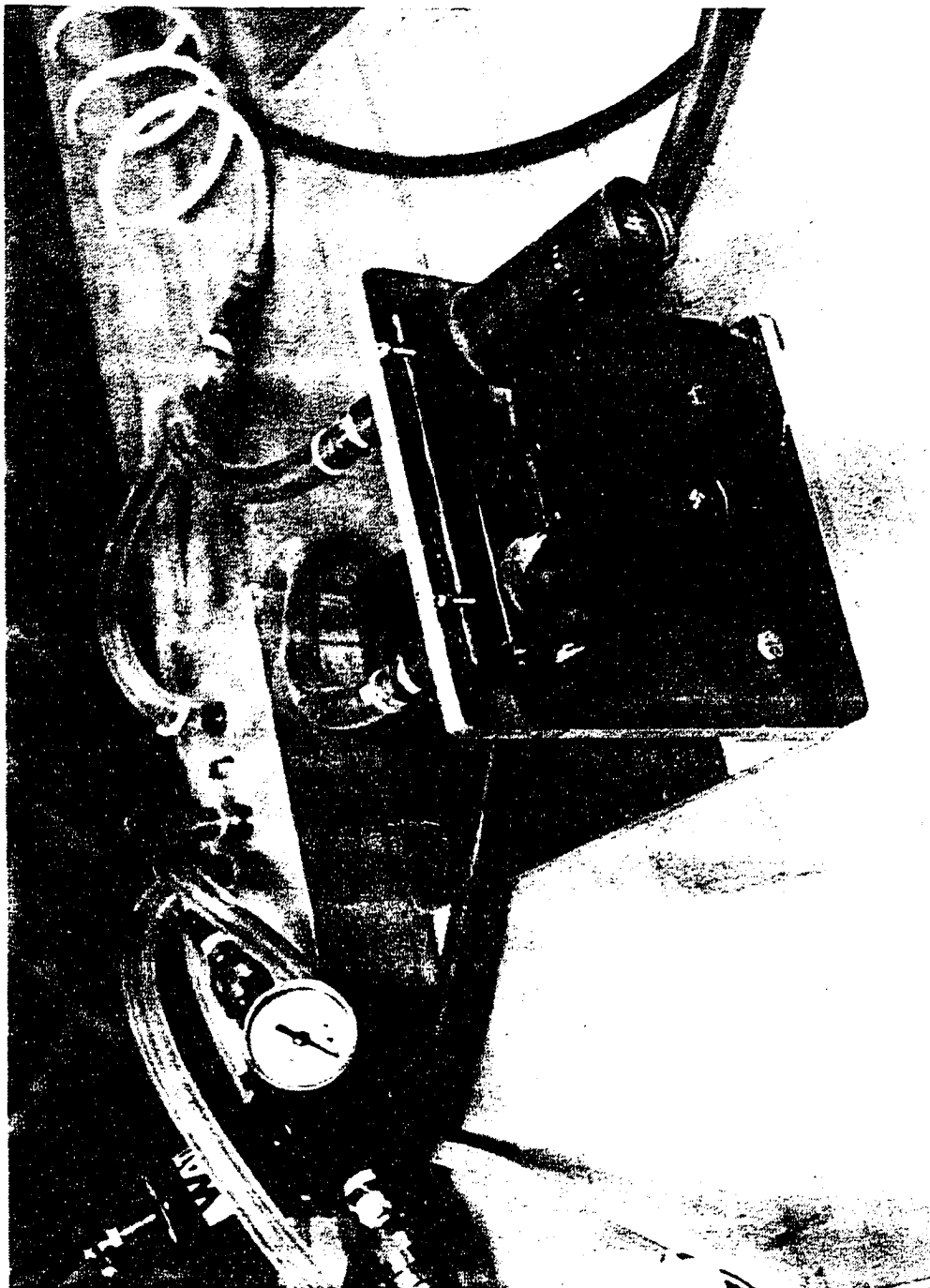
Figure 3.9   Alignment Roller Assembly Photograph
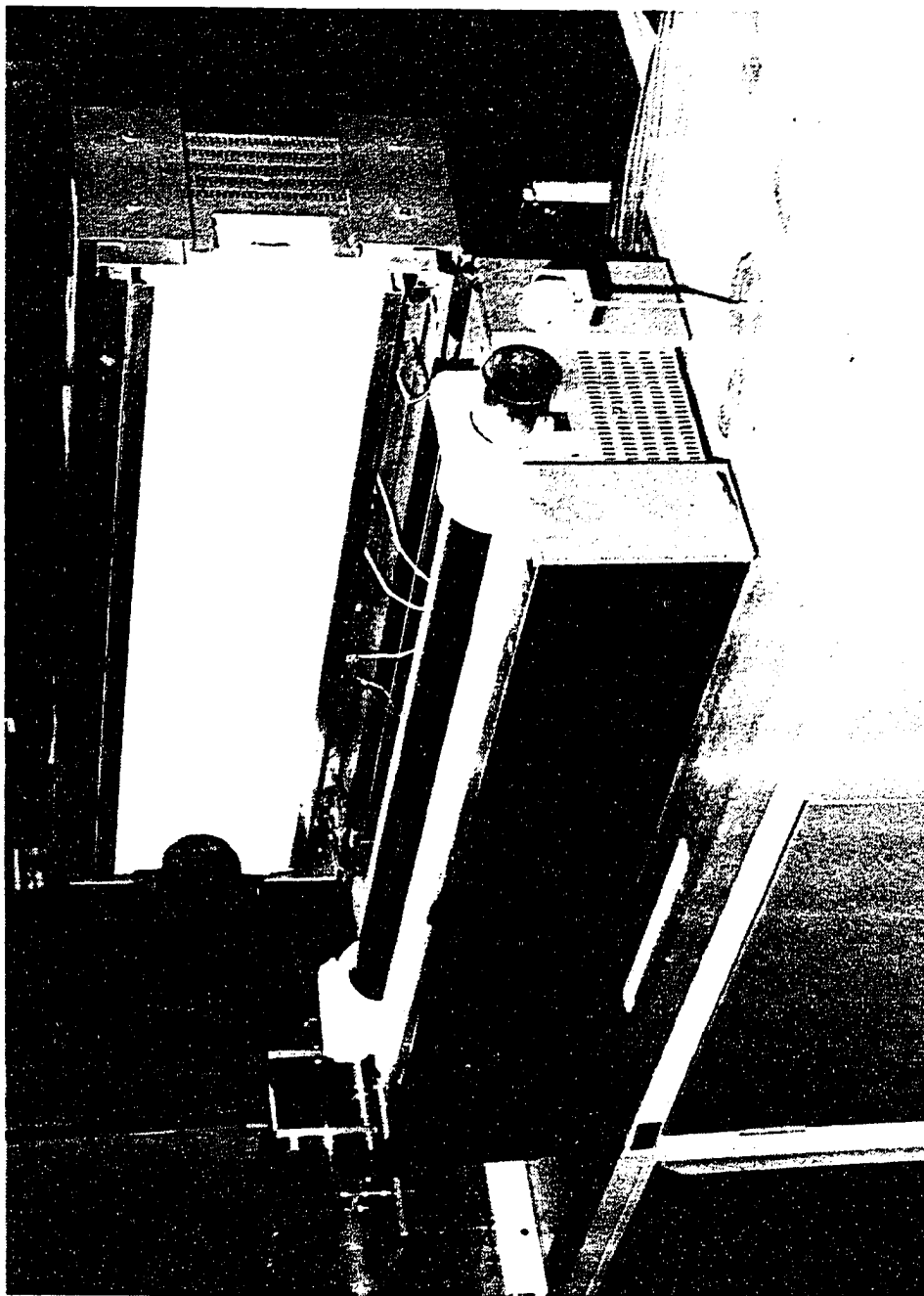
Figure 3.10 Tube Furnace Photograph
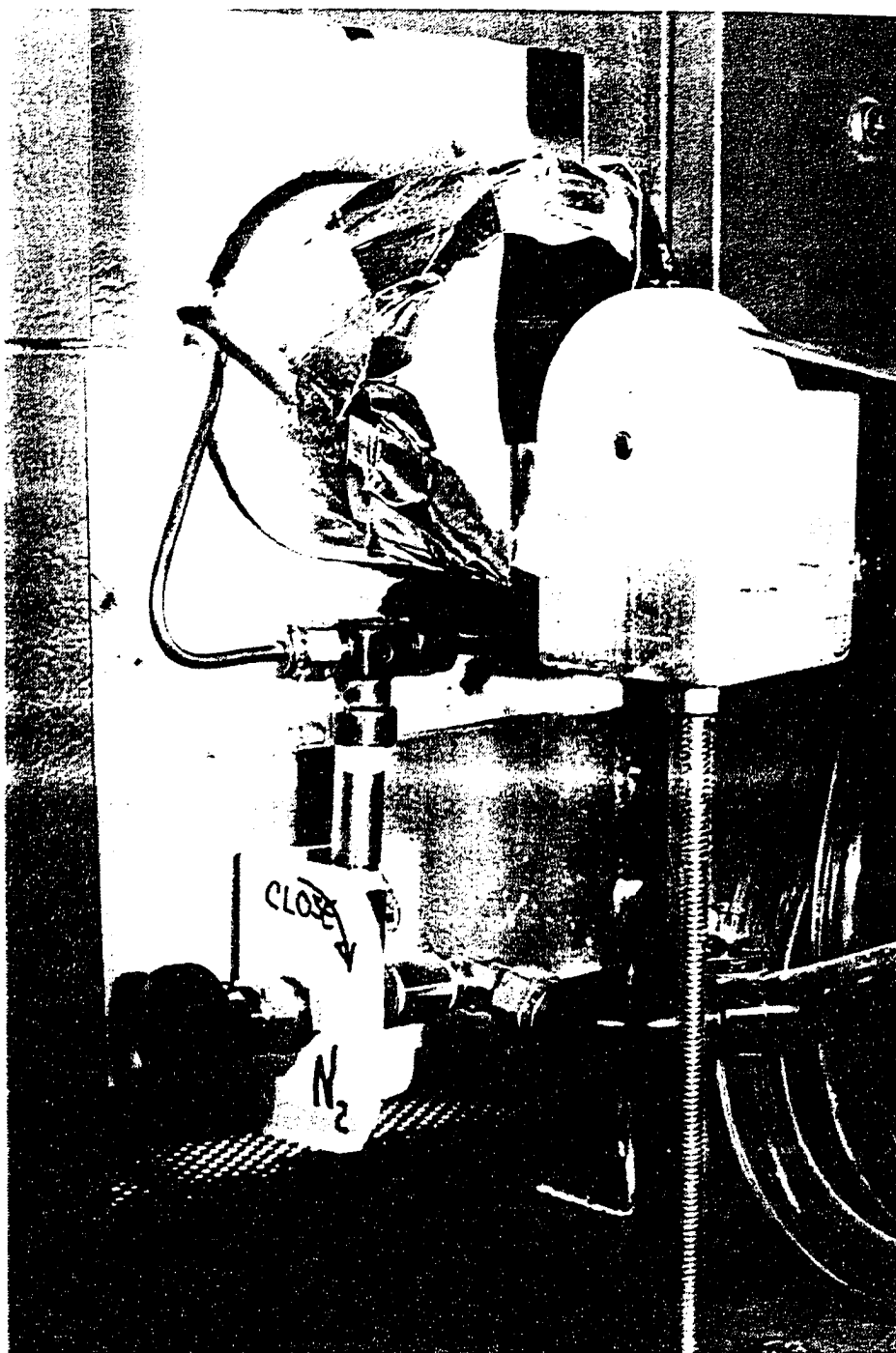
Figure 3.11   Nitrogen Bleed Assembly Photograph

Figure 3.12 Thermocouple Probe Assembly Photograph
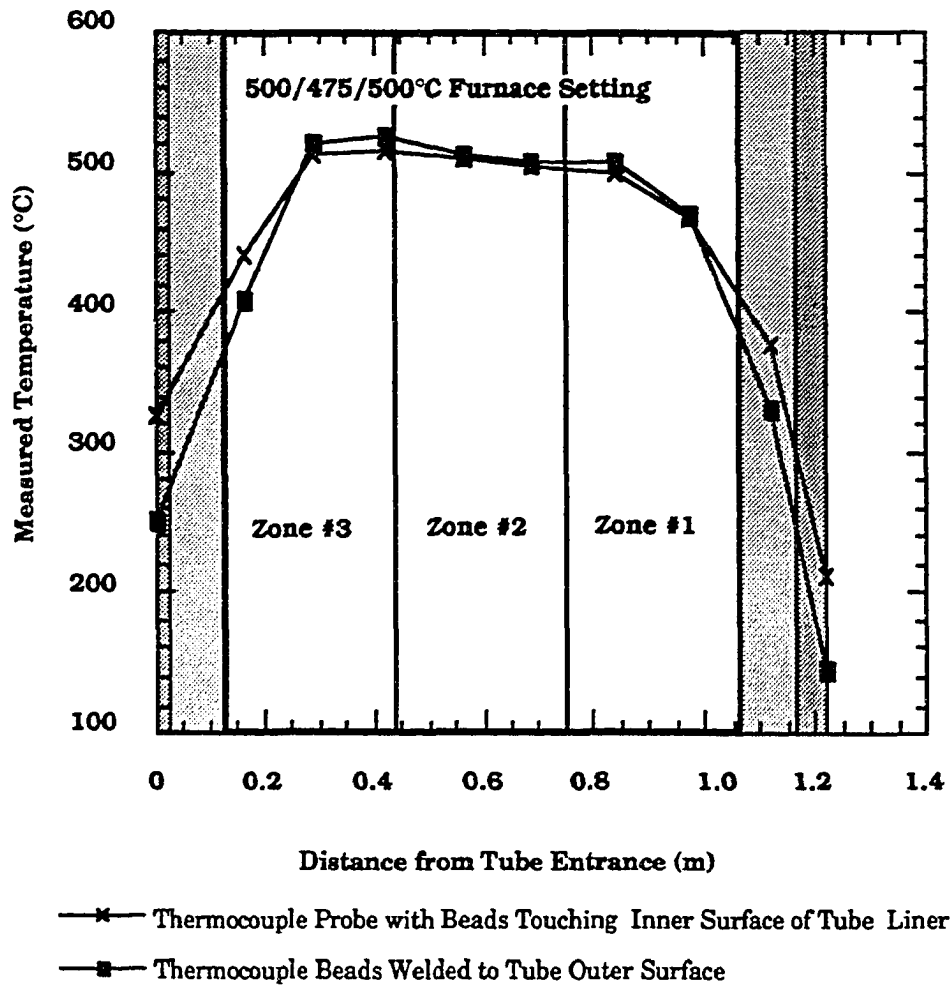
Figure 3.13 Tube Surface Temperature Profiles by Two Measurment Methods
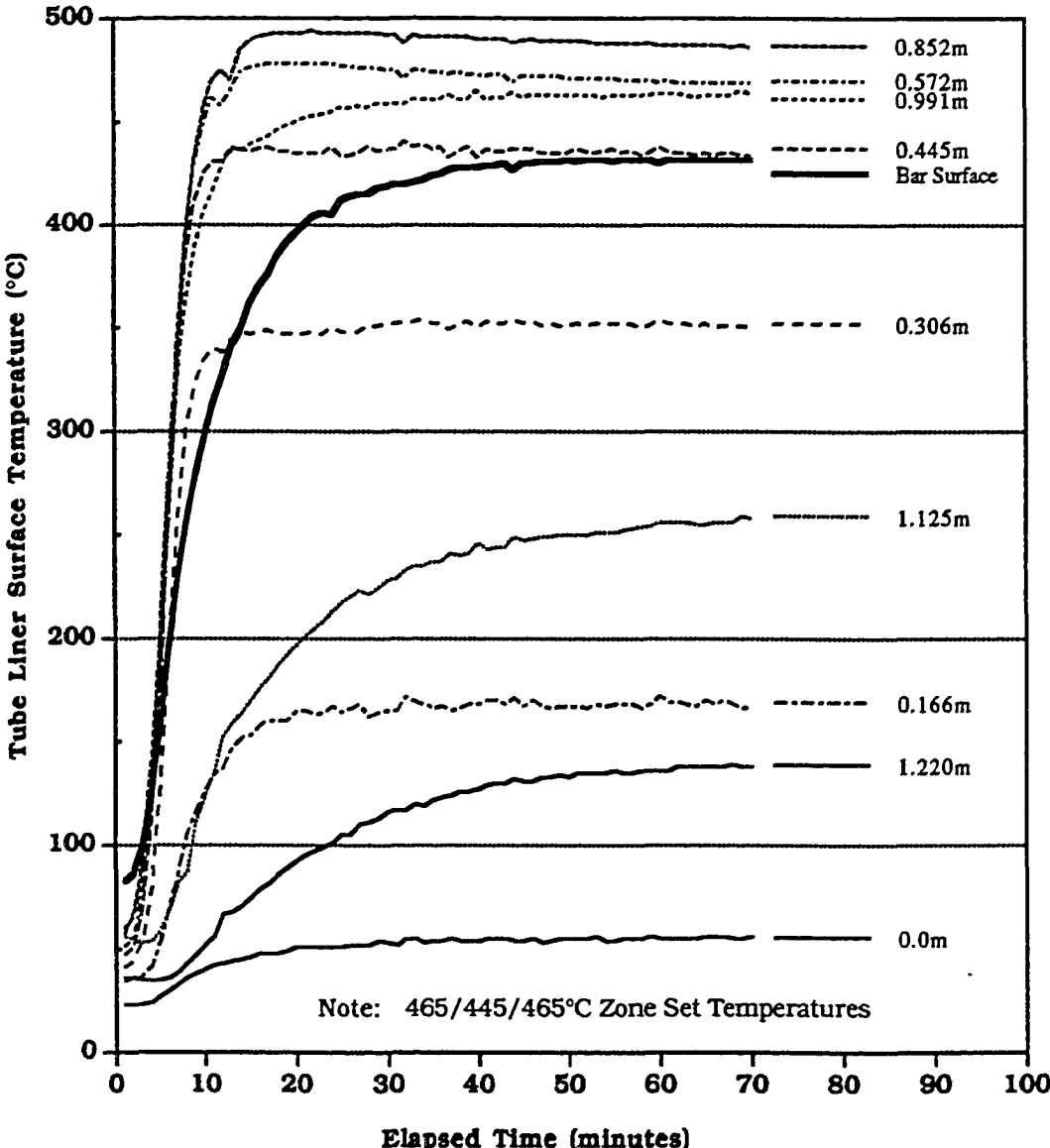
Figure 3.14 Tube Furnace Start-up
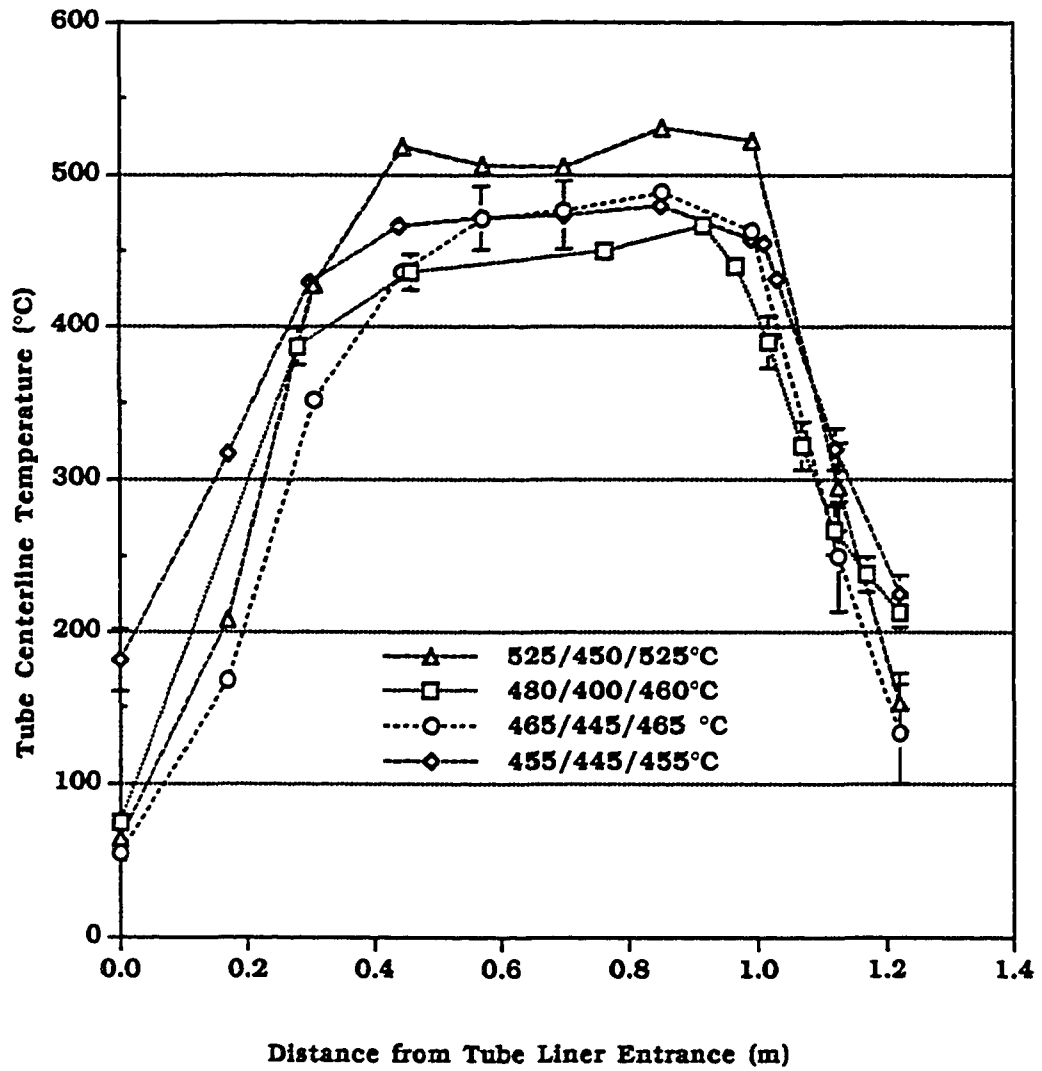
Figure 3.15 S.S. Tube Surface Temparature Profile Sensitivity to Zone Settings
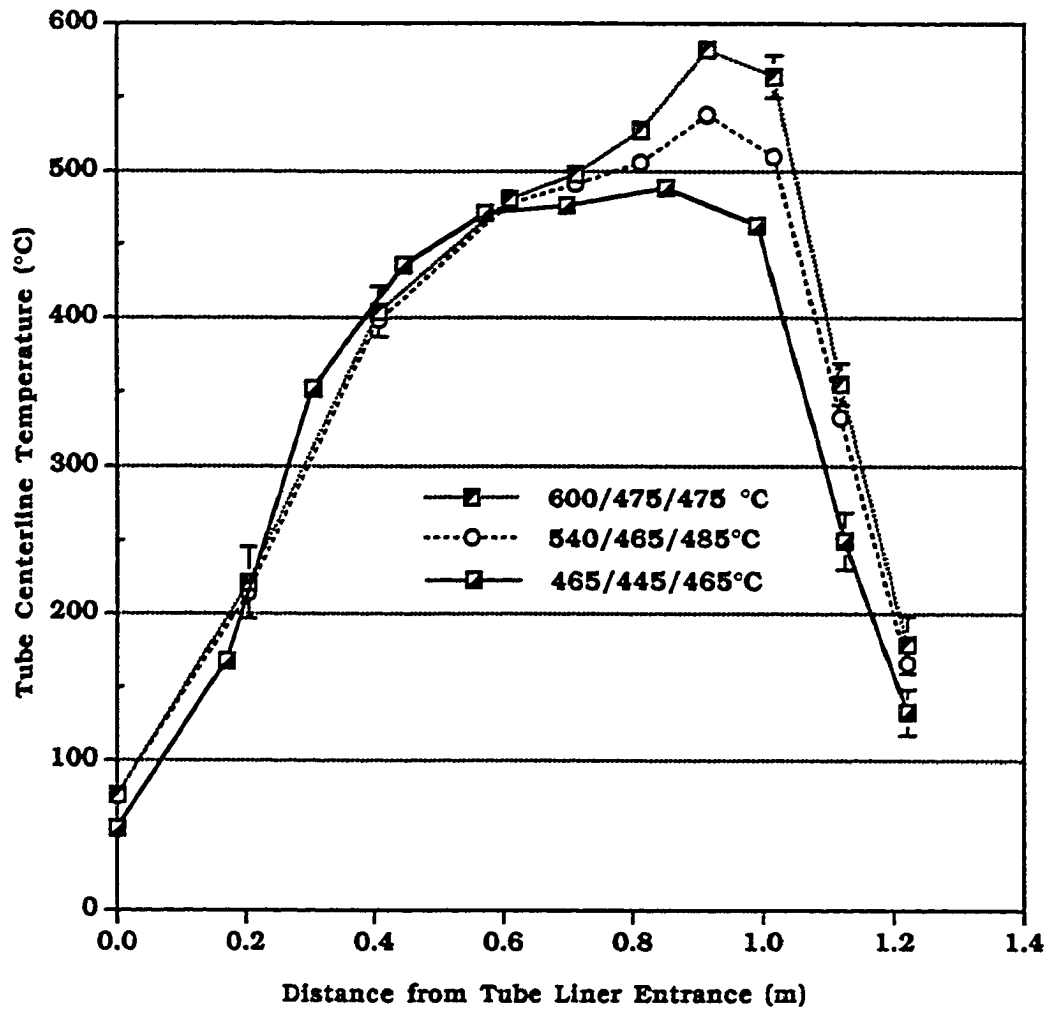
Figure 3.16 S.S. Tube Surface Temperature Profile Sensitivity to Zone #1 Setting
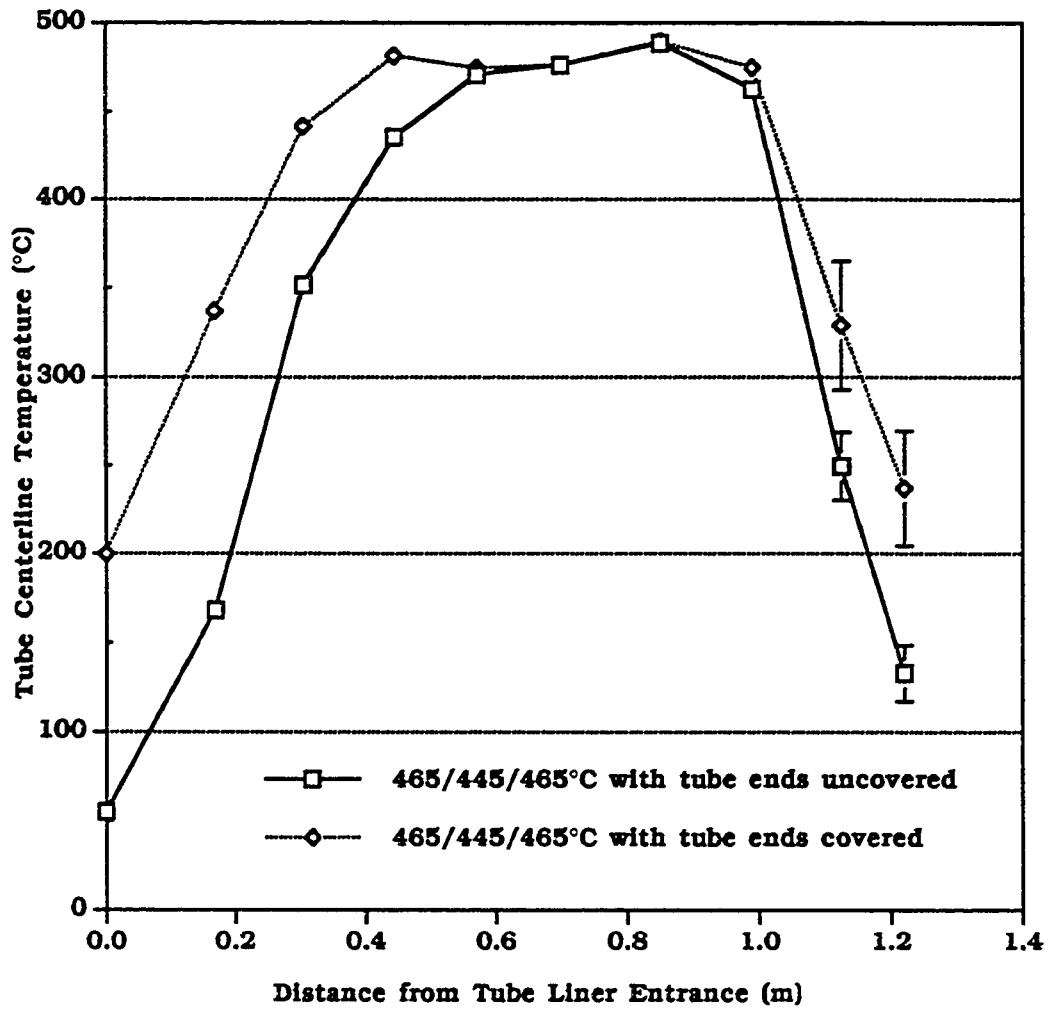
Figure 3.17 S.S. Tube Surface Temperature Profile Sensitivity to Tube End Covers
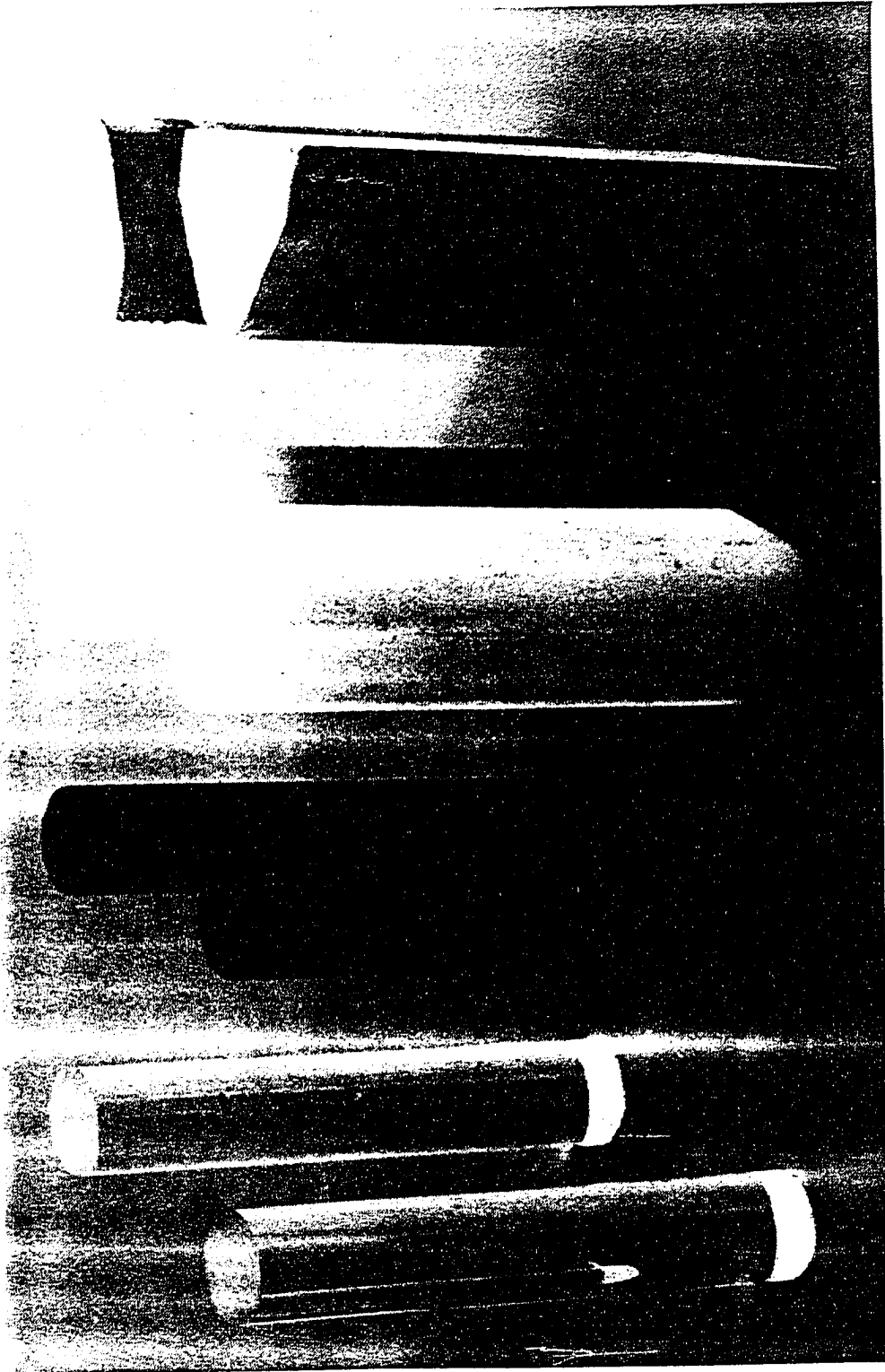
Figure 3.18 Four Types of Stationary Bars

SIDE VIEW

Thermocouple
Access Hole

Towpreg Path

TOP VIEW

① 387°C

385°C ②
409°C ③
375°C ④
387°C ⑤

Steady State at 475/490/465°C Zone Set Points
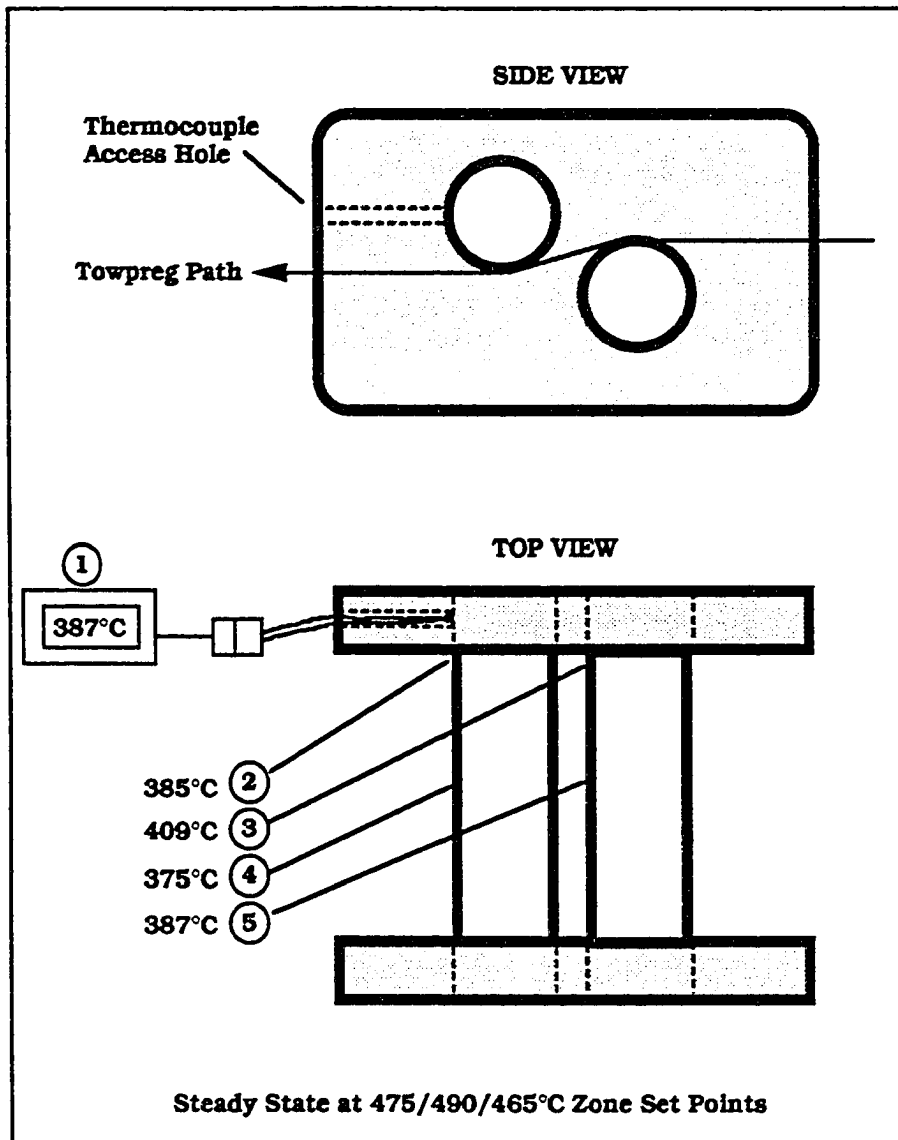
Figure 3.19 Bar Surface Temperature Distribution Illustration
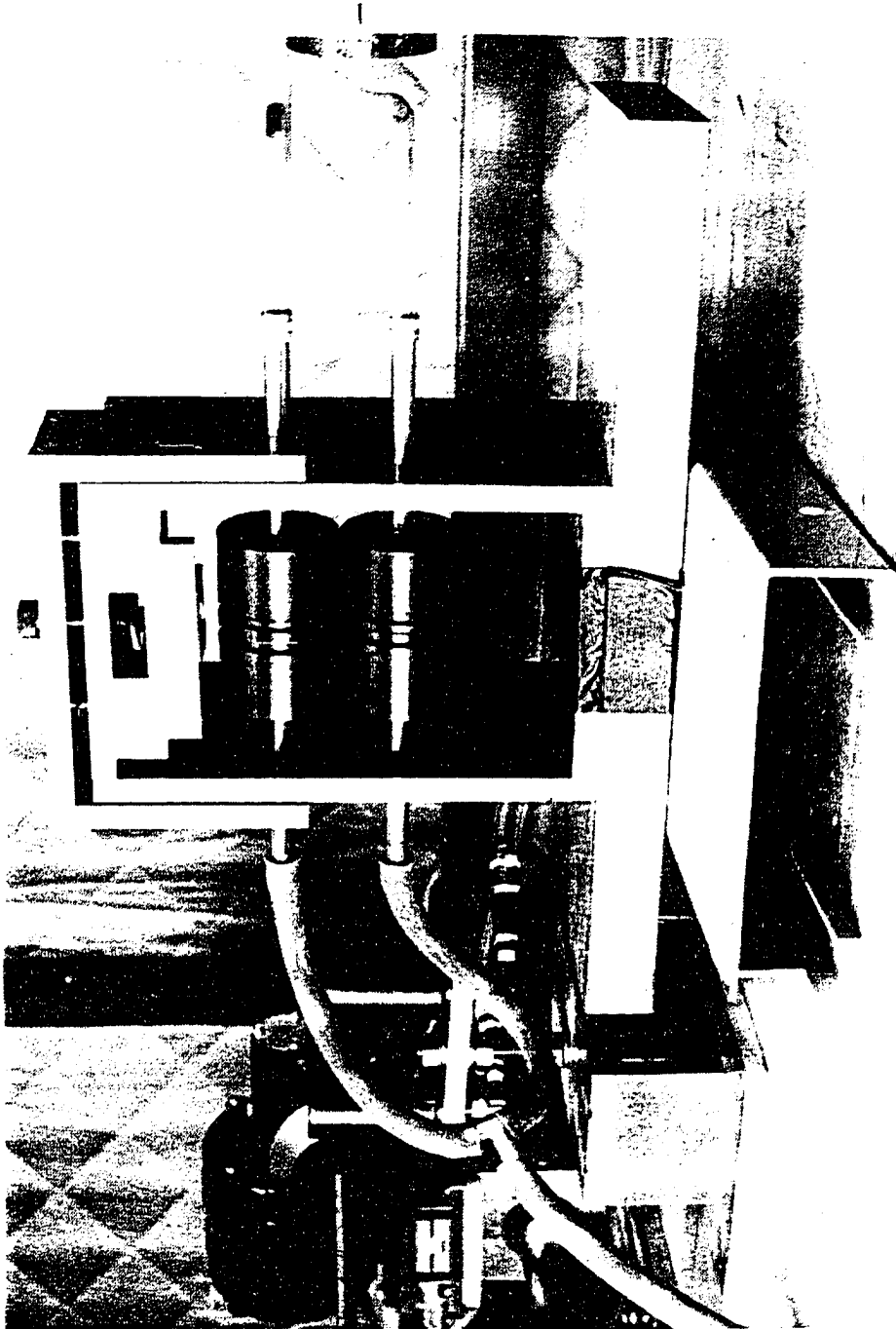
Figure 3.20   Nip Roller Assembly Photograph
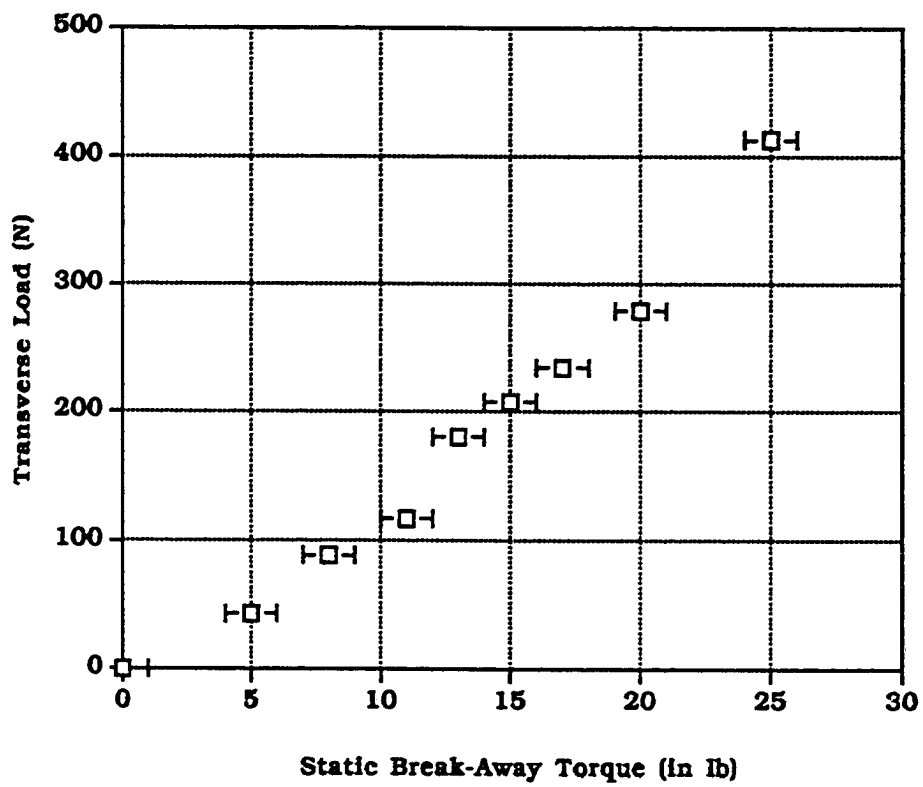
Figure 3.21 Transverse Nip Load Calibrated by Load Bolt
Break-Away Torque
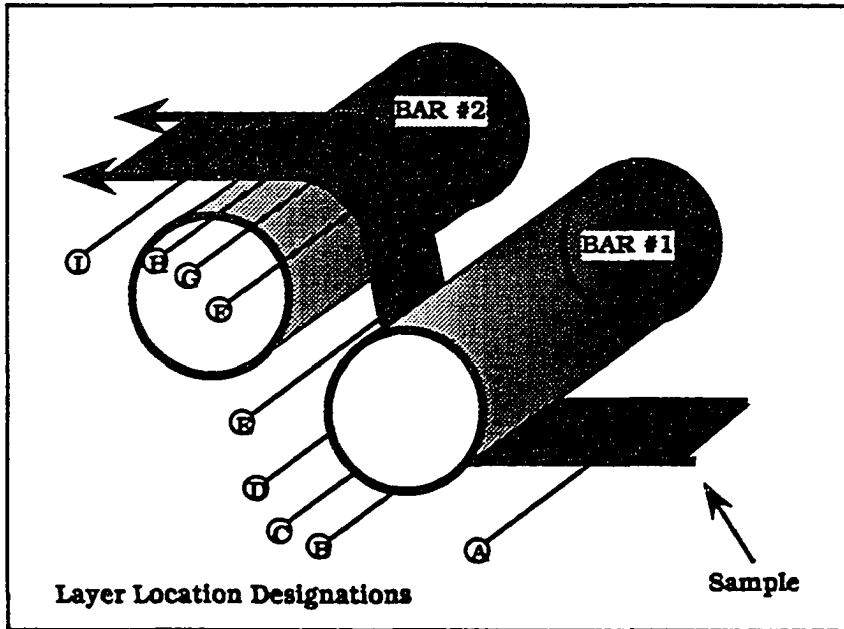
Figure 3.22 Towpreg Cross Section Sample Locator Key

Sample #062194 A

2 x 12 K IM-7/LaRC-IAX powder towpreg
V = 11 cm/s, T_c = 16N, RC = 39%
3 zones ≈ 355/355/355° C, T_b = 340° C
2 x 10 mm diameter Armalox™ ceramic bars
Template CL = 21.75 mm, ϕ = -9.2°, θ = 128°

0.10 mm

I

II

III

IV

V

Figure 3.23   Towpreg Sample #062194A Photomicrographs

Sample #062194 B

2 x 12 K IM-7/LaRC-IAX powder towpreg
V = 11 cm/s, T_c = 16N, RC = 39%
3 zones @ 355/355/355° C, T_b = 340° C
2 x 10 mm diameter Armalox™ ceramic bars
Template CL = 21.75 mm, ϕ = -9.20°, θ = 128°

0.10 mm

A

B

C

D

E

F

G

H

I
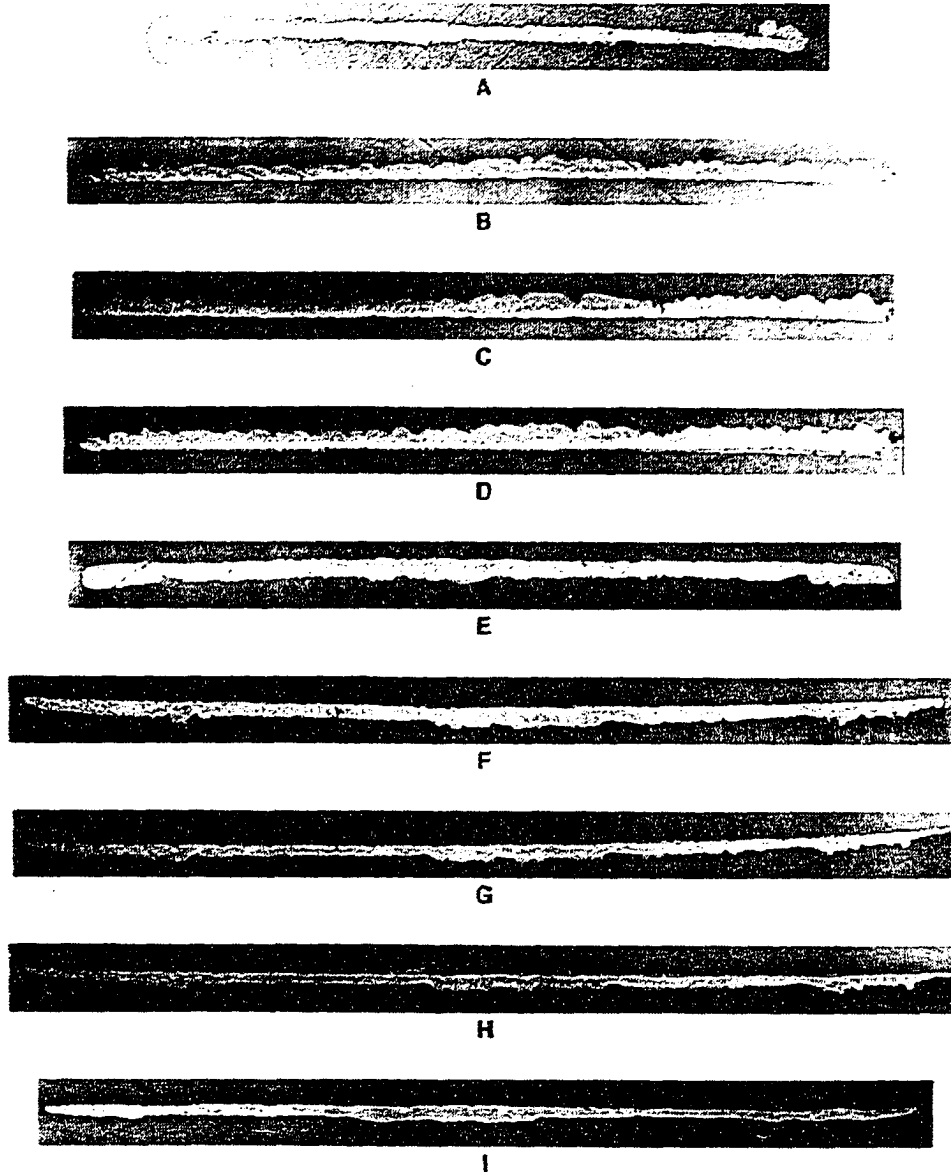
Figure 3.24   Towpreg Sample #062194B Photomicrographs

Sample #101893

2 x 12 K IM-7/Aurum-400A powder towpreg
$V = 8$ cm/s, $T_c = 10$ (N), RC = 39%
3 zones = 525/450/475° C, $T_b = 350°$ C
2 x 10 mm diameter carbon bars
Template CL = 16.5 mm, $o = 11°$, $\theta = 92°$

0.10 mm

N/A

A

B

C

D

E

F

G

N/A

H

I
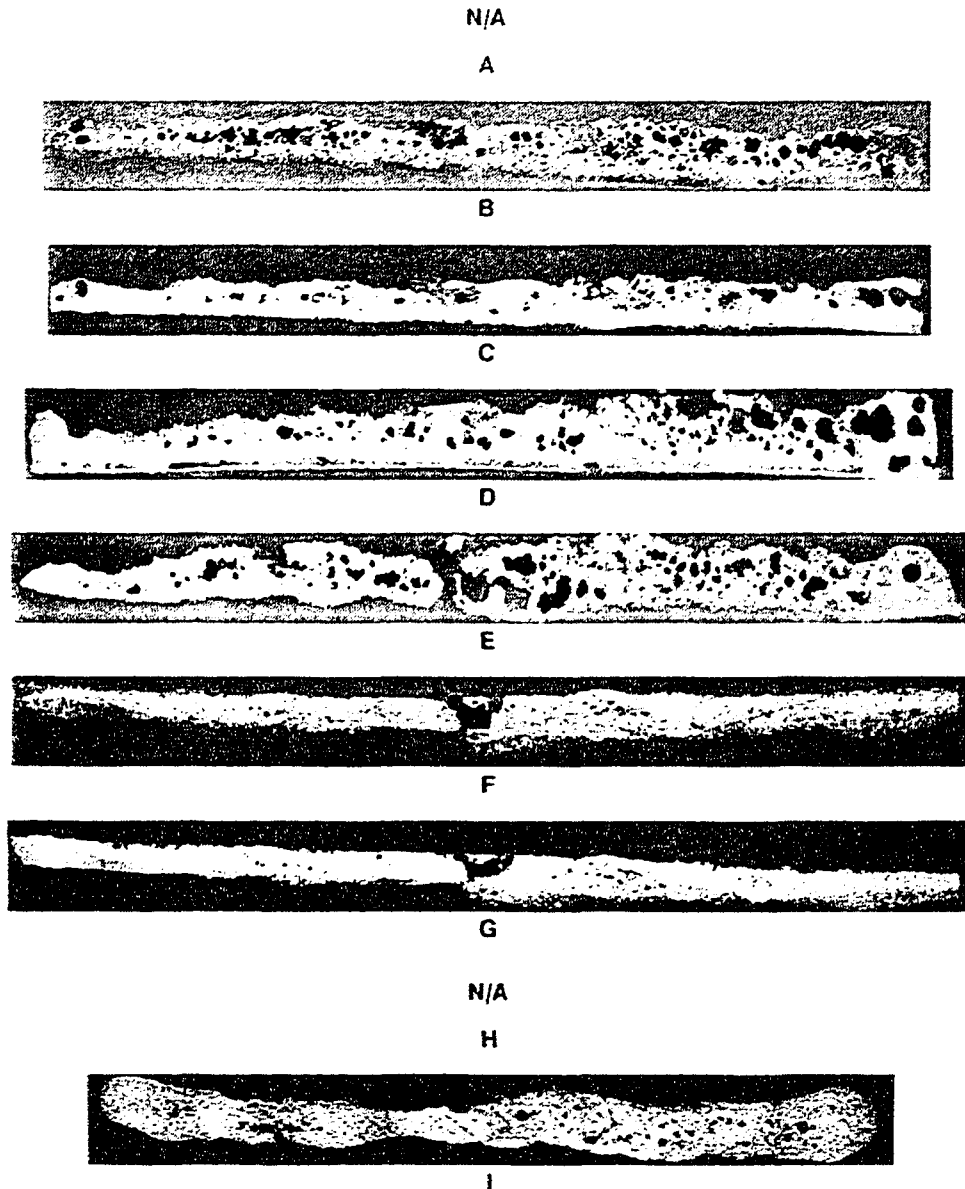
Figure 3.25   Towpreg Sample #011893 Photomicrographs

Sample #072594
_____

1 x 12 K IM-7/PIXA powder towpreg
$V = 11$ cm/s, $T_c = 5$ (N), RC = 37%
3 zones $\approx$ 500/490/525° C, $T_b = 370°$ C
2 x 10 mm Armalox™ ceramic bars
Template CL = 21.75 mm, $\varphi = -9.2°$, $\theta = 128°$

0.10 mm
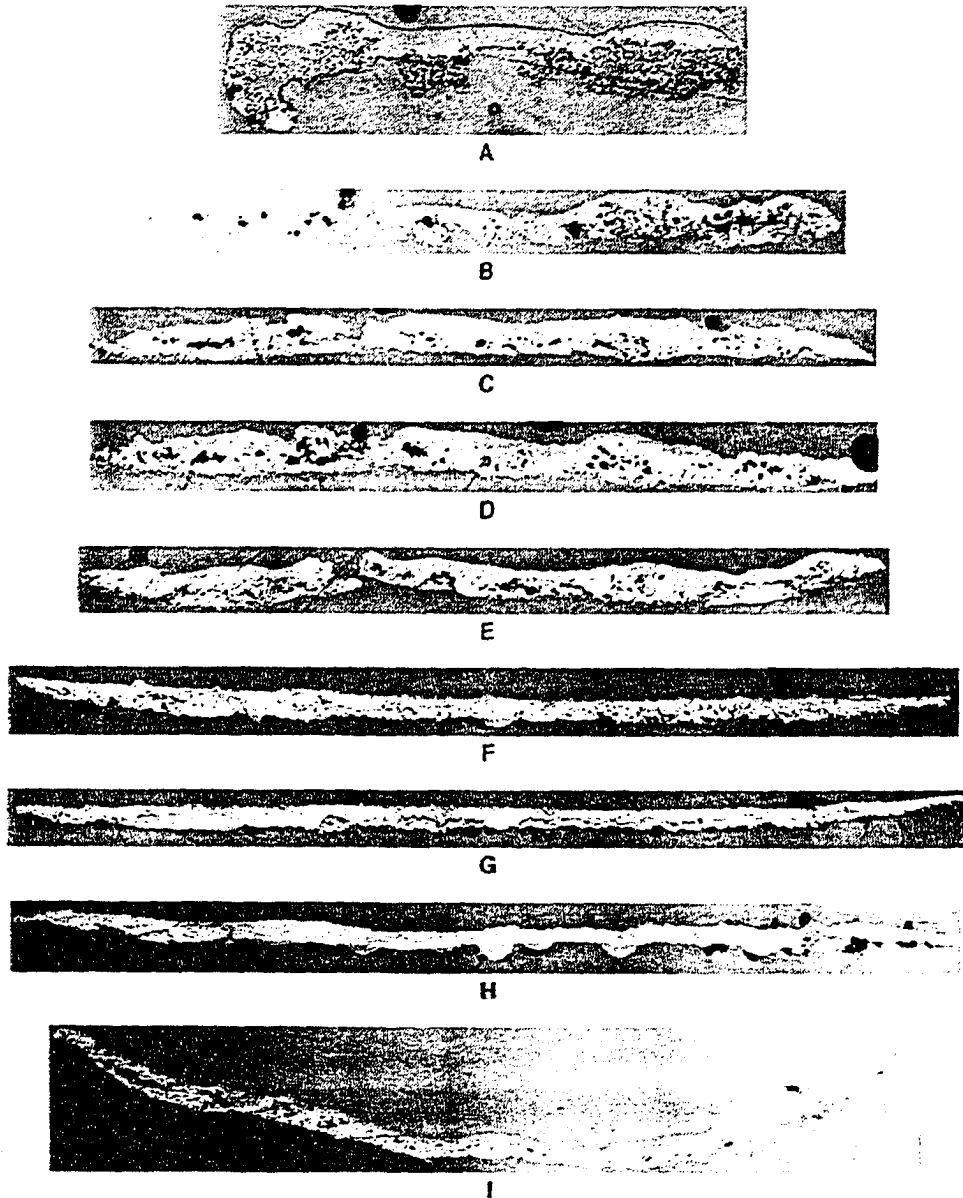
Figure 3.26   Towpreg Sample #072594 Photomicrographs

0.10 mm

A
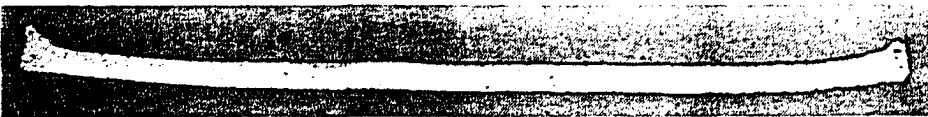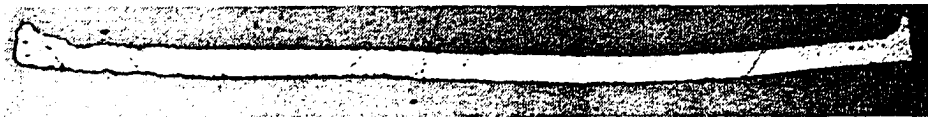
B
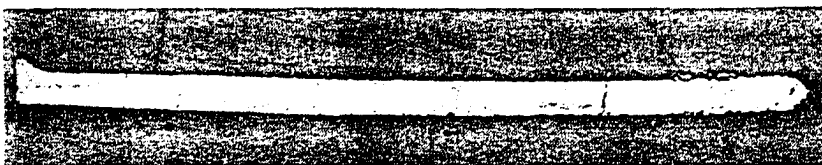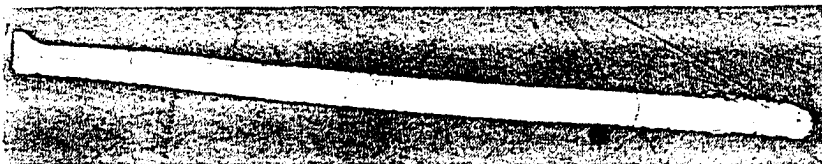
C

Figure 3.27   Common Cross Section Shape Photomicrographs
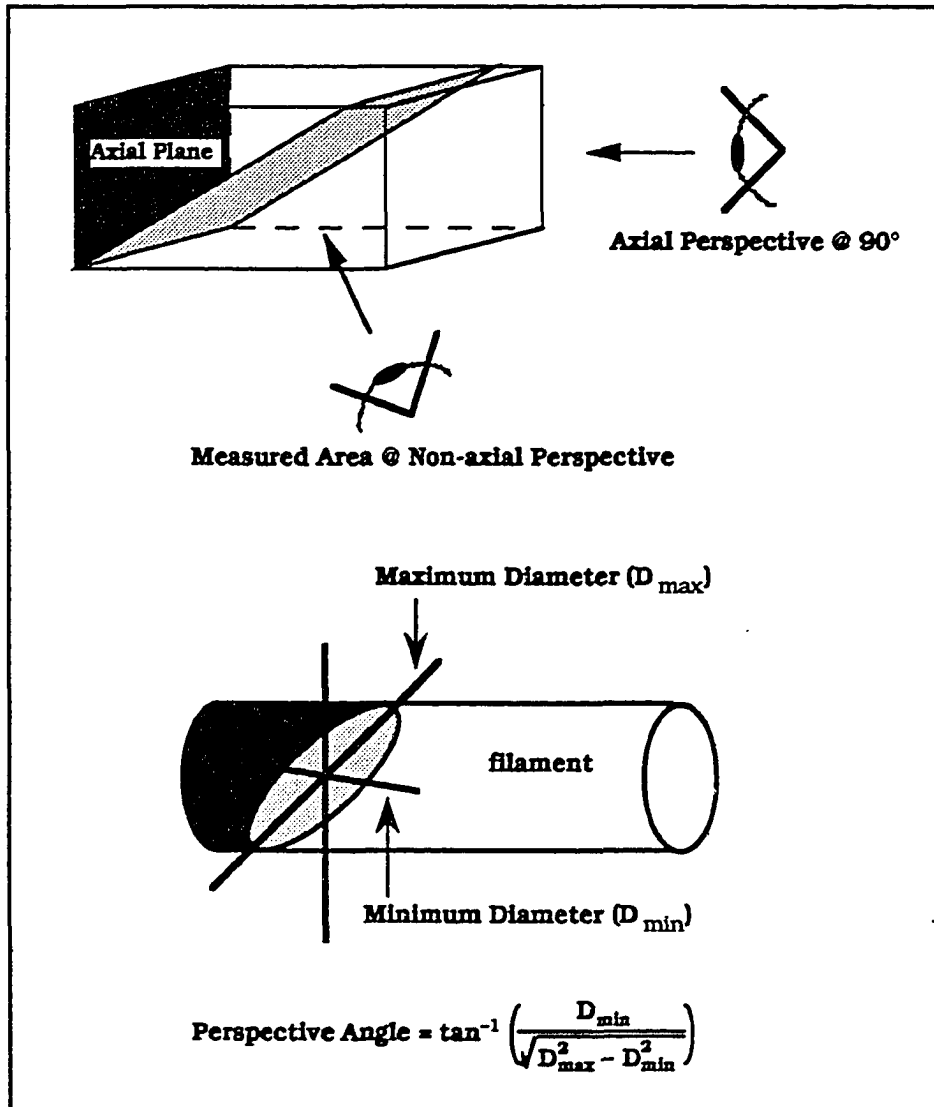
Figure 3.28 Sample Cross Section Perspective Angle Illustration

Figure 3.29 Towpreg Sample #101893 Cross Section Measured Areas vs. Location

Figure 3.30 Towpreg Sample #101893 Void Contents vs. Location

Figure 3.31 Towpreg Sample #072594 Cross Section Measured Areas vs. Location
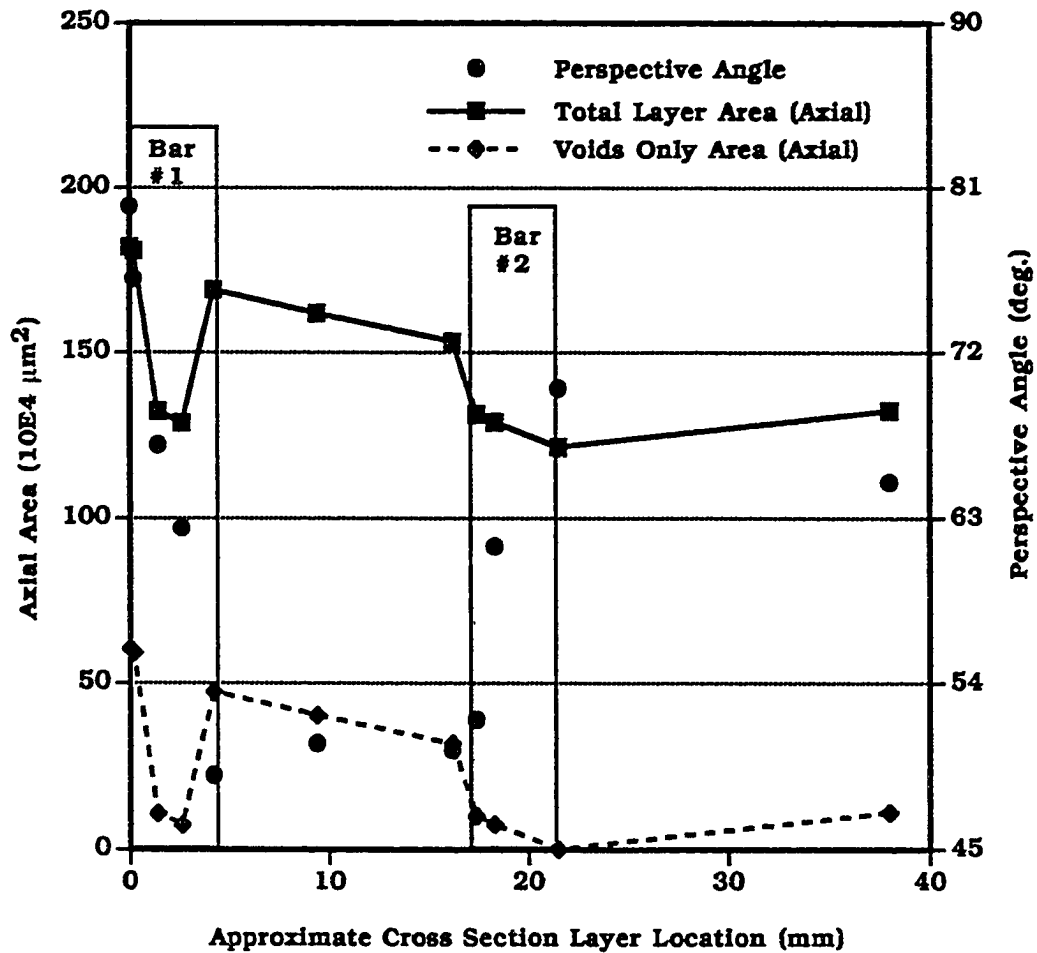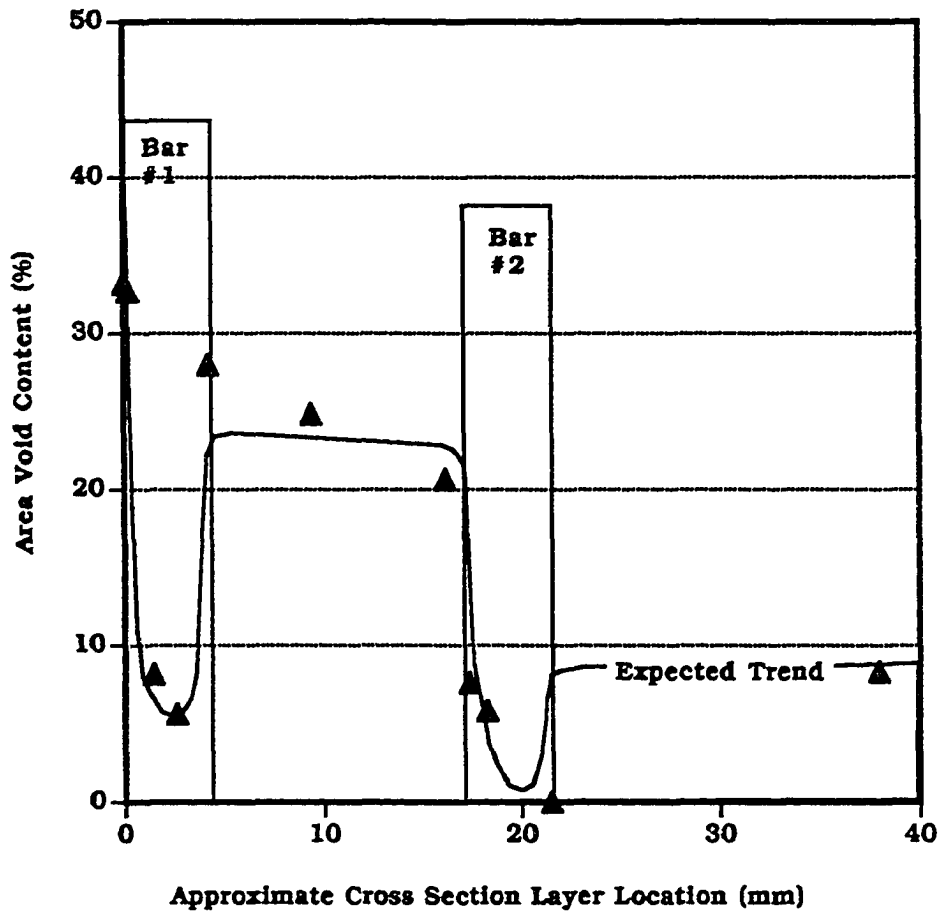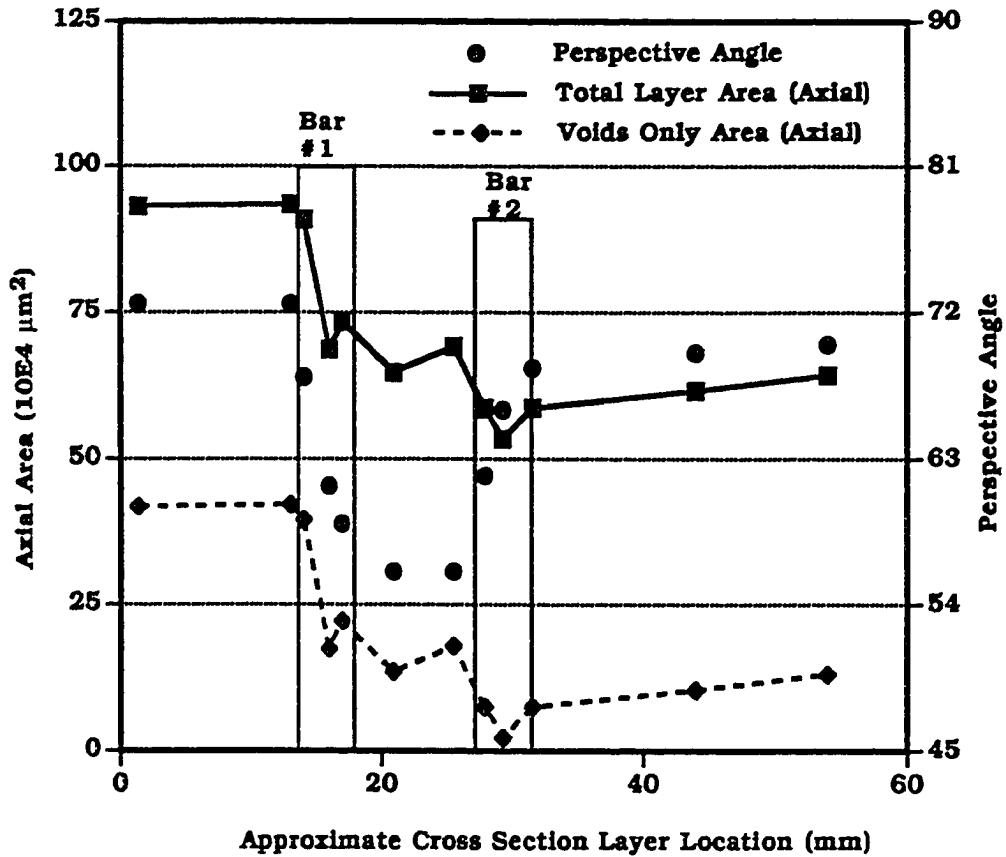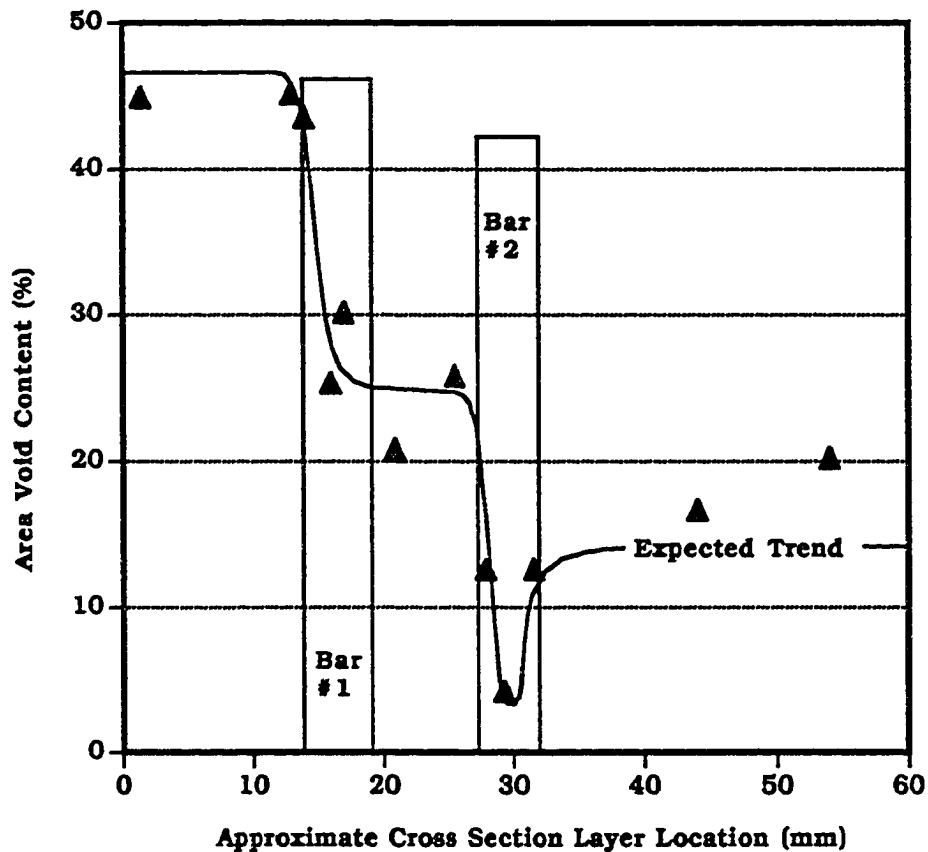
Sample # 072594 Ex Parte Ribbonization Processing Notes

1 X 12K IM-7™/PIXA™ Slurry Powder Towpreg
v = 11cm/s, Tc =2N, RC = 37%
3 Zones @ 500/490/525°C, Avg. Bar Temp. = 370°C
2 X 10mm Dia. Armalox™ Ceramic Bars
Combined Wrapping Angle for Both Bar Contacts θ = 128°

Figure 3.32 Towpreg Sample #072594 Void Contents vs. Location

4   Heat Transfer Analysis

4   Heat Transfer Analysis

When considering melt processing of a thermoplastic powder towpreg, the ideal

processing temperature can be obtained from the flow behavior of the neat polymer.

Rheometric and calorimetric analytical techniques can be used to determine an ideal

processing temperature range.   There usually exists a limit to the maximum

temperature for processing which is based on the materials inherent thermal oxidative

stability.   Alternative temperature constraints may be applied to material systems

which exhibit labile behavior above specific activation temperatures.   An example of

such a material is a primarily thermoplastic polymer, end-capped with molecules containing reactive moieties [1].

In the following analysis, the thermal history of the towpreg was evaluated experimentally and a quasi-steady-state (q.s.s.) towpreg heating profile model was developed to provide an unobtrusive means to predict the heating. This model also provided an engineering design tool and a method by which to parametrically study the roles of the processing parameters on the q.s.s. towpreg heating profile. The cooling phenomenon modeling was left for future work.

4.1　Towpreg Thermal History Characterization

The process heating and cooling scheme for the *ex parte* ribbonizer was expected to occur in four sequential components. **Figure 4.1** schematically illustrates the expected steady-state heat transfer phenomena where 1) preheating, 2) bar contact heating, 3) ambient cooling and 4) nip contact cooling occurred in series. The preheating occurred by radiation, with the towpreg translating through the tube furnace under tension. The preheat temperature T_p corresponds to the average temperature of the towpreg at a location just prior to contact with the first stationary bar. Next, bar contact heating occurred by conduction between the passively heated bars at nominal temperature T_b and the moving towpreg. The maximum temperature experienced by the towpreg T_{max} usually corresponded to the temperature attained by the towpreg, just prior to exiting the last bar. Ambient cooling occurred in the transition region between the bar assembly and the nip. The nip contact cooled the towpreg by conduction. With the proper distance between the tube furnace exit plane

and the nip roller assembly, the towpreg could be cooled below the polymers glass transition temperature on contact with the nip, to provide a form-stable ribbon of uniform cross section.

4.1.1   Average Towpreg Temperature Measurement

The enclosed geometry of the tube furnace apparatus posed a barrier to visual observation of the process within the tube and also limited the scope of practical techniques to measure the towpreg temperature. A compact optical pyrometer probe could have been positioned to indicate the towpregs radiant temperature at a particular location within the tube. Pyrometers typically offer a good means for process monitoring. If the temperature at several locations within the tube were measured this way, a steady-state temperature profile could be interpolated along the tubes length.

An alternative but obtrusive towpreg temperature measurement approach would be to place a very small thermocouple bead inside the towpreg and let it, and the wire, travel through the tube as an integral part of the towpreg. This bead would relay the changing temperature of the towpreg in real-time. The q.s.s. towpreg temperature profile could be obtained by scaling elapsed time by the axial velocity.

The direct pyrometer measurement approach was considered inappropriate, given the relatively hostile radiative environment within the premelting chamber, and the inherent uncertainty of pyrometer measurements on non-uniform, moving surfaces.

The thermocouple bead approach was selected and was expected to provide a reasonable indication of the average q.s.s. towpreg temperature profile.

Quasi-steady-state Towpreg Temperature Measurement

A fine gage thermocouple wire was incorporated into the powder towpreg and was then pulled, as an integral part of the towpreg, through the *ex parte* ribbonizer at a measured velocity. On exiting, the wire and bead remained an integral part of the towpreg. This technique provided real-time measurement of the towpreg temperature. Elapsed time was scaled by velocity and the resulting profile was assumed to reflect the q.s.s. towpreg temperature profile.

Experimental Set-up

The experimental process apparatus included the pay-out creel, two tensioning capstans, the tube furnace, the take-up puller and two powder-coated towpreg yarns of known composition.

A fine gage thermocouple wire was needed for flexibility and a small responsive bead. Due to the nature of the experimental set-up, the thermocouple wires were required to be approximately 20 feet long, yet flexible enough to mimic the mechanical behavior of the towpreg. Small thermocouple beads having small thermal masses tend to respond to temperature changes very fast, but long thermocouple leads can have inhibitive electrical resistance. Omega™ type K 30-2-305 (chromel-alumel) glass wrap-glass

braid thermocouple wire was selected for its flexibility, high temperature utility and reasonably fine wire gage.

Electrical discharge welding in inert gas, resulted in a substantially spherical thermocouple bead with 0.60mm nominal diameter. The lead wires were connected into a Hydra™ Data Acquisition Unit (Model 2620A) manufactured by John Fluke Mfg. Co., Inc. Each bead was tested at room temperature and 32°C after fabrication to check the lead connection. The bead end of the 20 foot long thermocouple wire was incorporated into the powder-coated towpreg by simply placing the about 5cm of the wire into the towpreg and helically wrapping (or serving) another fine wire around the bundle at approximately 3 revolutions per cm. The serving wire was retrieved from other discarded thermocouple wire. The tightly wrapped section of towpreg remained flexible due to the fine gage of the serving wire. The bead was positioned about 1cm downstream of the served section which constrained the wire and encapsulated the bead within the bundle. Note that the diameter of a bulky 24K IM-7 powder towpreg under tension was usually about 2mm while the thickness of a ribbon was usually near 0.15mm. This bead fit nicely within the bulky tow but was larger than the usual thickness of the resultant wide, flat ribbon.

The experimental temperature data were recorded with a Honeywell™ Omnilight 8M36 thermal chart recorder to provide real-time temperature measurement. Thermocouple voltage was stepped-up and calibrated to 1 (mV °C^{-1}) with a Fluke™ 80TK Thermocouple Module. The take-up speed was measured with a Computak™ speedometer made by Jones Corporation.

The fastest response rate for the bead (approximately 500 (°C s^{-1}) was obtained by dunking the room temperature bead into a container of boiling water and measuring the maximum slope of the temperature versus elapsed time curve. As long as the measured towpreg heating rates were less than the fastest response rate of the measurement technique, results were valid. In other words, for the range of temperature encountered in the experiment, the ratio of thermal masses had to be biased in favor of the towpreg, in order for the measurements to be meaningful.

The heating rates within the premelting chamber were usually below 30 (°C s^{-1}), and could therefore be considered valid. In contrast, heating rates were similar to, or higher than, the measured response time of the thermocouple bead, at the bar contact and the nip regions. This similarity between the bead response rate and the heating rates, tended to substantially bias the q.s.s. profiles for the bar contact heating and the nip cooling regions, and therefore, measurements at these locations were not considered valid, but did nonetheless, provide a general indication of the thermal history phenomenon.

Experimental Procedure

The tube furnace was turned-on and allowed to warm-up to steady-state. The chart recorder was cued and the take-up motor was engaged. The tow was pulled through the apparatus with the thermocouple wire attached. The served section proceeded through the tube furnace premelting chamber. When the served section contacted the take-up spool, the take-up and the data logging equipment were disengaged. The consumed material was inspected to determine whether or not the bead remained

encapsulated. To ensure repeatability, this experiment was repeated up to 5 times for each experimental variation. As long as care was taken in the serving operation, there was a reasonable certainty (>85%) that the bead would remain visibly encapsulated within the tow.

4.1.2   Q.S.S. Thermal History for Overall Process

The *ex parte* process was set-up for operation with each component in its normal configuration. The various polymer and fiber materials used throughout the analysis are listed in **Appendix B**. A typical overall process thermal history data set is illustrated by **Figure 4.2**. The chart speed of the data logger was set to 1 (cm s⁻¹) so that the horizontal axis corresponded to elapsed time. The vertical axis reflected thermocouple voltage, stepped-up and calibrated to 1 (°C mV⁻¹). The first distinguishable deviation from room temperature was assumed to correlate to position $z = 0$ (m) and time $t = 0$ (s) at the tubes entrance plane. This benchmark assumption did introduce some qualitative uncertainty in the experimental data however, was considered practical and reasonable since the assumption was utilized consistently.

The bending required for the served section of towpreg to translate through the stationary bar assembly was prohibitive for this experiment. Although maintaining full encapsulation of the thermocouple bead throughout contact was intermittent, the experiment was repeated many times until at least 3 fully encapsulated measurements were obtained.

The towpreg temperature, for the experimental data shown in **Figure 4.2**, was observed to increase a total of 50°C in two barely distinguishable steps corresponding to the two bar contacts. As the towpreg left the bar assembly behind, the tow temperature cooled accordingly. On contact with the cool nip rollers, the towpreg temperature dropped about 50°C. Note in the figure how the temperature after nipping was above the 250°C glass transition temperature T_g of the polymer. In this case, the ribbon was not fully cooled. Ideally, the nip would have been moved further down-stream so that prior to nipping the temperature would have been lower and therefore after nipping the towpreg temperature could have been below T_g.

The variance of these measurements in the region of the bar assembly and nip roller were characterized by comparing five independent sets of experimental data for similar processing conditions. The average heat-up at the contact with the stationary bars was 45°C with standard deviation of 14°C while the average cool-down at the nip was 55°C with standard deviation of 7°C. The relative magnitudes of these standard deviations reflected the tendency of the bar contact to force the thermocouple bead out of the bundle while the nip did not.

4.1.3 Q.S.S. Towpreg Temperature Profiles for Preheating Only

The nip was disengaged and removed. The bar assembly was also removed, so that the towpreg passed freely, suspended under tension, from the tensioning capstans to the take-up. Steady-state temperature measurements were again obtained by incorporating the thermocouple wire into the towpreg. The q.s.s. profiles were

obtained for only the heat transfer between the towpreg and the tube liner. These measurements indicated what was called "preheating only" q.s.s. profiles.

Figure 4.3 presents four sets of data converted to q.s.s. towpreg temperature profiles. Note the variance between samples C, D, E and F which were all obtained for identical tube furnace setting (500/490/500°C) and take-up speed ($v = 5.08$ (cm s^{-1})). Mean temperatures were calculated for several positions and were overlaid onto the towpreg profile data with error bars corresponding to ±1 standard deviation. Although the average uncertainty was about 20°C over the range of measurements, the shape of these profiles was shown to be consistent and repeatable. Of these four measurements, sample F matched the mean most closely. Sample F was also the best sample in terms of qualitative inspection because the bead appeared to remain encapsulated; there did not appear to be any slip of the wire relative to the towpreg and the experiment proceeded otherwise nominally. Independent of the variance analysis, qualitative experimental observation of repeated samples indicated sample F to be clearly the most representative.

The q.s.s. towpreg temperature profile shape was expected to reflect a dependence on take-up speed. Data at various speeds were obtained and converted to q.s.s. in **Figure 4.4**. Since experiments were repeated until clearly representative samples were obtained for each speed, and the variance of the measurements was not expected to depend on take-up speed, mean and standard deviation values were not calculated for all data.

Of particular importance was the towpreg temperature at position $z = 1m$ which corresponded to the axial location just prior to contact with the first stationary bar. This temperature corresponded to the previously defined preheating temperature T_p. Doubling the take-up speed was observed to decrease T_p by 100°C.

Another important process parameter was furnace zone temperature set points. **Figure 4.5** represents an overlay plot of a tube liner surface temperature for profile (455/450/455°C) and measured q.s.s. towpreg temperature profiles for two take-up speeds. The towpreg temperatures were assigned uniform error bars of ±10°C based on previously described variance observations. Comparison of **Figure 4.4** and **Figure 4.5** illustrated how lowering the average oven set point by 50°C reduced the preheat temperature by 60°C for similar take-up speed. This phenomenon was attributed to the independent control of the three zones of the tube. This observation re-emphasized the importance of the tube liner steady-state temperature profile characterizations discussed in Chapter 3.

4.2   Towpreg Temperature Profile Modeling

The entire heat transfer process was characterized experimentally, but only the first two heat transfer components were modeled by this analysis. The purpose of modeling the heating phenomenon was to better understand the role of take-up speed and furnace temperature set points on the heating scheme.

As a matter of convenience, scalar representations of the heat transfer phenomenon were evaluated and were considered reasonable approximations. Symmetry was

utilized advantageously to simplify the analysis of both components, such that the preheating, heat transfer was considered in cylindrical coordinates and the contact with the stationary bars was molded in rectilinear coordinates. The two model solutions were superimposed in a scalar representation to indicate the role of processing speed, bar temperature, and void content on the towpreg thermal heating history.

4.2.1 Relevant Heat Transfer Principles

Suppose that mass A, at a higher temperature than mass B, is placed in a closed system near B. When thermal equilibrium has been reached, A will be found to have undergone a temperature decrease and B, a temperature increase. When an energy transfer takes place by virtue of a temperature difference exclusively, it is heat flow. At one time this phenomenon was thought to be a flow of an invisible weightless fluid called *caloric*, but the work of Count Rumford (1753-1814) and Sir James Prescott Joule (1818-1889) established firmly that heat flow is an energy transfer.

Heat transfer within a control volume can occur via three primary modes; conduction, convection and radiation [2,3,4,5]. Conduction is the transfer of heat from one part of a body to another part or to another body by short-range interaction of molecules and electrons. Convection is the transfer of heat by the combined mechanisms of fluid mixing and conduction. Radiation is the emission of energy in the form of electromagnetic waves from one body to another. Radiation incident on a body may be absorbed, reflected and transmitted.

Thermal Energy Stored by a Mass

Consider a small quantity of heat which is transferred between a mass and its surroundings. The thermal energy dQ (J) needed to increase the temperature of the mass m (g) by an amount dT (K) with constant pressure heat capacity c_p (J g^{-1} K^{-1}) is known.

$$dQ = m\,c_p\,dT \qquad [4.1]$$

The time dependent form of this relationship defined the thermal state of the mass at any time t (s) during the heating or cooling process.

$$\dot{Q} = \frac{dQ}{dt} = m\,c_p\,\frac{dT}{dt} \qquad [4.2]$$

Conduction and Convection Heat Transfer

Fourier stated in 1822 that conduction heat transfer through a solid object was proportional to the normal area A and the temperature gradient ∇T to which the object was exposed. The scalar heat flow rate $\dot{Q}$ was expressed in energy per unit time or power (W).

$$\dot{Q} = k\,A\,\frac{dT}{dz} \qquad [4.3]$$

The proportionality constant k (W m^{-1} K^{-1}) is called the thermal conductivity and was a material constant which was actually temperature dependent itself.

Convection is simply an extension of conduction where heat transfer occurs between solid body and a fluid in motion. The scalar rate equation for convective heat transfer was first expressed by Newton in 1701, and is referred to as Newton's law of cooling.

$$\dot{Q} = h \, A \, \Delta T, \qquad\qquad [4.4]$$

where ΔT was the temperature difference between the surface and the main body of the fluid. Values of h ($W \, m^{-2} \, K^{-1}$) are determined experimentally and are known to depend on temperature and boundary layer flow conditions.

Electromagnetic Radiation Heat Transfer

Thermal energy flow rate from a radiating surface was shown to be proportional to the surface area A and to the fourth power of the absolute temperature T. This relation was deduced by Joseph Stephan on the basis of experimental measurements made by John Tyndall and was later derived from theoretical considerations by Ludwig Boltzmann. Radiative energy flow from an emitting surface is given by the Stephan-Boltzmann Law.

$$\dot{Q} = A \, \varepsilon \, \sigma \, T^4 \qquad\qquad [4.5]$$

The universal physical constant $\sigma = 5.6699 \, E\text{-}8$ ($W \, m^{-2} \, K^{-4}$) was called the Stephan-Boltzmann constant. Emissivity ε is the ratio of the total emissive power of a surface to the total emissive power of an ideally radiating blackbody at the same temperature.

Therefore, the radiative nature of a real surface is described by emissivity, which is between zero and unity. The effect of surface roughness on total hemispherical and specular reflectance of metallic surfaces was studied [6] in great detail in the 1960's. Emissivity is generally larger for dark, rough surfaces than for light, smooth ones. At room temperature [7], the emissivity of a smooth polished copper surface is about 0.3 while heavily oxidized steel is about 0.95.

Spectral hemispherical emissivity of real bodies is a function of radiation wavelength and direction. A materials emissivity is often characterized in terms of hemispherical emissivity which considers only the energy emitted into the hemispherical space averaged over all wavelengths. Opaque bodies have the characteristic that the hemispherical reflectivity plus absorptivity equal unity. To simplify the analysis of radiative heat transfer here, the spectral radiative properties were assumed uniform over the entire wavelength spectrum. Kirchoff's Law states that for a gray body system in thermal equilibrium, a surface's emissivity is equal to its absorptivity. This relationship is not applicable for steady-state conditions generally. Steady-state means that the time derivatives of temperature are zero while equilibrium refers to the equality of temperatures. However, for most materials in the usual range of temperature encountered in practice (room temperature to about 2000°F) the simple equality holds with good accuracy.

Emissivity describes the fraction of energy which can be emitted by one body, but does not address the issue of what percentage of that energy is incident on another body. The geometrical considerations of the apparatus may be included in the dimensionless view factor F. The view factor between two surfaces represents the

fraction of the radiative energy leaving one surface that strikes the other surface directly. There exists a reciprocity relationship between view factors of two surfaces i and j [8,9,10,11], such that the surface areas A_i and A_j determine the relative significance of each view factor.

$$A_i F_{A_i-A_j} = A_j F_{A_j-A_i}$$

[4.6]

4.2.2 The Preheat Heat Transfer Model Development

Figure 4.6 offers an illustrative representation of the geometry of the preheating region. The unit towpreg volume of length dz translated through the fixed tube liner in the positive z-direction at a constant speed v (m s^{-1}). Symmetry in the r-direction was assumed so that the tube furnace liner and the towpreg were modeled as concentric cylinders with the tube liner having inside diameter D_T (m) and the towpreg having diameter D (m). Heating by radiation and convection occurred as the towpreg passed through the tube liner. The heat sources increased the temperature of the towpreg element by conduction in the negative r-direction. Axial conduction within the towpreg flowed in the negative z-direction and therefore opposed the relative velocity of the element.

4.2.2.1   The Rigorous Preheat Temperature Model

The primary objective of this modeling effort was to characterize in scalar format, the q.s.s. heating profile for the towpreg as a function of processing variables. The

preheat, heat transfer component was first considered in terms of the anisotropic heat conduction equation in cylindrical coordinates.

$$\frac{k_r}{r}\frac{\partial}{\partial r}\left(r\frac{\partial T}{\partial r}\right) + \frac{k_\varphi}{r^2}\left(\frac{\partial^2 T}{\partial\varphi^2}\right) + k_z\left(\frac{\partial^2 T}{\partial z^2}\right) + g = \rho\, c_p\frac{\partial T}{\partial t} \qquad [4.7]$$

Two assumptions and one boundary condition of the second kind were utilized to simplify and reduce the order of the heat conduction equation . The heat generation term g (W m^{-3}) was assumed negligible. The temperature gradient in the φ direction was also considered negligible based on uniform heating resulting from the concentric symmetry. The conduction in the r-direction was assumed to be equal to the sum of heat supplies at the towpreg surface. The heat conduction in the r-direction was assumed equal to the sum of convection from the hot gas within the tube and net radiation from the interior tube liner surface. This imposed an adiabatic constraint for the system, which was considered appropriate and reasonable.

Assumption#1 $g = 0$ [4.8]

Assumption #2 $\dfrac{\partial T}{\partial\varphi} = 0$ [4.9]

B.C. #1 $\dfrac{k_r}{r}\dfrac{\partial}{\partial r}\left(r\dfrac{\partial T}{\partial r}\right) = \frac{1}{r}\, q_{conv.}\Big|_{r=D/2} + \frac{1}{r}\, q_{net\, rad.}\Big|_{r=D/2}$ [4.10]

Simplification provided the rigorous two dimensional time dependent conduction equation at steady-state.

$$\rho \, c_p \left(\frac{\partial T}{\partial t}\right) = k_z \left(\frac{\partial^2 T}{\partial z^2}\right) + \frac{1}{r} \, q_{conv.}\Big|_{r=D/2} + \frac{1}{r} \, q_{net \, rad.}\Big|_{r=D/2} \qquad [4.11]$$

4.2.2.2   Equivalent Scalar Energy Flow Balance

The q.s.s. experimental measurements were scalar and therefore a scalar model was required for comparison. The analogous and rigorous scalar representation of this same preheating process was derived by general energy flow rate balance of a control volume. **Figure 4.7** illustrates the energy flow balance of the differential control volume. All of the energy transfer was again assumed adiabatic. The energy balance for the cylindrical differential control volume, with previously described assumptions and boundary condition, was defined in terms of energy flow rates $d\dot{Q}$ $(J\,s^{-1})$.

$$d\dot{Q}_{stored} = d\dot{Q}_{cond.,L} - d\dot{Q}_{cond.,R} + d\dot{Q}_{conv.}\Big|_{r=D/2} + d\dot{Q}_{net \, rad.}\Big|_{r=D/2} \qquad [4.12]$$

The elemental mass, dm (g), was represented by the product of the composite towpreg density ρ (g m^{-3}) and a differential volume dV (m^3).

$$dm = \rho \, dV = \rho \, \frac{\pi}{4} D^2 \, dz \qquad [4.13]$$

The energy storage rate $d\dot{Q}_{stored}$ for the unit mass was defined in terms of T_2, representing the average temperature (K) throughout the cross section of the differential volume.

$$d\dot{Q}_{stored} = dm\, c_p \frac{dT_2}{dt},\qquad\qquad [4.14]$$

Substitution provided the rate at which the differential towpreg unit could absorb and store thermal energy.

$$d\dot{Q}_{stored} = \rho\, \frac{\pi}{4} D^2\, dz\, c_p \frac{dT_2}{dt}.\qquad\qquad [4.15]$$

Axial Conduction

The downstream (left) unit in **Figure 4.7** would have slightly higher temperature than the upstream (right) unit. Again, this analysis assumed that at any time or radial location, a towpreg yarn element had an average temperature T_2 throughout the entire radial thickness of the element and so the axial conduction energy flow rate was defined.

$$d\dot{Q}_{cond.L} - d\dot{Q}_{cond.R} = A_z\, k_z \left[\left(\frac{dT_2}{dz}\right)_L - \left(\frac{dT_2}{dz}\right)_R\right]\qquad\qquad [4.16]$$

The normal area for axial conduction A_z was known from the geometry.

$$A_z = \frac{\pi}{4} D^2\qquad\qquad [4.17]$$

Hot Gas Convection Mechanism

Conduction and convection occur in series during heat transfer between two different solids through a fluid. If the fluid were in motion, convection would be a very important heat transfer mechanism. The experimental premelting chamber was designed so that a low flow-rate bleed of bottled nitrogen gas was introduced into the chamber to minimize elevated temperature oxidation of the equipment and towpreg polymer. The gas within the tube at temperature T_1 was therefore an air mixture rich with nitrogen. Convection between the heated gas inside the chamber and the towpreg yarn element was defined by the differential form of Newton's law of cooling.

$$d\dot{Q}_{conv} = h\,(T_1 - T_2)\,dA_2 \qquad [4.18]$$

where the differential surface area dA_2, was given by the geometry.

$$dA_2 = \pi\, D\, dz \qquad [4.19]$$

The convection coefficient h characterized the boundary layer where buoyant, viscous and gravitational forces affect heat transfer. Boundary layer flow can be turbulent or laminar and its analysis and modeling require very involved fluid mechanics. Since there was no fan or blower to force convection, the gas flow rate within the premelting chamber was assumed to be low, so that free or natural convection was a good approximation.

Radiation Mechanism

The towpreg yarn was suspended within the tube by the braking tension applied by the pay-out capstan. The towpreg yarn element was assumed to be centered substantially evenly within the tube liner and therefore exposed equally to the entire cylindrical emitting surface.

Radiation from the tube liner was incident onto the yarn. Similarly, radiation was emitted by the yarn.

$$d\dot{Q}_{rad} = d\dot{Q}_{\text{ radiation } 1,2} - d\dot{Q}_{\text{ radiation } 2,1} \qquad [4.20]$$

For radiation between two long coaxial cylinders, a two-zone enclosure approach provided the relationship in terms of an equivalent radiation network of potentials and thermal resistancances in series [5,12,13,14]. The net radiant heat flow rate $d\dot{Q}_{rad}$ from the stainless steel tube liner differential unit at temperature T_1 to the towpreg yarn differential unit at T_2 was defined. The numerator of this expression was the driving thermal potential while the components of the denominator represented the pertinent thermal resistance.

$$d\dot{Q}_{rad} = \frac{\sigma\left(T_1^4 - T_2^4\right)}{\dfrac{1-\varepsilon_1}{dA_1\,\varepsilon_1} + \dfrac{1}{dA_1\,F_{1,2}} + \dfrac{1-\varepsilon_2}{dA_2\,\varepsilon_2}} \qquad [4.21]$$

The incremental radiating surface area dA_1 of the steel tube liner with interior surface diameter D_T was known by the geometry.

$$dA_1 = \pi \, D_T \, dz \qquad [4.22]$$

4.2.2.3   Quasi-Steady-State Scalar Preheat Model

The energy balance was expanded to represent each component.   [4.23]

$$c_p \, dm \left(\frac{\partial T_2}{\partial t}\right) = A_z k_z \left[\left(\frac{\partial T_2}{\partial z}\right)_L - \left(\frac{\partial T_2}{\partial z}\right)_R\right] + h \left(T_1 - T_2\right) dA_2 + \frac{\sigma \left(T_1^4 - T_2^4\right)}{\dfrac{1-\varepsilon_1}{dA_1 \, \varepsilon_1} + \dfrac{1}{dA_1 \, F_{1,2}} + \dfrac{1-\varepsilon_2}{dA_2 \, \varepsilon_2}}$$

Division of both sides by dz allowed for the application of the fundamental definition of the second derivative to the conduction term. On simplification, the time dependent integral form of the model was defined.

$$\frac{\rho \, D^2}{4} c_p \left(\frac{\partial T_2}{\partial t}\right) = \frac{D^2 k_z}{4} \left(\frac{\partial^2 T_2}{\partial z^2}\right) + h \, D \left(T_1 - T_2\right) + \frac{\sigma \left(T_1^4 - T_2^4\right)}{\dfrac{1-\varepsilon_1}{D_T \, \varepsilon_1} + \dfrac{1}{D_T \, F_{1,2}} + \dfrac{1-\varepsilon_2}{D \, \varepsilon_2}} \qquad [4.24]$$

The time dependence of the equation was reduced to a quasi-steady-state by multiplying the left hand side by dz/dz and again recognizing the processing speed v. The sign of the conduction term was changed to negative to reflect the observation that the axial conduction heat flow occurred in the negative z-direction. The scalar quasi-steady-state energy balance for the system was therefore defined.

$$\frac{\rho \, v \, D^2}{4} c_p \left(\frac{dT_2}{dz}\right) = -\frac{D^2 k_z}{4}\left(\frac{d^2 T_2}{dz^2}\right) + h \, D \, (T_1 - T_2) + \frac{\sigma\left(T_1^4 - T_2^4\right)}{\dfrac{1-\epsilon_1}{D_T \, \epsilon_1} + \dfrac{1}{D_T \, F_{1,2}} + \dfrac{1-\epsilon_2}{D \, \epsilon_2}} \qquad [4.25]$$

4.2.3 The Bar Contact Heat Transfer Model

Within approximately a 2cm length just prior to the bar initial point of contact with the bar surface, the towpreg transformed from a primarily cylindrical cross section to a rectangular cross section as described in Chapter 3. This symmetry transition was considered insignificant to the preheat heat transfer and was simply treated as though the transformation from cylindrical to rectilinear were instantaneous at the initial contact with the first bar. This approximation required a discontinuity between the heating process model components.

Unlike the preheat model, in cylindrical coordinates, the conduction with the bar surfaces lent itself to rectilinear coordinates. Figure 4.13 illustrates the preferred geometry.

$$k_z \frac{\partial^2 T_2}{\partial z^2} + k_y \frac{\partial^2 T_2}{\partial y^2} + k_x \frac{\partial^2 T_2}{\partial x^2} \, g = \rho \, c_p \frac{\partial T_2}{\partial t} \qquad [4.26]$$

Assumption #1 $\qquad\qquad g = 0 \;\; (W \, m^{-3}) \qquad\qquad [4.27]$

Assumption #2 $\qquad\qquad \dfrac{\partial T_2}{\partial x} = 0 \qquad\qquad [4.28]$

The heat generation term was assumed to be zero. As a first approximation, symmetry was advantageously interpreted such that the temperature variation across the width of the towpreg (x-direction here), in the rectilinear conduction equation, was considered insignificant.

The towpreg temperature just prior the first bar contact was uniform and known by the previous preheat model. A boundary condition of the third kind was assumed such that the heat flux at the free boundary surface was by convection with the ambient gas fluid. The radiation at the surface was ignored as an approximation. This imposed a limitation to the model's validity, however, based on precedence in the literature [13], this approximation was not expected to affect the overall bar contact conduction process significantly.

B.C. #1 $T_2\big|_{z=1.0} = T_p$ [4.29]

B.C. #2 $k_y \dfrac{\partial^2 T_2}{\partial y^2} = h_{gas}\left(T_{gas}-T_2\right)\big|_{y\,=\,thickness}$ [4.30]

The heat transfer which occurred at the bar contacts was modeled by the two dimensional equation in which the q.s.s. towpreg temperature profile was obtained by, again, reducing the time dependence by application of the axial velocity v to the conduction equation.

$$\left(\frac{\partial T_2}{\partial z}\right)_{q.s.s.} = \frac{1}{v\,\rho\,c_p}\left(k_z\,\frac{\partial^2 T_2}{\partial z^2} + h_{gas}\left(T_{gas}-T_2\right)\big|_{y\,=\,thickness}\right)$$ [4.31]

The heat transfer which occurred at the bar contact region was considered in two spatial dimensions rather than scalar since 1) composites are known to exhibit non-isotropic thermal conductivity and 2) the time interval of contact was usually less than 1/20th of a second. The resulting temperature gradients through the height of the axial cross section (y-direction here), were expected to be significant and therefore an equivalent scalar representation for the heating was not considered appropriate. Later in this chapter, the q.s.s temperature distributions were solved at four, equally spaced locations throughout the height of the cross section, and were subsequently averaged to represent mean scalar towpreg temperatures at q.s.s.

4.3   Model Evaluations

The restated goal of this evaluation was to solve for the q.s.s. heating profile as a function of processing variables. The primary control parameters for the premelting chamber heat transfer included take-up rate v, and tube liner surface temperature T_l. The velocity was set by an analog dial and the steady-state T_l temperature profile was measured as a function of position-z. Material specific variables were determined by experimentation or were obtained from the literature. Geometrical considerations were measured. Models were evaluated numerically as the exact solutions for the relationships were considered beyond the scope of this analysis. The preheat model solution was approximated by iteration while the bar contact model was approximated by finite difference representation. The preheat model was compared to experimentally obtained q.s.s. profiles for similar processing conditions and a good correlation was observed.

4.3.1   Parameter Evaluation

Several material parameters (e.g. D, D_T, ρ, ε_1, ε_2, c_p, h, k_z and k_y) were determined experimentally or by comparison with published values.

Tube Liner Surface Temperature Profile $T_1 = f\{z\}$

The temperature of the tube is a function of the heat transfer relationships between the heater elements and the tube.   As discussed in Chapter 3 thermocouple leads were welded directly onto the tube surface and temperature profile experiments were conducted which characterized the tube liner surface for a given set of oven control zone set temperature values.   For most zone set values, the temperature profile of the tube liner was hottest near $L/2$ and coolest at $z = 0$ and $z = L$.   The typical experimentally measured temperature profile could be approximated by a 5th order polynomial relationship with z as the operator.

Conductivity of the Towpreg

The axial conductivity of the towpreg was known to be dependent on the mass fraction of the constituent components according to the rule of mixtures [15].   The conductivity of carbon fibers is more than 100 times that of the polymer and therefore dominated conductivity [16].   The temperature dependence of composite conductivity was expected to be weak within the area of interest (20-500°C).   Thermal conductivity of the voidy towpreg was assumed constant and equal to published values, $k_z = 6.0$ (W

$m^{-1}K^{-1}$) and k_y = 0.72 (W $m^{-1}K^{-1}$), for APC-II® prepreg of fiber volume 60% at room temperature [17].

Free Convection for an Enclosed Cylindrical Annulus

For horizontal pipe openly exposed to air at atmospheric pressure, the convective coefficient could be approximated by 1.00E-4 $(\Delta T/D)^{1/4}$ in terms of (cal s^{-1} cm^{-2} K^{-1}) [3]. The coefficient of free convection h in enclosed spaces has been studied in detail and is at substantial variance with the previously stated approximation. For an enclosed cylindrical annulus, the isothermal free convection coefficient was determined [5] to be a function of the mean heat transfer coefficient h_m and the A_m mean area.

$$h = h_m A_m \qquad [4.32]$$

For a cylindrical annulus the mean area was known where A_o (m^2) and A_i (m^2) represented the surface areas of the outer and inner cylinders respectively.

$$A_m = \frac{A_o - A_i}{\ln\left(\frac{A_o}{A_i}\right)} \qquad [4.33]$$

The mean convection was defined as a function of the Nusselt number Nu_δ the gas conductivity k (W m^{-1} K^{-1}) and the thickness of the fluid layer δ (m).

$$h_m = Nu_\delta \frac{k}{\delta} \qquad [4.34]$$

For an annulus the fluid layer thickness is known to be a function of the geometry where D_o (m) and D_i (m) represented the diameters of the outer and inner cylinders.

$$\delta = \frac{D_o - D_i}{2} \qquad [4.35]$$

The Nusselt number is an empirical function of the Rayleigh number Ra_δ.

$$Nu_\delta = c \, (Ra_\delta)^n \left(\frac{H}{\delta}\right)^m \qquad [4.36]$$

Here, the height of the fluid layer H (m) was assumed equal to the thickness of the fluid layer in the annulus δ. The Rayleigh number is the product of the Grashof Number and the Prandtl Number.

$$Ra_\delta = Gr_\delta \, Pr \qquad [4.37]$$

For air, the Prandtl number is 0.72, representing the ratio of molecular diffusivity of momentum to the molecular diffusivity of heat. The molecular diffusivity of momentum v (m^2 s^{-1}) is the ratio of the gas viscosity to density. The acceleration due to gravity g (m s^2) is a known constant. The film temperature T_f (K) was assumed to be the mean value between the hottest temperature T_h (K) (on the tube liner surface) and the coolest T_c (K) temperature (on the towpreg surface) .

$$Gr_\delta = \frac{g \, \beta (T_h - T_c) \, \delta^3}{v^2} \qquad [4.38]$$

$$\beta = \frac{1}{T_f} \qquad [4.39]$$

$$T_f = \frac{1}{2}(T_h + T_c) \quad .$$ [4.40]

The empirical coefficients n and c are determined by the geometry. Rayleigh Number and Prandtl Numbers. For air, where the uniform gas temperature was 793K and the cooler body was 293K, the literature [5] values for conductivity k and kinematic viscosity v were obtained at the film temperature. The isothermal convectivity at the film temperature, for concentric cylinders similar to those modeling the heat transfer in this analysis, were calculated near 0.2105 $(W\ m^{-2}K^{-1})$.

View Factor for Concentric Cylinders $F_{1,2}$ and $F_{2,1}$

The view factor $F_{1,2}$ is defined by the ratio of D_T to D and L. For a tube furnace liner where $2L/D_T$ is greater than about 3, the view factor value is linear with the ratio of the diameters [5]. Here $2L/D_T = 32.9$ and $D/D_T = 0.002$, so that $F_{2,1} = 0.002$. The view factor of the tube liner to itself is the compliment to $F_{2,1}$ such that $F_{1,1} = 0.998$. The view factor of the towpreg yarn to the tube liner is $F_{1,2}$ the same as $F_{1,1}$.

Emissivity of the Tube Liner and Towpreg ε_1 and ε_2.

The tube liner emissivity can be found by comparison with published values for similar materials at similar temperatures. The tube liner was constructed of a non-magnetic, low 300 series stainless steel which "stained" from oxidation at elevated temperatures but did not build-up a heavy oxide layer. A published curve [5] for the hemispherical emissivity, within the temperature range (400°C-500°C) of normal

premelting chamber operating conditions, indicated a nominal range of $\varepsilon_1 = 0.21$ to 0.23 for 301 stainless steel.

The dry powder towpreg consisted primarily of black carbon filaments so the towpreg emissivity ε_2 was assumed to be constant with respect to any phase change experienced by the powder. This assumption allowed for the direct measurement of ε_2 from the consolidated ribbon product rather than from the powder towpreg.

McDonnell Douglas Aircraft (MDA) Company is a consumer of these towpreg ribbons and utilizes CO_2 and YAG laser technology as the primary heat source for robotic placement of thermoplastic ribbon. Consequently, MDA is concerned with the ribbon spectral properties at the corresponding wavelengths. Since the samples were opaque at the wavelengths measured, the Kirchoff's law emissivity curve for a typical polyimide, carbon-fiber ribbon was generated. Total hemispheric reflectance measurements were performed by B. Shawgo, on an IBM IR-38 FTIR with a Labsphere integrating sphere for the 2.5-14 μm band and a Perkin-Elmer Lambda-19 for the 0.200-2.5 μm band. Both measurements were performed using the 8-degree, angle-of-incidence port of the integrating sphere. Emissivity was equal to one minus the reflectance over the range of the experiment.

An independent verification for both the emissivity of the tube liner and that of the ribbon was performed by R. Wright at NASA Langley Research Center. Ambient temperature measurements of spectral specular and diffuse reflectance over the 2.5-16.4 mm range were taken with a custom grating spectrophotometer. Emissivity of the composite ribbon was found to be 0.81 and 0.78 at wavelengths corresponding to

450°C and 145°C respectively. The tube liner sample exhibited emissivities of 0.32 and 0.30 at wavelengths corresponding to 450°C and 300°C. The uncertainties in these data were estimated to be ±0.03 based on comparison with calibrated standards. Wright's measurements were only slightly at variance with Shawgo's ribbon emissivity and the published values for the tube liners emissivity. This comparison gives reasonable confidence in the measured emissivity values.

The approximately linear dependence, shown in **Figure 4.8**, of emissivity ε_2 on wavelength was moderate within the range of 1 to 10 (μm) dropping from 0.92 to 0.80. The corresponding relationship for emissivity of the towpreg yarn as a function of towpreg temperature T_2 was assumed constant over the range of normal use temperatures.

Specific Heat of the Towpreg C_p

The composite specific heat was measured directly with a DuPont 910 Differential Scanning Calorimeter. **Figure 4.9** is the differential calorimetric plot of a sample of a neat polyimide powder (Aurum™-400A), while **Figure 4.10** is the corresponding plot of the composite towpreg (Aurum™-400A/IM-7 @ resin content approximately 35% by weight in each case). The heat flow of the sample was compared to the heat flow of an empty reference pan. In accord with the manufacturer's recommended method, the heat capacity was defined [18].

$$C_p = \frac{60 \, E \, \Delta qs}{Hr} \frac{\Delta Y}{m} \qquad [4.41]$$

E was the calorimeter cell calibration coefficient at the average temperature of the range (dimensionless), Δqs was the y-axis range scaling in (mW cm^{-1}), Hr was the heating rate in (°C min^{-1}), ΔY was the difference in y-axis deflection between sample and blank curves at the temperature of interest (cm), m was the sample mass (mg). The heat capacity C_p was expressed in terms of (J g^{-1} K^{-1}). The experimentally determined heat capacity was conveniently approximated by a linear fit with absolute temperature.

Towpreg Density and Diameter

Void content had an important effect on the towpreg density and the nominal diameter of towpreg during the heating process. A simplistic approach was utilized where the values for density and diameter were corrected for void volume fraction v_v by comparison to the void-free composite values. The density of a void-free ribbon sample ρ_o could be measured via ASTM D-3171.

$$\rho = \rho_o (1-v_v) \qquad [4.42]$$

The cross sectional area of a void-free ribbon of width x (m) and thickness y (m) was defined here as A_{min}. The cross section of a void-free towpreg would have a similar area, so the theoretical diameter of a cylindrical void-free towpreg would therefore be defined.

$$D_{min} = \sqrt{\tfrac{4}{\pi} A_{min}} \qquad [4.43]$$

By applying a void volume, the nominal diameter of the towpreg was defined in terms of the void content, which also indicated the bulk of the towpreg.

$$D = \sqrt{\tfrac{4}{\pi}\,(1+v_v)\,A_{min}} \qquad [4.44]$$

4.3.2 Numerical Solution of the Models

The temperature dependent heat capacity, void content dependent density and diameter, and the non-isothermal tube liner temperature profile were all included in the preheat model solution. Two approximations were made which limited the accuracy of the model. Axial thermal conductivity of the voidy towpreg was assumed independent of temperature and the view factor was assumed independent of position-z. The isothermal conductivity approximation tended to slightly overestimate the cooling due to axial conduction while the constant view factor approximation tended to over-predict heating near the tube exit and entrance regions. Fiber volume fraction was neglected as a trivial variation of the model, since the heat capacity of the composite towpreg was utilized rather than a "rule of mixtures approach".

The exact solution to the premelting model ordinary differential equation did not need to be evaluated. A numerical algorithm was utilized to solve the model by iterative approximation. A commercially available software package called *Mathematica* and a Macintosh 960 with 36MB of RAM provided a convenient tool to solve for the approximate solution of the scalar ordinary differential equation by the NDSolve command. The NDSolve function was restricted to ordinary differential equations and required "initial conditions" for the operator and its derivatives. **Appendix C** is a copy

of a typical *Mathematica®* file which lists the code for the q.s.s. preheat model on the first two pages and the solution for a take-up speed of 25 (cm s⁻¹) plotted on the third.

Comparison Between Theoretical and Experimental

Theoretical heating profile predictions were generated numerically for several different throughput velocities. These profiles, the experimental tube liner temperature profile and the experimental data of **Figure 4.5** were superposed in **Figure 4.11**. A constant towpreg void content of 50% was assumed. Note that this void content was a little higher than the 40% to 45% void fraction observed in the microstructure analysis of Chapter 3. However, the thermocouple wire and its insulation took-up space within the tow and effectively contributed to the void content. The correlation between the theoretical scalar q.s.s. profiles and the measured q.s.s. temperature profiles was good. An increase in throughput velocity from 2.5 (cm s⁻¹) to 25 (cm s⁻¹) was predicted to result in nearly a 250°C difference in the towpreg preheat temperature Tp which corresponded to the location z = 1 (m).

Experimental observations indicated the presence of a neck-down or debulking phenomenon occurring as a result of polymer softening. This effect confused the assignment of a constant towpreg void content v_v because it suggested a more complicated dependence of the thermodynamic state of the matrix material. Rather than attempt to predict the void content directly, a parametric comparison of experimental towpreg temperature and model values were superposed in **Figure 4.12**. Near the entrance of the furnace, the data seemed to match more closely with the 70% void volume model. An apparent transition of void content was observed as the

material heated and translated through the tube where near the bar contact position, the data matched more closely the 50% void volume curve. This was consistent with experimental observations and made sense since as the polymer softened, local melt flow occurred and wet-out the fibers and therefore void content was reduced.

4.3.3 Bar Contact Temperature Model Solution and Evaluation

The heat transfer which occurred at the bar contact region was approximated by simple conduction. In situations where the preheat temperature T_p was sufficiently different than the bar surface temperature T_b, substantial temperature gradients were expected in the thickness direction (y-dimension). Finite difference approximations for the solutions provided the two-dimensional temperature distribution within the towpreg. The mean temperatures for each z-position were considered to represent the average scalar towpreg temperature at q.s.s.

Node Array Definition

The two bar contacts were modeled as a single continuous contact length Lz (m).

$$Lz = D \, \theta / 2 \qquad [4.45]$$

In terms of heat transfer, the width in the x-direction and the thickness of the towpreg in the y-direction were assumed constant for the duration of the contact. **Figure 4.13** illustrates surface nodes and boundaries for the model. The towpreg moved in the positive z-direction from nodes with m = 0 to m = M. The thickness of the towpreg

was also divided into an integer number of nodes ranging from i = 0 to i = I. The cell array (M by I) was divided into convenient increments of (thickness)/M = Δy and L_z/I = Δz.

The numerical approximation for the q.s.s. bar contact differential equation solution could have been obtained by an explicit finite-difference method or an implicit Crank-Nicholson method. Here, the explicit methods were utilized which provided reasonable solutions provided the stability criterion were met for each calculation.

Conducting Nodes

For the boundary nodes in contact with the bars and each of the interior conducting nodes $0 \le m < M$ and $0 \le i < I$, approximate solutions were obtained in terms of non-isothermal conductivity's k_z and k_y. The finite difference representations of the first and second derivatives of temperature in the two spatial directions z and y were known.

$$\frac{\partial T}{\partial z} = \frac{T_m^{i+1} - T_m^i}{\Delta z} \qquad [4.46]$$

$$k_z \frac{\partial^2 T}{\partial z^2} + k_y \frac{\partial^2 T}{\partial y^2} = \frac{k_z \left(T_m^{i-1} + T_m^{i+1} - 2 T_m^i\right)}{(\Delta z)^2} + \frac{k_y \left(T_{m-1}^i + T_{m+1}^i - 2 T_m^i\right)}{(\Delta y)^2} \qquad [4.47]$$

The anisotropic thermal diffusivities α were known in terms of other material properties. The finite difference approximations for the first and second derivatives were substituted into the q.s.s. bar contact heating model.

$$\frac{T_m^{i+1} - T_m^i}{\Delta z} = \frac{\alpha_z}{v} \frac{(T_m^{i-1} + T_m^{i+1} - 2\,T_m^i)}{(\Delta z)^2} + \frac{\alpha_y}{v} \frac{(T_{m-1}^i + T_{m+1}^i - 2\,T_m^i)}{(\Delta y)^2} \qquad [4.48]$$

where,
$$\alpha_z = \frac{k_z}{\rho\,c_p} \qquad [4.49]$$

and
$$\alpha_y = \frac{k_y}{\rho\,c_p} \qquad [4.50$$

The previous equation was rearranged and simplified to provide the approximation for the temperature of the node at location m,i+1 under q.s.s. constraints.

$$T_m^{i+1} = \left(\frac{1}{\Delta z} - \lambda_z\right)^{-1} \left[\frac{T_m^i}{\Delta z} + \lambda_z \left(T_m^{i-1} - 2\,T_m^i\right) + \lambda_y \left(T_{m-1}^i + T_{m+1}^i - 2\,T_m^i\right) \right] \qquad [4.51]$$

where,
$$\lambda_z = \frac{\alpha_z}{v\,(\Delta z)^2} \qquad [4.52]$$

and
$$\lambda_y = \frac{\alpha_y}{v\,(\Delta y)^2} \qquad [4.53]$$

These relationships were subject to stability constraints and a rational solution constraint.

$$\lambda_z \geq \frac{1}{2} \leq \lambda_y \qquad [4.54]$$

$$\left(\frac{1}{\Delta z} - \lambda_z\right) > 0 \qquad [4.55]$$

Convecting Nodes

The finite-difference approximation for the boundary nodes $m = M$ which were all subject to convection, was similarly derived from the boundary condition with the additional consideration for the effects of heat capacitance.

$$h_{gas}\left(T_{gas} - T_M^i\right) + \frac{k_y}{\Delta y}\left(T_{M-1}^i - T_M^i\right) = \frac{\rho\, c_p\, v\, \Delta y}{2\,\Delta z}\left(T_M^{i+1} - T_M^i\right) \tag{4.56}$$

The approximation for the surface boundary node temperature at a location one unit forward in the z-direction T_M^{i+1}, was obtained in terms of the q.s.s. assumption.

$$T_M^{i+1} = T_M^i + \frac{2\,\Delta z}{\rho\, c_p\, v\, \Delta y}\left[h_{gas}\left(T_{gas} - T_M^i\right) + \frac{k_y}{\Delta y}\left(T_{M-1}^i - T_M^i\right)\right] \tag{4.57}$$

Simultaneous Node Temperature Evaluation Method

A Microsoft™ Excel spread sheet was utilized to evaluate the solutions with increasing m and i step values corresponding to increasing y and z positions respectively. As a matter of convenience the thickness was divided into 3 unit cells. Since nodes were on cell boundaries, this required $M = 3$. Nodes with $m = 0$ corresponded to the bar contact surface nodes and nodes with $m = 3 = M$ corresponded to the free surface nodes. The other nodes were experiencing pure conduction. **Figure 4.14** illustrates the q.s.s. temperature profiles for each set of m nodes. The material parameter values for this analysis are listed in **Table 4.1**.

Table 4.1   Conduction Model Constant Values Utilized in Analysis

Conduction Model Variables
$k_z = 6.0 \left(\frac{W}{mK}\right)$
$k_y = 0.72 \left(\frac{W}{mK}\right)$
$c_p = 1.8 \left(\frac{J}{gK}\right)$
$h_{gas} = 0.2105 \left(\frac{W}{m^2 K}\right)$
$\rho = 1.104 \left(\frac{g}{cm^3}\right)$ @ 20% void content

The contact length was known to be a defined by the bar template geometry. The towpreg thickness during all of the contact was assumed to be 2.13E-4 m. The stability criterion for all nodes was satisfied by appropriate selection of Δz and Δy values which were not necessarily equal to each other. The temperature of the gas T_{gas} was assumed equal to the measured bar surface temperature $T_b = 663K$.

The average q.s.s. towpreg temperatures were calculated from the four node temperatures corresponding to each i-location, and were then plotted in **Figure 4.15** as a function of take-up speed. The preheat temperatures calculated for each throughput velocity, by the preheat temperature model, were indicated at location 1m. The maximum attainable temperature T_{max} was shown just prior to the towpreg exiting from the bar. The average towpreg temperature was predicted to change as the contact occurred.

At higher throughput speeds, not only was the preheat temperature lower, but the maximum temperature experienced by the towpreg was lower. For a throughput velocity of 12.19 (cm s^{-1}), the bar contact temperature model predicted approximately 50°C increase in average towpreg temperature, which was consistent with experimental observations for the same processing parameters.

4.3.4 Scalar Overlay of Heating Process

Figure 4.16 provides an example of theoretical temperature profiles at several processing rates. These processing conditions could be useful for a thermoplastic polyimide powder towpreg with a glass transition temperature above 250°C and a desired processing temperature between 300 to 350°C. Theoretical q.s.s., preheat towpreg temperature profiles, for an oven setting of 455/450/455°C, were calculated between 0 and 1.2 meters. Next, the preheat temperature at 1m was utilized as the starting temperature for the bar contact model within the range of contact $(1 < z \leq 1+L_z)$. As an illustrative approximation, the q.s.s. towpreg temperatures correlating to positions downstream from the last bar contact and upstream from the tube exit plane were obtained by simply shifting the residual preheat profile values upward to reflect the bar heating.

4.4   Observations and Suggestions

Temperature Measurements

The thermal history of the towpreg material was measured by incorporating a thermocouple lead into the towpreg. The time scale of the measurement technique was such that the measured changes in towpreg temperature were strictly valid at heating or cooling rates below 500 ($^{\circ}$C s^{-1}) only. The preheating phenomenon met this criterion. Under nominal processing conditions, with a substantial difference between the preheat temperature T_p and the bar surface temperature, T_b, the measured bar contact heating rates were not valid.

Preheat Modeling

The preheating heat transfer phenomenon was modeled and evaluated in scalar form. The scalar representation correlated well with measurements. Preheating was primarily driven by radiation from the tube liner and axial conduction opposing the relative velocity of the towpreg. Processing speed and furnace set temperatures were the most important variables for determining the q.s.s. preheat temperature profile. This heat transfer analysis has characterized the heating of the towpreg in terms of basic material properties, processing parameters and geometrical considerations. The approximations and assumptions did not substantially limit the accuracy of the theoretical model solutions.

The scalar preheat temperature model reasonably mimicked the observed preheating phenomenon. Process control could be implemented by utilizing the model to predict the q.s.s. profiles up to 1m and therefore would be useful for determining T_p. The

preheating temperature was not, however, strictly equal to the maximum temperature normally attained by the material.

Bar Contact Heat Transfer Modeling

The bar contact heat transfer phenomenon was modeled and evaluated first in two spatial dimensions. Several temperatures through the thickness were averaged to provide a scalar representation of the q.s.s. mean towpreg temperature profile. The scalar representation of the towpreg temperature increase, caused by contact with the stationary bars, provided a reasonable first approximation. Heating was driven by conduction with the bar surfaces. The two dimensional analysis revealed the potential for substantial temperature gradients throughout the towpregs thickness. This observation implied potential for non-isothermal bar contact squeeze flow at high or low processing speeds. Non-isothermal squeeze flow was considered undesirable in terms of steady-state operation and process control. An isothermal squeeze flow process control constraint was considered.

Overall Heating Profile

The two model components were integrated as an illustrative first approximation to demonstrate potential process thermal history scenarios. For a given set of processing conditions, velocities were considered too low if $T_p \gg T_b$ and too high if $T_p \ll T_b$.

Analysis of the heating models provided insight on the notion of process control at the region of the bar contact. At the bar contact, the towpreg was widened, flattened, voids were expelled and compressed, and some local flow occurred to provide limited wet-out of previously matrix-poor regions. A constraint for the process was chosen to impose the ideal processing situation. For the complex squeeze flow to occur under steady conditions, the entire cross section should ideally be isothermal. The isothermal preheating would ensure uniform viscosity throughout the cross section which was intuitively superior to having a viscosity distribution. **Figure 4.17** illustrates such a q.s.s. profile. The constraint would be defined so that the preheating temperature, the bar temperature, the maximum temperature and the desired processing temperature (from neat polymer rheometry) T^* were all equal.

$$T_p = T_b = T_{max} = T^* \tag{4.58}$$

In order to implement this process constraint, one needs to sample the tube liner temperature temperatures, interpolate the steady-state tube liner temperature profile, sense the bar surface temperature, and evaluate the model to determine the appropriate processing speed.

The utility of the heat transfer models extended beyond process control issues and contributed to process engineering and design. For a given set of process conditions, under the isothermal bar contact constraint, the process speed could be increased only by lengthening the tube liner or increasing the set temperature of the oven zones upstream of the bar contact location. The suggested processing speed subject to the previously described isothermal bar contact constraint (See **Figure 4.16**) would be

approximately 6.5 (cm s^{-1}). The model illustrates how by doubling the length of the tube furnace from 1.2 to 2.4 (m) nearly triples the processing speed. The oven zone set temperatures could be increased to allow for faster speeds, however, the risk of overheating during a momentary stoppage or slow-downs, would prohibit this approach in the extreme. The model also points out why actively heating the stationary bars would not increase processing speed under the isothermal bar contact constraint.

4.5   Future Heat Transfer Modeling

Continual on-line sensing of the tube liner surface temperature would provide a method to obtain a real-time preheat temperature prediction rather than actually sensing the towpreg temperature. If the heating models were integrated into a continuous coordinate system and a unified solution algorithm were developed, the real-time q.s.s. towpreg temperature profile could be utilized as a process control means.

As the towpreg approached and proceeded beyond the tube exit plane, cooling occurred because the towpreg was warmer than its surroundings. This cooling was primarily radiative and could be modeled similarly to the preheating model approach. Upon contact with the nip rollers, the towpreg was cooled and solidified. As a first approximation, this cooling could be modeled by the two dimensional heat conduction equation and analyzed by a finite difference approach.

4.6　End Notes

1　Hergenrother, P.M.; Bryant, R.G.; Jensen, B.J.; Havens, S.J. *J. Polym. Sci., A. Polym. Chem. Ed.*, **1995**, *35*, XX.

2　Welty X.; Wicks X.; Wilson X. "Fundamentals of Momentum, Heat & Mass Transfer", 2nd Ed.; John Wiley & Sons: New York, 1976.

3　Sears, F.W.; Zemansky M.W.; Young H.D. "University Physics", 6th ed.; Addison-Wesley : Reading Massachusetts, 1983, Chapter 15.

4　Van Wylen, G.J.; Sonntag, R.E.; "Fundamentals of Classical Thermodynamics", 3rd ed.; John Wiley & Sons: New York, 1986, Appendix A.

5　Ozisik M.N.; "Heat Transfer, A Basic Approach", McGraw-Hill: New York, 1985.

6　Birkebak R.C.; Sparrow E.M.; Eckert, E.R.G.; Ramsey J.W. *ASME J. Heat Trans. C,* **1964**, *86*, (2), 193-9.

7　Avallone E.A.; Baumeister T. "Marks' Standard Handbook for Mechanical Engineers", 9th ed.; McGraw-Hill, New York, 1987.

8　Sparrow, E.M. *ASME J. Heat Trans. C,* **1963**, *85*, (2), 81-8.

9　Perlmutter, M.; Howell J.R. *ASME J. Heat Trans. C,* **1964**, *86*, (2), 169-79.

10　Sparrow, E.M.; Loeffler, A.L.; Hubbard, H.A. *ASME J. Heat Trans. C,* **1961**, *83*, (4), 415-422.

11　Sparrow, E,M.; Albers L.U.; Eckert, E.R.G. *ASME J. Heat Trans. C,* **1960**, *84*, (2), 73-81.

12　Oppenheim, A.K. *ASME Trans.* **1956**, *78*, 725-35.

13　Zierling, M.B; Sarifim, A.F. *ASME J. Heat Trans. C,* **1966**, *88*, (3), 341-2.

14　Chipp R.E.; Viskanta R. *ASME J. Heat Trans. C,* **1966**, *88*, (3), 326-7.

15　Pitchumani, R; Yao, S.C. *J. Heat and Mass Trans.* **1992**, *35*, (9), 2185.

16   Lundblad, W.E.; Starrett, H.S.; Wanstall, C.W. *SAMPE Technical Series*, **1994**

26, 774-.

17   Ghasemi Nejad, M.N. University of Delaware, 1994, C.C.M. Report 92-52.

18   DuPont Company, Wilmington, DE, 1985, PM 9170037-002 Rev. A, 71-2.

4.7   Chapter 4 Figures
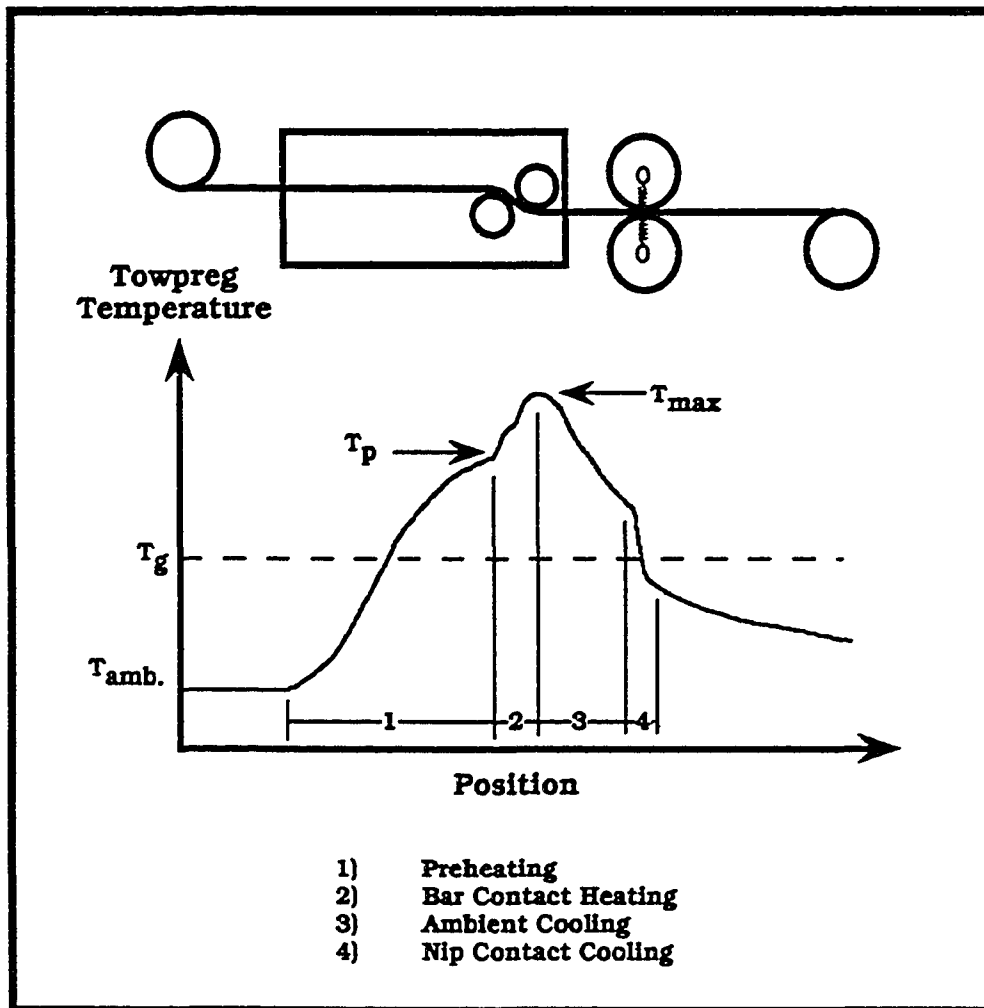
Figure 4.1   Expected Steady State Towpreg Temperature Profile
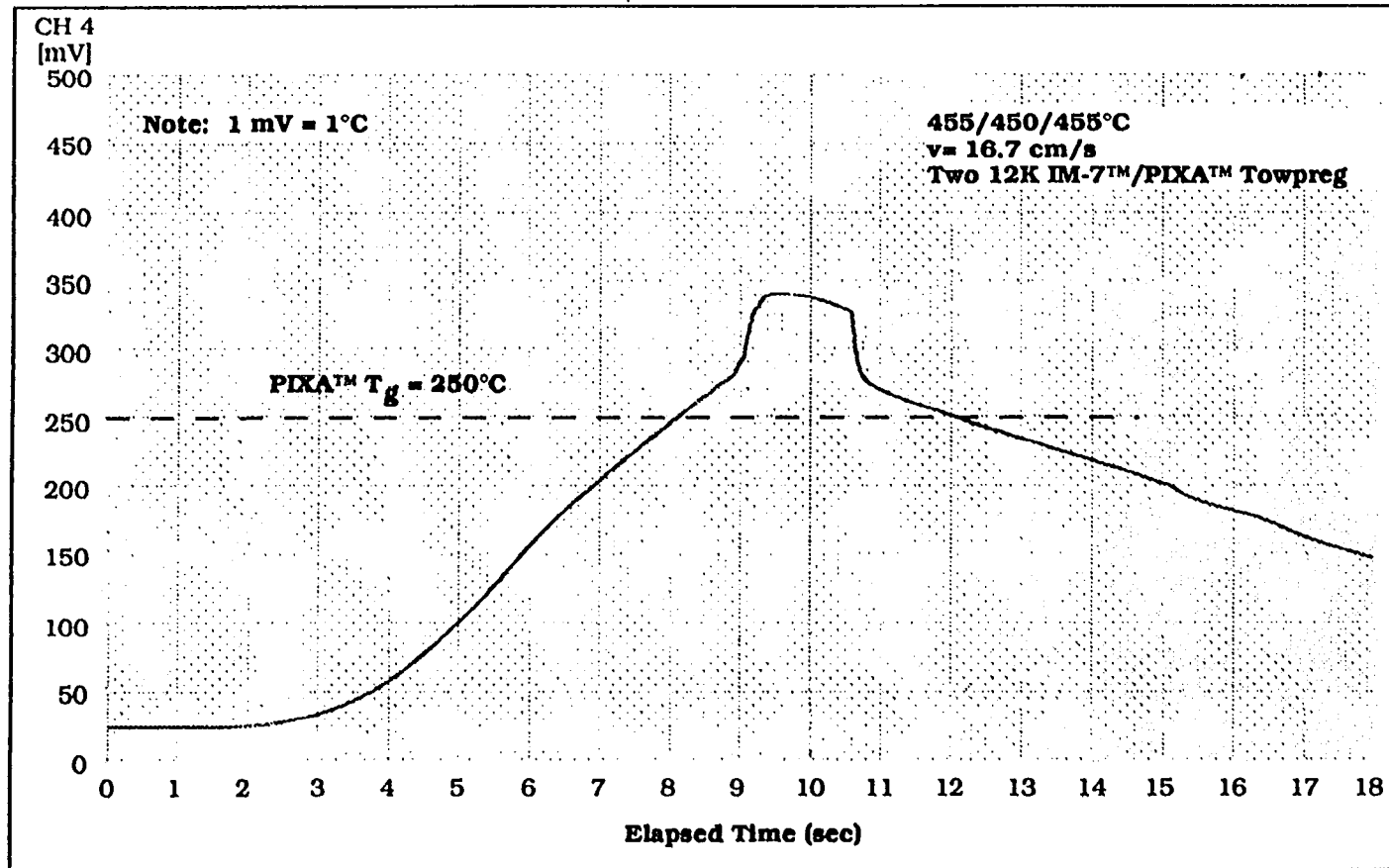
Figure 4.2 Typical Q. S. S. Towpreg Temperature Profile Data for Complete *Ex parte* Process
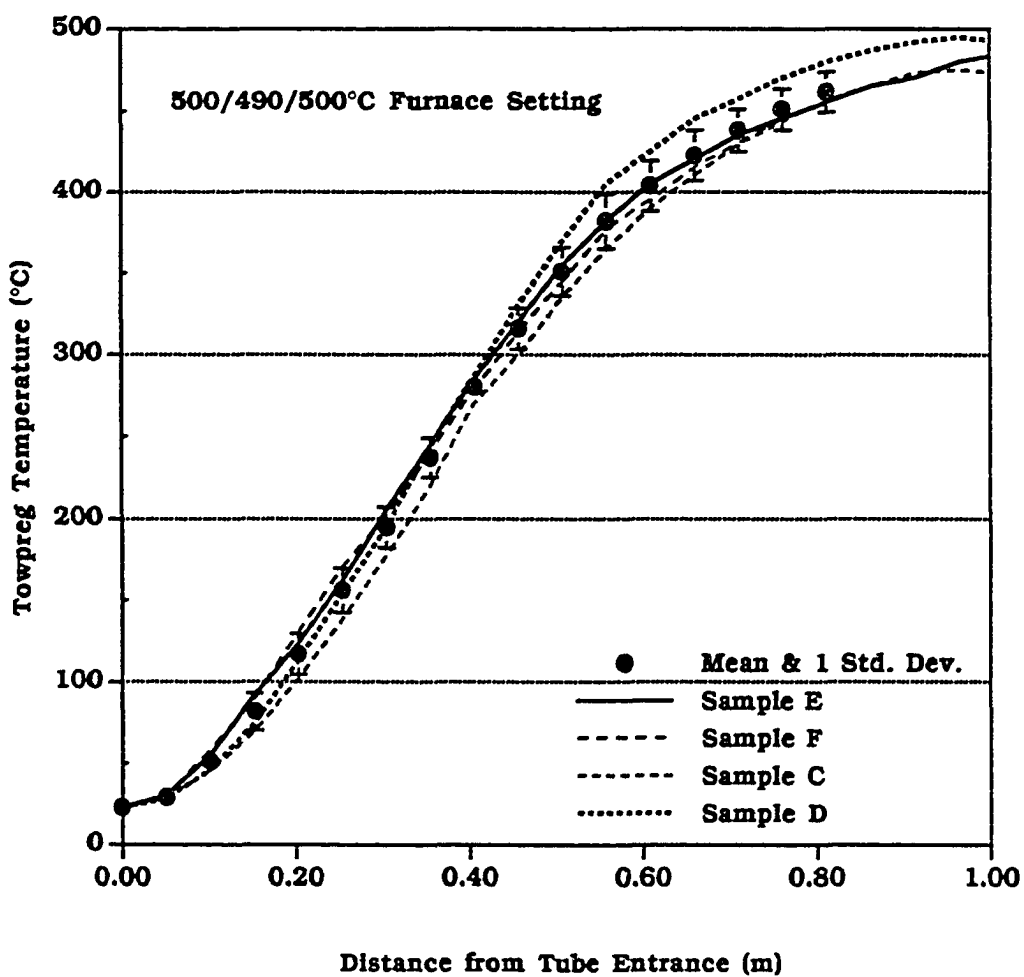
$$\frac{\text{Chart Position (m)}}{\text{Chart Speed} \left(\frac{m}{s}\right)} \times \text{Take-up Speed} \left(\frac{m}{s}\right) = \text{Q.S.S. Position (m)}$$

Figure 4.3 Repeatibility of Measured Q.S.S.Towpreg Temperature (T_2) Profiles
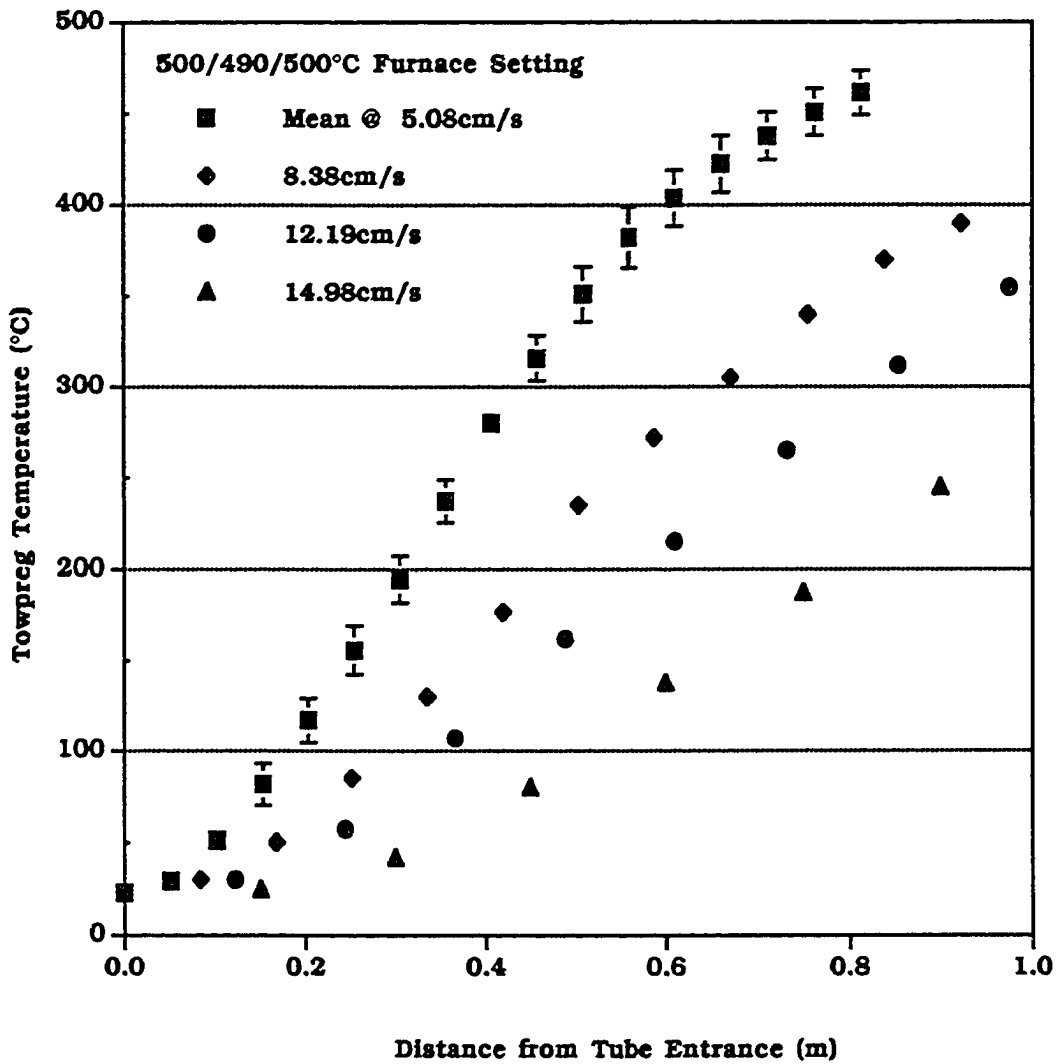
Figure 4.4 Effect of Velocity on Q.S.S. Measured Towpreg Temperature.
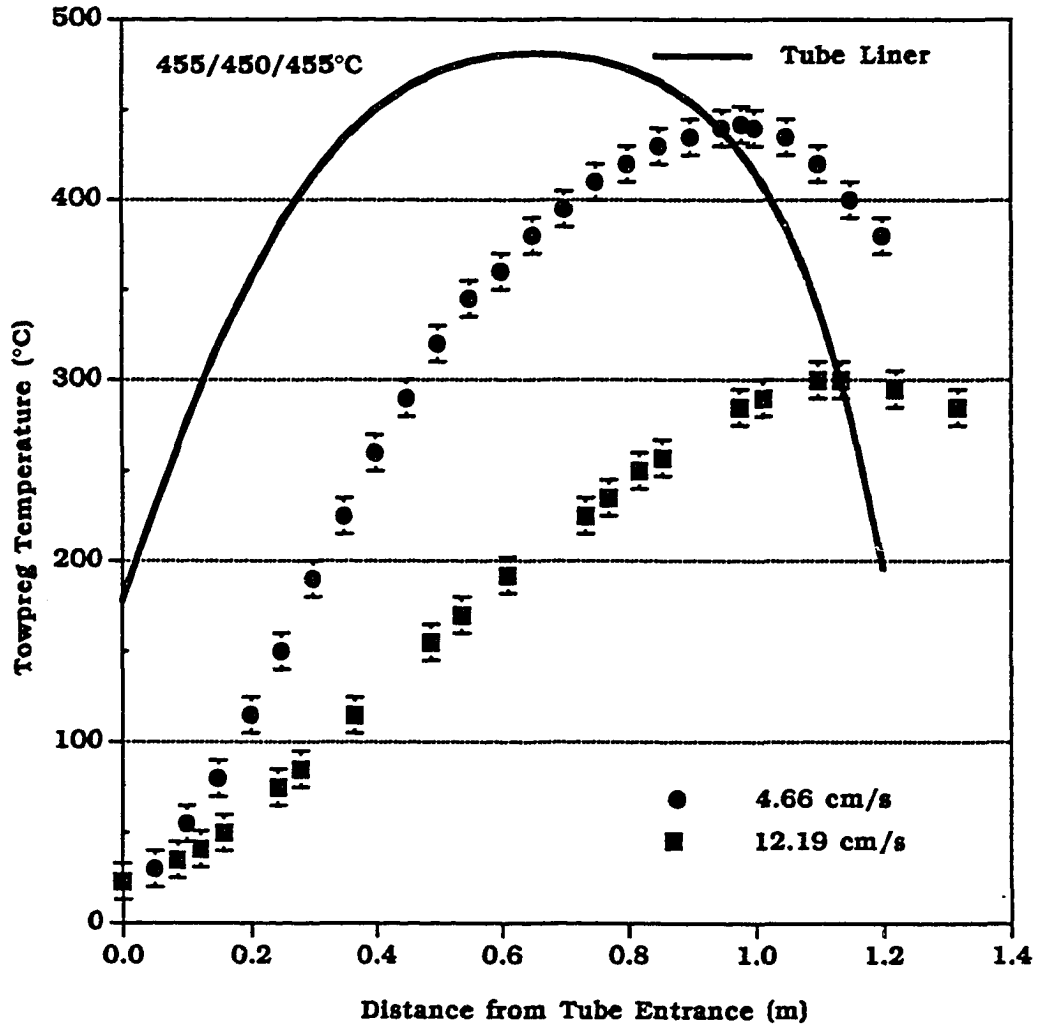
Figure 4.5 Measured Towpreg Temperature Profiles for Two Take-up Speeds
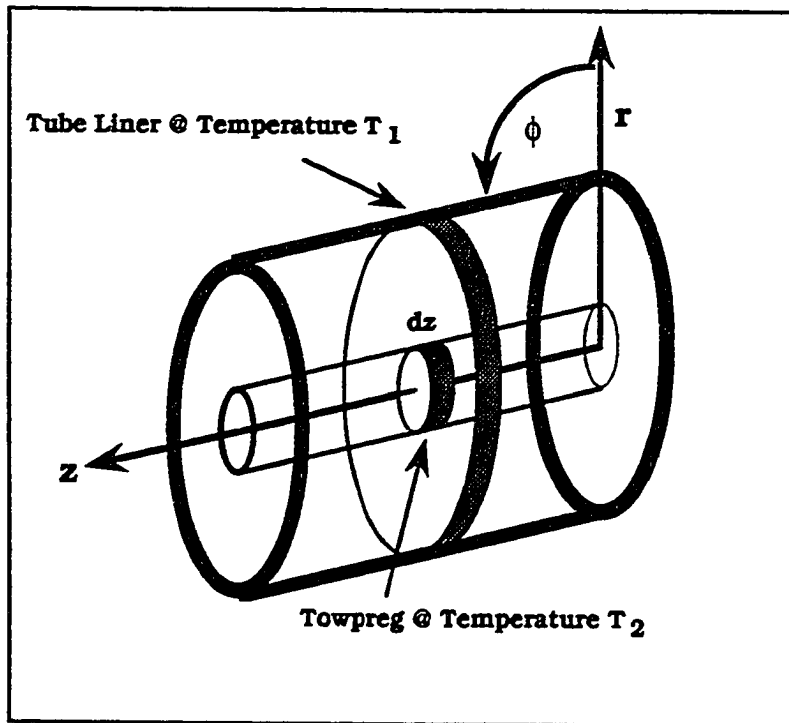
Figure 4.6 Isometric Illustration of Towpreg and Tube Liner in Cylindrical Coordinates

$$d\dot{Q}_{net\ rad.}\Big|_{r=D/2}$$

$$r$$

$$z$$

$$d\dot{Q}_{cond.L} \qquad dz \qquad d\dot{Q}_{cond.R}$$

$$d\dot{Q}_{stored}$$

$$L \qquad R$$

$$d\dot{Q}_{conv.}\Big|_{r=D/2}$$

$$\left(\frac{J}{s}\right)_{Stored} = \left(\frac{J}{s}\right)_{Flowing\ In} - \left(\frac{J}{s}\right)_{Flowing\ Out}$$

$$d\dot{Q}_{stored} = d\dot{Q}_{cond.L} - d\dot{Q}_{cond.R} + d\dot{Q}_{conv.}\Big|_{r=D/2} + d\dot{Q}_{net\ rad.}\Big|_{r=D/2}$$
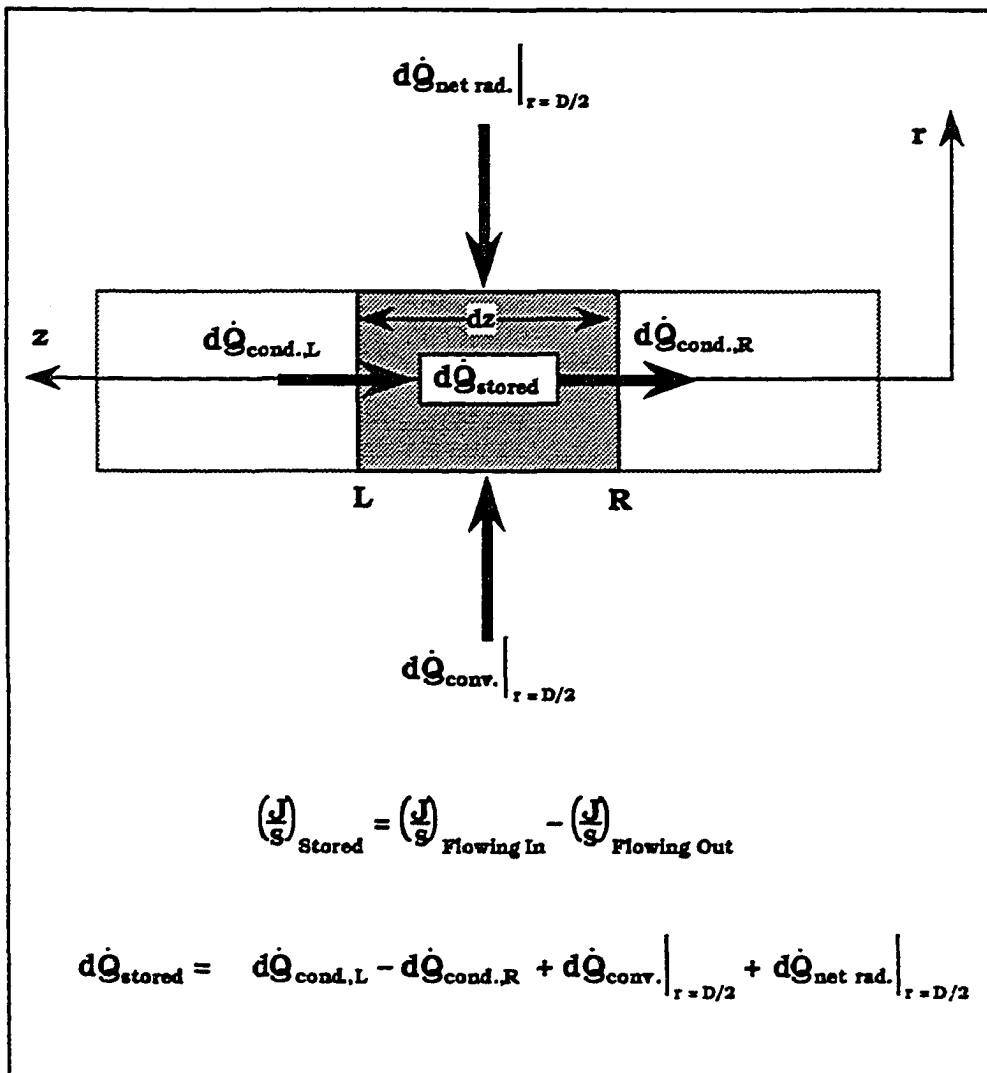
Figure 4.7 The Differential Towpreg Element Steady State Energy Balance

```
                                            Aurum^TM/IM-7^TM Ribbon

1.0

0.9

0.8
E  0.7
M
I  0.6        Perkin-Elmer Lambda-19
S            0.200-2.5μm band
S  0.5        IBM IR-38 FTIR
I            2.5-14 μm band                    Nd: YAG laser (1064nm)
V  0.4
I
T  0.3        Emissivity = (1-reflectance)
Y
0.3                                            Measurments Conducted and
                                               Provided by B. Shawgo
0.2                                            Dept. 254, Station 49088
                                               McDonnell Douglas Aerospace
0.1                                            St. Louis, MO. 63166-0516

0.0
    0    2    4    6    8    10   12   14   16
              WAVELENGTH (microns)
```
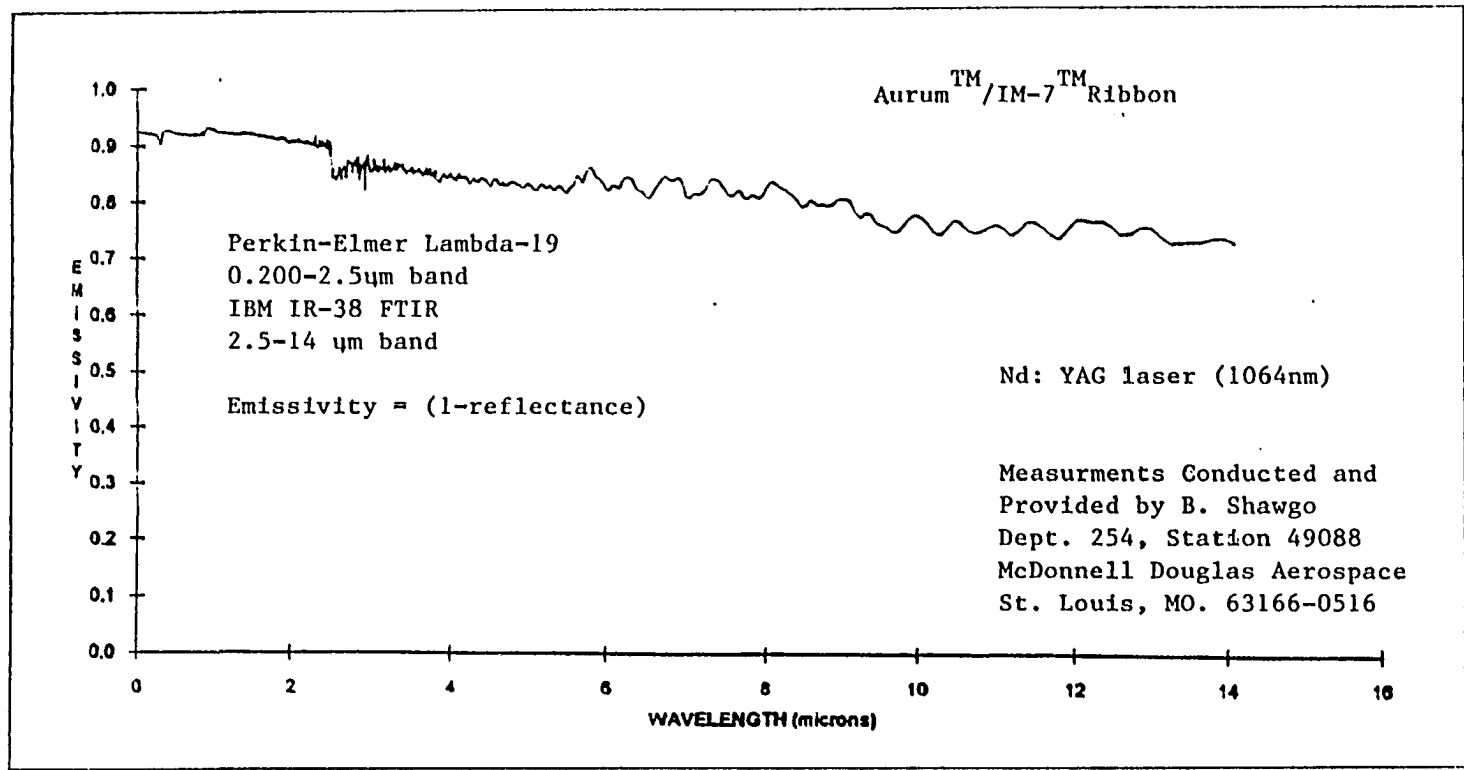
4.8   Emissivity of Aurum-400A/IM-7 Towpreg Ribbon

146

Sample: AURUM 400A/IM7 TOWPREG RIBBON DSC File: 1778.01
Size: 3.8967 mg Operator: WHITLEY
Method: RT-400°C 10°C/MIN Run Date: 03/22/93 15:42
Comment: SANDUSKY
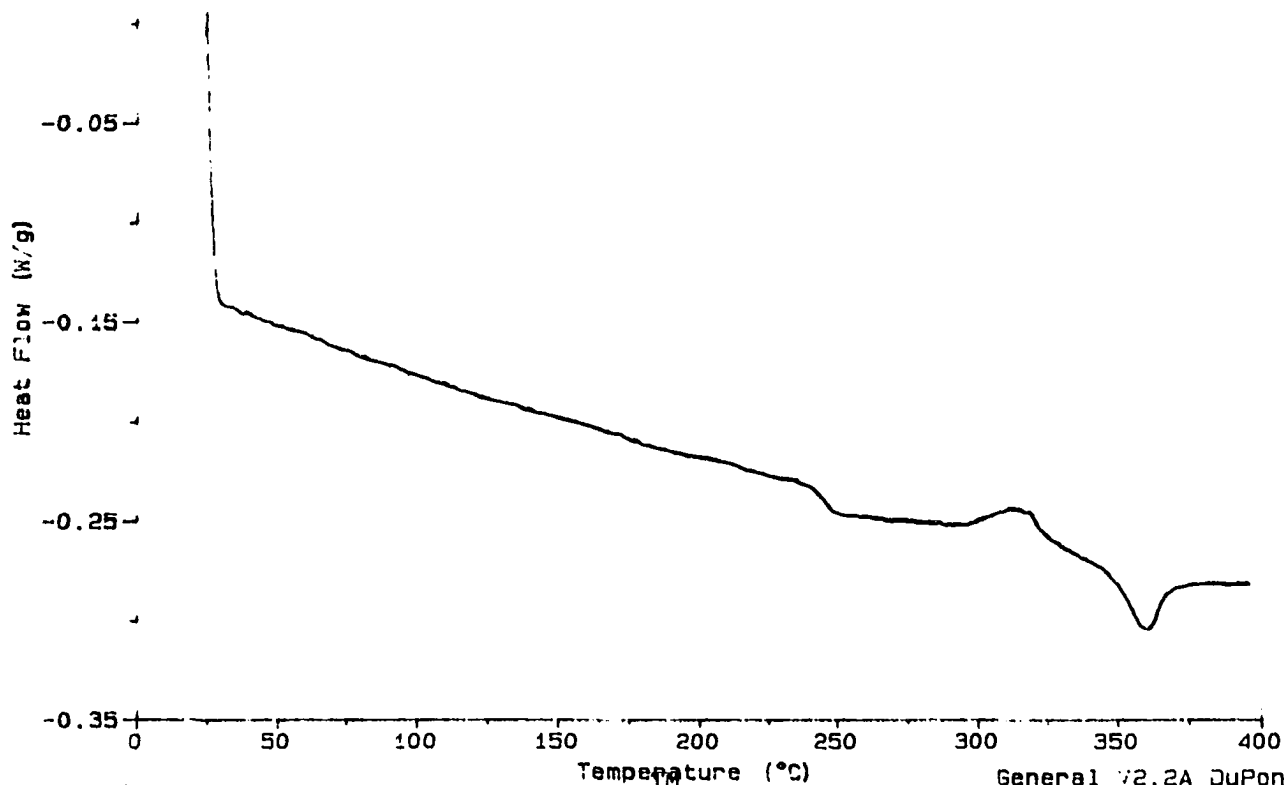
Figure 4.9 Calorimetric Response of Aurum™-400A Powder to Increasing Temperature

General v2.2A DuPont 9900

147
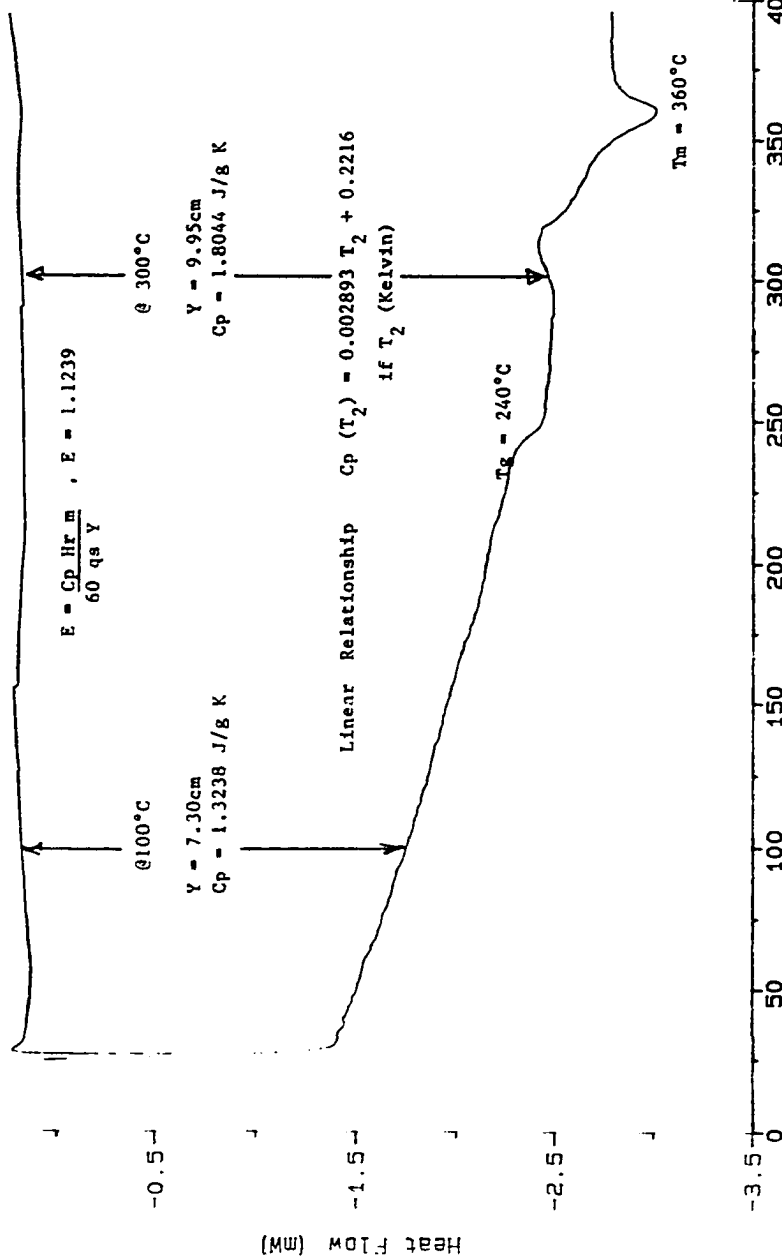
Figure 4.10 Aurum^{TM}-400A/IM-7^{TM}Towpreg Heat Capacity as a Function of Temperature
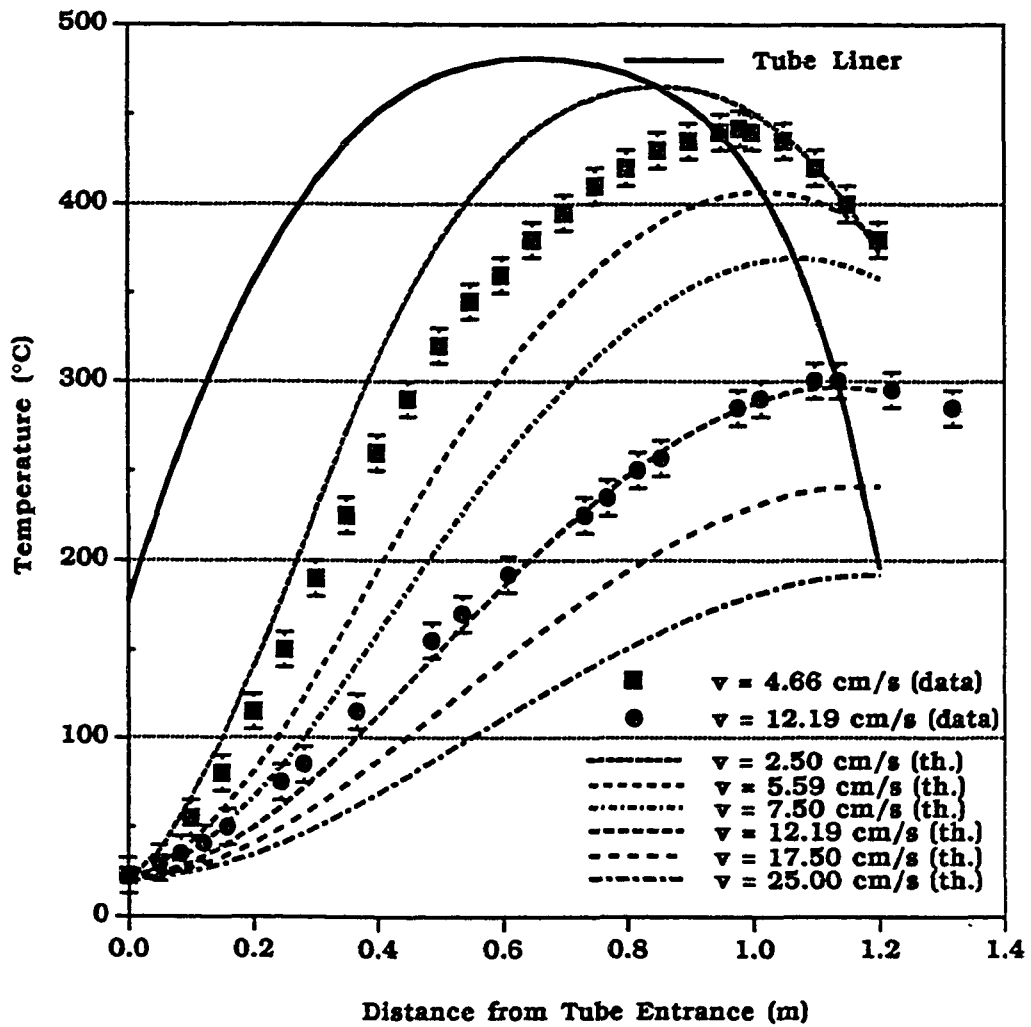
Figure 4.11 Effect of Velocity on Q.S.S. Towpreg Temperature Profile.
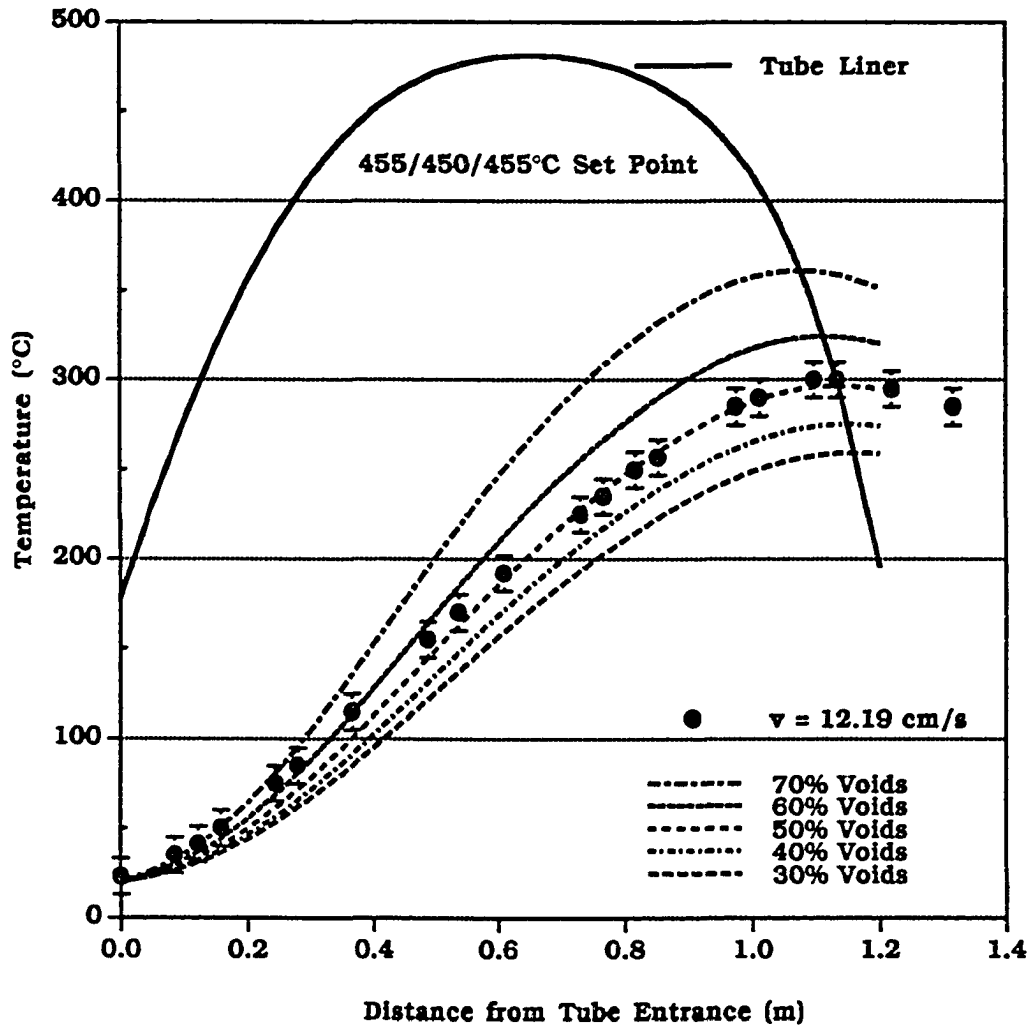
Figure 4.12 Effect of Void Content on Q.S.S. Towpreg Temperature Profile
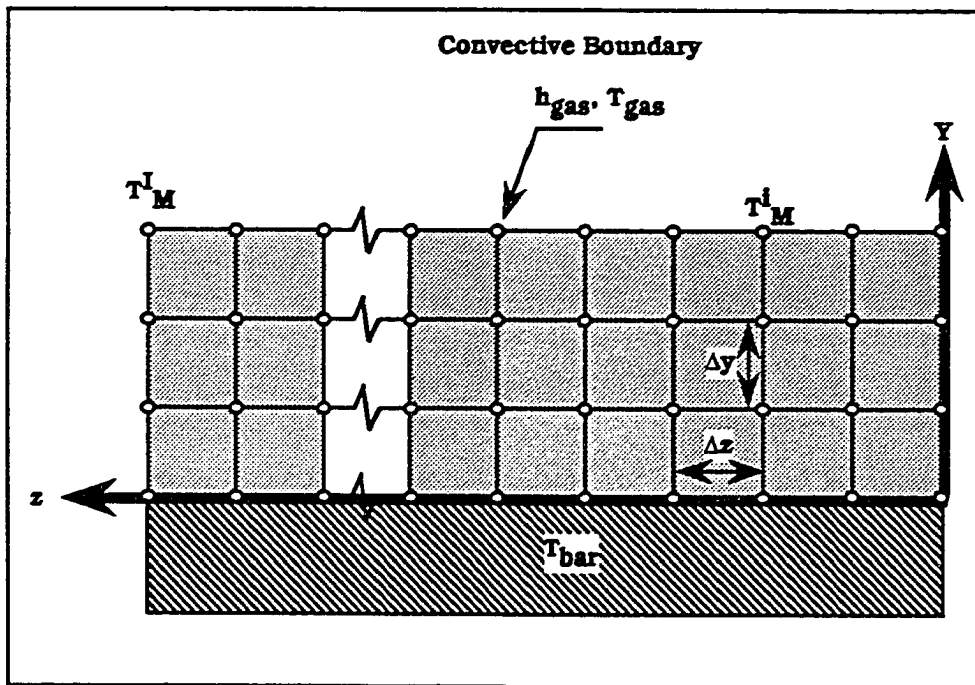
Figure 4.13 Conduction Heat Transfer Model Node Diagram in Rectiliniar Coordinates
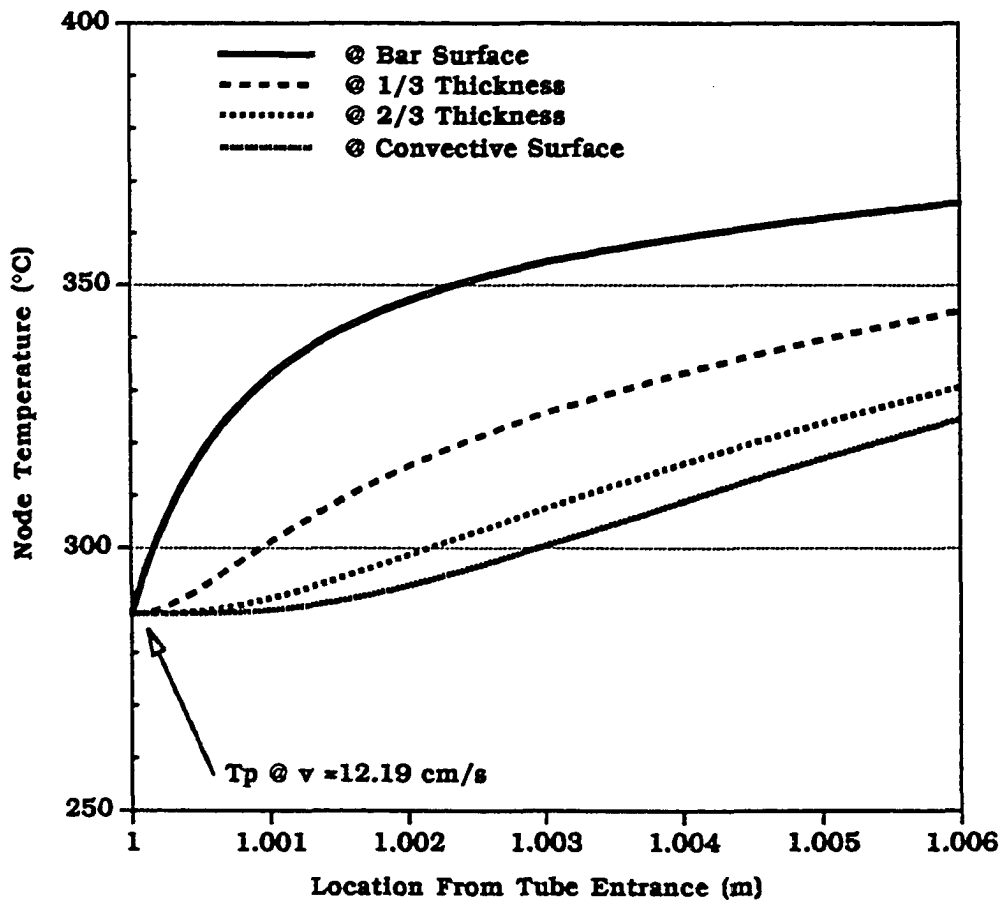
Figure 4.14 Steady State Node Temperatures for Bar Contact Conduction Model
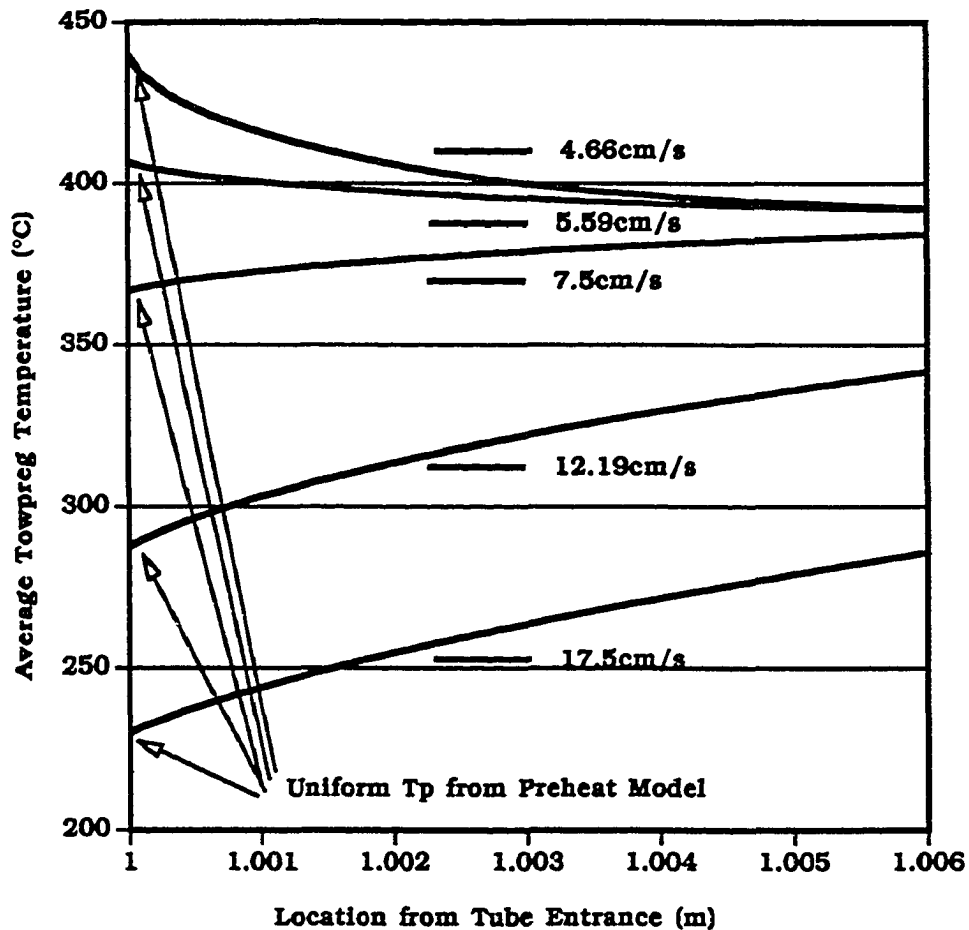
Figure 4.15 Axial Velocity Effect on Bar Contact Heating Model Solution
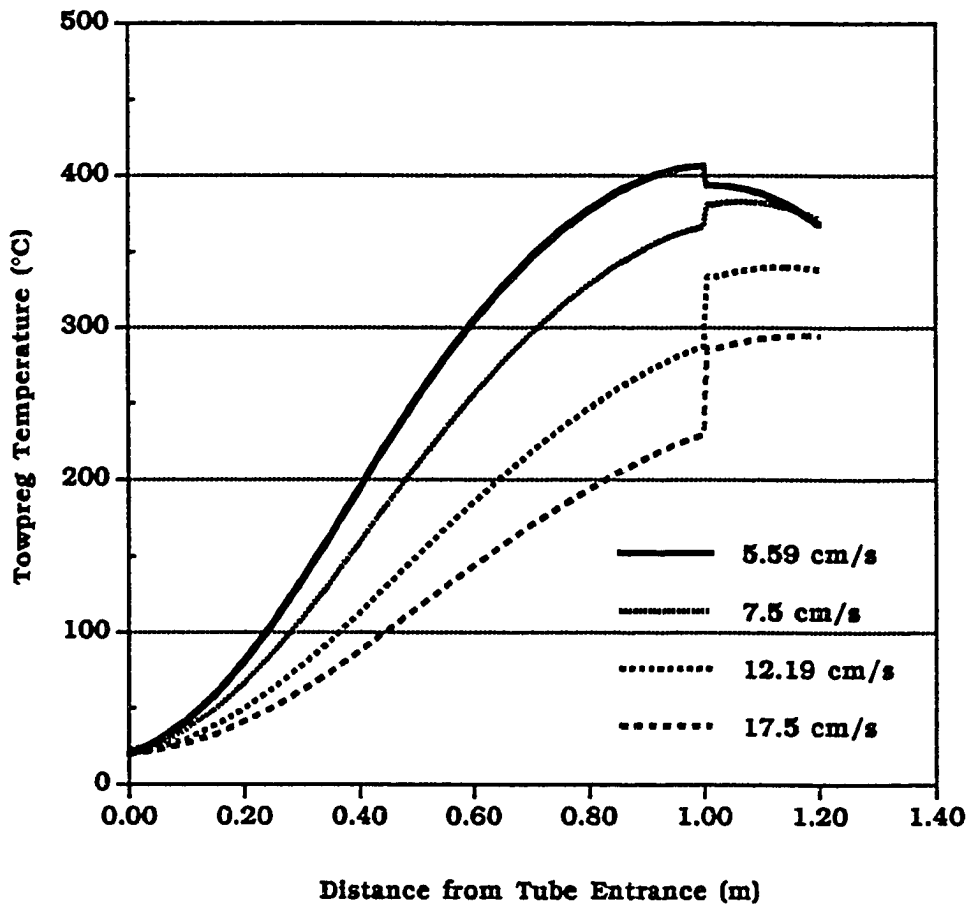
Figure 4.16 Effect of Take-up Speed on Overall Q.S.S. Heating Process.
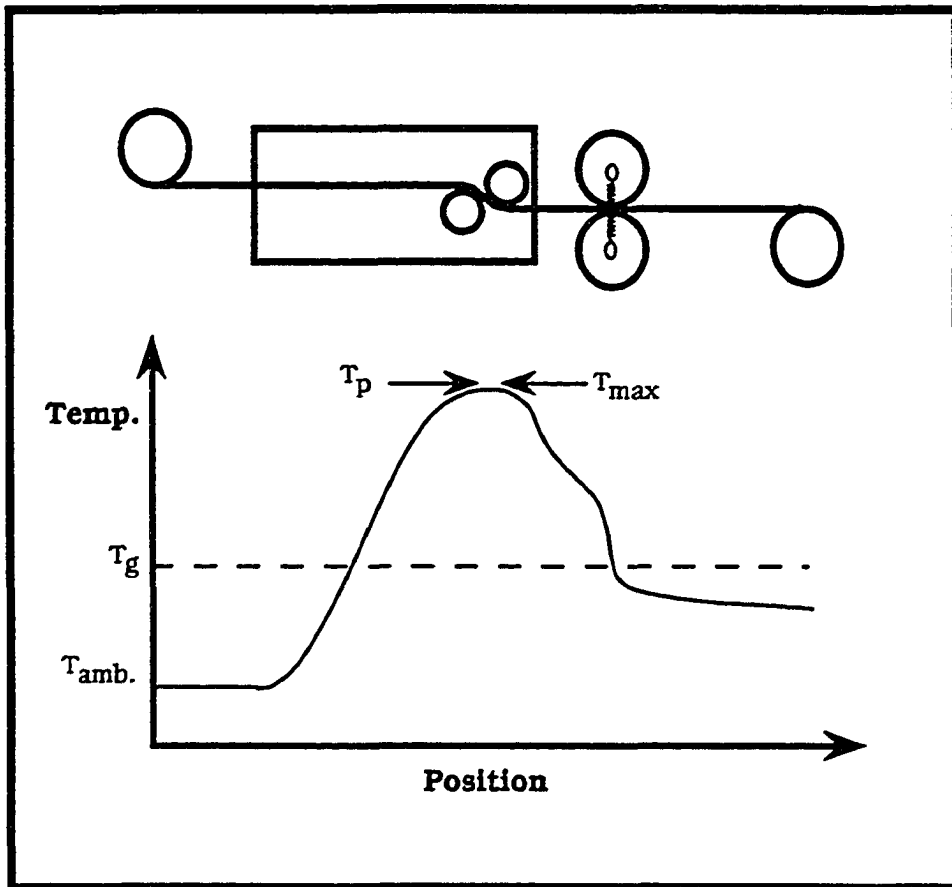
Figure 4.17   Ideal Steady State Towpreg Temperature Profile

5   Pulling Force Analysis

The aggregate pulling force in *ex parte* ribbonizing consists of three primary components: capstan tension Tc, bar drag force Td, and axial nip tension Tn. The capstan tension is independent of processing parameters and material properties due to the nature of the magnetic capstan braking mechanism. The capstan tension is set between 2 and 10 (N) per towpreg. The bar drag force is a consequence of the friction between the stationary bar surfaces and the moving towpreg. The axial nip tension constitutes the added pulling force required to pull the ribbon through the nip. The nip rollers are not driven by external means, so the axial nip tension represents the compaction of the towpreg into a consolidated ribbon and the associated bearing friction.

The axial nip tension is less substantial than the capstan tension and the bar drag force. The bar drag force is 10 to 20 times greater than the axial nip force. The bar drag force is usually 5 to 10 (N) per bar contact, within the most likely range of processing conditions. By comparing experimental pulling force measurements with theoretical models, the boundary layer condition is determined. The utility of sensing bar drag force to indicate process control is discussed.

5.1 Goal: Identify Important Flow Mechanisms

The microscopic cross-section analysis of Chapter 3 illustrated how the towpreg lamina was substantially consolidated on contact with the stationary bars. Voids were expelled in the transverse direction as a consequence of the towpreg flattening. Most of the redistribution of the towpregs constitutive components (filaments, matrix polymer and gas bubbles) occurred on contact with these bar surfaces.

Note that the observed redistribution of components of the microstructure analysis in Chapter 3 were only valid over the time scale of the experiment. The towpreg samples were cooled over 20 to 30 minute time intervals in which case, transverse flow could certainly occur. Normally, the contact with the bars actually occurred over 1/30th to 1/10th of a second. Determining the "flow" mechanisms for time intervals corresponding to nominal fabrication, is paramount to understanding the process. Determining the boundary condition at the bar contacts is the present objective. A defined boundary condition is required to understand the flow potentials and therefore is useful as a starting point for future flow modeling and analysis.

How can bar drag contribute to the characterization of the flow mechanism?

Based on the pultrusion modeling literature, several possible mechanisms for the component redistribution at the bar contact were considered. 1) If the contact at the bars imposed a pressure gradient through the thickness (in the transverse direction), buoyant forces could drive gas bubbles outward and transverse permeative flow by the viscous polymer melt could wet-out dry regions within the towpreg. 2) If an axial pressure distribution were imposed, polymer and bubble flow "plug flow" could occur in the axial direction. In contrast, 3) if the contact at the bars imposed a uniform pressure through the thickness, the polymer could not obtain a velocity relative to the fibers, and therefore transverse and axial polymer flow could not occur. In the third case, some other flow mechanism would be required to explain wet-out and bubble expulsion.

How can bubbles be expelled without imposing a transverse flow potential to the bubbles relative to the polymer melt?

Consider the possibility that the bubbles do not actually move relative to the bars, but rather the entire composite towpreg spreads wider and thinner and consequently moves away from the bubbles. A "multiphase, anisotropic squeeze flow" can occur wherein the towpreg is flattened and bubbles are consequently released. This means that the in the ideal extreme, the towpreg should be flattened at the bars so that the entire band is one fiber diameter thick. In this ideal and unfortunately, impractical case, only the bubbles significantly smaller than the fiber diameter could possibly remain within the towpreg.

This squeeze flow phenomenon may contribute to the understanding of the flow mechanisms contributing to the conversion of a towpreg to a ribbon, but is not expected to contribute to the pulling force directly. It is considered a consequence of the capstan tension. If the boundary condition at the bar contacts do not permit axial or transverse polymer matrix flow potentials, this multiphase anisotropic squeeze flow mechanism is more likely than not.

Bar Drag Force Modeling

The drag force caused by drawing the viscous towpreg over the stationary bar surfaces was considered from two distinct perspectives; a slip or a no-slip boundary condition. The slip condition is the simpler of the two, because the drag force is independent of the relative velocity between the towpreg and the bar surface. The no-slip condition requires a viscous boundary layer borne by an increasing drag force with increasing velocity and viscosity. For flexible and homogeneous materials, both boundary layer conditions do not ordinarily occur simultaneously. Since powder-coated towpreg is anisotropic, this mixed boundary condition is even possible. Prior to experimental evaluation, no compelling boundary condition preference was obvious.

The slip condition implies sliding friction where the drag force is dissipated as heat. In this case, pulling force would not be a substantially useful process control indicator because the pulling force would be independent of processing speed and temperature.

The no-slip condition suggests a viscous boundary layer where most of the drag force

is dissipated by viscous fluid shear. A no-slip viscous boundary layer flow condition defines the shear stress in a viscous boundary layer as the sole contributor to the bar drag force T_b. With a viscous boundary layer, the limiting processing rates are described in terms of the fluid viscosity, and therefore describe the interdependence of material properties and processing parameters.

5.2   Pulling Force Measurement

Off-line dynamometry techniques are often used to calibrate the performance of rotating machinery by measuring shaft work. In this method, several known masses are lifted at measured velocity and motor armature power draw, to provide a fundamental relationship, known empirically, within the range of measured work loads. This off-line take-up motor calibration approach was inappropriate for the *ex parte* ribbonizer because it eliminates the capability of real-time process monitoring. Off-line dynamometry offered no potential for closed-loop sensing for process control. Consequently, on-line measurement of the pulling force is a priority for this analysis. The ideal pulling force measurement technique is one that is on-line and unobtrusive. Two on-line pulling force sensing methods were considered: 1) the take-up motor power draw was measured and converted to yield pulling force, and 2) a custom designed load cell was utilized as a take-up motor platform to provide the normal reaction force experienced by the take-up motor.

5.2.1   Motor Power Draw Technique

The electric power required for the motor to pull the yarn through the apparatus

under a steady-state condition was defined in terms of potential E (V dc), current I (A) and some motor efficiency f. This power was also considered in terms of the total pulling force T_T (N) and the axial velocity v (m s^{-1}) of the towpreg.

$$Power = f\,E\,I = T_T\,v \qquad\qquad [5.1]$$

The analog controller which delivered current to the puller motor armature was fitted with a Amphenol™ (model 14S-9P) electrical port so that the armature voltage and current could be measured continually. The puller motor field supported a constant 115 volts DC and 0.13 amperes. The motor armature supported a constant 115 volts DC but drew current according to load and speed. Again, the shaft speed and load were both integrally related to armature current draw. At low loads, the armature consumed 10 Watts while at high loads 200 Watts.

Motor efficiency data was obtained from the manufacturer of the motor. The motor performance was characterized by an off-line dynamometer technique. **Figure 5.1** illustrates the motor manufacturers data [1] obtained via a common brake test. The motor was initially warmed up and set to a known shaft speed. Load was applied to the shaft. For increasing load, a decrease in shaft speed was observed. Similarly, as the power draw increased, the motor efficiency increased to a plateau value of approximately 75%. As the motor was overloaded, the efficiency decreased. The important observation here was that both shaft load and speed were interdependent with respect to efficiency. Furthermore, the nature of DC motors was such that application of the previously described linear relationship between shaft work and motor power draw did not apply generally.

The manufacturer suggested that the actual efficiency of the take-up motor also included a 50% knock-down for the 40:1 gear box which constituted a single reduction, right angle power take-off. Unlike the motor, the reduction gears were expected to be more efficient at lower loads. The efficiency of the motor and gear box were considered in series so that the nominal take-up efficiency, within the normal range of operation of the take-up motor, was 37.5%.

5.2.2　Load Cell Technique

A custom load-cell was designed and built to indicate the bar drag force experienced by the motor and to serve as a permanent motor mount. The load cell was fixtured between the take-up motor base and the traverse platform of the take-up apparatus. This dual role allowed for unobtrusive, real-time measurement of bar drag force.

Under normal operation of the *ex parte* process, the take-up traversed regularly. The loading of the take-up motor base plate was transient in all directions except the "normal". The transient moments applied to the base-plate needed to be eliminated from the pulling force measurement as they would simply provide extraneous load information.

The four post load-cell design was similar to those used for drag and lift analysis of aerodynamic structures in wind tunnel experiments. This particular load cell design [2] was unique due to the specific nature of its application. Since only normal force was desired, all other moments were eliminated by the combined design of the posts

and the strain gauge array.

A billet of 7075-T6 aluminum was wire E.D.M. machined and fixtured with Wheatstone bridge strain gage assemblies. **Figure 5.2** illustrates the load cell and the normal force (NF), axial force (AF), side force (SF) and pitch moment (PM), yaw moment (YM) and roll moment (RM) of interest. The design of the four load bearing beams was such that the stiffness (Young's Modulus times Area Moment of Inertia) was lowest in the (NF) direction of the desired measurement. The pitch stiffness was over 5,000 times greater than the normal stiffness. The roll stiffness and yaw stiffness were respectively 60 and 11,400 times greater than the normal stiffness. This provided a load cell which elastically deflected most, in the normal direction.

The wiring diagram for the strain gauges of the load cell is shown in **Figure 5.3**. A 10.000 VDC bridge potential was specified so a Hewlett Packard 6205C Dual DC Power Supply was utilized. A balanced bridge was designed which isolated the normal load voltage. When pitch, roll or yaw moments were induced, the bridge received both positive and negative voltage signals for each unwanted strain. Each of the voltage signals for these moments, canceled out. Only the normal force signal prevailed.

Load Cell Calibration

The load cell was calibrated with known weights. The linear interpolation between the signal voltage and the weights, provided the sensitivity constant 1.753 (lb mV^{-1}) for a 10V DC input. The load cell was then calibrated with known normal loads in combination with known pitch moments. Next, another calibration was conducted

with known normal loads and known roll moments. The maximum error between the three calibration techniques was found to be ± 0.26%.

As a free standing load cell, the electrical zero voltage -0.357 (mV) was measured with a digital Hewlett Packard 3478A Multimeter. After the load cell was installed onto the traverse platform, the electrical zero increased to -0.531 (mV). When the motor was installed, the load cell indicated approximately 134 (mV). This was expected since the center of gravity of the motor could not possibly be perfectly aligned with the moment center of the load cell. In other words, the table was slightly slanted. After the motor had been operated approximately 10 minutes and had reached its steady-state temperature, the load cell indicated approximately 136mV varying less than 0.1 (mV). The sensitivity constant was independent of the electrical zero, the axial load and thermal strain load. The normal load voltages were positive so the 136 (mV) steady-state voltage was subtracted from the measured load voltage.

To view load cell pulling force voltage signal in real-time a Honeywell™ Omnilight 8M36 Thermal Chart Recorder was utilized. Since the signal from the bridge was on the order of (mV), a Stanford Research Systems™ SR560 Low Noise Preamplifier was utilized at 100gain and 3Hz filter cut-off to boost the signal to a range compatible with the chart recorder.

5.2.3 Measurement Evaluation

An on-line calibration experiment was conducted to determine the utility of the two different pulling force measurement techniques. Only the material handling system

was utilized. There was no contact with the stationary bars or the nip rollers and therefore this was a pure calibration exercise. Four different braking loads were applied at four different take-up rates to identify any dependence on speed or load for either the capstan brake or the take-up motor. The load cell voltage and the motor armature amperage were measured simultaneously.

The take-up motor speed was measured by a hand-held Jones® CT-2000 tachometer made by Computak™. The capstan tensions were both set to a similar load which was measured with a hand-held SAXL™ Tension Meter (Model TM-2000 w/scooped roll) made by Tensitron®. The nominal motor armature amperage was indicated by a Fluke™-87 multimeter connected to the Amphenol™ access port of the motor controller. The load cell pulling force signal was monitored via a previously described technique.

The take-up motor and the traverse motor were engaged at maximum speed and were left unrestrained for several minutes to allow warm-up. The take-up motor armature current draw and the load cell voltage signal were recorded for four different linear take-up speeds. A zero load was guaranteed by performing this first experiment with the unrestrained take-up motor which was allowed to spin freely. The remaining experiments were conducted with two 12K IM-7™ carbon fiber tows and known capstan loads of 14, 21 and 27 (N) respectively.

Figure 5.4 illustrates the resulting load values determined by the calibration experiment. The results of armature method were unexpected. The load cell method on the other hand, indicated a pulling force which was both uniform and reasonably

accurate and a barely distinguishable deviation of load with increasing speed. This slightly upward shift in the load cell signal was attributed to unavoidable bearing friction and non-ideal braking.

Important knowledge was gained by this experiment in addition to the demonstration of the utility of the load cell for on-line pulling force sensing. The transient moment loading caused by the traverse mechanism did not effect the axial pulling force measurements which served as testimony to the load cell design. Also, the capstan tension, measured by the load cell, was shown to be reasonably independent of pulling rate. Capstan tension was independent of any material properties, and all other process control parameters.

5.2.4 Experimental Characterization of Pulling Force

Pulling force experiments were conducted to determine the relative importance of the three pulling force components, capstan tension Tc, bar drag tension Td and axial nip tension Tn. The axial nip tension was expected to increase with increasing transverse nip load.

$$T_T = T_c + T_d + T_n \qquad [5.2]$$

Two powder towpreg yarns were ribbonized with the *ex parte* process under normal operating conditions. **Figure 5.5** is an overlay plot of experimentally obtained load cell output voltage for two configurations; 1) nip rollers disengaged (Td + Tc) and 2) the nip rollers engaged (Tn+Td+Tc). Note the vertical axis voltage is scaled by a

sensitivity constant to indicate pulling force and the horizontal axis corresponds to elapsed time. The first experimental configuration provides a steady signal over time. The total load signal indicates a sinusoidal force measurement with a regular amplitude and period. This is attributed to nip roller bearing misalignment or eccentric nip roller shape.

Figure 5.6 illustrates measured pulling force as a function of transverse nip load. Neither capstan load nor bar drag were affected by transverse nip load since they were both applied upstream of the nip assembly. Of particular interest was the pulling force at 175N transverse nip load, which corresponded to the load under normal operational conditions. This indicated a measured bar drag force about 10 times greater than the resultant axial nip load contribution under normal processing conditions.

Experimental to Determine Contact Interface Boundary Condition

Several bar templates were fabricated with the intent to characterize the role of contact angle on pulling force. The values for bar curvature diameter D (m), centerline distance between diameters CL (m) and the relative centerline angle ϕ were laid-out on the template material prior to template construction and were therefore known. The geometrical deflection angle β shown in **Figure 5.7**, was known from measurable quantities.

$$\beta = \tan^{-1}\left(\frac{D - CL \sin(\phi)}{CL \cos(\phi)}\right) \quad , \qquad\qquad [5.3]$$

Note that if the sign of ϕ is negative the relation holds. As a matter of convenience, templates with positive centerline angle are designated Z and those with negative centerline angle are designated S configurations. From geometry, the total contact angle θ for the bar assembly was obtained. For two bars of either Z or S configuration, the total contact angle is known to be $\theta = 4\beta$, as illustrated by **Figure 5.8**. For three bars, the contact angle is doubled $\theta = 8\beta$.

Table 5.1   Bar Template Geometry Specifications

Template	D (mm)	CL (mm)	ϕ (°)	β (°)	θ (β)	θ (°)
Gr. A (2Z)	10.0	18.66	12.0	18.5	4	74
Gr. B (2Z)	10.0	27.16	8.4	12.7	4	51
Gr. C (2S)	10.0	25.00	-26.5	43.4	4	174
Gr. D (2S)	10.0	25.00	-13.7	33.3	4	133
Gr. E (3S)	10.0	21.63	-3.7	27.8	8	223
Gr. F (3S)	10.0	20.62	-28.3	47.4	8	380
CB A (2Z)	10.0	16.50	11.0	23.0	4	92
CB B (2S)	10.0	16.50	-8.8	40.0	4	150
MC A (2S)	10.0	21.80	-9.2	32.1	4	128
MC B (2Z)	10.0	20.14	3.0	23.9	4	96
MC C (2S)	10.0	21.00	-19.3	40.5	4	162

Table 5.1 lists the specifications of each template designated Gr. A ("Greenleaf A") through Gr. F, "Carbon Bar A " (CB A and CB B) and "Machinable Ceramic bar A" (MC A, MC B and MC C). The information within the parentheses of the "Template" column indicate the number of bar surfaces contacted and the wrapping configuration.

Based on previous experience, nominal zone temperatures 500/490/525°C were selected. The tube furnace was allowed to heat-up to steady-state. The low quality towpreg material (32% powdered PIXA™/IM-7™ towpreg, slurry-impregnated by CYTEC Engineered Materials, Anaheim, CA) was observed to have non-uniform resin content such that the surface of the towpreg was resin rich while the interior was resin poor. The two towpregs were set-up adjacently for normal ribbonization of 1/4 inch wide ribbon.

A temperature profile experiment was conducted to determine the steady-state tube liner temperature profile. For convenience, the tube surface temperature distribution T_1 (z) was characterized by a polynomial expression in terms of z-position (m) from the entrance plane of the tube liner.

$$T_1(z) = 2942\, z^5 - 12484\, z^4 + 18484\, z^3 - 12517\, z^2 + 4006\, z + 300 \ (\text{KELVIN}) \qquad [5.4]$$

The steady-state bar surface temperature was measured. The preheating heat transfer model, described in Chapter 4, was utilized to interpolate the optimum take-up speed so that the preheat temperature at position z = 1(m), was within 5°C of the measured steady-state bar surface temperature. A speed of 11 (cm s^{-1}) ensured an isothermal boundary layer for the duration of bar contacts because 11 (cm s^{-1}) was the speed which corresponded to a preheat temperature nearly equal to the measured steady-state bar temperature of 370°C.

Only one of the listed bar assemblies could be evaluated at a time. At least 50

minutes of heat-up time was allowed for evaluation of each assembly configuration. The role of contact angle on the bar drag force was evaluated by disengaging the nip rollers and setting the temperature, speed and capstan tension constant. The two capstans were both set by checking the towpreg tension with the hand-held tensiometer and adjusting the brake to provide a common tension to both towpregs. The capstan braking tension was then recorded by the load cell at 11 (cm s^{-1}) take-up rate. Next, the bar drag plus capstan pulling force measurements were recorded.

The measured capstan tension was subtracted from the measured pulling force. **Figure 5.9** illustrates the bar drag force components (Td), in Newtons, for each of the 11 templates. The bar drag force was observed to increase almost linearly with contact angle. The error bars reflect the average variation in the measured load cell output. The total error appeared to increased with increased load. This was expected since load cell sensitivity increased with normal load magnitude, and the maximum load for the cell was about 45 (N). Note linear trend did not vary substantially for any of the three different bar materials and bar types.

The role of capstan tension on pulling force was evaluated by utilizing only template "Gr. A" and the same temperature settings and take-up speed as the previously described experiment. The capstan tension was increased from a minimum of 16 (N) to just under 26 (N). The bar drag component was observed to be reasonably independent of capstan tension in **Figure 5.10**.

The role of pulling speed or temperature could not be isolated for experimental evaluation as the two parameters were interdependent. Observations did, however,

suggest that bar drag force increased with increasing speed and the corresponding decrease in temperature. This dependence on temperature suggested that the polymer viscosity contributed to pulling force.

5.3   Pulling Force Modeling

Modeling of the pulling force of *ex parte* ribbonizing provided a means to interpret and analyze the experimental measurements. The objective here was to understand the stationary bar contact phenomenon in terms of fundamental principles so that the role of pulling force for process control could be determined. The interface between the towpreg and the bar surfaces was recognized as the primary contributor to the pulling force. Prior to modeling, the boundary condition of this contact region was unknown. Two independent boundary condition models were developed. The "slip model" was based on simple Coulomb friction, while the "no-slip model" built upon viscous Tribology principles [3], sometimes referred to as hydrodynamic friction. The no-slip model, which incorporated the geometrical considerations of the apparatus, material properties of the towpreg and the process control parameters such as temperature and take-up rate, was therefore useful for indicating process control.

5.3.1 Literature Review

The *ex parte* ribbonizer has been shown to be novel in terms of U.S. patent records and, a as a result, limited pertinent process science literature presently exists. The closest analogue to the *ex parte* ribbonizer, thermoplastic pultrusion, has been addressed by the research community for some time. Many important phenomena

such as permeative flow [4,5,6,7,8], axial capillary (plug) flow or back flow [9,10,11], squeeze flow [12,10], elastic filament network deformation [13], have been investigated and are in the literature.

Three key processing models provided the background to understanding consolidation mechanism for the pultrusion process. One model for thermoset pultrusion and two thermoplastic pultrusion models are discussed in the following paragraphs.

Pulling Force Model #1   Bibbo; Gutowski (M.I.T.), (1986)

Pultrusion processes have historically been treated as supporting both viscous boundary layer forces and frictional forces simultaneously. Bibbo and Gutowski [11] described the pulling force of thermoset pultrusion to include three mechanisms: 1) friction of the fibers on the pultrusion die wall, 2) viscous flow in a very thin layer of resin between fibers and the die wall, and 3) the drag resistance on the fibers due to the back flow in a contracting section. The authors implied that both fiber friction and viscous flow occurred simultaneously at the interface between the part and the pultrusion die wall. Such an assumption was intuitively appropriate given the inherently low viscosity of molten thermosetting polymer precursors. A practical analogy to this approach is found by considering a soapy steel wool pad scrubbing a stainless steel frying pad. The contact was both abrasive and lubricating. Most of the friction between the abrasive pad and the pan surface can be attributed to the contact between the two solids; and, therefore, in modeling the phenomenon, dry friction would be the dominant mechanism.

The Coulomb friction drag force was obtained from a friction coefficient and the effective normal stress caused by fluid pressure and elastic filament network stress [14,15]. The Newtonian hydrodynamic friction forces were obtained by assuming a uniform viscous boundary layer of thickness equal to the distance between fibers δ (m) of a hexagonal array of fiber volume V_f (%) and fiber radius r_f (m) .

$$\delta = 2\, r_f\left[\sqrt{\frac{\pi}{2V_f\sqrt{3}}}-1\right]$$

[5.5]

The "back flow" forces were attributed to the shear stress of the resin moving in the opposite direction to the fibers. This relationship was determined by force balance on an interior differential volume element. The relative velocity between the fibers "u" (m s^{-1}) and resin "v" (m s^{-1}) was related to resin viscosity "η" (Pa s). a modified permeability constant "S" (m^2), and resin pressure gradient "P_r" (Pa m^{-1}) in the axial direction "x" (m). The permeability constant was given as a function of fiber radius and volume, and the empirical Darcy's Law permeability "k" constant.

$$u - v = -\frac{S}{\eta}\frac{dP_r}{dx}$$

[5.6]

$$S = \frac{r_f^{2}(1-V_f)^3}{4k}\frac{}{V_f^2}$$

[5.7]

The model predicted the friction forces to be 2 to 4 decades more important than the viscous forces for composites with fiber volume near 50% and a friction coefficient of 0.50. This prediction was expected given the magnitude of the normal stress approximation. The back flow forces (opposing the prepreg axial velocity) caused by

the contracting die were predicted to be within a decade but not as substantial as the friction forces. These predicted pulling forces corresponded favorably to measured values obtained by Price and Cupshalk [16]. The pulling force for pultruding epoxy-carbon fiber prepreg into a rectangular cross section die (with exit geometry 20 mm wide, 2 mm high and 50 mm long) was calculated to vary between 10 (N) and 1000 (N) depending on the compaction ratio of the die. This corresponded to shear stresses between 5 (MPa) and 500 (MPa). Since this analysis involved an epoxy thermoset polymer precursor fluid which characteristically exhibited low melt viscosity, it was not surprising that the viscous forces were negligible by comparison to frictional forces.

The fundamental criticisms of this model focus on the dependence on a permeability constant and the guess at the friction coefficient. Both of these empirical values affected the load predictions substantially. Thermoplastic pultrusions are usually different than thermosetting pultrusion for a couple of key reasons. First is the difference in fluid viscosities. Thermoset pultrusion begins with very low molecular weight mer units which polymerize downstream from the tapered section of the die. Thermoplastic pultrusion begins and ends with high polymer. Second, thermoset pultrusion advantageously benefits from the part constriction away from the die walls which occurs on polymerization, while thermoplastic pultrusion does not.

Pulling Force Model #2   Hepola (U. Delaware C.C.M.), (1993)

Pultrusion of unidirectional thermoplastic polymer prepreg required modified modeling scenarios with substantial dependence on polymer viscosity and fluid

mechanics. A detailed study [9] was conducted by Hepola to categorized the pulling force of thermoplastic pultrusion in terms of axial plug flow induced by fiber drag and back flow resultant from the axial pressure gradients caused by the pultrusion die taper. This model also included a detailed description of polymer melt viscosity, including Carreau shear rate dependence and viscous dissipation heating effects.

A detailed fluid mechanics based analysis of the pulling force in thermoplastic pultrusion was conducted wherein the primary pulling force component was hypothesized to be comprised of the axial flow of viscous polymer relative to the filaments. All of the pulling force was attributed to counter flow in the interior sections of the unidirectional . The boundary layer drag was assumed to be insignificant.

This modeling approach overestimated pulling forces and did not exhibit substantial validation by experimental comparison. The shear stress for uniform viscous flow (throughout the thickness) along the very large surface area required pulling forces greater than the measured values. Uniform "plug flow" did not likely occur for high molecular weight thermoplastic unidirectional composites during pultrusion.

Pulling Force Model #3   Lee; Springer (Stanford); Smith (ALCOA). (1991)

Lee, Springer and Smith published a pulling force model [10] for pultrusion of unidirectional thermoplastic semicrystalline poly (arylene ether) prepreg. The model describes four factors contributing to the pulling force of thermoplastic pultrusion: 1) "pretension" of the prepreg. 2) pressure exerted by the composite (polymer/fiber

viscous mixture) on the die, 3) Coulomb friction between the "solid" composite and the die wall and 4) hydrodynamic friction resulting from shearing of the thin "fluid" resin layer contained between the composite and the die wall.

This modeling attempt cast aside the notions of permeable flow and axial plug flow, in favor of a transverse composite squeeze-flow concept. A "saw tooth" representation defined the surface roughness of a unidirectional ply where the rectangular "teeth" were a (m) tall and b (m) wide in the ξ -direction.

$$u = - \frac{a^2}{12\,\eta_{mf}} \frac{dP}{d\xi} \qquad [5.8]$$

The transverse flow velocity u (m s^{-1}) of the matrix-fiber mixture with viscosity "η_{mf}" (Pa s) was defined in terms of the pressure gradient in the ξ -direction. This composite viscosity and the geometrical considerations were utilized with a conservation of mass relation under a laminar flow constraint to provide the drag force due to squeeze-flow during unidirectional thermoplastic pultrusion. The total pulling force per unit width was defined in terms of three components and a "pretension" F_t (N) applied at the pay-out supply.

$$F = 2 \int_0^L \left[P_{av} \left(\tan(\theta) + f \right) + \eta_{mf} \frac{V}{\delta} \right] dx + F_t \qquad [5.9]$$

The average pressure P_{av} (Pa) was a function of the continuity model. The friction drag was defined by an empirical parameter f_c and the normal component of average pressure, and the hydrodynamic friction contribution was a function of the processing

speed V (m s^{-1}) and the composite squeeze flow viscosity.

It is important to note that the authors referred to a two-section pultrusion die, commonly used for thermoplastic processing where the tapered section was maintained above the melt temperature of the polymer and the subsequent straight section was maintained below the glass transition temperature of the polymer. The hydrodynamic friction was applied as the boundary condition for the heated section and the Coulomb friction was applied as the boundary condition of the cooled section.

The tapered section had an exit height of 0.086 (in) for 20 consolidated plies of APC-2™ prepreg with constant taper angle and a 10 (in) long straight section of similar height. The width of both sections was 10 (in). This heated and cooled die design provided a form stable composite article.

In the analysis of a sample problem, pulling forces of 500 to 2,000 (lbf) were calculated for speeds of 0.5 to 2 (in s^{-1}). The maximum transverse pressure at the die walls of the tapered section reached 1,000 to 2,000 (psi). The majority of the pulling force was attributed to the tapered section axial component of force required to debulk and consolidate the laminate. By an unexpected assumption, the pretension and the shear thinning fluid layer were both considered negligible. If the entire pulling drag force were attributed to the heated taper section of the die, shear stress values would have been expected between 4 to 17 (MPa). The boundary condition of the tapered section was neglected altogether. This model predicted substantial pulling force contribution by the contact interface and that suggested the Coulomb friction in the cooled section was more important than the hydrodynamic friction in the hot section.

Comments on the Pertinent Literature

Each of these three thermoplastic pultrusion pulling force models identified similar contributions to pulling force. For pultrusion pretension was generally disregarded as it was usually small by comparison to the total pulling force. Each model development considered the remaining pulling components and characterized their contributions uniquely. Although each pulling force model was sensibly derived and intuitively sound, none of the pulling force models was broadly validated by experimentation. It is likely that the lack of experimental data speaks to the challenge of measuring pulling force and the particularly difficult task of isolating individual contributions to the total pulling force for complex processes.

The two thermoplastic pultrusion models (#2 and #3) neglected the pulling force contribution by the viscous boundary layer between the composite and the heated die surfaces altogether. For thermoplastic pultrusion this assumption was of particular concern because high molecular weight polymers tend to be very viscous in the melt, and therefore tend to sustain high shear stresses at viscous shear interfaces. In pultrusion, these shear stresses are usually aligned axially and therefore can contribute to pulling force. The significance of these shear stress loads would be greatest for pultruded articles with a high surface area to cross section area ratio, and would be less important for large cross section annular articles. The shear forces would also be greater at higher processing speeds. The pultruded article of the sample problem in model #3 was a part with high surface area and was pulled through the die at over 100 (cm min^{-1}). Ignoring the shear stresses at the part-die interface was a fundamental limitation but did not invalidate the models altogether.

By way of example, in the analysis of model #3, dry friction between the solidified composite article and the straight section of the cooled pultrusion die was proposed to contribute to pulling force with friction coefficients greater than unity. This is expected to have been an inappropriate compensatory adjustment. The model should be reanalyzed by including the hydrodynamic shear interface contribution and reducing the friction coefficient below unity.

Many important concepts were demonstrated by these model studies. 1) In unidirectional pultrusion, significant elastic stresses were encountered by the compaction of the non-uniformly aligned filament array. The squeeze-flow of the fiber/matrix viscous prepreg was an important contributor to the pulling force in pultrusion and was shown to be primarily a consequence of the enclosed tapered section. 2) If a dry friction interface existed between the straight cooled section of a pultrusion die and the prepreg material, the contribution to pulling force would be defined in terms of the transverse component of residual elastic stress within the filament array, but would be independent of the hydrostatic pressure in the viscous fluid. 3) If, on the other hand, a viscous boundary layer existed between the fibers and the pultrusion die walls, viscous shear could substantially contribute to the required pulling force under high pulling speeds or high surface area ratio.

Fundamental Modeling Differences Between Pultrusion and *ex parte* Ribbonizing

It was expected that the primary contributor to the pulling force in the *ex parte* ribbonizer was imposed by the bar contact interface. The *ex parte* ribonizer did not clearly support the boundary conditions for axial pressure gradient and therefore, it

was expected that axial plug flow could not possibly occur. Furthermore, the flow field boundary condition (a source of fluid with a well defined pressure gradient) did not exist to support a Darcy's law, permeation-type flow in any direction. Permeative polymer flow and plug flow in pultrusion of thermoplastics requires high pulling forces. The flow potential constraints for plug flow and permeative flow are met by the contracting section of a pultrusion die but can not be met by the one sided bar contacts of the *ex parte* ribbonizing process.

5.3.2 Stationary Bar/Towpreg Interface Modeling

The type of interface was unknown but was expected to contribute entirely to the bar drag force component of pulling force. An objective of experimentation was to characterize the interface as a dry friction, viscous boundary layer, or a combination of both. Models for the strict slip and strict no-slip were formulated with the intent of determining the extremes.

Slip Condition (Coulomb Friction) Drag Force Model

If a slip condition applied between the towpreg and the bar surfaces, the Coulomb friction drag force could be characterized by an empirical dynamic coefficient of friction μ and the normal reaction force N (N). This slip model was based on the premise that the fluid boundary layer between the towpreg yarn and the surface of the bars could be continually wiped away by the abrasion of the filament array.

The representative diagram of the bar contact region is illustrated in **Figure 5.11**.

The tension on the tight side is equal to the tension on the slack side T(θ) (N) plus an increment dT(θ). The bar is pressing outward on the towpreg band with a normal reaction force dN (θ). Assuming a slip condition at the interface, the dynamic coefficient of friction μ and the normal reaction force component describe the increment of drag tension dT (θ).

$$dT(\theta) = \mu \ dN(\theta) \qquad [5.11]$$

Since the angle dθ is very small, the inward component from the tangential forces is T(θ) dθ.

$$dT(\theta) = \mu \ T(\theta) \ d\theta \qquad [5.12]$$

The tension varied from the capstan tension T_c (N) to the bar drag force plus the capstan tension Td + Tc (N) and the angle varied from 0 to θ. The exact solution for the bar drag force T_d (N) is known.

$$T_d = T_c \left[e^{\mu\theta} - 1 \right] \qquad [5.13]$$

As expected, this solution is independent of processing speed and temperature. All of the various contributing material properties were lumped together into a friction coefficient.

No-Slip Condition (Hydrodynamic Friction) Drag Model

If the no-slip boundary condition applies, the bar drag force could be modeled by

viscous boundary layer flow [17] between the filament array and the stationary bar surface. The most obvious indication of the no-slip condition would be evident if the bar drag force increases with increasing velocity. The modeling of viscous boundary layer flow required development from fundamental principles.

Polymer melt viscosity is known to exhibit dependence on molecular weight, molecular weight distribution, temperature, and chain branching for both Newtonian and non-Newtonian shear rate regimes [18]. As a first approximation this model neglects all but the temperature and shear rate dependence of viscous flow. This imposes a substantial limit such that the pulling force model can only apply within a predetermined range of temperatures and shear rates, wherein the molecular weight and polydispersity are invariant over the duration of the contact. The physical interpretation of this assumption imposes a constraint on the reactivity and thermal oxidative stability of the polymer itself. To account for this limitation, careful rheometric characterization [19,20,21] of the neat polymer is required.

Shear Rate Dependence of Viscosity

When a viscous fluid is subjected to shear forces, it deforms [22] at a strain rate inversely proportional to its coefficient of viscosity η. The resultant shear stress can be defined by a viscosity term and a linear velocity gradient or velocity distribution.

$$\tau = \eta \frac{d\Theta}{dt} = \eta \frac{du}{dy} \qquad [5.14]$$

Many fluids such as water (η = 10E-3 Pa s) and glycerol (η = 1 Pa s) exhibit Newtonian flow behavior [23], such that viscosity is independent of shear rate. For Newtonian liquids, η is often called the coefficient of viscosity but it is more commonly referred to simply as the Newtonian viscosity. In contrast, polymer processing melt flow situations often involve non-Newtonian behavior called pseudoplastic, where shear forces change the polymers structure. **Figure 5.12** illustrates the shearing effect on molecular structure [24]. Higher shear rates reduce polymer chain entanglements (reduce molecular entropy) and therefore reduce the polymer melt viscosity.

Polymer melt flow at high shear rates γ (s^{-1}) is usually non linear and is often modeled by a power law variation of Newton's postulate.

$$\eta = m \, \dot{\gamma}^{n-1} \qquad\qquad [5.15]$$

The power law index n is the parameter which indicates the shear sensitivity of the polymer. A fluid that exhibits viscous shear thinning is called a power law fluid. The viscous constant m (sometimes referred to as "consistency") and the power law index n are material-specific empirical values which are dependent on molecular weight, polydispersity, chain connectivity, and temperature. The values of m and n can be obtained by the expanded linear relationship for isothermal steady mode rheometry.

$$\log \eta = (n-1) \log \dot{\gamma} + \log m \qquad\qquad [5.16]$$

As the value of n approaches 1, (Newtonian fluid) the fluid is less shear sensitive, and if n approaches 0, (ductile yielding material) it is more shear sensitive. Values of n<1

indicate pseudoplastic (shear thinning) fluids, whereas n>1 defines dilatant (shear thickening) materials. At predetermined processing temperatures, semicrystalline (PEEK™) exhibits moderate shear thinning behavior [23] with n = 0.80, while semicrystalline polypropylene (PP) exhibits a particular affinity n = 0.43 for shear thinning response to high shear rates.

The Newtonian equation can be utilized over the range of shear rates from very low up to the point where deviation with linear behavior corresponding to the relaxation time of the polymer begins. The power-law equation can be used to describe the shear thinning behavior for very high shear rates. Between these two models a substantial range of transition behavior can be neglected. The primary limitation of the power-law relationship is found in this transition region between linear and non-linear behavior. The Carreau description of viscosity is a three-parameter relationship which incorporates both Newtonian and shear-thinning flow behavior.

$$\eta = \eta_\lambda \left[1 + (\lambda \dot{\gamma})^2\right]^{\left(\frac{n-1}{2}\right)}$$ [5.17]

The time constant λ (s) is a material parameter which is the reciprocal of the shear rate corresponding to the relaxation time of the polymer. The linear viscosity prior to that key shear rate η_λ (Pa s) is scaled by the power law index to provide a uniform transition from Newtonian to power-law behavior at high shear rates.

Viscous Dissipation of Heat

All substances undergoing flow dissipate viscous forces into heat. The act of shearing generates heat within the liquid and may thus change the temperature enough to decrease the viscosity, unless steps are taken to remove the generated heat. The rate of work energy dissipated into heat energy per unit volume of a sheared Newtonian liquid is the product of shear stress and shear rate or, equivalently, the product of the viscosity and the square of the shear rate. For low viscosity fluids the resulting temperature rise can be negligible. For polymer melts and other high viscosity fluids (lubricants), viscous flow heating can be an important factor. This rate of viscous heat dissipation per unit volume θ_v (W m^{-3}) for non-Newtonian fluids depends on shear rate.

$$\theta_v = \tau\,\dot{\gamma} = m\,\dot{\gamma}^{n+1} \tag{5.18}$$

The non-adiabatic rate of temperature rise in a polymer material which is subjected to shear, is obtained by energy balance.

$$\frac{dT}{dt} = \frac{\theta_v}{\rho\,c_p} \tag{5.19}$$

After integration and substitution the increase in temperature ΔT (K) of a power-law fluid, caused by irreversible viscous dissipation is related to shearing time t_s (s), heat capacity c_p (J g^{-1} K^{-1}) and density ρ (g m^{-3}).

$$\Delta T = \frac{m \, \dot{\gamma}^{n+1} \, t_s}{\rho \, c_p}$$
[5.20]

Polymer fluids which are cyclically loaded over long time duration (fatigued) are most susceptible to such heating. Viscous dissipation heating is very important for continuous large amplitude vibrational damping applications.

Temperature Dependence of Viscosity

Another important aspect of polymer melt flow behavior, is the temperature dependence of viscosity. In general, liquid viscosities decrease and gas viscosities increase with increasing temperature. For processing temperature below Tg+100°C, the polymer exhibits behavior well predicted by the familiar time-temperature superposition WLF relationship.

$$\log (a_t) = \log \left(\frac{\eta}{\eta_g} \right) = - \frac{a \, (T-T_g)}{b + T - T_g}$$
[5.21]

The familiar constant a_t is the WLF shift factor, and a and b are constants given by fitting data of a glass forming substance onto a viscosity-temperature plot. The viscosity at the glass transition temperature η_g is about 10^{13} poise for many polymers.

An Arrhenius relationship more accurately models the temperature dependence of polymer melt viscosity at processing temperatures greater than Tg+100°C. A shear

rate may be arbitrarily chosen, but here the theoretical zero shear rate melt viscosity η_o is defined.

$$\eta_o = A_o^{T=\infty} \, e^{\left(\frac{\Delta E}{RT}\right)}$$

[5.22]

Here the absolute temperature T is given in Kelvin and R is the universal gas constant (8.314 $(J \text{ mol}^{-1} \text{ K}^{-1})$). The frequency factor $A_o^{T=\infty}$ (Pa s) is the theoretical minimum value of viscosity at infinite temperature, and usually at a known low shear rate of 1 Hz. The activation energy term $(\Delta E/R)$ is usually obtained by the slope of the curve defined by a plot of natural logs.

$$\ln\left(\eta_o^{T=\infty}\right) = \left(\frac{\Delta E}{R}\right)\frac{1}{T} + \ln\left(A_o^{T=\infty}\right)$$

[5.23]

The slope is positive for conventional treatment of this relationship; when the horizontal axis is defined to be reciprocal temperature. The larger value of flow activation energy increment ΔE $(J \text{ mol}^{-1})$ in a certain region of temperature, the greater the temperature dependence of viscosity.

Interpretation of the Physical Contact

The arc length ζ (m) for bar contact is mapped out by the bar contact angle θ and the bar surface diameter D as discussed in section 5.2.4.

$$\zeta = \frac{D}{2}\theta$$

[5.24]

The shear stress is known in terms of viscous drag force T_d applied over the contact area. The total shear area A_s (m^2) is defined by the bar contact curvature ζ and the average bar contact width w (m). The shear stress τ (Pa) in the boundary layer is therefore defined.

$$\tau = \frac{T_d}{A_s} = \frac{T_d}{2\zeta w}$$

[5.25]

The shear rate is equal to the quotient of the linear take-up rate v and the average thickness of the viscous polymer boundary layer $\bar{h}$ (m), between the stationary bar surface and the towpreg filament array.

$$\dot{\gamma} = \frac{v}{\bar{h}}$$

[5.26]

Modeling Assumptions

Figure 5.13 illustrates the expected viscous boundary layer between the towpreg and the stationary bar surface. The boundary layer shape and distribution was unknown but was expected to resemble a distribution thinnest near the middle of the contacted length and thickest at the entrance and exit regions. Cross-section photographs discussed in Chapter 3 indicated distinguishable viscous slag layers only near the entrance and exit contact locations. In accordance with the pultrusion pulling force model of Bibbo and Gutowski, a uniform boundary layer is approximated by the spacing between fibers of a close-packed hexagonal array.

$$\bar{h} = \delta \qquad\qquad [5.27]$$

Note that the fiber volume fraction V_f is not necessarily equal to the fiber volume of the composite, but rather is the fiber fraction of the boundary layer. This distinction is considered important since 1) viscous slag is never observed to drip off of the bars during processing and 2) viscous fluids tend to migrate toward shear fields. The boundary layer is possibly experiencing a control volume type of steady flow and there exists the possibility for causing a slightly resin rich surface as a result of this shear field. The fiber volume fraction of the boundary layer is expected to be slightly lower than that of the towpreg itself.

Power-law shear-dependent flow behavior was assumed since the area of interest for processing was usually within a 100°C range and the shear rates of the boundary layer were expected to be very high. Based on the previous assumptions for the boundary layer thickness, normal processing shear rates ranged from 10^4 to 2×10^5 (Hz) for velocities corresponding to 2.5 to 50 (cm s^{-1}). Shear deformation was assumed to be a consequence of the relative motion of the towpreg yarn filament array to the stationary bar surfaces. Viscous dissipation heating effects were considered negligible since the shearing time t_s of contact was very small. Arrhenius temperature dependence was assumed to characterize the polymer melt flow behavior since processing temperatures were normally higher than T_g + 100°C.

Viscous Drag Model Definition

The two governing relations for the shear stress were set equal to each other which provided the fundamental relationship.

$$\frac{T_d}{2\zeta w} = \tau = m\,\dot{\gamma}^n \qquad\qquad [5.28]$$

Substitution and addition of the capstan tension, yielded a fundamental model equation to predict the bar drag force.

$$T_d = w\,D\,\theta\,(\eta_o\,\dot{\gamma}^n) \qquad\qquad [5.29]$$

5.4   Pulling Force Model Evaluations

The two types of drag models were evaluated under conditions most likely to occur during normal operation of the *ex parte* process. An increase in pulling force with increased pulling velocity would provide a clear indication that there existed a hydrodynamic friction interface, however the experiment could not be easily accomplished in under isothermal conditions. As shown in the previous chapter, the pulling speed and the heat transfer (towpreg temperature) were interdependent. Geometrical considerations and capstan tension were independent parameters which could be set to constant values. The only independent processing parameters common to both models were contact angle θ and capstan tension Tc. Accordingly, their contributions to bar drag force were of particular interest. For Coulomb friction, the bar drag force was expected to increase linearly with capstan tension and increase

exponentially with contact angle. The hydrodynamic viscous friction drag was expected to increase linearly with contact angle but was independent of capstan tension.

Model Comparison with Experimental Data

The previously described bar drag force measurements were compared to calculated values obtained from each of the two theoretical models. The experimental parameters and material properties of the experiment were listed in **Table 5.2**.

Table 5.2   Nominal Processing Parameters for PIXA™/IM-7™ *ex parte* Ribbonizing

Parameter	Value
D (m)	0.01
r_f (m)	2.5E-6
v (m/s)	0.11
ΔE (J/mol K)	1.30E5
A (Pa s)	2.70E-8
n	0.42
T (K)	643
V_f	0.45
T_c (N)	17.63

Plots of the theoretical bar drag force as a function of contact angle are compared to the experimental data in **Figure 5.14**. The experimental bar drag force clearly

increased linearly, however, it was only at high contact angles where the distinction between boundary conditions was obvious. These high bar contact angles corresponded to larger contact areas. Although not presented here, the corresponding shear stress plot versus bar contact angle would be a line of 70 (KPa) magnitude and zero slope as expected for a viscous boundary layer.

It is interesting to note that by assuming a very low friction coefficient, the shape of the Coulomb friction model tended to be more linear and therefore mimicked the data more closely. This plot alone was not sufficient to define the boundary condition as dry friction, or viscous friction, or a combination of the two.

The bar drag force was calculated as a function of the capstan tension. The processing parameters listed in **Table 5.2** were utilized again except where noted on **Figure 5.15**. Again, the hydrodynamic model predictions mimicked more accurately the bar drag force data.

5.5   Pulling Force Observations and Suggestions

The measured viscous boundary layer shear stress for this ribbonizing process was near 10 (KPa) for 400°C bar temperature and 20 (cm s^{-1}) take-up speed. The viscous boundary layer model predicts a similar shear stress value. The previously discussed model #3 for thermoplastic pultrusion, predicts shear stresses 1000 times higher. This observation indicates a fundamental difference between pultrusion and *ex parte* ribbonizing.

Viscous fluids tend toward shear fields and therefore it is reasonable to expect a slightly resin-rich region near the towpreg/bar interface. The microstructure photographs of Chapter 3 offer tangible evidence of a polymer boundary region of about one fiber radius in thickness. The actual fiber volume fraction of the towpreg used to generate the data in **Figure 5.14** was near 60%. In order to fit the model to the data a theoretical fiber volume fraction of 45 to 50% are required. The fiber volume fraction used in the calculation of the boundary layer thickness δ is not the overall ribbon fiber volume fraction but rather is the fiber volume fraction of the boundary layer.

As T_c was increased, towpreg spreading at the bar contacts first increased, then encountered a maximum and then decreased. This phenomenon is attributed to the competition between the towpreg catenary effect which tends to draw the material into a cylindrical cross section and the squeeze-flow at the bar contacts which tends to spread the material into a wide flat cross section. The hydrodynamic model required that the shear stress in the boundary layer be independent of capstan tension, but the data presented in **Figure 5.15**, indicated a clear maximum of T_b with increasing capstan tension. This was attributed to the changing surface area presented to the shear field with changing band with. At maximum spreading, maximum pulling force was encountered. This observation did suggest a potential optimum value for capstan tension such that maximum spreading was achieved.

Material Considerations

The bar drag force model relied profoundly on accurate description of the polymer

viscosity. Polymer melt viscosity is related to molecular weight, polydispersity, chain branching, temperature and shear rate. For polymer processing, this very complex secondary material property is typically characterized in terms of only the latter two. The assumption of constancy among polymerization batches is considered reasonable. As mentioned in a previous section of this chapter, the difference in melt behavior for different thermoplastic polymers is significant. Just as important, the flow behavior of a polymer melt varies significantly with temperature and shear rate. The complication here is that the shear rate and temperature effects are interdependent.

The recent literature on polymer melt processing science has consistently utilized Arrhenius values, power-law index, relaxation time and even zero shear rate viscosity values to evaluate processing models. Most of the thermoplastic composite processing science has made use of the matrix polymer PEEK™ with carbon fibers. **Table 5.3** is a compilation of published viscosity relationships for PEEK™ and several different types of thermoplastic polymers. The published viscosity relationships for PEEK™ were variant.

It is suggested that the Arrhenius frequency factor A_0 and flow activation energy ΔE, be obtained via cone and plate, steady-mode rheometry. The frequency factor should be considered to represent the theoretical viscosity at infinite temperature and 1 Hz shear frequency. The power law index and relaxation time of the polymer melt are both dependent on temperature and so the likely temperature range should be established. The values for power law index n should be obtained for several isothermal frequency sweeps within the established temperature range. An average value for the power law index should be sufficient within a narrow processing

temperature range.

Table 5.2   Literature Values for Temperature and Shear Rate

Dependence of Polymer Melt Flow

Polymer	$\Delta E/R$ (K^{-1})	A_0 (Pa s)	n	η_0 (Pa s) @°C	λ (s)
PEEK[5]	16,260	6.6E-9	0.916	N/A	N/A
PEEK 150P[12]	19,100	1.13E-10	N/A	N/A	N/A
PEEK[25]	N/A	N/A	0.787	280@ 375	0.038
PEEK[26]	N/A	N/A	0.8	280 @ 400	0.04
PEEK[27]	N/A	N/A	N/A	3,500 @ 390	N/A
PEEK 150P[28]	5,523	N/A	0.71	1,090 @ 380	N/A
PEEK 380P[28]	5,523	N/A	0.67	3,600 @ 380	N/A
PEEK 450P[28]	5,523	N/A	0.63	5,870 @ 380	N/A
APC-2[10,29]	2,969	133	N/A	N/A	N/A
APC-2[12]	26,300	1.14E-12	N/A	N/A	N/A
PP[30]	5,600	2.6E-3	N/A	528@ 185	1.0
PPS[31]	N/A	N/A	N/A	N/A	0.1
PA[27]	N/A	N/A	N/A	33 @ 215	N/A
PPS[27]	N/A	N/A	N/A	2,500 @ 315	N/A
PEI[27]	N/A	N/A	N/A	2,000 @ 350	N/A
PIXA[32]	15,600	2.7E-8	0.42	N/A	0.01
PS[27]	N/A	N/A	N/A	2,000 @ 350	N/A
PEKK[33]	12,000	1.42E-6	0.35	N/A	0.003

The expected shear rate range for processing should be approximated. Polymer melts can exhibit strictly Newtonian, power-law or Carreau-type flow. PIXA™ and PEEK™ are strictly power-law fluids within the nominal temperature and shear rate ranges

encountered in ribbonizing. If the polymer rheometry indicated Carreau flow behavior, the hydrodynamic model should be adjusted to incorporate the relaxation time.

Sensitivity Analysis of the Hydrodynamic Boundary Layer Model

The relative importance of speed and temperature was evaluated within the range of probable processing conditions. **Figure 5.16** is an isometric representation of the hydrodynamic bar drag force model for two 12K, PIXA™/IM-7™ powder towpregs with both take-up speed and boundary layer film temperature increasing simultaneously. To process at moderate pulling force, this curve suggests processing at the maximum temperature and minimum speed. Temperature appears to be more important than the speed. For an increase in temperature of 40°C at 20 (cm s⁻¹), the bar drag was reduced by at least 75%. At 400°C the bar drag force leveled-off quickly with increasing take-up speed. This curve suggests that at high processing temperatures, there is no fundamental pulling force limitation on processing speed.

Summary of Pulling Force Analysis Observations

The pulling force for *ex parte* ribbonizing is comprised of 3 major components, capstan tension, bar drag tension and axial nip tension. Capstan tension is a process control variable. Bar drag tension is a complex function of processing conditions. The axial nip tension is observed to increase with increasing transverse nip load and is also expected to be a function of processing conditions. Under nominal processing conditions, bar drag is more significant than the axial nip load.

As capstan tension is increased, spreading at the bar contacts encounters a maximum width, which was attributed to the competitive mechanisms of squeeze-flow spreading and catenary effect narrowing. The shear stress in the boundary layer is independent of capstan tension, but the bar drag tension exhibits a secondary dependence on capstan tension related to the spread width.

The bar drag force is entirely attributed to hydrodynamic friction between the towpreg and the stationary bars. This implied that axial plug flow was not possible. The bar drag tension increases linearly with contact angle. Since the bar drag force component was found to be dependent on material properties, temperature, process geometry and take-up speed, sensing the bar drag force could be useful for indicating process control.

5.6   End Notes

1   Bodine Electric Company, 1975, Brush Motor Test Report, 32DSBEPM.

2   Stokes, T. (Modern Machine & Tool Co. Inc.), Newport News, VA.; Rhew, R. (NASA LaRC), Hampton, VA., 1994, NASA CONTRACT NAS1-19369 Report.

3   Suh, N.P. "Tribophysics", Prentice-Hall: Englewood Cliffs, New Jersey, 1986.

4   Williams, J.G.; Morris, C.E.M.; Ennis, B.C. *J. Polym. Eng. Sci.* **1974** *14* (6),413.

5   Seo, J.W.; Lee, W.I.. *J. Comp. Mat.* **1991**, *25*,1127.

6   Yang, H.; Colton, J.S. Preview Copy for *J. Polym. Comp.* **1993**.

7   Ahn, K.J.; Seferis, J.C.; Price, J.O.; Berg, A.J. *SAMPE Journal*, **1991**, 27(6), 19.

8   Hou, T.H. Soc. Plast. Eng. Tech. Papers, ANTEC'86, 1986, 1300.

9   Hepola, P.J., Ph.D. Dissertation, The University of Delaware, Newark, DE.,

1993.

10 Lee, L.I.; Springer, G.S.; Smith, F.N. *J. Comp. Mat.* **1991**, *25*, 1632.

11 Bibbo, M.A.; Gutowski, T.G. Soc. Plast. Eng. Tech. Papers, ANTEC'86, **1986**, 1430.

12 Mantell, S.C.; Springer, G.S. *J. Comp. Mat.* **1992**, *26*, (16), 2348.

13 Gutowski, T.G.; Cai, Z.; Bauer, S.; Boucher, D.; Kingery, J.; Wineman, S. *J. Comp. Mat.* **1987**, 21, 650.

14 Gutowski, T.G. *SAMPE Series*, **1985**, *30*, 925.

15 Gutowski, T.G. *SAMPE Quarterly*, **1985**, *16* (4).

16 Price, H.L.; Cupschalk, S.G. in "Polymer Blends and Composites in Multiphase Systems", C.D. Han, ed. *ACS Advance in Chemistry Series* **1984**, *206*.

17 White, F.M. "Fluid Mechanics", 2nd Ed., McGraw-Hill: New York, 1986; Chapter 1.

18 Barnes, H.A.; J.F. Hutton; Walters, K. "An Introduction to Rheology", Elsevier: New York, 1989; Chapter 1.

19 Walters, K, "Rheometry", Chapman and Hall: New York, 1975, p.52.

20 Rosen, S.L. Fundamental Principals of Polymeric Materials for Practicing Engineers, Barnes and Noble: New York,X.

21 Kumar, N.C. *J. Polym. Sci. Macromol. Rev.* **1980**, *15*, 255-325.

22 Sears, F.W.; Zemansky M.W.; Young H.D. "University Physics", 6th ed.; Addison-Wesley : Reading Massachusetts, 1983, Chapter 13.

23 Avallone E.A.; Baumeister T. "Marks' Standard Handbook for Mechanical Engineers", 9th ed.; McGraw-Hill: New York, 1987.

24 Cheng, J.T. "Applied Rheology and Polymer Processing", from Cheremisinoff, X. "Encyclopedia of Fluid Mechanics", Vol. 7, Gulf Publishing: Houston, 1988.

25   Burns, J.S. *J. Thermopl. Comp. Mat.*, **1994**, *7*, 100-.

26   Carpenter, C.E.; Colton, J.S. *SAMPE Series*, **1993**, *38*, 205-.

27   Iyer, S.I.; Drzal, L.T. *J. Thermopl. Comp. Mat.*, **1990**, *3*, 325-.

28   Qizian, L.; Ziaoming, Z. *SAMPE Series*, **1993**, *38*, 1594-.

29   Ranganathan, S.; Advani, S.G.; Lamontia, M.A. *SAMPE Technical Series*, **1993**,

        25, 630.

30   Ye, L.; Klinkmuller, V.; Freidrich, K., *J. Thermopl. Comp. Mat.*, **1992**, *5*, 32-.

31   Baird, D.G.; Sun, T.; Done, D.S.; Wilkes, G.L. *J. Thermopl. Comp. Mat.*, **1990**,

        3, 31-.

32   Personal Correspondence with Y. Sugita, Mitsui Toatsu, 1993.

33   Personal Correspondence with J. Pratt, DuPont Advanced Materials, 1993.

5.7   Chapter 5 Figures
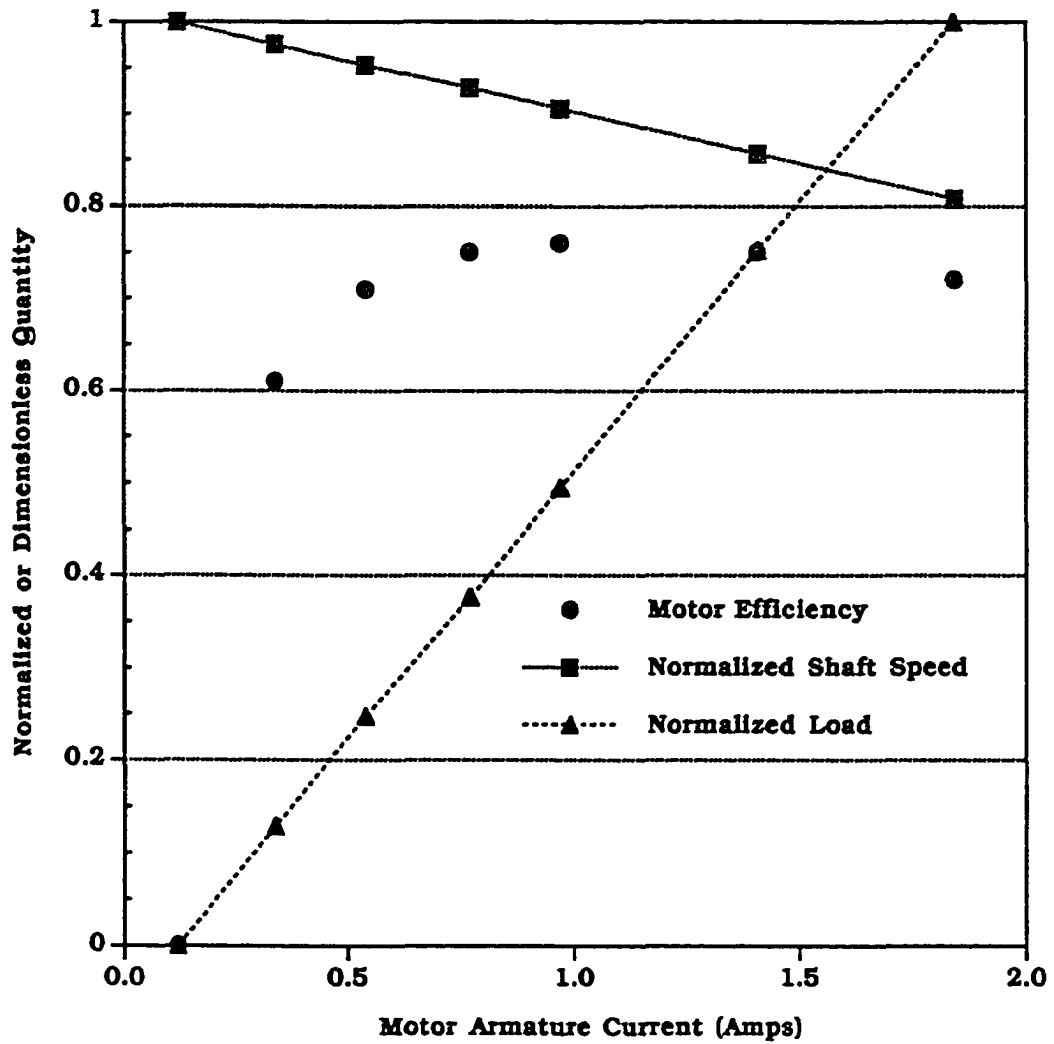
Figure 5.1 Take-up Motor Performance for a Steadily Increasing Load
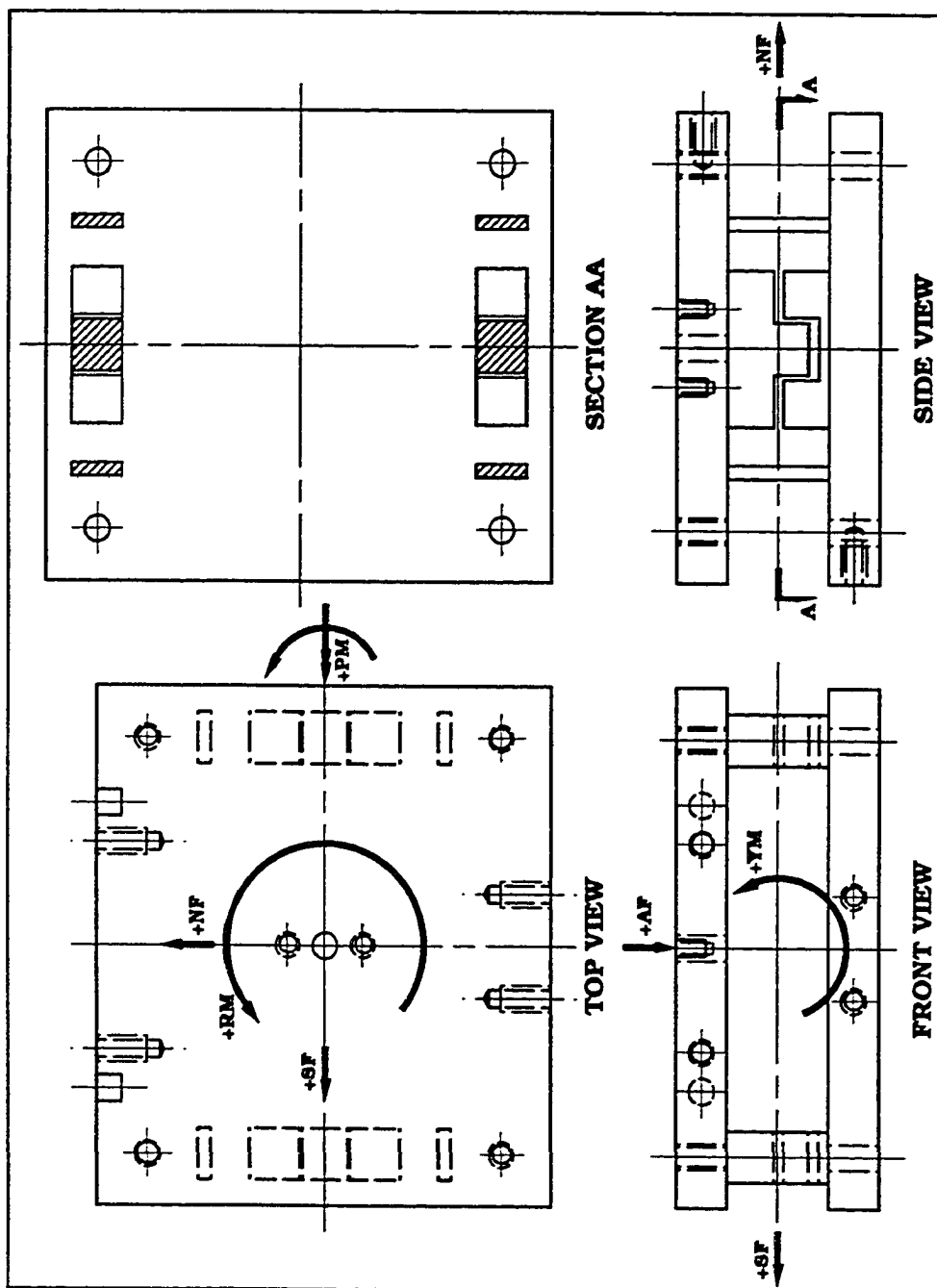
Figure 5.2 Pulling Force Load Cell Design Illustration.
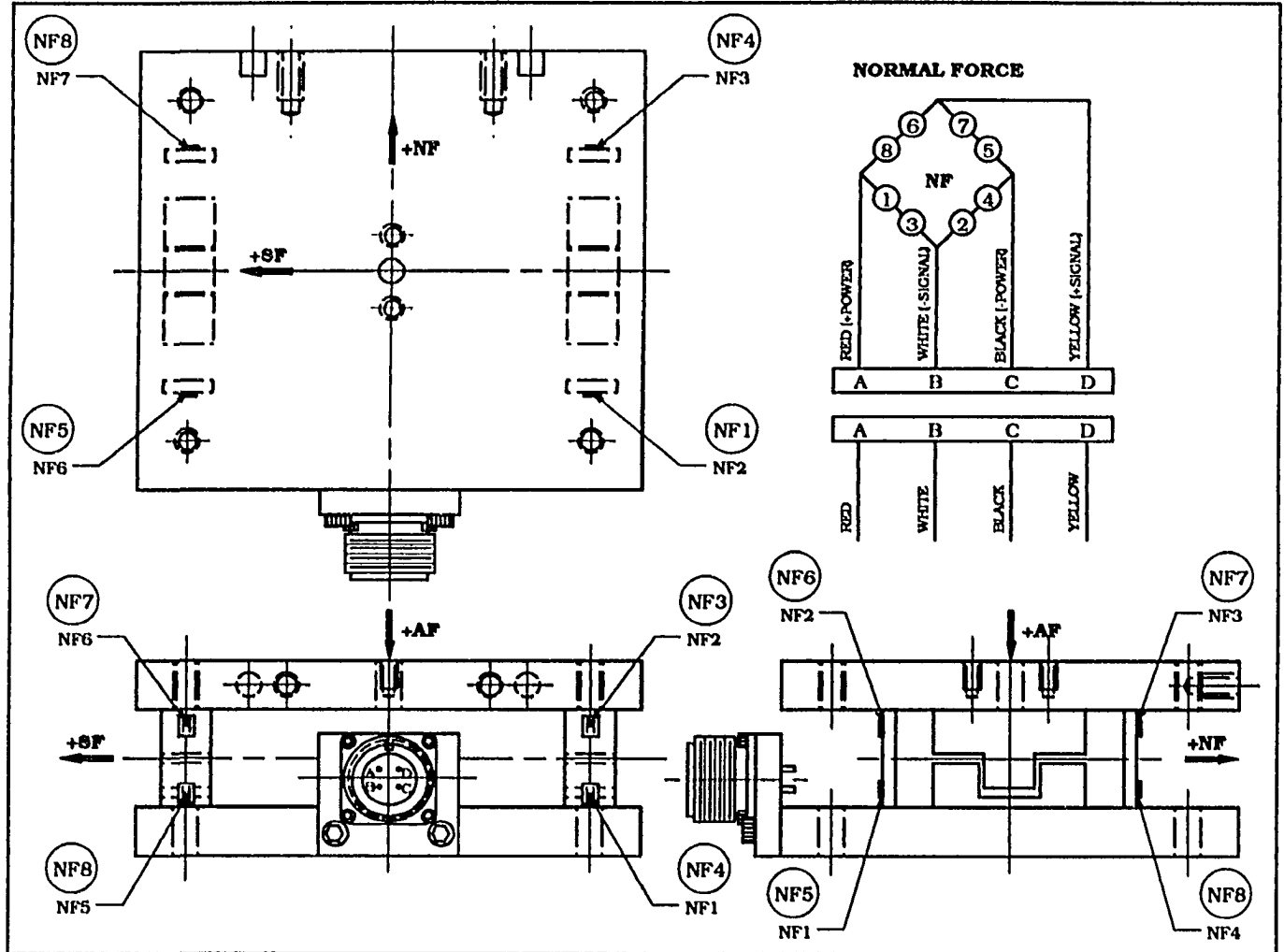
Figure 5.3 Pulling Force Load Cell Wiring Illustration.
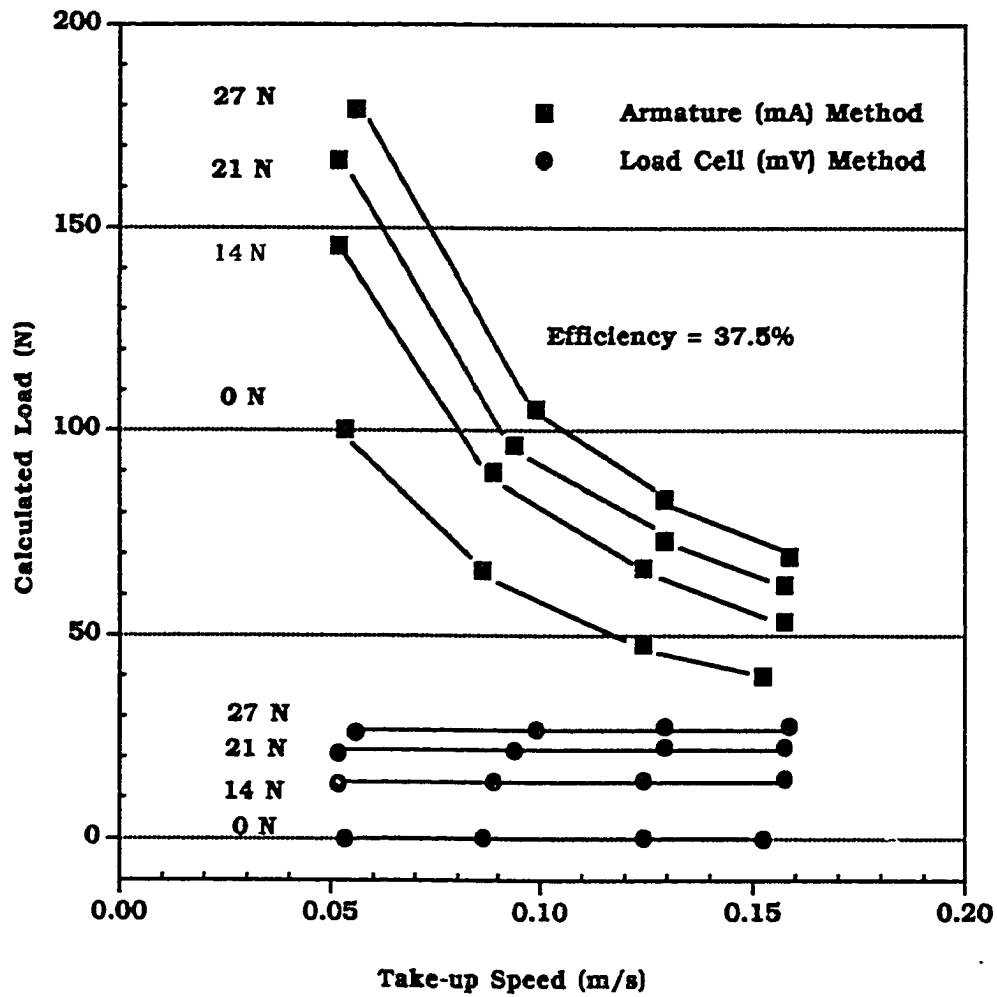
Figure 5.4 Comparison of Two Different Pulling Force Measurement Techniques at Four Different Capstan Loads and Four Different Speeds.
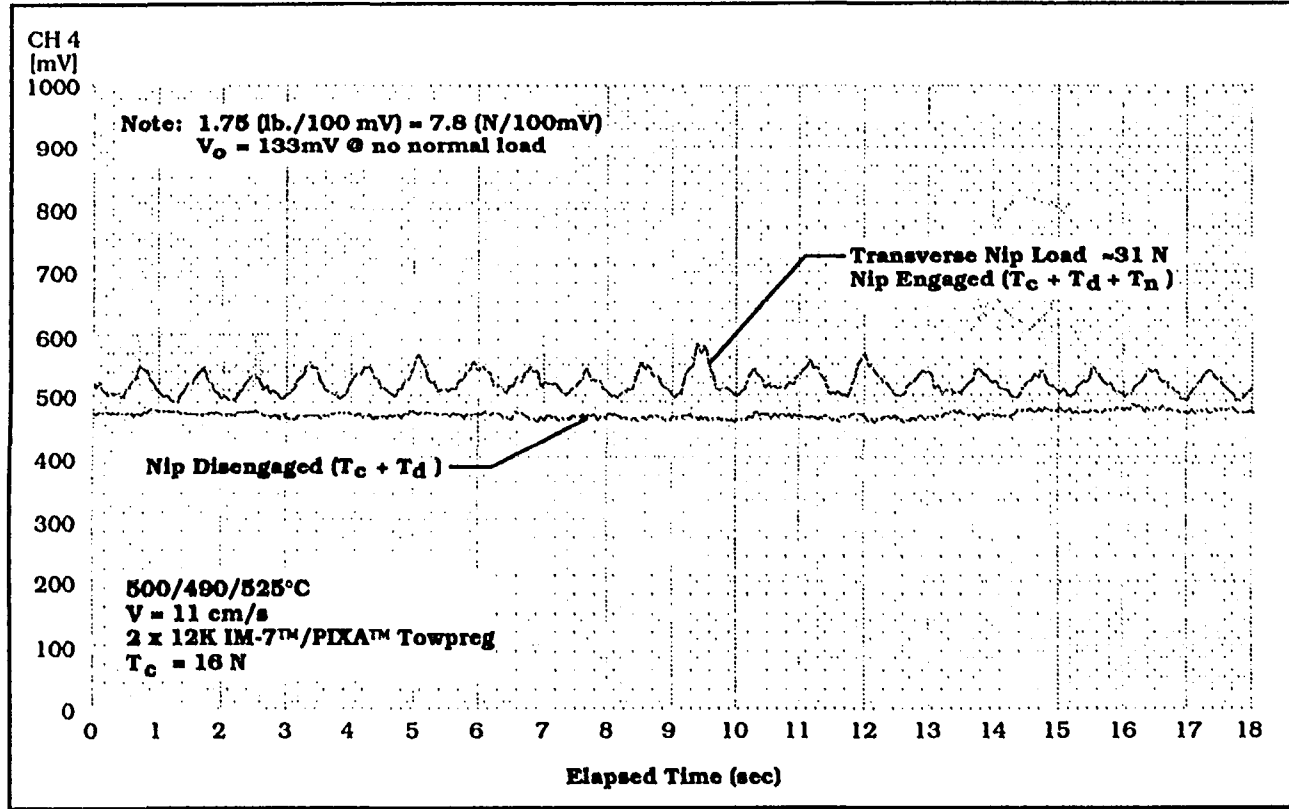
Figure 5.5 Typical Pulling Force Data for the Nip Engaged and Disengaged
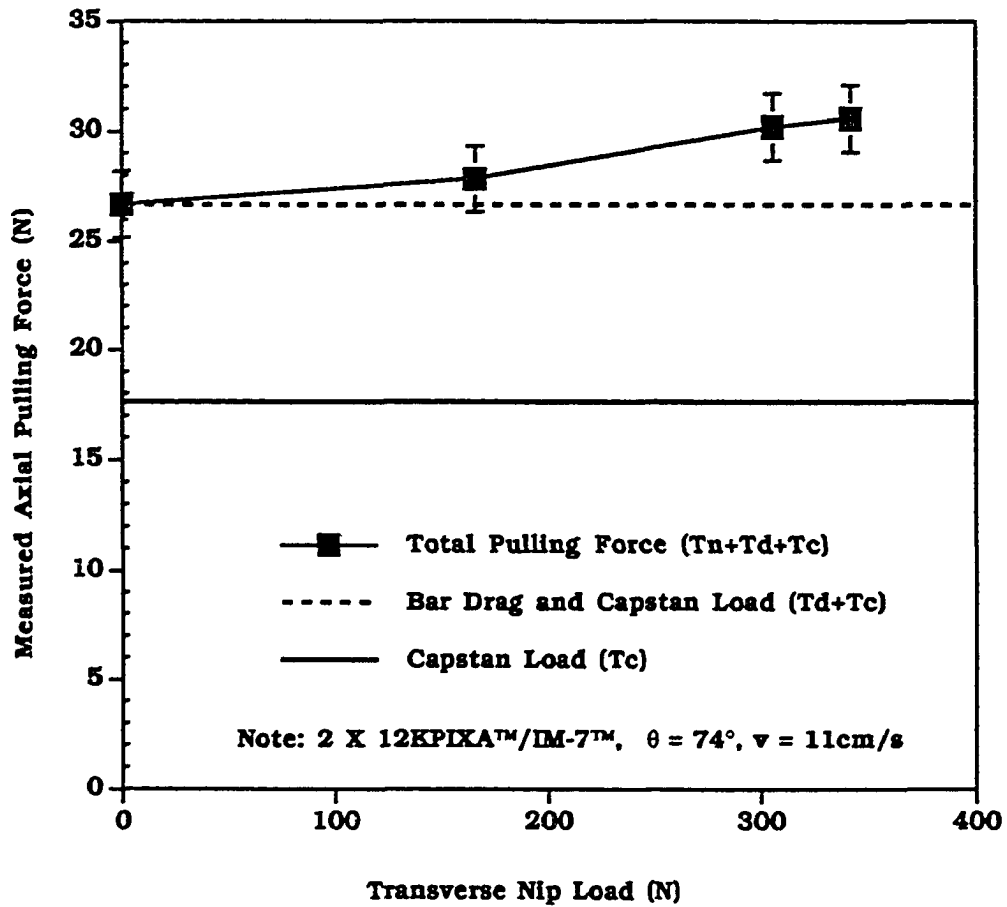
Figure 5.6 Relative Importance of the Three Pulling Force Components.
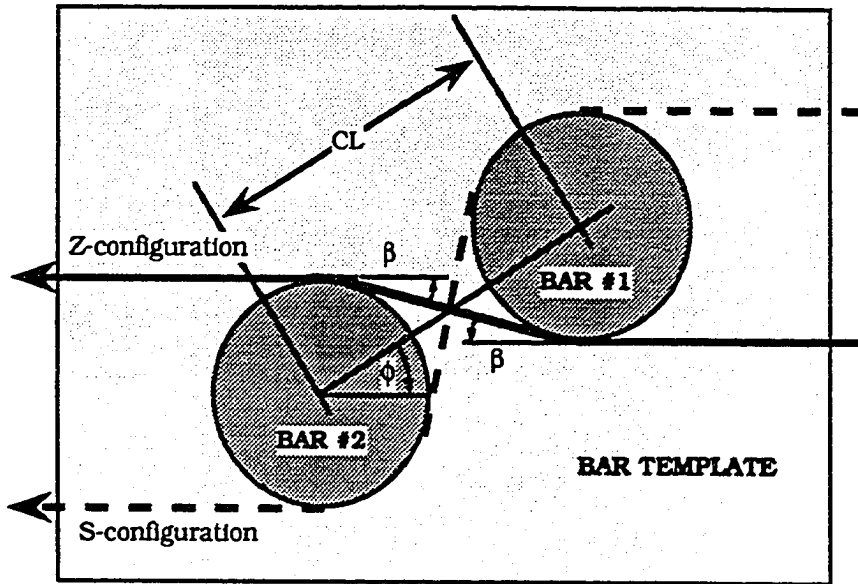
Figure 5.7 Template Geometry and Wrapping Configurations
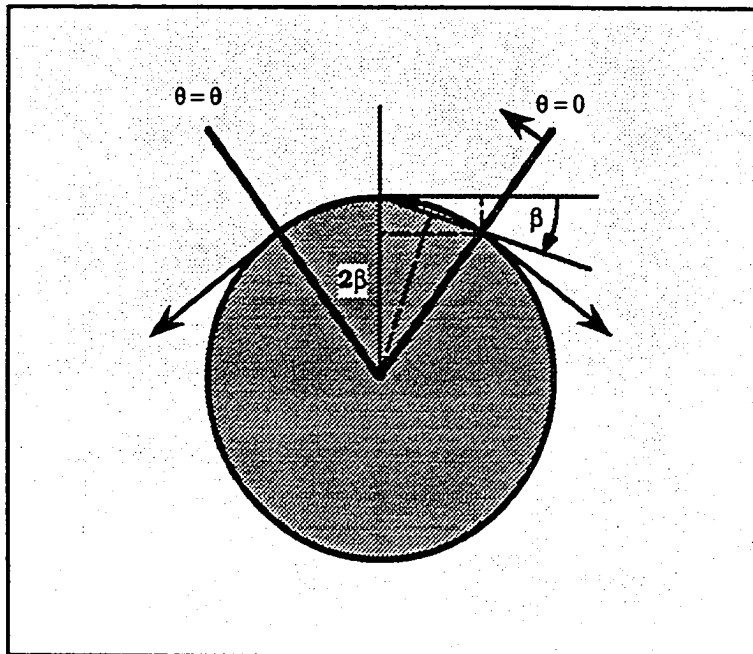
Figure 5.8 Geometry of Bar Surface Contact
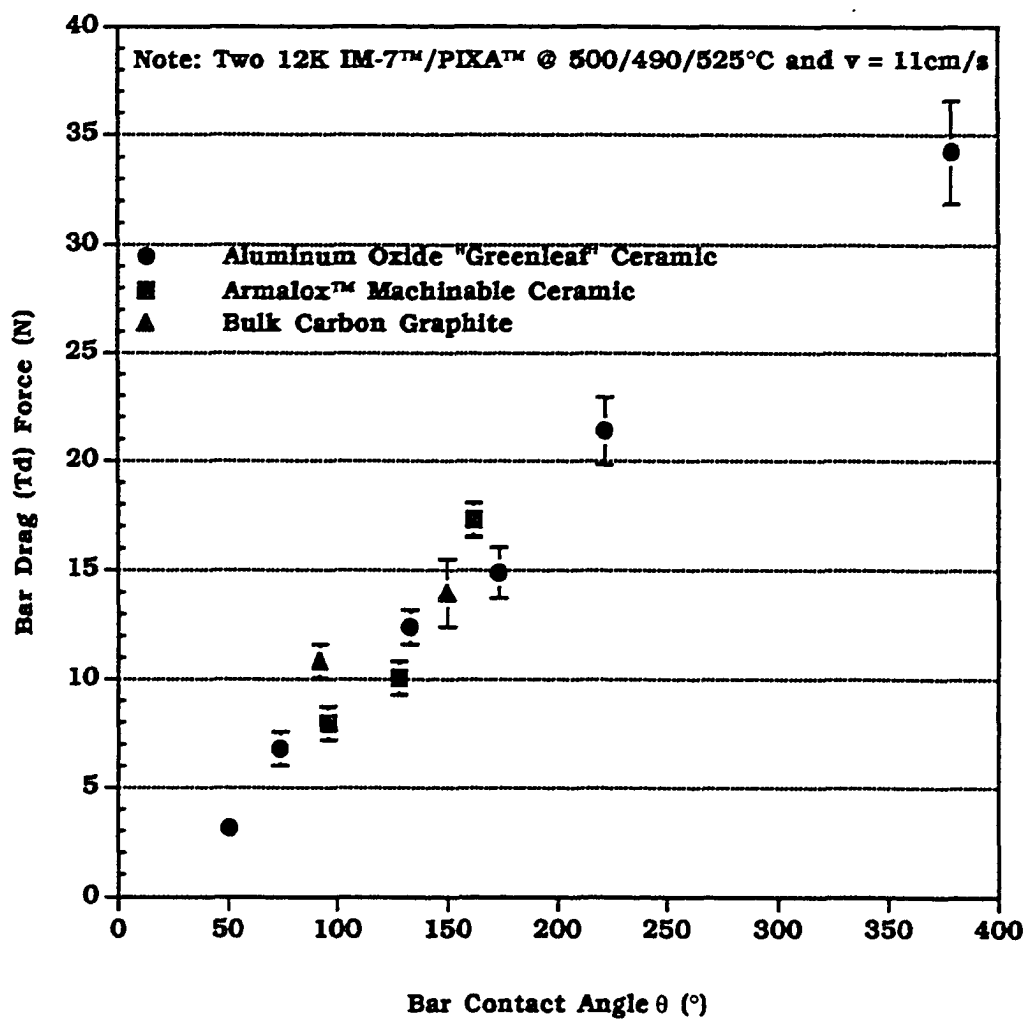
Figure 5.9 Bar Drag Force vs. Contact Angle for Three Different Stationary
Bar Materials.
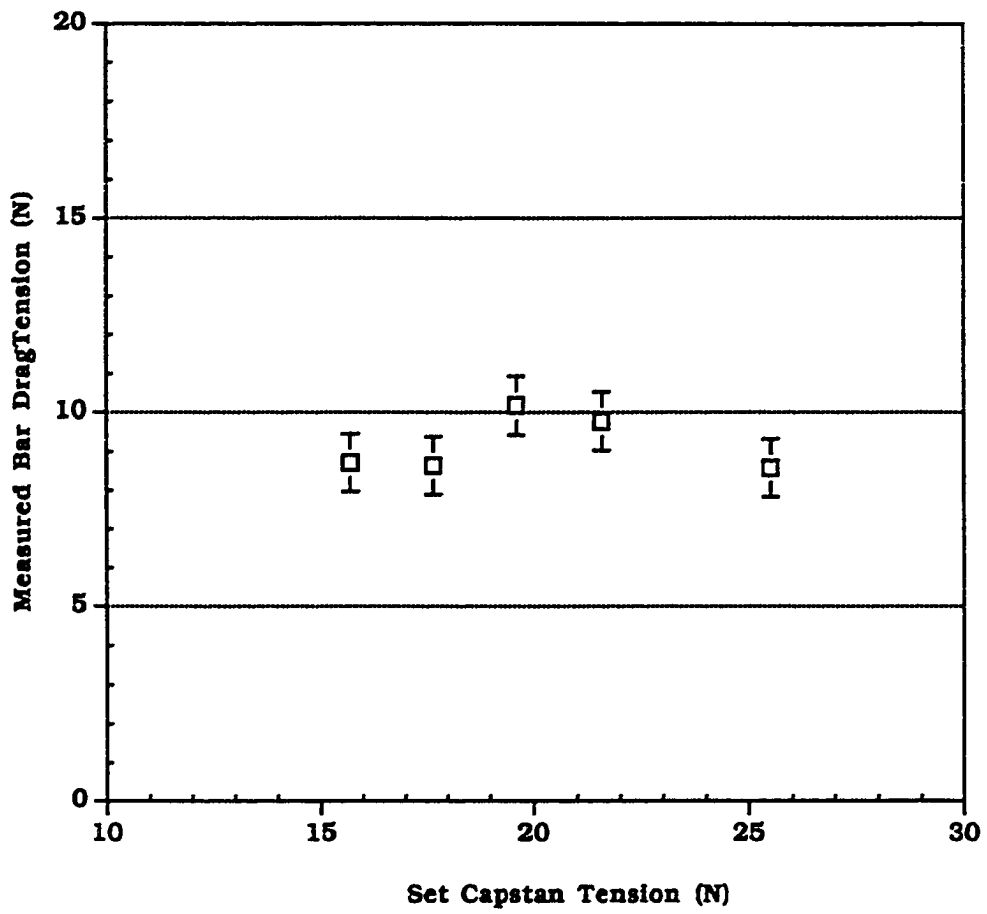
Figure 5.10 Bar Drag Force Data as a Function of Capstan Tension

Total Contact Angle = θ

$d\theta$

$T(\theta) + dT$

$T(\theta)$

dN

$Td + Tc$

Tc

Velocity = v

D/2

Stationary Bar

Contact Length = θ D/2

$\theta = f (D, CL, \phi)$

$$T_d = T_c \, [\, e^{\mu\theta} - 1\,]$$
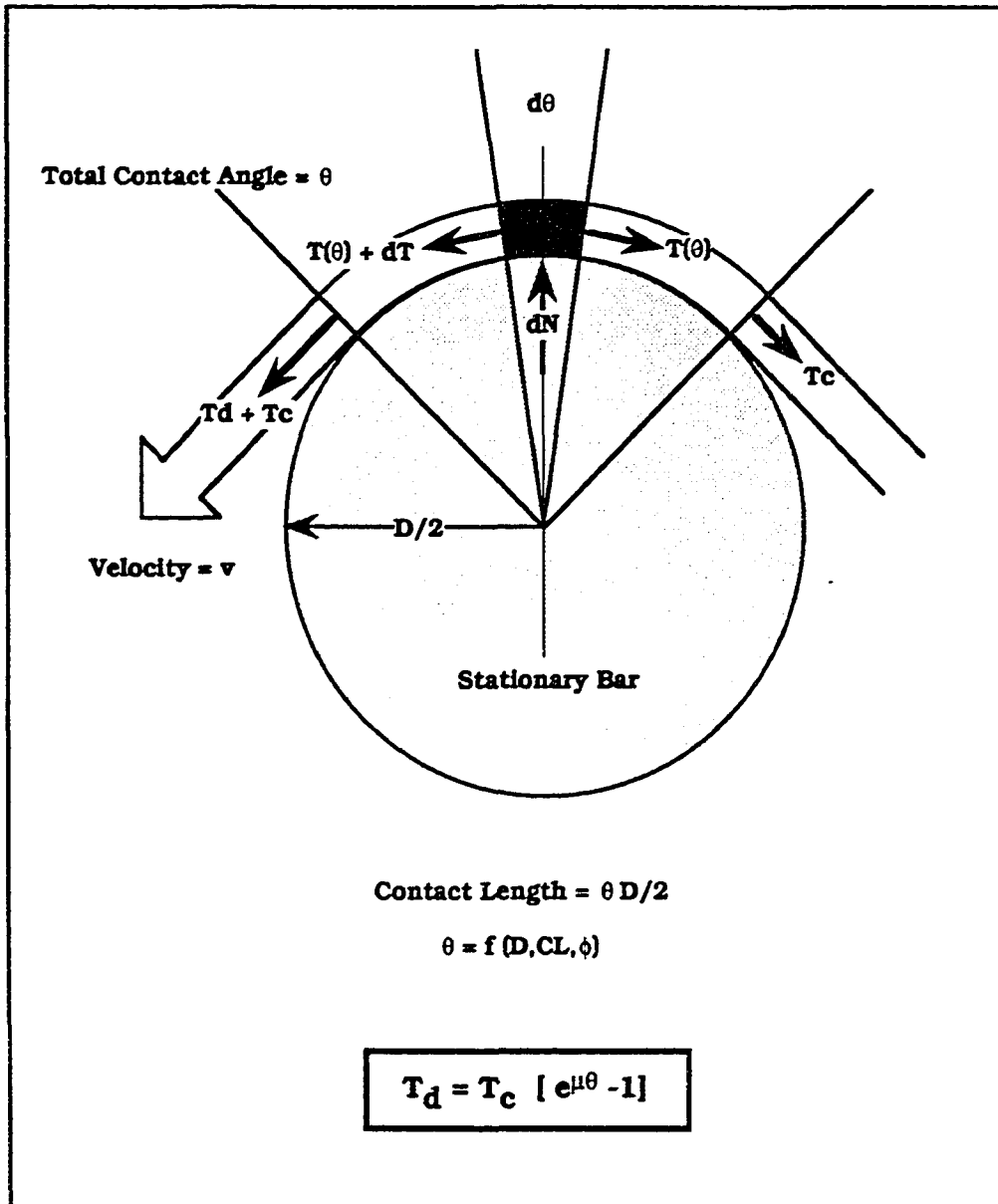
Figure 5.11 Representative Diagram of Towpreg Section Under Dry Friction
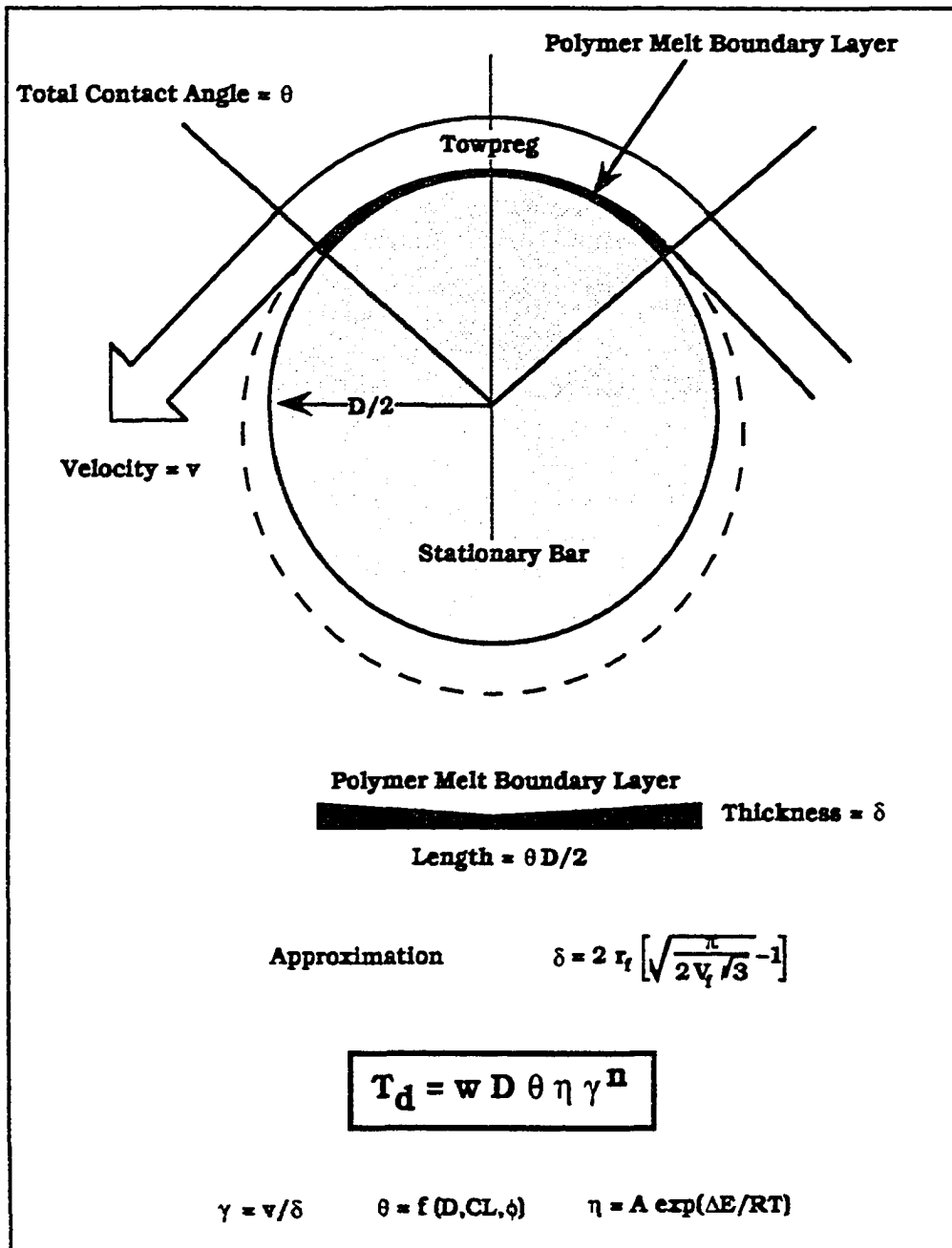
Figure 5.12 Viscous Boundary Layer Illustration and Drag Force Model Definition
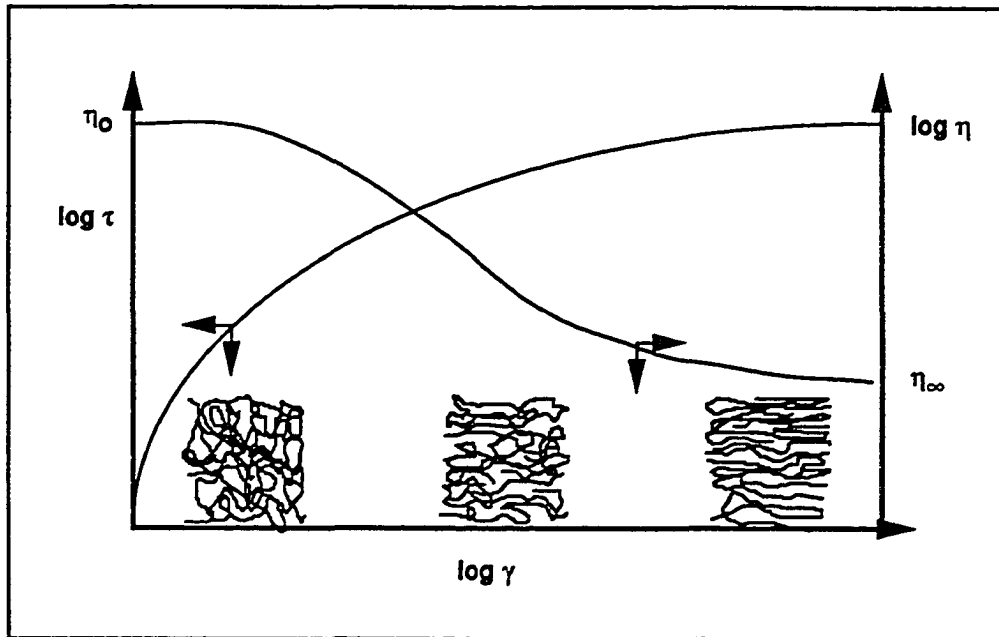
Figure 5.13 Effect of Shear Rate on Polymer Melt Shear Stress, Viscosity and Molecular Entropy
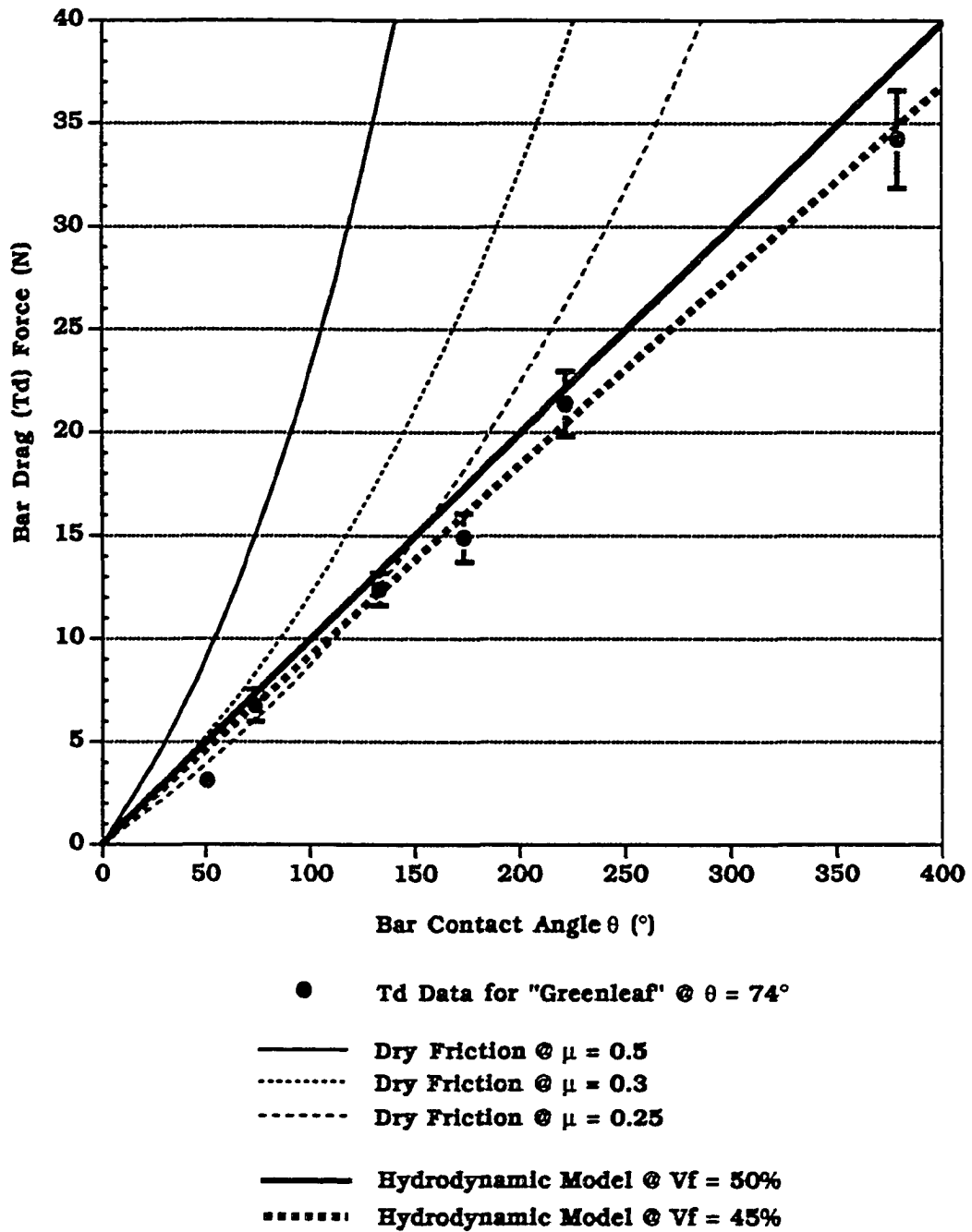
Figure 5.14 Bar Drag vs. Contact Angle Data Compared to Two Types of
Bar Drag Force Models
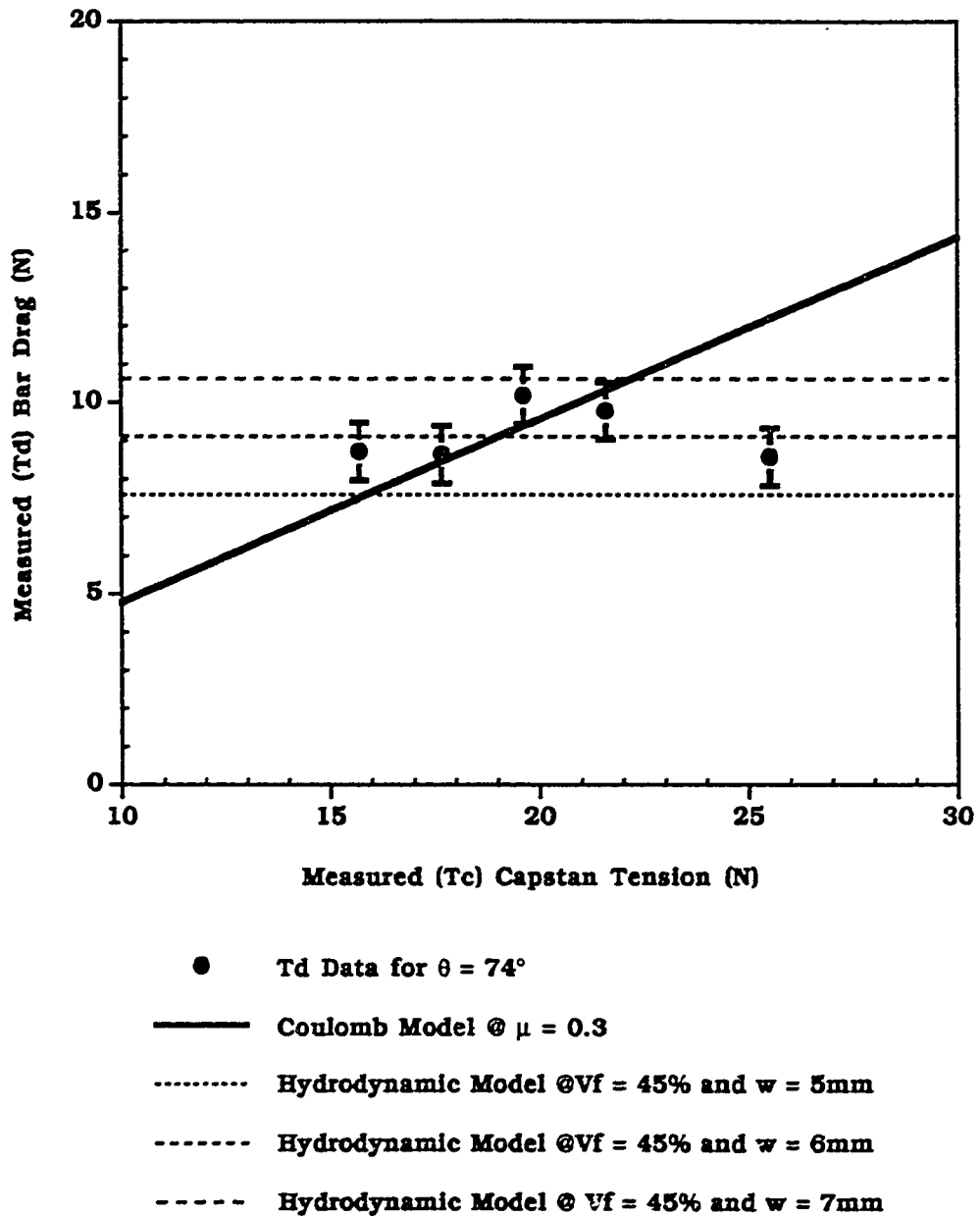
Figure 5.15 Bar Drag Force Data as a Function of Capstan Tension
Compared to Two Types of Drag Force Models

2 X 12K IM-7/PIXA Powder Towpreg @ Nominal Processing Conditions

Bar Drag Force (T_d)

(0 - 16 N)

Take-up Speed

(0 - 20 cm/s)

Temperature

(360 - 400°C)
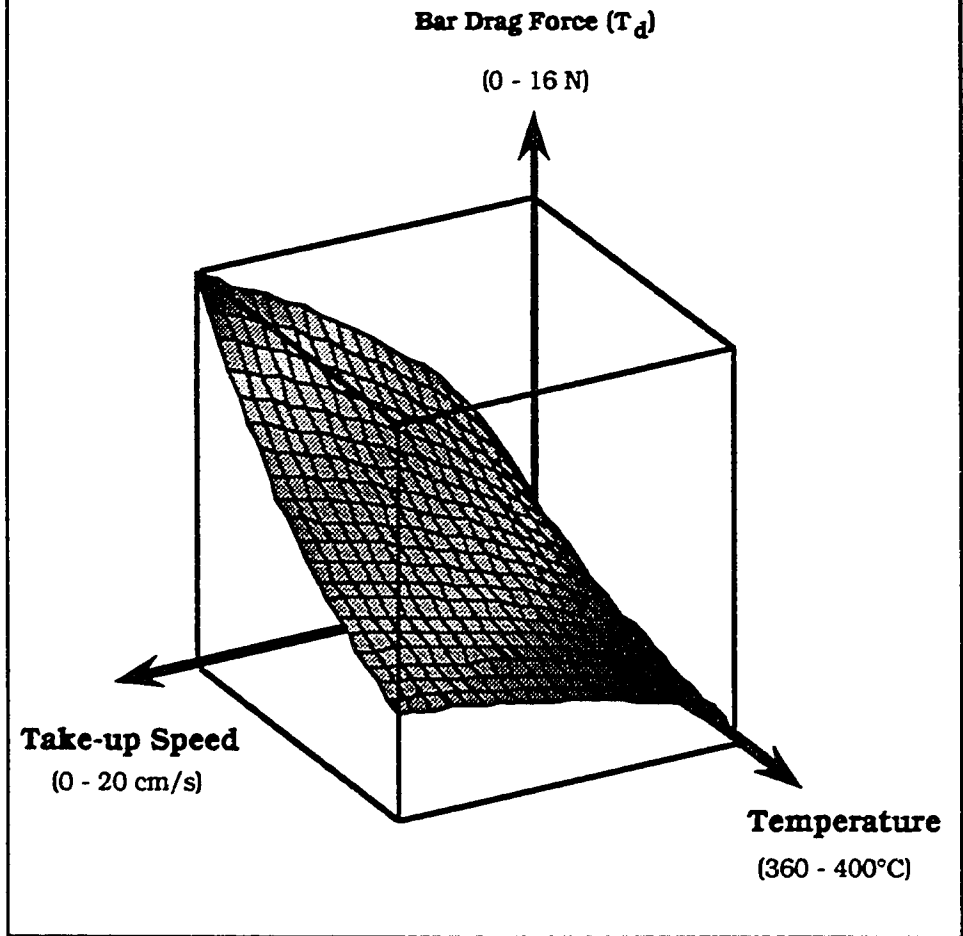
$$Td = w \, D \, \theta \, \eta \, \gamma^n$$

$\gamma = v/\delta$ $\qquad \theta = f(D,CL,\phi)$ $\qquad \eta = A \exp(\Delta E/RT)$ $\qquad \delta = 2 \, r_f \left[\sqrt{\dfrac{\pi}{2 V_f /3}} - 1 \right]$

Figure 5.16 Typical No-Slip Boundary Layer Model Isometric Plot.

Chapter 6   Summary of Conclusions

The goal of this research was to develop a controllable process to convert a thermoplastic powder-coated carbon-fiber towpreg into uniform and consolidated ribbon. The approach comprised four primary activities. 1) The patent and processing literature was studied to evaluate the state of-the-art. 2) A functional ribbon fabrication technique was developed by scaling-up, in a novel (*ex parte*) configuration some of the hardware components found in the literature. 3) The *ex parte* ribbonizing process was characterized by calibrating equipment, determining steady-state and studying cause and effect between process parameters and ribbon quality. 4) Process design and control methods were derived from heat transfer and pulling force analyses.

The *ex parte* ribbonizer process comprises a material handling system, a preheat region, a heated stationary bar assembly, and a cooled nip roller assembly. Appropriate timing of important contacts is key to fabricating quality ribbon. Process characterization and analyses revealed key flow mechanisms. Ribbon microstructure changes most at the bars. Ribbon macrostructure changes most at the nip. An isothermal bar contact is a practical processing constraint for ensuring uniform squeeze flow bar spreading. All bar drag force is attributed to shear stress in the interfacial viscous boundary layer between the towpreg and the stationary bar surface. Continually sensing pulling force is a good indication of process control.

The research goal was achieved because the *ex parte* ribbonizer can be used to convert polymer powder towpreg into uniform and fully-consolidated ribbon in a

controllable manner.

Summary of Observations

A study of the state of-the-art in polymer composite prepregging revealed the key approaches for converting thermoplastic powder-coated towpreg into consolidated and uniform cross section ribbon. For this objective, towpreg band spreading was accomplished best by heated bar spreading and ribbon forming was accomplished best by cooled nip rolling. A novel process called the *ex parte* ribbonizer was developed comprising a material handling system, a premelting chamber, a stationary bar assembly and a cooled nip roller assembly.

The *ex parte* process was characterized in terms of hardware description and calibration. The material handling system control parameters: capstan tension (7.5 to 20 (N)) and pulling speed (0 to 50 (cm s^{-1})), were variable by analog setting. The premelting chamber control variables comprised three zone set temperatures. The stationary bar assembly control parameter was the total contact wrap angle (50 to 400°). The stationary bars were passively heated by the steel tube liner of the premelting chamber. The cool nip roller control parameter was transverse nip load (10 to 25 lbf.). All of the process control parameters affected ribbon quality to some extent.

A microstructure analysis revealed key phenomenon encountered by the towpreg which were 1) gas bubble (void) redistribution, 2) transverse, permeative melt flow (general wet-out), 3) filament alignment, 4) residual void compression, 5) elastic

compaction of the filament network, and 6) net axial cross section shaping. The least significant of these mechanisms is transverse melt flow due to the high shear stress and the short time-scale of the perturbation. Axial melt flow is not likely a key component of the flow phenomenon because the axial viscous flow potential only exists at the tangent point of initial bar contact.

The towpreg "void content" comprises two components, incompletely wet-out regions and gas bubbles. The cylindrical symmetry assumed by the towpreg during preheating is attributed to "towpreg catenary effect". Spreading at the bar contacts is attributed to composite squeeze flow. After exiting the last bar contact, the towpreg cross section is generally wide and flat but usually contains some gas bubbles near the center plane. Filament alignment and elastic compaction of the filament network are implicit by towpreg band spreading. Fabrication of void-free towpreg ribbon is dependent on the initial quality of the powder towpreg. The key to forming good ribbon microstructure is to maximize wet-out and minimize entrapped gas bubbles. The key to good macrostructure is to optimize bar spread width to be nearly identical to the desired ribbon width.

The heat transfer phenomenon of the *ex parte* process comprises 1) preheating, 2) bar contact heating, 3) ambient cooling and 4) nip cooling. The first two components were modeled to predict heating thermal history up to the maximum temperature experienced by the material.

The preheating phenomenon was modeled and evaluated in scalar form. The scalar representation correlates well with measurements. Preheating is primarily driven by

radiation from the tube liner and axial conduction opposing the relative velocity of the towpreg. Processing speed and furnace set temperatures are the most important variables for determining the q.s.s. preheat temperature profile in terms of basic material properties, processing parameters and geometrical considerations. The model is useful for predicting the q.s.s. towpreg temperature profiles up to the bar contact location.

The bar contact heat transfer phenomenon was modeled and evaluated first in two spatial dimensions. Several temperatures through the towpreg bands thickness were averaged to provide a scalar representation of the q.s.s. mean towpreg temperature profile. The scalar representation of the towpreg temperature increase, caused by contact with the stationary bars, provides a reasonable first approximation. Heating is driven by conduction with the bar surfaces. The two dimensional analysis revealed the potential for substantial temperature gradients throughout the towpregs thickness. This observation implies potential for non-isothermal bar contact squeeze flow at high or low processing speeds. Non-isothermal squeeze flow is considered undesirable in terms of steady-state operation and process control. An isothermal squeeze flow process control constraint is considered practical.

The two heat transfer model components were integrated as an illustrative approximation to demonstrate potential process thermal history scenarios. For a given set of processing conditions, velocities are considered too low if $T_p \gg T_b$ and too high if $T_p \ll T_b$. An isothermal constraint is imposed on the bar contact region such that the preheating temperature, the bar temperature, the maximum temperature and the desired processing temperature are all equal. This constraint ensures uniform

viscosity throughout the cross section. In order to implement this process constraint, the previously established steady-state tube liner temperature profile, and continual sensing of the bar surface temperature, are used to evaluate the heat transfer model providing the appropriate processing speed.

The utility of the heat transfer models extends beyond process control issues and contributes to process engineering and design. For a given set of process conditions, under the isothermal bar contact constraint, the process speed can be increased by lengthening the tube liner or increasing the set temperature of the oven zones upstream of the bar contact location. The oven zone set temperatures can be increased to allow for faster speeds, however, the risk of overheating during a momentary stoppage or slow-down, prohibit this approach in the extreme.

The pulling force for *ex parte* ribbonizing comprises 3 major components; 1) capstan tension, 2) bar drag, and 3) axial nip tension. The capstan tension is a process control variable. As the capstan tension is increased, the spreading at the bar contacts encounters a maximum width, which is attributed to the competitive mechanisms of squeeze-flow spreading and towpreg catenary effect narrowing.

Under nominal processing conditions, the bar drag force is more significant than the axial nip load. The axial nip tension was observed to increase with increasing transverse nip load. The bar drag force is entirely attributed to hydrodynamic friction between the towpreg and the stationary bars. The bar drag tension increases linearly with contact angle. The shear stress in the boundary layer is independent of capstan tension, but the bar drag tension exhibits a secondary dependence on capstan tension

related to the spread width. Since the bar drag force component is dependent on material properties, temperature, process geometry and take-up speed, sensing the bar drag force is useful for indicating process control.

The novel *ex parte* ribbonizer together with the mechanism study, heat transfer model and pulling force model provide a controllable process which is useful for converting thermoplastic powder-coated towpreg into high-quality ribbon for use in ATP fabrication of composite structures.

Future Work

Continued process development is necessary to fully exploit the *ex parte* ribbonizer. The take-up should be redesigned so that a separate winder and puller exist. The nip design should be redesigned for better ribbon dimensional tolerances. An automatic slag removing and bar cleaning mechanism is necessary to allow for long duration (over 2 hour) fabrication runs. A ribbon splice tool is necessary to join continuous ribbons allowing the operator to remove poor quality ribbon which can result in the middle of a fabrication run. A variable bar contact angle mechanism is necessary to allow for analog settings as a readily variable control parameter.

Continued process control development is necessary to gain a closed-loop control mechanism for the *ex parte* ribbonizer. Permanent thermocouple attachments to the tube liner surface should be put in place to sense, in real-time, the driving potential for heating so that the q.s.s. towpreg profile could be evaluated continually. A method for determining the natural tolerance of pulling force should be developed for common

fabrication conditions to establish the process control range. A closed-loop process control mechanism should be developed by integrating the q.s.s. towpreg temperature profiles and the pulling force natural tolerance, along with the appropriate control logic, into an interactive platform.

APPENDIX A

Ribbonizing Powder-Impregnated Towpreg

Donald A Sandusky
The College of William & Mary Williamsburg, VA 23185

Joseph M. Marchello
Old Dominion University, Norfolk, VA 23529

Norman J. Johnston and Robert M. Baucom
NASA Langley Research Center, Hampton VA 23681

ABSTRACT

Dry powder prepregging of thermoplastics is efficient in distributing solid polymer particles throughout continuous filament tows. The resulting towpreg yarn is flexible, bulky and abrasive. Robotic placement material handling systems are generally designed to utilize stiff, preconsolidated ribbons with consistent cross-section. The research included herein summarizes efforts toward developing a bench-scale processing method to convert a single powder coated towpreg yarn into a fully preconsolidated ribbon. A comprehensive study of debulking techniques revealed a variety of issues critical to effective ribbonizing, including towpreg material quality, transverse squeeze flow, appropriate timing for heating and pressure application, and tool contact/release.

Several processing techniques have been designed, built and experimentally evaluated to serve as a basis for understanding the unique characteristics of the towpreg ribbonizing process. Use of reactive plasticizers or solvents was excluded altogether. Due to availability, three powder towpreg yarn materials, Aurum (500)/IM-8 (prepregged by BASF), LaRC-IA/IM-7 and PEEK/AS-4 (prepregged by NASA LaRC), were used in the evaluation of these processes.

By utilizing desirable attributes of several of the experimental processes, a novel processing technique was developed. This powder coated towpreg ribbonizer was comprised of two primary components. The hot bar fixture facilitates transverse melt squeeze flow while the cool nip-roller assembly solidifies the ribbon into a preconsolidated ribbon with consistent cross-section. The process has been shown to provide quality ribbon from various high-temperature performance thermoplastic powder-coated towpreg yarns. The observed experimental rates and temperature ranges indicate that this technique could be readily integrated as a final step in the powder prepreg manufacturing process. The resulting process has been scaled-up to simultaneously convert multiple powder coated yarns into multiple ribbons and has also been used to produce a single 3 inch wide prepreg tape.

KEYWORDS: Thermoplastic Powder Towpreg, Melt Processing, Prepreg Tape, Polyimides, Ribbonizing.

INTRODUCTION

High Temperature Performance, Fiber Reinforced Thermoplastics

Future aircraft are being designed to fly faster, resulting in increased air frame surface temperatures. If fiber reinforced polymeric matrix materials are to be utilized in structural components, they must exhibit high temperature stability in addition to high strength-to-weight ratios. NASA is conducting research efforts to develop high temperature performance, fiber-reinforced, thermoplastic composites for use in future aircraft. Material development research has provided a number of thermoplastic polymers which have the potential to qualify under high performance conditions. In order to properly characterize these polymers as matrix materials, an extensive evaluation of the composite parts is required.

Robotic Composites Manufacture

Automated robotic placement of fiber reinforced thermoplastics (ATP-Advanced Tape Placement) is generally known to offer important advantages for in-situ composite manufacturing. Many commercial research efforts are developing the robotic hardware and software to bring this technology into widespread use in building aircraft parts. Ambitious projects are attempting to push the limits of the robotic technology by building complex curvature parts. Simultaneously, the robot manufacturers and users are learning how to reduce the size and bulk of the placement equipment [1]. As time progresses and the technology develops, this manufacturing method promises opportunities for thermoplastic composites assembly and repair in commercial composites shops as well as in the vacuum of earth orbiting space.

As these ATP developmental research efforts succeed and fail, important limitations and "bottle-neck" issues have been discovered. Examples include open section residual stresses, turning radius limitations, autohesion requirements, compliant roller issues, prepreg material quality and post processing annealing of crystalline polymers. Most basic of these is the requirement for high quality thermoplastic prepreg ribbon.
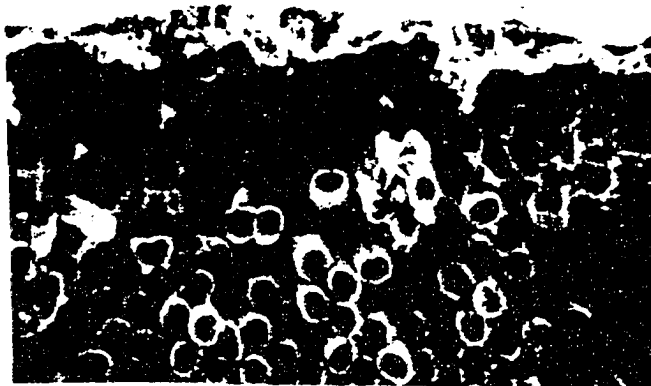

Figure 1.   This LaRC-TPI-1500/T-800 hot-melt prepreg tape exhibits poor wet-out.

2613

Dry Powder Prepregging:

Many high-temperature performance thermoplastics (e.g., fully-imidized polyimides with Tg=250°C) are not particularly amenable to dissolution in organic solvents due to their stiff back-bone structure and are therefore not well suited for conventional solution (dip-pan impregnation) prepregging methods [2]. The high melt viscosity of these same polymers precludes conventional hot-melt prepregging methods. Figure 1 shows a Scanning Electron Micrograph cross-section of hot-melt prepreg tape which appears as a bundle of dry carbon filaments covered by a polymer sheath. This prepreg was not "wet-out" because the viscosity of the polymer was far too high for the melted polymer to penetrate the fiber bundle. Melt viscosity could be reduced, and therefore wet-out could be promoted, by adding a flow enhancing additive (plasticizer) to the polymer prior to prepregging. Residual plasticizer [3] has been shown to effect matrix dominated composite part properties.

In response to these concerns, powder prepregging technology [4] continues at NASA Langley Research Center. In contrast to the previously mentioned conventional prepreg forms, dry powder prepregging does not include the use of solvents or plasticizers. As a consequence, the typical dry powder-coated towpreg is more likely to retain maximum matrix dominated composite properties. Contemporary commercial research compliments NASA's efforts in the development of towpreg yarn and ribbon material. CYTEC Engineered Materials (formerly BASF) offers a high-quality dry powder towpreg yarn made via their slurry impregnation processing [5]. CYTEC is currently evaluating ribbonizing methods for the conversion of towpreg yarn into preconsolidated ribbon. Similarly, Quadrax Advanced Materials Systems Inc. has a powder slurry process [6] followed by pultrusion, which is being used to develop ribbon for automated placement research.

Figure 2. The surface topology of a typical thermoplastic powder coated towpreg yarn (PEEK/AS-4) exhibits powder particles trapped within the filament array and/or partially fused polymer which is adhered to the filaments.

2614

Typically, powder towpreg yarn is bulky and voidy [7] compared to its solution-coated towpreg counterpart. Figure 2 is a photograph of a typical powder coated towpreg yarn made at NASA LaRC's Composites Laboratory. In this bulky state, high Tg, thermoplastic powder towpreg yarns are not well suited for conventional robotic ribbon placement.

Many powder towpreg yarns generally exhibit these characteristics:

- Abrasive surface texture below the glass transition temperature.
- Even filament/polymer distribution.
- Accurate fiber volume percentage.
- Peripheral broken filaments and inconsistent surface characteristics varying with fiber type, sizing and modulus.
- Bulky and flexible characteristics (ranging from 50% to 80% voids).
- Inconsistent thickness and width due to variable "bulk" of yarn.

High Quality Prepreg Ribbon Manufacturing

Commercial prepregging technology is being elevated to meet the stringent material specifications required by automated robotic placement. Some commercial prepreg suppliers already have technologies which are capable of providing high quality ribbons (e.g., PEEK/AS-4, PEKK/AS-4 and PPS/AS-4). Some of the NASA funded robotic placement research efforts require the use of polymer matrix systems which are not commercially available in ribbon form. The term "ribbonizing" is used here as an analog to manufacturing a prepreg tape that is less than about 10 mm wide. Once a reasonable ribbonizing method is developed, the scale-up to making multiple ribbons or a more conventional prepreg tape, is a natural progression. **The primary goal of this research was to develop a process which converts powder towpreg yarn into ATP quality ribbon.** Secondly, this activity intends to provide technological opportunities to suppliers of other material systems so as to broaden the scope of the available materials for robotic placement of thermoplastic composites.

In order for the towpreg yarns described above to be considered for utilization in automated tow placement operations, the yarn must be converted to discrete cross-section ribbons with the following characteristics.

- Surface texture of the ribbons must be uniform and smooth to the touch. This eliminates the allowance of "hair-balls" and irregular surfaces.
- Filaments must be evenly distributed within the polymeric matrix.
- The fiber volume of the towpreg ribbon must be equal to that which is required for the finished part, since no squeeze-out or "flash" is removed in robotic placement processing.
- Ribbon must be reasonably void-free (1% to 3% maximum) for most high performance applications.
- Ribbons must have precise width (e.g. 0.125 in. to 0.250 in.).
- Ribbon must not be unevenly tapered or rounded on ends.
- Thickness is specified within some tolerable range but is not typically considered a critical dimension for thin ribbons.

Experimental Evaluation of Ribbonizing Techniques

Each of the following processing methods were thoroughly evaluated. Two major categories of techniques were chosen: Heated and Cooled Apparatus.

2615

I   Heated Tools and Machines

Pull Dry Powder Towpreg Yarn:

1   Through a Conventional Thermoplastic Melt Pultruder.
2   Through an Over-Sized Die Melt Pultruder.
3   Through an Ultrasonically Enhanced Melt Pultruder. *
4   Through a Preheated Ultrasonically Enhanced Melt Pultruder. *
5   Over a Heated. Stainless Steel Roller.
6   Over a Heated. Grooved S.S. Roller.
7   Over a Heated. Grooved Ceramic Roller.
8   Over a Heated. Grooved. Silica-Glazed. Ceramic Roller.
9   Through Matched Set of Hot. Flat. S.S. Nip-Rollers.
10   Over and Under Stationary Hot S.S. Rods (3/8 inch o.d.).
11   Over and Under Stationary. Hot. Ceramic or Bulk Graphite Bars.
12   Over and Under Stationary. Hot. Glass Rods.
13   Over a Heated. Curved. Ceramic Shoe.
     by Thermoplastic Composites Inc., Bartlesville. OK.

II   Cooled Tools and Machines

Pull Dry Powder Towpreg Yarn Through a 4 Foot Long Tube Furnace to Soften the Polymer. then After Exiting:

14   Over an Ambient Air-Cooled. Chrome Rod (1 inch o.d.).
15   Through a Cooled. Grooved. Silica-Glazed. Curved. Ceramic Shoe.
16   Over a Cooled. Stationary. S.S. Tube Array (3/8 inch o.d.).
17   Through Cooled. Spring-Loaded. Nip-Rollers.
18   Through Cooled. Grooved. Spring-Loaded. Nip-Rollers.

III   Combination Processes

19   Process # 12 and # 18.
20   Process # 11 and # 18.

Figure 3 on the following page. arranges qualitative attributes associated with each of the 20 listed processing techniques. The heated apparatus typically facilitated melt flow and therefore promoted polymer/filament redistribution and void expulsion. The cooled apparatus typically provided good product release and consistent cross-sections. The combination processes take advantage of the beneficial attributes of the others and consequently provide a novel approach to consolidating prepreg yarns [8].

EXPERIMENTAL DISCUSSION

I   Heated Tools and Machines

Ribbonizing techniques #1.#2.#3 and #4 above refer to a group of variations on the common theme of pultrusion: the dry towpreg yarn is pulled through a stationary tapered die having an inlet area greater than the exit area. which is heated at the entrance and may or may not be cooled at the exit. Manufacture of thermoplastic composite parts via pultrusion techniques is commonly known to be useful for a variety of products. Large cross-section pultruded (fiberglass/epoxy) parts [9.10] routinely make use of random short-fiber mats which surround the major load bearing unidirectional filaments inside. One of the purposes for the random mat. shown in Figure

2616

Attributes

Ribbonizer Process #

Legend: ● Good ◉ Average ○ Poor

| Attribute	1	2	3	4	5	6	7	8	9	10	11	12	13	14	15	16	17	18	19	20
General Quality of Resulting Ribbon	◉	◉	◉	●	◉	◉	◉	◉	◉	●	●	●	◉	◉	◉	◉	◉	◉	●	●
Uniformity of Polymer Distribution	◉	◉	◉	◉	◉	◉	◉	◉	◉	●	●	●	◉	◉	◉	◉	◉	◉	●	●
Transverse Melt Flow	○	○	◉	◉	◉	◉	◉	◉	◉	●	●	●	●	○	○	○	○	◉	●	●
Longitudinal Melt Flow	◉	◉	◉	◉	○	○	◉	◉	◉	●	●	●	◉	○	○	○	○	◉	●	●
Uniformity of Fiber Alignment	●	●	●	●	○	○	◉	◉	◉	◉	●	●	◉	○	○	○	○	◉	●	●
Ribbon Customization Capability	●	◉	●	●	○	○	○	○	◉	○	○	○	◉	○	○	○	◉	●	●	●
Surface Texture Smoothness	◉	◉	◉	●	○	○	◉	○	◉	●	●	●	◉	◉	○	○	◉	◉	●	●
Custom Cross-Section Shape Control	◉	◉	●	●	○	◉	◉	◉	◉	○	○	○	◉	○	○	○	◉	●	●	●
Response to Defects in Powder Yarn	○	◉	◉	◉	○	○	◉	◉	◉	●	●	●	◉	◉	○	◉	●	●	●	●
Fiber "Hair" Balls	○	○	○	○	◉	◉	◉	◉	◉	●	●	●	◉	●	○	●	●	●	●	●
Broomed Filament Ends	○	○	○	○	○	○	○	○	○	◉	◉	◉	○	◉	○	◉	●	●	●	●
Peripheral Dry Filaments	◉	◉	◉	○	○	○	○	○	○	◉	◉	◉	○	◉	○	◉	●	●	●	●
Low Fiber Volume Percentage	◉	◉	◉	◉	◉	◉	◉	◉	○	◉	◉	◉	●	●	○	◉	●	●	●	●
Efficacy of Tooling and Fixturing	◉	◉	◉	◉	○	○	◉	◉	◉	●	◉	●	◉	◉	○	◉	◉	◉	◉	●
Resistance to Friction and Wear	○	◉	◉	●	●	●	◉	○	○	◉	○	●	◉	●	○	◉	●	●	◉	●
Product Release from Tool	◉	◉	◉	◉	○	○	◉	○	○	◉	◉	●	◉	◉	○	◉	●	●	◉	●
Tool / Fixturing Simplicity	◉	◉	◉	◉	●	●	●	○	◉	●	●	●	◉	●	○	●	◉	◉	●	●
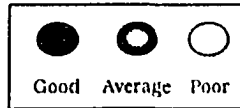
Figure 3. Qualitative Attributes for Each Attempted Process

2617

228

4 is to facilitate a desirable surface contact between the part and the interior walls of the pultrusion die. much like a cotton sock provides a comfortable interface between the foot and shoe. More importantly. the random surface mat acts as a bleeder ply. for transverse polymer flow. Unfortunately, when pultruding ATP ribbon. use of a random mat is inappropriate. Without the mat. pultrusion typically exhibits an exaggerated sensitivity to surface irregularities (e.g. broomed or dry fiber ends) of the incoming towpreg yarn material. Barring use of release coatings or extravagant surface preparations. high temperature performance thermoplastics were observed to stick to just about any surface above Tg.

The time required to melt the dry polymer powder was naturally dependent upon the method of heat application. For practical reasons. the towpreg yarn was preheated (melting the polymer) before it contacted the die entrance. Benefits included entrance lubrication. reduction of required tension and enhanced processing speed. Most importantly. due to the mechanics of the process and the lack of a bleeder ply. pultrusion and its derivatives promoted only limited melt flow transverse to the fibers while the primary flow was longitudinal (axial). For high melt-viscosity thermoplastic polymers. this characteristic is detrimental since it tends to limit processing rates.

Ribbon pultrusion of these polymers on carbon fibers is typically very slow (near 2 to 10 ft/min). Polymer slag build-up was common and tended to complicate processing.
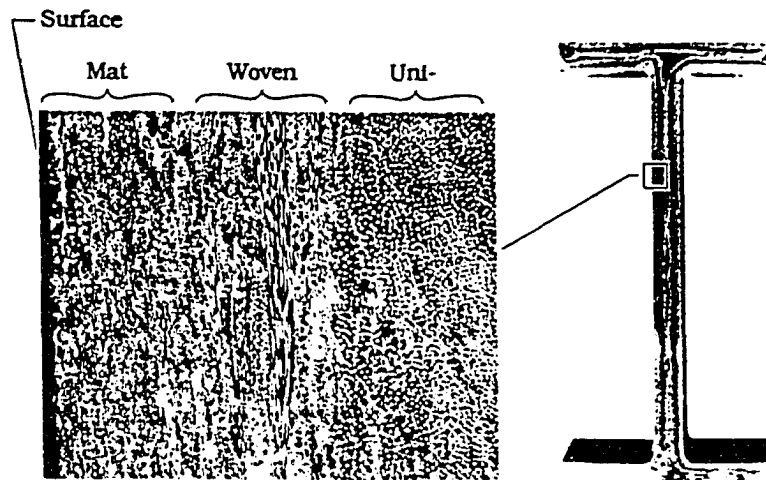
Figure 4. This is a cross-section of a commercially available S-Glass/Vinyl ester, 4 inch tall, pultruded beam. Close inspection of the beam reveals the "lay-up". Note the thickness and heavy polymer content of the chopped fiber mat surrounding the part.

Although state-of-the-art powder coated towpreg is reasonably uniform and consistent. occasional anomalies exist. such as "fiber-balls" and broomed fiber ends. These irregularities routinely cause failure of the pultrusion process. Ultrasonic augmentation has been shown to reduce the sensitivity of the pultrusion process to these material irregularities [11] but it is

impractical. on such a small scale. to expect the pultrusion process to survive ingestion of a fiber-ball without "jamming" the entrance. When the throat of a pultrusion die was plugged with fibers and polymer slag. tension was observed to build-up and sometimes jeopardize the integrity of the towpreg yarn. It is expected that pultrusion of individual carbon fiber towpreg yarns is particularly sensitive to adjacent fiber crossing during debulking. There is a relatively small size ratio (approx. 20 to 1) of the mold cavity's smallest dimension to the filament diameter. Smaller diameter filaments reduce this ratio and likely change the consequential filament crossing effects.

Alternatives to the pultrusion process (techniques #5 through #9) were built and evaluated [12] with the objective of 1) full wet-out of the fibers. 2) a reasonable degree of melt squeeze flow transverse to the fibers. 3) smooth ribbon surface character and 4) a "robust" process which would allow for incidental fiber-balls and other towpreg yarn anomalies. Upon experimental evaluation. adhesion between the melted polymer and most heated tool surfaces was observed for all rotating (e.g. heated roller) apparatus.
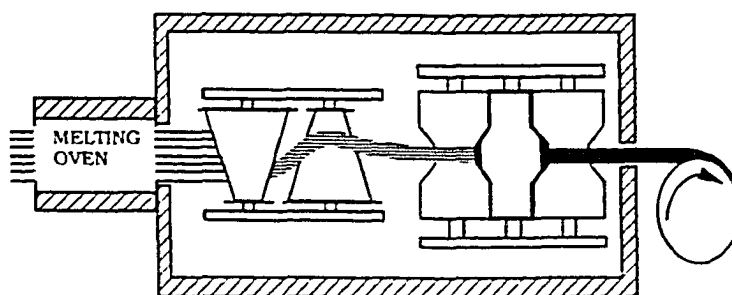

Figure 5.   This is a schematic diagram of the heated box assembly used to evaluate techniques #5 through #9: "the heated roller machinery".

The process shown in Figure 5 was relatively unsuccessful. The heated roller process evaluation did contribute the notion that when melted towpreg yarn was passed over any heated roller (regardless of the surface finish) stray fiber ends tended to become wrapped around the circumference of the roller. This eventually resulted in a filament stripping and process failure in every trial. It became very clear that no heated roller shaping device was going to be capable of converting towpreg into fully preconsolidated ribbon.

Processes #10 #11 and #12 involved drawing a pre-melted towpreg yarn over and under two stationary rods which were fixtured near the exit of a tube furnace. Upon exiting the tool. an operable distance was provided to the "take-up" puller so that the ribbon was allowed to cool below Tg in ambient conditions prior to being taken-up onto a 3 inch cardboard spool (Figure 6). The rod fixture geometry was varied between a classic "S-wrap" to a much gentler under and over pattern. Filament buckling and excessive adhesion between the melted polymer and the heated rods were observed to contribute to process failure under the "S-wrap" configuration but became less detrimental as the yarn was routed through a gentler trajectory. Furthermore. the effect of filament buckling with the "S-wrap" was observed to be more pronounced for larger diameter filaments (AS-4) than for smaller filaments (IM-7) and was casually attributed to the differences in the bending stiffness (Young's Modulus * Area Moment of Inertia) of each type of filament.

Fire-Polished Glass Rods

Towpreg Yarn

Take-Up
Spool
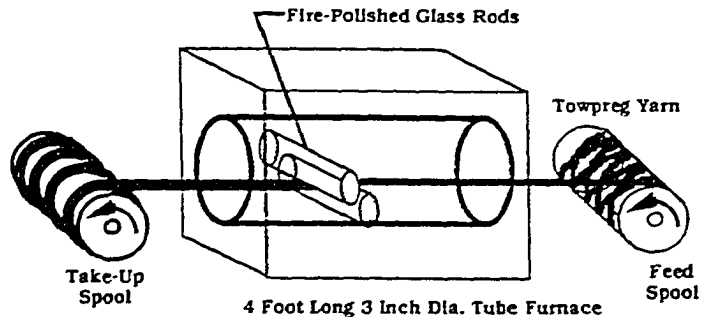
Feed
Spool

4 Foot Long 3 Inch Dia. Tube Furnace

Figure 6. Processes #11 & #12. The incoming yarn passes sequentially, over the first bar and under the second. Void expulsion and polymer flow result in a wide and flat ribbon whose dimensions are a function of rod diameter, fixture geometry and the feed spool tension.

By reducing the angle of wrap, the total yarn surface area contacting the bars was reduced and therefore the ribbon take-up tension required to draw the yarn through the device was correspondingly reduced. (Axial drag force must be optimized to reduce the detrimental processing effects caused by filament/tool adhesion.) The gentler rod configuration used in process #12 was observed to effectively facilitate flow transverse to the unidirectional fibers (wet-out), while causing reasonable values (approximately 150 g) of pulling force. The reaction tension measured just prior to take-up, was observed to change with wrapping area defined by the fixture, but was found to be independent of take-up rate within the range of 5 fpm to 50 fpm. Ribbon width was observed to vary with the processing temperature, amount of wrapping and take-up speed. An example cross-section of the ribbon is shown in Figure 7.
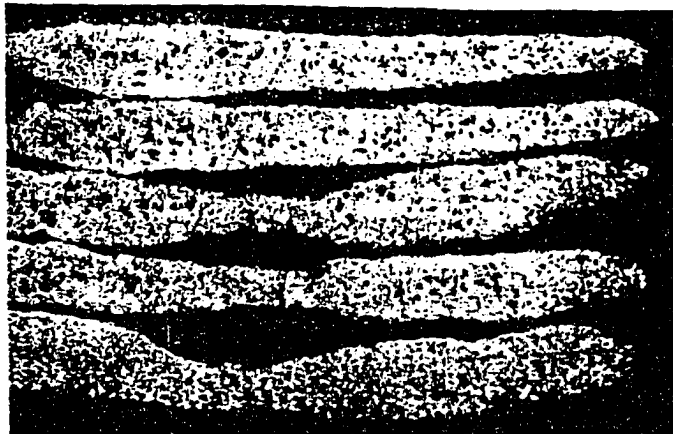

Figure 7. Several representative cross-sections of ribbon made from process #12 are shown to have even polymer distribution and reasonable void content. Aurum-500/IM-8 powder coated towpreg was processed at 50 fpm. The large dark region between the second and third ribbon is a void which resulted during sample potting.

After a typical 45 minute experimental ribbonizing run, the take-up was shu down and the oven was turned off. After the polymer was solidified, produc was cut and removed so that the fixture containing process #12 wa withdrawn from the tube furnace with a section of product adhered withir The rod assembly was then dismantled. The two glass rods were observed t remain adhered to the product. The rods were removed from the polyme material by lightly twisting the rod and holding the rigid ribbon stationary The glass rods exhibited abrasion and wear. Efforts to remove the residua polymer and filament slag included soaking the rods in organic solvents anc fire-polishing techniques. Polar aprotic solvents removed the polymer anc revealed carbon filaments which had cut through and stuck into the surfac of the glass rods. Fire-polishing compromised the dimensional stability o the glass. The abrasion of the glass rods revealed that silica glass would no be useful for long duration processing runs nor could the glass be routinely reused. Wear resistant materials have replaced the glass rods. Both bulk graphite and fired ceramic and have been used in repeated long-duration ribbonizing runs.

The section of ribbon which was attached to the glass rods was potted in epoxy and polished for microscopic evaluation. Sectioning along the length of the sample revealed the motion of voids to be transverse to the filament array. Void size and shape varied from small spheres to large slugs. Transverse void expulsion (per unit length) is known to require a larger pressure gradient than axial void expulsion. Fortunately, this process flattens the towpreg to a thickness near 10 to 100 filament diameters so that the voids do not have far to travel before they escape. As a consequence of the thinning cross-section, the pressure gradient was compounded. The cross-sections also revealed the movement of the filaments within the polymer matrix. As the yarn passed over the first bar, the filaments were pulled upward toward the bar surface, relative to the viscous polymer melt. Upon contact with the lower surface of the second bar, the filaments were observed to move upward toward the second bars surface. These observations suggest that the polymer is being redistributed within the filament array via melt squeeze-type flow. The photomicrograph of the
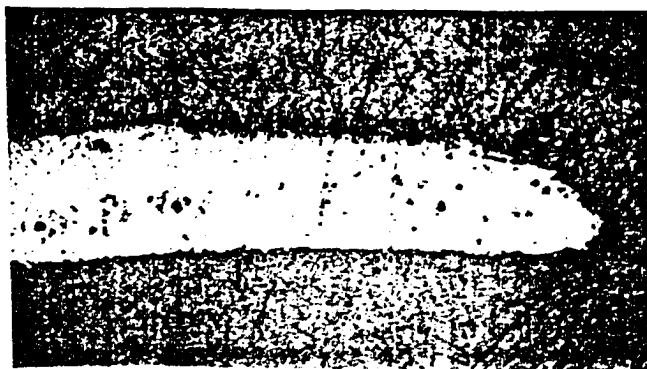

Figure 8. Aurum-500/IM-8 powder coated towpreg was processed via #12 at 30 fpm take-up speed. The ribbon cross-section exhibits many desirable attributes including low void content, smooth surface character and good wet-out.

resulting ribbon further revealed an enhanced, even distribution of the two components. By slowing process #12 down from 50 fpm to 30 fpm. (Figure 8), void content was observed to be reduced. Similar effects were observed when the temperature was increased or wrapping angle was increased, instead of slowing the process from 50 fpm. The contact time required for processing is limited by complex two-phase viscous fluid flow and is the matter of future process modeling research activities.

Since the fibers carried 100% of the tensile load, the matrix was cooled under approximately ambient conditions. To make a ribbon of uniform cross-sectional shape along its length, the ribbon must have been constrained in the form of that desired shape until below Tg (reformed). Otherwise, surface energy effects, thermal stresses, and uneven tension on the filament ends, had the opportunity to alter the intended shape of an otherwise smooth, flat ribbon.

II Cooled Tools and Machines

Several alternative techniques (previously designated #14 through #18) were evaluated with the goal of providing full product release from the tool as well as uniform net shape. Process #14 was accidentally discovered. In attempts to divert the softened yarn exiting apparatus #12, it was discovered that the polymer did not adhere to a cool chrome rod. Furthermore, the polymer solidified quite evenly on the side which contacted the rod. This led to an attempt to use the ceramic shoe in an altered configuration so that it could be heated on the inlet side and cooled on the exit side. Figure 9 illustrates the salient aspects of process #15. Experimental evaluation of the polished cross-section, revealed that the ribbon made from the tool was insufficiently wet-out and was unevenly shaped along its length.
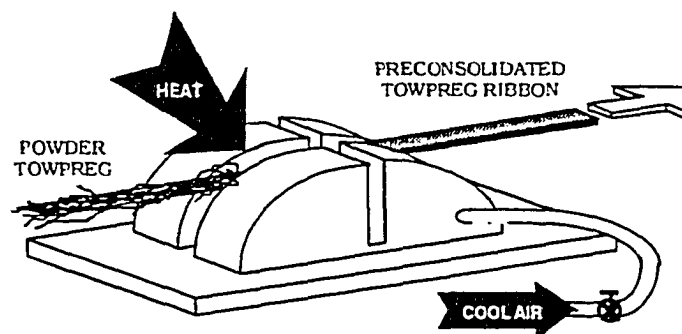
Figure 9.   This schematic diagram illustrates the configuration of the apparatus #15. The front half of the die was passively heated by a hot air gun while the hollow back half was cooled with a steady stream of air.

The next apparatus involved pulling pre-melted towpreg yarn through a stationary, cooled tube array (#16). Unexpectedly, a steady low frequency "hum" could be heard emanating from the machinery. This hum was observed to vary with take-up speed within a limited range. The melted towpreg yarn instantly stuck to the tube. As the polymer cooled well below Tg it shrank according to the difference in the thermal coefficient of expansions for the two different materials. Within a very short period of time (approximately 1/20 th of a second) the melted polymer adhered to the tube

2622

and solidified. While the polymer contracted, the take-up winder tension overcame the adhesive bond so that the polymer "popped-off" the tube allowing the melted section directly behind to impact the cool tube and instantly stick. This set of simultaneous events caused the hum. The resulting ribbon surfaces were "scaled" and rough. Upon observation of the polished ribbon cross-sections, techniques #14, #15 & #16, were determined to be mostly ineffective at facilitating melt squeeze-flow transverse to the fibers. The most important benefit of these three cooled processes was consistent product release from the tool. This was known to be a critical issue for scale-up production. Due to the elevated temperatures used for melt processing of polyimides, conventional release papers (or cloths) were predetermined to be impractical.

Next, the #17 apparatus involved pre-melting the yarn in a long oven and then drawing it through cooled, nip-rollers. This apparatus was placed approximately 1 inch from the exit of the melting oven. At a moderate take-up rate of approximately 15 ft/min. and proper temperature setting for the melting oven, the molten polymer was observed to cool to below Tg upon contact with the nip rollers. Product release between the polymer and the cool metal surfaces was observed to be consistent. No vibration hum was heard. Incidental towpreg yarn defects were allowed to pass freely through the die by the nature of the spring-loaded nip. Given a conduction mode of heat transfer from the towpreg yarn to the contacting tool surface, the rate of heat removal was subjectively observed to be a function of the processing rate, the thickness of the yarn and the respective material heat capacities. In one example, Aurum-500/IM-7 was pre-melted (above Tm = 375°C long enough to melt crystalline regions) then entered the nip point at 300°C and exited at 100°C which corresponded to a roller surface temperature increase from 49°C to 55°C. The nip roller temperature was observed to be effected by the flow rate of cooling fluid (pressurized dry air) through the hollow roller shafts as well as the temperature difference between Tg and the steady-state roller nip surface temperature. Process # 18 and, was shown to be effective as a means of constraining the moving towpreg yarn in a specific rectangular shape while it solidified.

Although process #18 was successful in constraining the moving yarn under pressure while its temperature was lowered below Tg, the overall goal of a void-free, consistent shaped ribbon was not realized. By inspecting the polished ribbon cross-section, incomplete wet-out (via melt squeeze-flow transverse to the fibers) was observed. Changing the nip-pressure (approximated 10 psi to 400 psi) was observed to result in only minor improvements in the wet-out. Inspection of the polished cross sections of the ribbon revealed residual voids within the bundle. Additional pressure would normally compress these voids in the neat resin, but further evaluation of the ribbon revealed that the limited debulking could be attributed to extensive fiber cross-over within the towpreg yarn itself. This detrimental processing effect is expected to be more pronounced with higher fiber volume and larger diameter fibers (e.g., AS-4 compared to IM-8). Studies of squeeze-flow from a "closed" mold containing viscous oil and long fibers [13], have shown the platen movement to be ultimately halted; not by impermeable network viscous flow limitations, but by the compounded occurrences of fiber cross-over contact [14]. Prior to the cool nip in process #18, some filament alignment as well as filament/polymer redistribution was clearly required.

III Combination Processes

Approach # 19 was arranged to utilize the beneficial attributes of processes # 12 and # 18 simultaneously.

Take-Up Spool

Incoming Towpreg Yarn

Ribbon

Process # 17 Spring-Loaded Nip-Rollers

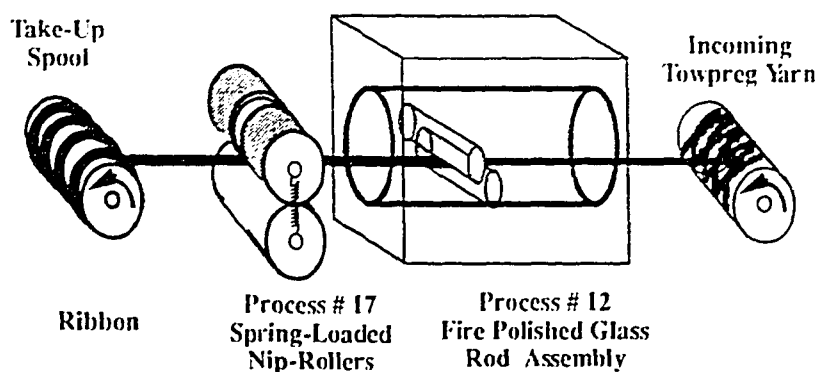**Process # 12 Fire Polished Glass Rod Assembly**

Figure 10. Schematic for process # 19 and # 20. Yarn movement is right to left.

As illustrated in Figure 10, the oven was retrofitted with fixturing which held two fire-polished glass rods in an optimized pattern which caused the incoming melted towpreg yarn to contact the under surface of the first rod and the upper surface of the lower rod. As observed previously, the material which exited tool #12 was debulked and exhibited low void content. Due to physical interference of the apparatus, approximately one inch of linear distance was required between the exit of the melting oven, and the entrance to the spring-loaded nip-roller assembly # 18. Exposure to ambient cooling

Figure 11. Representative cross-sections of Aurum-500 / IM-8 ribbon made via process #19 at 40 fpm on a table-top experimental scale. This ribbon exhibited desirable attributes such as good polymer/filament distribution. low void content. highly consistent cross-sectional dimensional integrity. and smooth surface texture.

2624

through this space was a direct function of take-up speed. Upon entering the nip-point, the "malleable" softened towpreg was solidified into a uniform 0.121 in. wide by 0.0085 in. thick ribbon (Figure 11).

Process # 20 is similar to process #19 with the exception that the glass rods were replaced by a wear resistant ceramic material. The critical control variable was found to be back tension rather than pulling tension or take-up rate. An advanced material handling system was implemented to ensure accurate control of the process variables. Uninterrupted experimental processing (120 minutes at 30 fpm linear take-up) indicated that process #20 was the best candidate to scale-up for manufacturing multiple ribbons and broad tapes.

SUMMARY

A systematic investigation of powdered towpreg ribbonizing has provided the following experimental observations:

1   Melted towpreg will stick to surfaces which are above the polymers Tg.
2   To expel voids from a towpreg yarn, a process must contact the viscous melt, without excessive adhesion.
3   To fully preconsolidate towpreg yarns a process must provide fiber alignment and polymer/filament redistribution.
4   Melted towpreg cannot be roller processed unless rollers are cooled.
5   To make a ribbon of uniform cross-sectional shape along its length, the ribbon must be partially constrained in the form of that desired shape as it is changes from the viscous melt to the solid phase.
6   Ribbonizing is sensitive to intra-yarn fiber crossing.
7   Ribbonizing may be sensitive to fiber volume and diameter.
8   Thinning the yarn reduces the transverse void travel distance.
9   Stationary hot bar processing requires bar material which resists abrasion of carbon fibers at elevated temperatures.

Process (#19 or #20) can be readily integrated as a final step in state-of-the-art powder prepreg manufacturing techniques to convert high temperature performance powder towpreg yarn into fully preconsolidated ribbon. The nip-roller groove can be customized to form many alternative cross-sectioned [15] ribbons. With appropriate treatments, derivatives of process # 20 promise to be cost-effective and robust for long duration ribbonizing runs.

REFERENCES

[1]   Felderhoff, K, Steiner, K, "A New Compact Robotic Head for Thermoplastic Fiber Placement", 38th International SAMPE Symposium. p. 138-151, (1993).
[2]   St. Clair, TL, Johnston, NJ, Baucom, BM, "High Performance Composite Research at NASA Langley", SAE/SP-88/748, paper 880110, pp. 1-19, SAE International Congress, Feb., 1988.
[3]   Hou, TH, Johnston, NJ, St. Clair, TL, "Processing and Properties of IM-7/LaRC-ITPI Polyimide Composites", 38th International SAMPE Symposium, Volume 38, Book 1, P. 334-356, (1993).
[4]   Baucom, RM, Marchello, JM, "Powder Curtain Prepreg Process", 38th International SAMPE Symposium, Volume 38, Book 2, P. 1902-1915, (1993).

[5] Baucom. RM. Marchello. JM. "Powder Curtain Prepreg Process". 38th International SAMPE Symposium. Volume 38. Book 2. P. 1902-1915. (1993).

[6] Soules. DA. "Apparatus and Process for Improved Thermoplastic Prepreg Materials". U.S. Patent No. 5.019.427 . May 28. 1991.

[7] Ramasamy. Y. Wang. Y. and Muzzy. J. "Characterization of Powder Coated Towpregs and 2-D Preforms". 38th International SAMPE Symposium. Volume 38. Book 2. p. 1882-1891. (1993).

[8] Sandusky. DA. U.S. patent appl.. NASA LAR-15173-1-CU. 1992.

[9] Lee. W. I.. Springer. G.S.. "Pultrusion of Thermoplastics. "36th International SAMPE Symposium Transactions. p.1309-1317. April (1991).

[10] Fanucet. JP. Nolet. S.C.. Koppernaes. C. Kim. YR. "Measurement of Internal Die Pressure Distributions During Pultrusion of Thermoplastic Composites". 22nd International SAMPE Technical Conference. P.50-64. (1990).

[11] Taylor. SR. Thomas. W.M.. "High-Speed Pultrusion of Thermoplastic Composites". International SAMPE Technical Conference Series. 22. p.78-87.(1990).

[12] Sandusky. DA. Marchello. JM. Baucom. RM. Johnston. NJ. "Customized ATP Towpreg". 24th International SAMPE Technical Conference. p. T591-T605. (1992).

[13] Gutowski. TG. Cai. Z. Bauer. S. Boucher. D. Kingery. J and Wineman. S. "Consolidation Experiments for Laminate Composites". *Journal of Composite Materials*. Vol. 21. p.650-669. (July. 1987).

[14] Holty. DW. Greene. TL. Carpenter. CE. Davies. RM. "Variables Affecting the Physical Properties of Consolidated Flexible Powder-Coated Towpregs". 38th International SAMPE Symposium. Volume 38. Book 2. P. 1916-1929. (1993).

[15] Sandusky. DA. Marchello. JM. Baucom. RM. Johnston. NJ. "Customized ATP Towpreg". 24th International SAMPE Technical Conference. p. T591-T605. (1992).

Appendix B

PAN-Carbon Fibers	Diam. (μm)	Modulus (Msi)	Strength (Ksi)
AS-4™(Herculese)	7	33	580
IM-7™(Herculese)	5	40	785

Polyimide Powders	Tg (°C)	Tm (°C)
LaRC™-IAX (4%)	235	285
Aurum™-400A	250	none
PIXA™	252	361

APPENDIX C

$\varepsilon 1=0.8$

0.8

$\varepsilon 2=0.3$

0.3

$\sigma=5.67*10^{\wedge}-8$

$5.67 \ 10^{-8}$

$F12=0.004$

0.004

$Vv=0.5$

0.5

$\rho=(1.38*10^{\wedge}6)*(1-Vv)$

690000.

$d=Sqrt[(9.7326*10^{\wedge}-8)*(1+Vv)]$

0.000382085

$dT=0.072$

0.072

$L=1.2$

1.2

$k11=6$

6

$h=0.2105$

0.2105

$T1=451+1054*x-555*x^{\wedge}2-1960*x^{\wedge}3+3100*x^{\wedge}4-1402*x^{\wedge}5$

$451 + 1054 \ x - 555 \ x^{2} - 1960 \ x^{3} + 3100 \ x^{4} - 1402 \ x^{5}$

$cp=0.002893*T2[x]+0.2216$

$0.2216 + 0.002893 \ T2[x]$

$v=0.250$

0.25

$\Omega=(\rho*v*cp*(d^{\wedge}2))/4$

$0.00629578 \ (0.2216 + 0.002893 \ T2[x])$

zip=(1-ε1)/(dT*ε1)

3.47222

dee=1/(dT*F12)

3472.22

doo=(1-ε2)/(d*ε2)

6106.84

Σ=(σ/(zip+dee+doo))

$5.91701 \ 10^{-12}$

don=((d^2)*k11)/4

$2.18984 \ 10^{-7}$

jen=(h*d)

0.0000804289

rhs=Ω*T2'[x]

0.00629578 (0.2216 + 0.002893 T2[x]) T2'[x]

lhs=-don*T2''[x]+Σ*(T1^4-T2[x]^4)

$5.91701 \ 10^{-12}$ ((451 + 1054 x - 555 x^2 - 1960 x^3 + 3100 x^4 - 1402 x^5)
^{4} - T2[x]^4) - 2.18984 10^{-7} T2''[x]

Sol025=NDSolve[{rhs==lhs,T2[0]==293,T2'[0]==0},T2,{x,0,1.2}]

{{T2 -> InterpolatingFunction[{0., 1.2}, <>]}}

Sol0559=NDSolve[{rhs==lhs,T2[0]==293,T2'[0]==0},T2,{x,0,1.2}]

{{T2 -> InterpolatingFunction[{0., 1.2}, <>]}}

Sol075=NDSolve[{rhs==lhs,T2[0]==293,T2'[0]==0},T2,{x,0,1.2}]

{{T2 -> InterpolatingFunction[{0., 1.2}, <>]}}

Sol1219=NDSolve[{rhs==lhs,T2[0]==293,T2'[0]==0},T2,{x,0,1.2}]

{{T2 -> InterpolatingFunction[{0., 1.2}, <>]}}

Sol175=NDSolve[{rhs==lhs,T2[0]==293,T2'[0]==0},T2,{x,0,1.2}]

{{T2 -> InterpolatingFunction[{0., 1.2}, <>]}}

Sol250=NDSolve[{rhs==lhs,T2[0]==293,T2'[0]==0},T2,{x,0,1.2}]
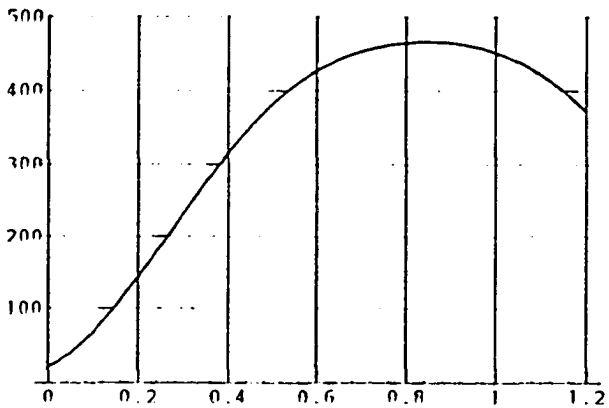
{{T2 -> InterpolatingFunction[{0., 1.2}, <>]}}

```
Sol250B=NDSolve[{rhs==lhs,T2[0]==293,T2'[0]==0},T2,{x,0,1.2}]

{{T2 -> InterpolatingFunction[{0., 1.2}, <>]}}
```

```
mps025=Plot[Evaluate[(T2[x]-273)/.Sol025],{x,0,1.2},
PlotRange ->{0,500},GridLines->Automatic]
```
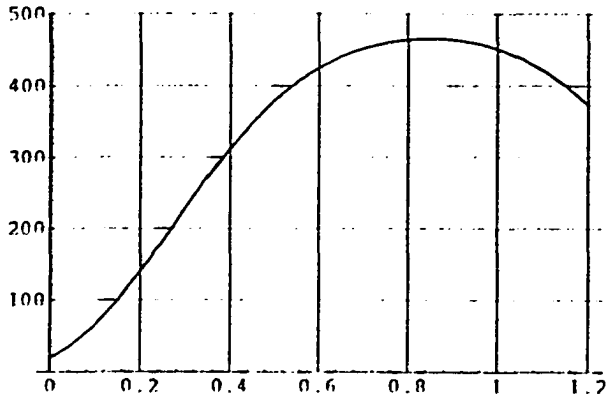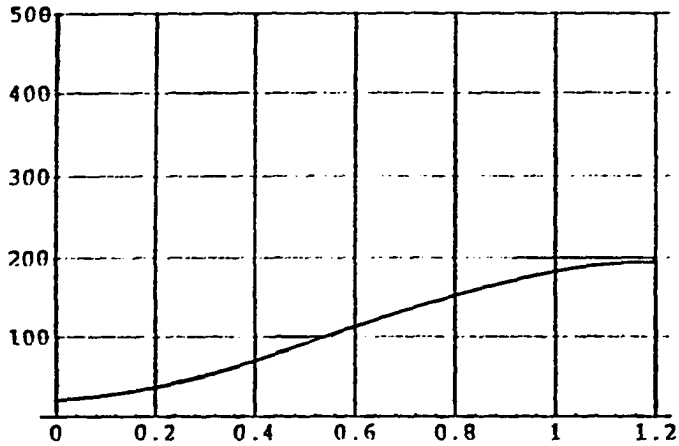

-Graphics-

```
mps025all=Plot[Evaluate[(T2[x]-273)/.Sol025B],{x,0,1.2},
PlotRange ->{0,500},GridLines->Automatic]
```
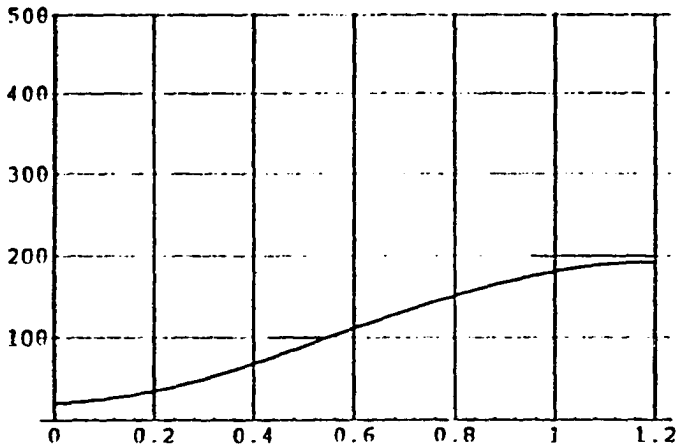

-Graphics-

```
mps250all=Plot[Evaluate[(T2[x]-273)/.Sol250B],{x,0,1.2},
PlotRange ->[0,500],GridLines->Automatic]
```


-Graphics-

```
mps250=Plot[Evaluate[(T2[x]-273)/.Sol250],{x,0,1.2},
PlotRange ->[0,500],GridLines->Automatic]
```


-Graphics-

Bibliography

1   Ahn, K.J.; Seferis, J.C.; Price, J.O.; Berg, A.J. *SAMPE Journal*, **1991**, 27(6),
        19.

2   Angell, Jr., R.G.; Michno, Jr., M.J.; Konrad, J.M.; Hobbs, K.E. U.S. Patent
        4 804 509, 1989.

3   Avallone E.A.; Baumeister T. "Marks' Standard Handbook for Mechanical
        Engineers", 9th ed.; McGraw-Hill, New York, 1987.

4   Avis, V.A.; Matthews, A.J. U.S. Patent 3 737 352, 1973.

5   Baird, D.G.; Sun, T.; Done, D.S.; Wilkes, G.L. *J. ThermopL Comp. Mat.*, **1990**,
        3, 31-.

6   Barnes, H.A.; J.F. Hutton; Walters, K. "An Introduction to Rheology",
        Elsevier: New York, 1989; Chapter 1.

7   Baucom, R. M.; Marchello, J. M. *SAMPE Series*, **1993**, *38*, 1902-15.

8   Baucom, R. M.; Snoha, J.; Marchello, J. M. U. S. Patent 5 057 338, 1991.

9   Beever, W.H.; Selby, L.M. U.S. Patent 4 820 366, 1989.   ·

10   Bibbo, M.A.; Gutowski, T.G. Soc. Plast. Eng. Tech. Papers, ANTEC'86, 1986,
        1430.

11   Birkebak R.C.; Sparrow E.M.; Eckert, E.R.G.; Ramsey J.W. *ASME J. Heat
        Trans. C*, **1964**, *86*, (2), 193-9.

12   Bodine Electric Company,1975, Brush Motor Test Report, 32DSBEPM.

13   Burns, J.S. *J. ThermopL Comp. Mat.*, **1994**, *7*, 100-.

14   Carpenter, C.E.; Colton, J.S. *SAMPE Series*, **1993**, *38*, 205-.

15   Chabrier,G.; Moine, G.; Maurion, R.; Szabo, R. U.S. Patent 4 626 306, 1986.

16   Cheng, J.T. "Applied Rheology and Polymer Processing", from Cheremisinoff, X. "Encyclopedia of Fluid Mechanics", Vol. 7, Gulf Publishing: Houston, 1988.

17   Chipp R.E.; Viskanta R. *ASME J. Heat Trans. C,* **1966,** *88,* (3), 326-7.

18   Cogswell, F.N.; Hezzell, D.J. U.S. Patent 4 549 920, 1985.

19   Cogswell, F. N.; Staniland, P.A. U.S. Patent 4 541 884, 1985.

20   Courtney, A.L. U.S. Patent 3 249 484, 1966.

21   DuPont Company, Wilmington, DE, 1985, PM 9170037-002 Rev. A, 71-2.

22   Dyksterhouse R.; Dyksterhouse, J.A.; Handermann, A.C.; Western, E.D. U.S. Patent 4 919 739, 1990.

23   Ghasemi Nejad, M.N. University of Delaware, 1994, C.C.M. Report 92-52.

24   Gutowski, T.G.; Cai, Z.; Bauer, S.; Boucher, D.; Kingery, J.; Wineman, S. *J. Comp. Mat* **1987,** 21, 650.

25   Gutowski, T.G. *SAMPE Series,* **1985,** *30,* 925.

26   Gutowski, T.G. *SAMPE Quarterly,* **1985,** *16* (4).

27   Hardwick, J.G. G.B. Patent 1 434 926, 1976.

28   Hartland, U.S. Patent 2 702 408, 1955.

29   Hashizume, S. Japanese Patent 405 050 432, 1993.

30   Hepola, P.J., Ph.D. Dissertation, The University of Delaware, Newark, DE., 1993.

31   Hergenrother, P.M.; Bryant, R.G.; Jensen, B.J.; Havens, S.J. *J. Polym. Sci., A. Polym. Chem. Ed.,* **1995,** *35,* XX.

32   Hinckley, J.A.; Grenoble, R.W.; Marchello, J.M. *SAMPE Series,* **1995** *40,* XX-.

33   Hou, T.H. Soc. Plast. Eng. Tech. Papers, ANTEC'86, 1986, 1300.

34   Iyer, S.I.; Drzal, L.T. *J. Thermopl. Comp. Mat.*, **1990**, *3*, 325-.

35   Johnston, N. J.; Towell, T. W. U. S. Patent 5 252 168, 1993.

36   Kumar, N.C. *J. Polym. Sci. Macromol. Rev.* **1980**, *15*, 255-325.

37   Lee, L.I.; Springer, G.S.; Smith, F.N. *J. Comp. Mat.*, **1991**, *25*, 1632.

38   Lundblad, W.E.; Starrett, H.S.; Wanstall, C.W. *SAMPE Technical Series*, **1994**
      26, 774-.

39   Mantell, S.C.; Springer, G.S. *J. Comp. Mat.* **1992**, *26*, (16), 2348.

40   Moyer, R.L. U.S. Patent 3 993 726, 1976.

41   Muzzy, J.D.; Varughese, B. U.S.Patent 5 094 883,1992.

42   Muzzy, J.D.; Colton, J.S. U.S. Patent 5 295 064, 1994.

43   O'Conner, J.E. U.S. Patent 4 680 224, 1987.

44   O'Conner, J.E.; Beever, W.H.; Dancer, J.W.; Beaulieu, W.B.; Selby, L.M.;
      Rhodes Jr., V.H. U.S. Patent 4 883 552, 1989.

45   Oppenheim, A.K. *ASME Trans.* **1956**, *78*, 725-35.

46   Ozisik M.N.; "Heat Transfer, A Basic Approach", McGraw-Hill: New York,
      1985.

47   Peltonen, P.; Lahteenkorva, K.; Paakkonen, E.J.; Jarvela, P.K.; Tormala, P.
      J. Thermopl. Comp. Mat., **1992**, *5*, 318-43.

48   Perlmutter, M.; Howell J.R. *ASME J. Heat Trans. C*, **1964**, *86*, (2), 169-79.

49   Pitchumani, R.; Ranganathan, S.; Don, R.C.; Gillespie, Jr., J.W. in,
      "Mechanics of Materials Processing and Manufacturing", Moon and Nejhad
      Eds., ASME Press, 1994.

50   Pitchumani, R; Yao, S.C. *J. Heat and Mass Trans.* **1992**, *35*, (9), 2185.

51   Pratt, J., DuPont Advanced Materials, 1993.

52 Price, H.L.; Cupschalk, S.G. in "Polymer Blends and Composites in Multiphase Systems", C.D. Han, ed. *ACS Advance in Chemistry Series* **1984**, *206*.

53 Qizian, L.; Ziaoming, Z. *SAMPE Series*, **1993**, *38*, 1594-.

54 Rammoorthy, M. M.S. Thesis, Georgia Institute of Technology, Atlanta, GA., 1993.

55 Ranganathan, S.; Advani, S.G.; Lamontia, M.A. *SAMPE Technical Series*, **1993**, *25*, 630.

56 Rosen, S.L. Fundamental Principals of Polymeric Materials for Practicing Engineers, Barnes and Noble: New York,X.

57 Sandusky, D.A.; Marchello, J.M.; Johnston, N.J. *SAMPE Series*, **1994** *39*, 2612-25.

58 Sears, F.W.; Zemansky M.W.; Young H.D. "University Physics", 6th ed.; Addison-Wesley : Reading Massachusetts, 1983, Chapter 15.

59 Sears, F.W.; Zemansky M.W.; Young H.D. "University Physics", 6th ed.; Addison-Wesley : Reading Massachusetts, 1983, Chapter 13.

60 Seo, J.W.; Lee, W.I.. *J. Comp. Mat.* **1991**, *25*,1127.

61 Soules, D.A. U.S. Patent 5 019 427, 1991.

62 Sparrow, E.M.; Albers L.U.; Eckert, E.R.G. *ASME J. Heat Trans. C*, **1960**, *84*, (2), 73-81.

63 Sparrow, E.M. *ASME J. Heat Trans. C*, **1963**, *85*, (2), 81-8.

64 Sparrow, E.M.; Loeffler, A.L.; Hubbard, H.A. *ASME J. Heat Trans. C*, **1961**, *83*, (4), 415-422.

65 Stokes, T. (Modern Machine & Tool Co. Inc.), Newport News, VA.; Rhew, R.

(NASA LaRC), Hampton, VA.,1994, NASA CONTRACT NAS1-19369 Report.

66   Sugita, Y. Mitsui Toatsu, 1993.

67   Suh, N.P. "Tribophysics", Prentice-Hall: Englewood Cliffs, New Jersey, 1986.

68   Towell, T. W.; Hirt, D. E.; Johnston, N. J. *IntL SAMPE Tech. Conf. Series,* **1990,** *22,* 1156-69 .

69   Van Wylen, G.J.; Sonntag, R.E.; "Fundamentals of Classical Thermodynamics", 3rd ed.; John Wiley & Sons: New York, 1986, Appendix A.

70   Walters, K, "Rheometry", Chapman and Hall: New York, 1975, p.52.

71   Welty X.; Wicks X.; Wilson X. "Fundamentals of Momentum, Heat & Mass Transfer", 2nd Ed.; John Wiley & Sons: New York, 1976.

72   White, F.M. "Fluid Mechanics", 2nd Ed., McGraw-Hill: New York, 1986; Chapter 1.

73   Wickwire, A.M., Jr. U.S. Patent 2 407 335, 1946.

74   Williams, J.G.; Morris, C.E.M.; Ennis, B.C. *J. Polym. Eng. ScL* **1974** *14* (6), 413.

75   XXX. U.S.S.R. Patent 422 469, 1974.

76   Yang, H.; Colton, J.S. Preview Copy for *J. Polym. Comp.* **1993**.

77   Ye, L.; Klinkmuller, V.; Freidrich, K., *J. ThermopL Comp. Mat.,* **1992**, *5,* 32-.

78   Zierling, M.B; Sarifim, A.F. *ASME J. Heat Trans. C,* **1966,** *88,* (3), 341-2.

Vita

Donald A. Sandusky was born in Washington D.C., October 16, 1966. He graduated from Presque Isle High School in Presque Isle, Maine in June, 1985. He graduated from the University of Maine in Orono, Maine in May, 1990 with a B.S. in Mechanical Engineering. He was awarded a NASA Graduate Research Fellowship in August, 1991. He entered The College of William and Mary Program in Applied Science (Polymer Track) in January, 1992. During his tenure as a graduate student he was awarded two U.S. patents, published three technical articles, and received four NASA Tech. Brief awards. The author successfully defended his Ph.D. dissertation in February 1995. Following the completion of his work at William and Mary, he will join DuPont Advanced Materials as a Senior Engineer.